

School of Civil and Mechanical Engineering

**Development and Application of Swarm Intelligence and Neural
Network Techniques for Structural Identification**

ZhengHao Ding

0000-0001-6814-7672

**This thesis is presented to the Degree of
Doctor of Philosophy
of
Curtin University**

August 2020

Declaration

To the best of my knowledge and belief this thesis contains no material previously published by any other person except where due acknowledgement has been made.

This thesis contains no material which has been accepted for the award of any other degree or diploma in any university.

Signature:

Date:

LIST OF ACRONYMS

AI: Artificial Intelligence
ABC: Artificial Bee Colony Algorithm
ABCHSS: Artificial Bee Colony Algorithm with Hybrid Search Strategy
AFS: Artificial Fish Swarm Algorithm
ANN: Artificial Neural Network
ALO: Ant Lion Optimizer
Arc-tan DBN: Arc-tan based Deep Belief Network
BA: Bat Algorithm
BMO: Birds Mating Optimizer
BP: Back-propagation Algorithm
CD: Contrastive Divergence
CNN: Convolutional Neural Network
CS: Cuckoo Search algorithm
CSS: Charged System Search
C-TSA: Clustering based Tree Seeds Algorithm
DA: Dragonfly Algorithm
DBN: Deep Belief Networks
DE: Differential Evolutionary algorithm
DE-ANN: Differential Evolutionary based Artificial Neural Network
DMI: Damage Measure Index
DOFs: Degrees Of Freedom
DPSO: Disturbed Particle Swarm Optimizer
EA: Evolutionary Algorithm
EKF: Extended Kalman Filter
FA: Firefly Algorithm
Faster-RNN: Faster Region-based Convolutional Neural Network
FFT: Fast Fourier Transform
FNN: Feed-forward Neural Network
GA: Genetic Algorithm
GABC: Global-best Artificial Bee Colony Algorithm
GA-ANN: Genetic Algorithm based Artificial Neural Network
GBABC: Gaussian Bare-bones Artificial Bee Colony Algorithm
GBSO: Global Brain Storm Optimization
GWO: Grey Wolf Optimizer
GP: Genetic Programming
GSA: Gravitation Search Algorithm
HWA: Hierarchic Wolf Algorithm
Hybrid C-Jaya-TSA: Hybrid Clustering based Jaya and Tree Seeds Algorithm
ICA-ANN: Imperialist Competitive Algorithm based Artificial Neural Network
IGHS: Improved Global-best Harmony Search Algorithm
INM-PSO: Improved Nelder-Mead Particle Swarm Optimizer
I-TSA: Improved Tree Seeds Algorithm
IUKF: Iterated Unscented Kalman Filter
I-Jaya: Improved Jaya
Log-sum DBN: Log-sum based Deep Belief Network
LSHADE: Adaptive DE with Linear Population Size Reduction Mechanism
MA: Monkey Algorithm

MABC: Modified Artificial Bee Colony Algorithm
MAC: Model Assurance Criteria
MDE: Modified Differential Evolutionary Algorithm
MDOF: Multi Degree Of Freedom
MVP: Most Valuable Player Algorithm
PCA: Principle Component Analysis
PDFs: Probability Density Functions
PoDE: Possibility of Damage Existence
PSO: Particle Swarm Optimizer
QABC: Quicker Artificial Bee Colony algorithm
RBF: Radial-Basis Function
RBMs: Restricted Boltzmann Machines
SHM: Structural Health Monitoring
SDI: Structural Damage Identification
SDOF: Single Degree Of Freedom
SPSO: 2011 version of Standard Particle Swarm Optimizer
SRF: Stiffness Reduction Factor
ST: Search Tendency
SVM: Support Vector Machine
TSA: Tree Seeds Algorithm
UKF: Unscented Kalman Filter
VWNN: Volterra/Wiener Neural Network

LIST OF REPRESENTATIVE SIMBOLS

\mathbf{K} : Global stiffness matrix

\mathbf{M} : Global mass matrix

Φ : Mode shape

\mathbf{k}_{ei} : *ith* elemental stiffness matrix

α : Damage index

\mathbf{K}_d : Global stiffness matrix under damaged status

\mathbf{P} : Modal vector to be identified

\mathbf{B} : Best-so-far solution in each cycle

θ_i : An arbitrary feasible solution in the Jaya algorithm

\mathbf{T}_i : An arbitrary feasible solution in the Tree Seeds Algorithm

E : Energy function

$p(\theta | \mathbf{D})$: Probability Density Function

$p(\mathbf{D} | \theta)$: Likelihood Function

$d(X_i, X_j)$: Euclidean distance

$d(\theta_j, \theta_c)$: Manhattan distance

nel : Total number of elements

c'_i : New clustering center

ω : Natural frequency

r : Restoring force

u : Displacement response

\dot{u} : Velocity response

\ddot{u} : Acceleration response

c : Damping

λ : Regularization parameter

v_i : Visible unit i

h_j : Binary state of the hidden unit j

b_j : Bias weight

$p(v, h; \lambda)$: Joint probability

$p(h_{L-1} | h_L)$: Conditional probability

ABSTRACT

Civil engineering structures may accumulate damage during the service period, due to various reasons, such as material degradation, fatigue, overloading, excessive deformation and vibration under normal operating environment and/or extreme conditions. Therefore, it is necessary to perform structural condition monitoring and detect structural damage at an early stage by using the vibration data to prevent structural failures. The nonlinear hysteretic effect could be observed when severe damage occurred in structures. Several nonlinear models, such as the Bouc-Wen model and the bilinear model, are usually used to describe the nonlinear hysteretic effect of civil engineering structures. Identifying these nonlinear parameters is important for understanding the vibration behavior and performance of nonlinear structures. When using the traditional methods, such as the response sensitivity method, to tackle the above-mentioned two problems, the gradient information and good initial values will be required. However, acquiring good initial conditions and gradient is difficult, especially for large-scale structures with strong nonlinearity. Therefore, this research mainly develops improved approaches based on swarm intelligence and neural network techniques, as well as their hybridization methods, which do not demand the good initial values and gradient, for structural identification. Owing to the modeling errors and measurement noise, the difficulties for structural identification increase. The good robustness of swarm intelligence and neural network techniques can be used to effectively overcome this limitation.

The swarm intelligence methods are essentially global optimization algorithms, which are usually based on machine learning techniques to learn and search through data instead of explicit formulations. Structural identification can be formulated as an optimization problem. An appropriate objective function relevant to structural parameters is defined, and mathematical optimization is conducted to identify the best-fit parameters with physical meanings. Thus, swarm intelligence methods could be used for structural identification. Two emerging swarm intelligence techniques, namely, the Tree Seeds Algorithm (TSA) and the Jaya algorithm, are used and further improved for structural identification and their performance is investigated with numerical and

experimental studies. TSA employs the propagation of the trees as a framework while the Jaya is inspired by the concept that the feasible solution acquired for a given problem should move towards the best solution and avoid the worst one. Compared with traditional swarm intelligence techniques, such as the Genetic Algorithm (GA), Particle Swarm Optimizer (PSO) and Differential Evolution (DE), these two algorithms have a simpler algorithmic structure but stronger global search ability. Furthermore, to enhance the performance of these two algorithms, several modified versions are developed, such as, the clustering based TSA (Chapter 2), the improved TSA (Chapter 3), and the improved Jaya (Chapter 4). Then these developed methods are combined with different objective functions to perform structural damage identification and nonlinear parameter identification. Identification results show that the clustering based TSA by using the modal data based objective function can be used effectively to identify damage in a plane truss structure and a frame structure. The improved TSA combining with the time-domain data can be used to well identify the Bouc-Wen model and two bilinear models. The improved Jaya combining with the modified objective function based on the Bayesian inference and the sparse regularization can be used to identify damage in some relatively large scale structures.

Neural network techniques belong to an important branch of artificial intelligence algorithms. The working principle of this type of method is to simulate human brains, through learning a large number of samples to train the network's 'inference ability'. The Deep Belief Neural (DBN) network, as a representative deep network, is used and further developed to investigate the development and application of neural network techniques for structural identification. To enhance the performance of the DBN, an arctan-based sparse constraint is employed to ensure the hidden units to become sparse, which is easily achieved by adding an arctan norm on the whole of the hidden units' activation probabilities. The modified DBN is termed as the 'Arc-tan DBN' and undetermined damage identification is conducted. The identification results demonstrate that the proposed Arc-tan DBN can be used to identify the damages effectively for a building frame structure, even when the modeling uncertainty and measurement noise exist, and only limited data is available.

The hybridization methods mean combining at least two different intelligent

methods to solve more complex identification problems. A hybrid swarm intelligence method based on Jaya and TSA is proposed, termed as the ‘C-Jaya-TSA’. Specifically, the clustering strategy is employed to replace solutions with low-quality objective function values in the Jaya algorithm. Then the search strategy of the TSA is introduced into the best-so-far solution of each cycle. The C-Jaya-TSA combining with the modal data based objective function is used to conduct the undetermined damage identification for the Guangzhou New TV tower benchmark and a simply supported beam with 100 elements. Furthermore, a non-probabilistic method is used to quantify the damage index. A hybrid method based on K means Jaya and Artificial Neural Network (ANN) is proposed, termed as the ‘ANN-K means Jaya’. The used ANN is a representative shallow network. To enhance the ability of the ANN, the K means Jaya algorithm is used to replace the back-propagation algorithm during the training process. The acceleration responses are used as the input, while the corresponding output contains the improved Dahl nonlinear model parameters and the damage index. Even though high-level measurement noise is introduced, the proposed two hybridization methods can yield satisfactory identification results.

Overall, this thesis develops novel swarm intelligence approaches to conduct structural identification, including structural damage identification and nonlinear parameter identification. To make these methods more powerful, some modifications are suggested. Comprehensive numerical and experimental verifications demonstrate the necessity and rationality of the developed modifications and the effectiveness and performance of using the proposed approaches for various structural identification problems.

ACKNOWLEDGEMENTS

First at all, I would like to express my sincere gratitude and respect to my supervisors Prof. Hong Hao and Dr. Jun Li, who have been giving me invaluable guidance and persistent encouragement during my PhD study period. I would never accomplish this thesis without their generous assistances.

Many thanks go to the staff and postgraduate students in the School of Civil and Mechanical Engineering and Centre for Infrastructure Monitoring and Protection (CIMP) for their friendship and kindness during my study at Curtin University.

I would like to acknowledge the China Scholarship Council (CSC) and Curtin University for providing Curtin International Postgraduate Research Scholarship (CIPRS) to support me pursuing this study.

Last but not least, I wish to express my profound appreciation to my parents and family, for their unconditional love and support.

LIST OF PUBLISHED WORK AND/OR WORK PREPARED FOR PUBLICATION

This thesis contains published work and/or work prepared for publication, which have been co-authored. The bibliographical details of the work and where it appears in the thesis are outlined below.

Chapter 2

Ding, Z., Li, J., Hao, H. & Lu, Z. (2019). Structural damage identification with uncertain modelling error and measurement noise by clustering based tree seeds algorithm. *Engineering Structures*, 185, 301-314. <https://doi.org/10.1016/j.engstruct.2019.01.118>.

Chapter 3

Ding, Z., Li, J., Hao, H. & Lu, Z. (2019). Nonlinear hysteretic parameter identification using an improved tree-seed algorithm. *Swarm and Evolutionary Computation*, 46, 69-83. <https://doi.org/10.1016/j.swevo.2019.02.005>.

Chapter 4

Ding, Z., Li, J., & Hao, H. (2019). Structural damage identification using improved Jaya algorithm based on sparse regularization and Bayesian inference. *Mechanical System and Signal Processing*, 132, 211-231. <https://doi.org/10.1016/j.ymssp.2019.06.029>.

Chapter 5

Ding, Z., Li, J., & Hao, H. (2020). Structural damage identification by sparse deep neural network using uncertain and limited data. *Structural Control & Health Monitoring*, 27(5), e2522. <https://doi.org/10.1002/stc.2522>.

Chapter 6

Ding, Z., Li, J., & Hao, H. (2020). Non-probabilistic method to uncertainty in structural damage identification based on Hybrid Jaya and Tree Seeds algorithm, *Engineering Structures*, 220, 110925. <https://doi.org/10.1016/j.engstruct.2020.110925>.

Chapter 7

Ding, Z., Li, J., & Hao, H. Simultaneous identification of structural damage and nonlinear hysteresis parameters by an evolutionary artificial neural network based on time domain data, *International Journal of Non-linear Mechanics*. (Under review).

STATEMENT OF CONTRIBUTION OF OTHERS

The works presented in this thesis were primarily designed, numerically executed, interpreted and written by the candidate and also the first author of the publications (ZhengHao Ding). Significant input to the works was also provided by co-authors. Contributions of the co-authors are described below. The signed contribution form is attached in the appendix.

Chapters 2 and 3

Hong Hao and Jun Li defined the overall scope and objectives of the works and suggested research methodologies and approaches. Zhong-Rong Lu provided some suggestions about how to conduct modeling. All the numerical simulations and experimental verification were realized by ZhengHao Ding. The manuscript was written by ZhengHao Ding. Hong Hao and Jun Li revised and edited this manuscript and also offered additional intellectual input in the discussions of the results.

Chapters 4

All the simulation works are carried out by ZhengHao Ding. Hong Hao provided valuable suggestions. Jun Li offered the experimental data. Hong Hao and Jun Li offered additional intellectual input in the discussions of the results, revised and edited this manuscript.

Chapters 5, 6 and 7

All the simulation works are carried out by ZhengHao Ding. Hong Hao provided valuable suggestions. Hong Hao and Jun Li offered additional intellectual input in the discussions of the results, revised and edited this manuscript.

LIST OF RELEVANT ADDITIONAL PUBLICATIONS

The additional publications relevant to the thesis with the bibliographical details are list as follows

1. **Ding, Z.**, Li, J., & Hao, H. (2020). Structural Damage Detection with Uncertainties Using a Modified Tree Seeds Algorithm. In: *Mechanisms and Machine Science*, 75, 751-760. https://doi.org/10.1016/978-3-030-27053-7_63.

TABLE OF CONTENTS

ABSTRACT.....	I
ACKNOWLEDGEMENTS.....	IV
LIST OF PUBLISHED WORK AND/OR WORK PREPARED FOR PUBLICATION.....	V
STATEMENT OF CONTRIBUTION OF OTHERS.....	VI
LIST OF RELEVANT ADDITIONAL PUBLICATIONS.....	VII
TABLE OF CONTENTS.....	VIII
LIST OF FIGURES.....	XI
LIST OF TABLES.....	XIV
CHAPTER 1 INTRODUCTION.....	1
1.1 Background.....	1
1.2 Research objectives.....	4
1.3 Research outline.....	5
References.....	7
CHAPTER 2 STRUCTURAL DAMAGE IDENTIFICATION WITH.....	11
UNCERTAIN MODELLING ERRORS AND MEASUREMENT NOISE BY CLUSTERING	
BASED TREE SEEDS ALGORITHM.....	11
2.1 Introduction.....	11
2.2 Mathematical Model and Problem Formulation.....	15
2.2.1 Structural damage model.....	15
2.2.2 Objective function for damage identification.....	15
2.3 Methodology.....	16
2.3.1 Standard TSA.....	16
2.3.2 The proposed approach.....	18
2.4 Numerical Simulations.....	23
2.4.1 Colony diversity analysis between TSA and C-TSA on classical benchmark.....	24
2.4.2 Comparison with state-of-the-art algorithms on CEC benchmarks.....	26
2.4.3 Numerical simulation on a truss structure.....	28
2.4.4 Damage identification without modeling uncertainty.....	29
2.4.5 Damage identification with modeling uncertainty.....	33
2.5 Experimental Verification.....	39
2.5.1 Initial finite element model.....	40
2.5.2 Damage identified results.....	41
2.6 Conclusions.....	42
References.....	44
CHAPTER 3 NONLINEAR HYSTERETIC PARAMETER IDENTIFICATION USING AN	
IMPROVED TREE SEEDS ALGORITHM.....	47
3.1 Introduction.....	47
3.2 Nonlinear Hysteretic Models and Parameter Identification.....	51
3.2.1 Nonlinear hysteretic models.....	51
3.2.2 Nonlinear system identification formulation.....	53
3.3 Improved Tree seeds Algorithm (I-TSA).....	55
3.3.1 Original TSA.....	55
3.3.2 Proposed modifications.....	57
3.4 Numerical Studies.....	60

3.4.1 Benchmark Study.....	62
3.4.2 Nonlinear model parameter identification for a SDOF system.....	71
3.4.3 Nonlinear model parameter identification for a MDOF system.....	76
3.5 Conclusions.....	83
References.....	85
CHAPTER 4 STRUCTURAL DAMAGE IDENTIFICATION USING IMPROVED JAYA ALGORITHM BASED ON SPARSE REGULARIZATION AND BAYESIAN INFERENCE	89
4.1 Introduction.....	90
4.2 Theoretical background.....	94
4.2.1 Damage identification of structures.....	94
4.2.2 Proposed objective function.....	96
4.3 Optimization algorithm.....	99
4.3.1 Jaya algorithm.....	100
4.3.2 Improved Jaya algorithm.....	102
4.4 Numerical Studies.....	105
4.4.1 Benchmark tests.....	105
4.4.2 Numerical Simulations.....	106
4.4.3 Comparison with other optimization techniques.....	113
4.4.4 Comparison with the standard Jaya algorithm and other method.....	114
4.5 Experimental verification.....	117
4.5.1 Experimental setup and initial model updating.....	117
4.5.2 Damage identification for the testing model.....	119
4.6 Conclusions.....	121
References.....	123
CHAPTER 5 STRUCTURAL DAMAGE IDENTIFICATION BY SPARSE DEEP BELIEF NEURAL NETWORK USING UNCERTAIN AND LIMITED DATA.....	126
5.1 Introduction.....	126
5.2 Structural damage model.....	131
5.3 Sparse Deep Belief Network.....	131
5.3.1 Restricted Boltzmann Machine.....	132
5.3.2 Deep Belief Network.....	134
5.3.3 Sparse RBM based on Arc-tan.....	136
5.4 Numerical studies.....	139
5.4.1 Numerical Model.....	139
5.4.2 Data generation for training.....	140
5.4.3 Damage identification results.....	144
5.5 Experimental verification.....	147
5.5.1 Initial finite element model updating.....	148
5.5.2 Data generation for training.....	149
5.5.3 Damage identification results.....	151
5.6 Conclusions.....	155
References.....	157
CHAPTER 6 NON-PROBABILISTIC METHOD TO CONSIDER UNCERTAINTIES IN STRUCTURAL DAMAGE IDENTIFICATION BASED ON HYBRID JAYA AND TREE SEEDS ALGORITHM.....	160
6.1 Introduction.....	161

6.2 Theoretical background.....	166
6.3 Hybrid algorithm: Hybrid C-Jaya-TSA.....	168
6.3.1 Jaya algorithm.....	168
6.3.2 Clustering-based Jaya algorithm.....	170
6.3.3 Tree Seeds Algorithm.....	171
6.3.4 The proposed Hybrid C-Jaya-TSA.....	172
6.3.5 Non-probabilistic method to consider uncertainties.....	173
6.4 Numerical Studies.....	176
6.4.1 Optimization for the classical benchmark.....	177
6.4.2 Damage identification for the Guangzhou New TV tower.....	178
6.4.3 Verification with a benchmark structure.....	190
6.5 Experimental validations.....	192
6.6 Conclusions.....	197
References.....	199
CHAPTER 7 SIMULTANEOUS IDENTIFICATION OF STRUCTURAL DAMAGE AND NONLINEAR HYSTERESIS PARAMETERS BY AN EVOLUTIONARY ARTIFICIAL NEURAL NETWORK BASED ON TIME DOMAIN DATA.....	202
7.1 Introduction.....	202
7.2 Nonlinear Hysteretic Model and Parameter Identification.....	207
7.2.1 Improved Dahl hysteresis model.....	207
7.2.2 Nonlinear Model Parameter Identification.....	208
7.3 Methodology.....	210
7.3.1 Artificial Neural Network.....	210
7.3.2 K-means Jaya algorithm.....	212
7.4 Numerical studies.....	216
7.4.1 Training data generation.....	216
7.4.2 Parameters setting for the ANN-K means Jaya for a SDOF system.....	217
7.4.3 Training process and identification results.....	217
7.5 Identification for a MDOF system.....	222
7.5.1 Training data generation.....	224
7.5.2 Parameters setting for the ANN-K means Jaya.....	225
7.5.3 Training process and identification results.....	225
7.6 Conclusions.....	228
References.....	230
CHAPTER 8 CONCLUSIONS AND RECOMMENDATIONS.....	233
8.1 Main findings.....	233
8.2 Recommendations for future study.....	235

LIST OF FIGURES

Figure 2-1 The flowchart of the proposed C-TSA.....	21
Figure 2-2 The diagram of operating the K-means clustering in the proposed C-TSA.....	22
Figure 2-3 The pseudo-code of the proposed C-TSA.....	23
Figure 2-4 The diversity values on several benchmark functions by using TSA and C-TSA.....	25
Figure 2-5 Friedman rank test for the CEC'05 benchmarks.....	28
Figure 2-6 A planar truss structure in the numerical study.....	29
Figure 2-7 The evolutionary process of Scenario 1.....	30
Figure 2-8 Damage identification results of Scenario 1.....	31
Figure 2-9 The evolutionary process of Scenario 2.....	31
Figure 2-10 Damage identification results of Scenario 2.....	32
Figure 2-11 The identified damage and boundary condition of Scenario 3.....	33
Figure 2-12 The identified results of Scenario 4.....	35
Figure 2-13 Damage identification results of Scenario 4.....	36
Figure 2-14 The evolutionary processes of the identified damage in Scenario 5.....	37
Figure 2-15 Damage identification results in Scenario 5.....	38
Figure 2-16 Damage identification results in Scenario 6.....	38
Figure 2-17 A steel frame model in the laboratory.....	39
Figure 2-18 Introduced damages in the frame model.....	42
Figure 2-19 Identified damage results in the experimental tests.....	42
Figure 3-1 The flowchart of the TSA.....	56
Figure 3-2 The pseudo code of I-TSA.....	61
Figure 3-3 The iteration process of two benchmark functions.....	63
Figure 3-4 A nonlinear SDOF system with hysteretic effect.....	71
Figure 3-5 The evolution process of the objective function in Case 1 (without noise).....	72
Figure 3-6 The evolution process of the nonlinear parameter identification in Case 1 with 10% noise effect by using I-TSA.....	73
Figure 3-7 The true and identified hysteresis loop in Case 1 (with noise).....	73
Figure 3-8 The simulated measured response and calculated response with identified parameters in Case 2.....	74
Figure 3-9 The colony distributions at the initial time instant and 381 seconds.....	75
Figure 3-10 A seven-storey shear building with nonlinear hysteretic effect.....	77
Figure 3-11 The hysteresis loop of a bilinear model in the shear building.....	78
Figure 3-12 Comparison of the evolutionary processes in objective function values by using different approaches in Case 4.....	79
Figure 3-13 The identified system parameters by using responses with 5% noise.....	80
Figure 3-14 The identified system parameters by using responses with 10% noise.....	80
Figure 3-15 Comparison of the evolutionary processes in objective function values by using input data.....	82
Figure 4-1 The pseudo-code of operating the K-means clustering.....	104
Figure 4-2 The flowchart of the proposed I-Jaya algorithm.....	105
Figure 4-3 The convergence line for the classical benchmarks based on Jaya and the proposed I-Jaya algorithm.....	106
Figure 4-4 The model of the truss structure.....	107
Figure 4-5 The convergence processes of the identified damage index α_{10} with different objective	

functions.....	108
Figure 4-6 Damage identification results of Case 1 in the numerical study.....	108
Figure 4-7 Damage identification results of Case 2 in the numerical study.....	110
Figure 4-8 The iteration processes of the damage indices in damaged elements in Case 3.....	112
Figure 4-9 Damage identification results in Case 3 based on different inputs.....	112
Figure 4-10 Damage identification results of Case 4 with different optimization methods.....	113
Figure 4-11 The evolutionary process of the objective values.....	115
Figure 4-12 The evolutionary process of the identified damage index in the damaged element based on I-Jaya.....	116
Figure 4-13 Identification results for Case 5: (a) I-Jaya; (b) Jaya; (c) MDE; (d) DPSO.....	116
Figure 4-14 The experimental testing model.....	118
Figure 4-15 Dimensions (unit: mm) of the experimental concrete bridge model and the placed sensor location.....	118
Figure 4-16 The finite element model of the experimental bridge model.....	119
Figure 4-17 The measured and updated frequencies in the experimental studies.....	119
Figure 4-18 Observed cracks in the web elements of the concrete bridge model.....	120
Figure 4-19 Damage identification results of the testing bridge model in the experimental study with limited input data.....	121
Figure 5-1 The architecture of the proposed DBN.....	135
Figure 5-2 Demonstration of the functions used for approximating the L_0 norm, the Log-sum norm and the proposed Arc-tan norm with a hyper-parameter $\varepsilon = 0.01$	137
Figure 5-3 The building structure model used in numerical study.....	141
Figure 5-4 The activation probability of hidden units for the trained samples.....	141
Figure 5-5 The activation times of each hidden unit on training samples.....	143
Figure 5-6 Identification results for a single minor damage case by using.....	145
Figure 5-7 Identification results for a case with two minor damages.....	146
Figure 5-8 Identification results for a minor damage and a large damage case.....	146
Figure 5-9 Identification results for the case with three damages.....	147
Figure 5-10 A eight-storey steel frame model.....	148
Figure 5-11 Measured and analytical frequencies of the laboratory model before and after updating.....	149
Figure 5-12 The fitting results on all the elements of the trained and observed samples based on the proposed Act-tan DBN.....	150
Figure 5-13 Identification results based on the Arc-tan DBN.....	152
Figure 5-14 The iteration processes of all damage indices based on swarm intelligence methods.....	153
Figure 5-15 Identification results by using three swarm intelligence methods and the Arc-tan DBN.....	154
Figure 6-1 The flowchart of the proposed Hybrid C-Jaya-TSA.....	172
Figure 6-2 Damaged and undamaged regions of the hth element.....	175
Figure 6-3 Situation of uncertain α_h	176
Figure 6-4 The Guangzhou New TV tower and its simplified finite element model.....	181
Figure 6-5 The evolutionary processes of the objective function values by using different methods.....	182
Figure 6-6 Identification results for the single damage case without uncertainties.....	183
Figure 6-7 The evolutionary process of the damage indices based on the proposed method.....	184
Figure 6-8 Identification result for the multiple damage case without uncertainties.....	185
Figure 6-9 The evolutionary process of the damage index at the 37th element by the proposed.....	185

method with uncertain modal data.....	186
Figure 6-10 PoDE and DMI value of each element in the single damage case with uncertain modal data.....	187
Figure 6-11 PoDE and DMI values for the multiple damages case with uncertain modal data.....	188
Figure 6-12 The evolutionary processes of the upper bound, lower bound and middle value of the damage index of the 9th element in the minor structural damage case.....	189
Figure 6-13 Identification results for the minor structural damage case.....	189
Figure 6-14 A truss model.....	191
Figure 6-15 Identification results of the truss model; (a) Case 1, (b) Case 2.....	191
Figure 6-16 The cantilever beam structure and the locations of accelerometers.....	192
Figure 6-17 The first six measured mode shapes of the undamaged model.....	194
Figure 6-18 The lower bound, upper bound, DMI values of each element for Case 1 in the experimental verification.....	195
Figure 6-19 PoDE and DMI values of each element for Case 2 in the experimental verification...	196
Figure 6-20 PoDE and DMI values of each element for Case 3 in the experimental verification...	197
Figure 7-1 The improved Dahl nonlinear hysteretic model.....	208
Figure 7-2 The improved Dahl model in SDOF system.....	209
Figure 7-3 Three-layer neural network architecture.....	210
Figure 7-4 Flowchart of using the proposed ANN-K means Jaya for nonlinear model identification.....	215
Figure 7-5 Nonlinear system behavior with an improved Dahl hysteresis model.....	216
Figure 7-6 Iterations of objective function values for the network training process of the nonlinear SDOF system.....	219
Figure 7-7 Fitted results on all parameters in the model vector based on the training dataset by using the proposed method.....	219
Figure 7-8 Regression results on all parameters in the modal vector based on the testing data set by using the proposed method.....	220
Figure 7-9 Evolutionary processes of objective function values based on state-of-the-art swarm intelligence methods.....	222
Figure 7-10 Five-storey benchmark building model.....	224
Figure 7-11 The acceleration response of the 1st floor.....	224
Figure 7-12 Iterations of objective function values for the network training process of the nonlinear MDOF system.....	226
Figure 7-13 Regression results on all parameters in the model vector based on the testing dataset by using the proposed method.....	227

LIST OF TABLES

Table 2-1 Classical mathematical benchmarks.....	24
Table 2-2 Statistical results obtained by TSA and C-TSA on classical benchmarks.....	25
Table 2-3 Performance results of various algorithms on CEC05 functions: 10D.....	27
Table 2-4 Performance results of various algorithms on CEC05 functions: 30D.....	27
Table 2-5 Performance results of various algorithms on CEC05 functions: 50D.....	28
Table 2-6 Damage identification results in numerical simulation.....	33
Table 2-7 Damage identification results in numerical simulation with modelling uncertainty.....	38
Table 2-8 Measured and analytical natural frequencies of the experimental model before and after updating.....	40
Table 3-1 Classical benchmark functions employed for tests.....	62
Table 3-2 Classical benchmark tests results.....	63
Table 3-3 Performance of I-TSA on CEC14 Functions---Results of 10D.....	68
Table 3-4 Performance of I-TSA on CEC14 Functions---Results of 30D.....	69
Table 3-5 Performance of I-TSA on CEC14 Functions---Results of 50D.....	70
Table 3-6 Identified results for a SDOF system with different nonlinear models.....	75
Table 3-7 Comparisons between I-TSA and other heuristic algorithms on the identification of a nonlinear seven-storey shear building.....	79
Table 3-8 Identification of a nonlinear seven-storey shear building under different noise.....	81
Table 3-9 Comparisons on using different input data for nonlinear system identification by using I-TSA.....	83
Table 4-1 Statistic results obtained by the Jaya and I-Jaya algorithms for the classical benchmarks.....	106
Table 4-2 Damage identification results in the numerical studies.....	109
Table 4-3 Used modal data in different scenarios and regularization parameters for Case 3.....	111
Table 4-4 Identified damage extents for Case 3 in the numerical studies.....	111
Table 4-5 Reported typical cracks in the tested structure (Li et al.,2018).....	121
Table 6-1 Classical mathematical benchmarks.....	178
Table 6-2 Statistical results obtained by TSA, C-TSA, Jaya and C-Jaya-TSA on benchmarks.....	178
Table 6-3 Identification results of single damage case without uncertainties.....	182
Table 6-4 Identification results of multiple damage case without uncertainties.....	184
Table 6-5 Damage locations and extents for the experimental verifications.....	193
Table 6-6 The first six natural frequencies of the initial and updated finite element models.....	194
Table 6-7 Measured modal data of the beam under the undamaged and damaged states.....	194
Table 7-1 Identified results for a nonlinear SDOF system with improved Dahl model.....	222
Table 7-2 Structural properties of the five-storey benchmark building model (Yu et al., 2018).....	223
Table 7-3 Identified results for a nonlinear MDOF system with improved Dahl model.....	228

CHAPTER 1 INTRODUCTION

1.1 Background

With the development of human society, the quantity and scale of all kinds of structural engineering facilities across the world have soared up in recent decades. However, no matter how well these large-scale structural projects are designed and constructed, during their service periods, due to a variety of reasons, under operating and extreme loading conditions such as earthquake and impact loading, almost all in-service structures will accumulate certain level of condition deteriorations owing to fatigue and corrosion damage, and damage caused by extreme loadings, which lead to strength and stiffness of the structures to decrease. If these deteriorations are not detected timely, great threats could be posed since some damages may cause catastrophic destruction to structures, especially to some bridge structures. In 1994, the 48-meter-long concrete slab in the middle of the Shengshui bridge in South Korea collapsed, leading to 33 deaths and 17 injures. In 1967, the silver bridge on the Ohio river toppled down, resulting in 50 cars falling into the river and 46 deaths. Furthermore, at least 8 people were killed and 79 were injured when the I-35W Mississippi river bridge suddenly collapsed in 2007. Therefore, it is of great significance to assess the condition of structures timely and accurately, which is beneficial to avoid the occurrence of accidents and minimize the maintenance costs (Farrar & Worden, 2007; Fan & Qiao, 2011).

Structural Health Monitoring (SHM) system can be used to record the dynamic responses of a structure in real time. Through a series of sensing, acquisition, communication and some other means as well as the assistance of data processing system, it could automatically monitor the operation status of a structure, evaluate the structural safety, and guide the maintenance work. Damage identification is an important component of a SHM system. When a structure has damage under the earthquake excitation, some nonlinear hysteresis phenomena could be observed (Berger & Krousgrill, 2002; Katsaras et al., 2008; Wang et al., 2016). Several mathematical models, such as Bouc-Wen and bilinear models, have been widely used to describe the nonlinear hysteretic behavior of civil engineering structures (Belbas & Mayergoyz, 2002; Ikhoulane & Rodellar, 2005; Lu et al., 2017). Identifying these nonlinear parameters is important and necessary for understanding the damage process and vibration behavior of structures. Therefore, the vibration based structural identification has attracted attentions in

recent decades and many different types of methodologies have been developed (Salawu, 1997; Sirca Jr & Adeli, 2012). These methods could be classified into two types, depending on the fact that structural identification is conducted in the frequency-domain or in the time-domain.

The former one denotes that the identification is performed by utilizing structural modal information, such as the natural frequencies, mode shapes, flexibility, damping ratios and some other frequency domain data. Chinchalkar (2001) localized the damage positions of a beam structure through the alteration of the first three natural frequencies, and also compared the localized effects with difference damage extents. Xia and Hao (2003) developed a statistical method using the change of frequencies to conduct the damage identification and also investigated the effect of noise on identification accuracy. Lu and Law (2007) proposed a response sensitivity method for structural damage identification and this method was also extended into the vehicle bridge coupling system (Lu & Liu, 2011) and the crack identification (Lu et al., 2013). Chang and Shi (2010) applied the wavelet multiresolution analysis method to conduct identification for the Bouc-Wen system. Besides, the power spectral approach (Zheng et al., 2015; Pedram et al., 2017; Guo et al., 2020), the flexible matrix (Yang & Sun, 2011; Zhang et al., 2013), the modal strain energy (Yan et al., 2012; Fan & Qiao., 2012; Ramesh & Rao, 2018) have been respectively applied to conduct structural identification in the frequency-domain.

Furthermore, the structural identification methods in the time-domain have been developed in recent years. Hu et al. (2017) used the homotopy continuous algorithm to identify cracks in beam structures, in which the acceleration data were employed to formulate the objective function. An enhanced sensitivity method, in which a trust-region constraint was used to enhance the convergence performance of the original sensitivity method, was widely used to perform structural damage identification and nonlinear hysteretic parameter identification (Lu & Wang, 2016; Lu et al. 2017). The extended/unscented Kalman filter (Corigliano & Mariani, 2004; Yang et al., 2006; Wu & Smyth, 2008; Xie & Feng, 2012), the Volterra series method (Shiki et al., 2017; Villani & Silva, 2019), are the commonly used methods to handle the nonlinear parameter identification in the time-domain.

Although the abovementioned methods can basically achieve satisfactory identification, challenges still exist. Most of the above methods require a good initial condition and good gradient information. Furthermore, difficulties may increase when using these methods to

perform structural identification for large-scale structures when limited measurement data are available. Therefore, a large number of intelligence methods have been widely used to conduct structural identification. These intelligence methods are usually categorised into two types, namely, the swarm intelligence techniques and the neural network based methods. The swarm intelligence techniques are essentially the optimization algorithms, which are usually based on machine learning techniques to learn and search through data instead of explicit formulations (Ding et al., 2019). Compared with some traditional optimization methods, the distinguished feature of the swarm intelligence techniques is that they do not require good initial values and gradient information. By defining the objective function relevant to structures, it is easy and convenient to employ the swarm intelligence methods for structural identification. Therefore, the Genetic algorithm (GA) (Guo & Li, 2009, 2012), the Particle Swarm Optimizer (PSO) (Kang et al., 2012; Chen & Yu, 2018), the Artificial Fish Swarm (AFS) algorithm (Yu & Li, 2014), the Artificial Bee Colony (ABC) (Sun et al., 2013, 2014; Ding et al., 2016, 2017, 2018), and the Most Valuable Player (MVP) algorithm (Jahangiri et al., 2019) are respectively adopted to settle the linear and nonlinear structural identification. In terms of the neural network based methods, it is actually an important branch of the artificial intelligence technique. The main principle of this type of methods is to simulate a human's brain. Through a large number of samples, the trained network would equip the 'inference ability' and therefore could do some identification or prediction work. Usually, the input of the network is some vibration data while the corresponding output is the vector of structural parameters to be identified. Many researchers have also applied the neural network to perform structural identification. Zapico et al. (2003) utilized the Back-propagation (BP) network to conduct the model updating of a real bridge. Jiang et al. (2006) integrated the probabilistic neural network with the data fusion technique to perform damage identification. Furthermore, the Feed-forward Neural Network (FNN) (Truong et al. 2020), the Radial-Basis Function (RBF) network (Morfidis & Kostinakis, 2019), the Convolutional Neural Network (CNN) (Modarres et al., 2018; Xu et al., 2019; Khodabandehlou et al., 2019) are gradually becoming major choices when dealing with the structural identification by using the neural network methods.

Apart from the abovementioned intelligence methods, two novel swarm intelligence methods, named as the Tree Seeds Algorithm (TSA) (Kiran, 2015) and the Jaya algorithm (Rao, 2016) are employed to perform complex optimization. TSA employs the trees propagation as

the algorithmic framework while the Jaya is inspired by the conception that feasible solutions always approach the best-so-far solution and avoid the worst one. Compared with the traditional swarm intelligence methods, such as the GA, PSO and the ABC, etc, these two algorithms have simpler algorithmic structures and are successfully applied to solve different engineering problems (EI-Fergany & Hasnien, 2018; Zhou et al., 2018; Rao & Saroj, 2017; Xu et al., 2019; Jian & Weng, 2020; Warid, 2020). Regarding the neural network methods, the Deep Belief Networks (DBN), due to its excellent generalization ability, has been widely used in supervised classification problem (Geng et al. 2018; Rizk et al. 2019), data processing (Zhang et al. 2019), biomedical field (Chen et al. 2018), etc. Considering that these methods have been proven to be successful in tackling some other engineering problems, it is feasible to extend these methods, as well as their further developments and hybridization methods to structural parameter identification, considering some problems linked with the limitations that exist in real applications such as using incomplete and a limited amount of measurements as input and considering uncertainties in identification.

1.2 Research objectives

The primary objective of this study is to develop state-of-the-art intelligence methods for structural identification considering uncertainties. Numerical studies and experimental verifications are conducted to demonstrate the effectiveness and efficiency of the proposed approaches. The detailed tasks include:

1. To develop the clustering based Tree Seeds Algorithm to effectively identify structural linear damages considering modeling errors and measurement noise;
2. To develop the Improved Tree Seeds Algorithm to effectively identify structural nonlinear parameters;
3. To investigate an objective function that is sensitive to structural damage and to develop the Improved Jaya algorithm for structural damage identification, in which only a limited number of measurement data is required;
4. To develop a sparse Deep Belief Neural network for undetermined structural damage identification;
5. To develop a non-probabilistic interval analysis method to quantify structural damage and to develop a hybrid Jaya and Tree Seeds Algorithm for structural damage identification

considering uncertainties;

6. To develop a hybrid clustering Jaya and Artificial Neural Network for simultaneous identification of structural damages and nonlinear parameters considering high-level measurement noise.

1.3 Research outline

This thesis comprises eight chapters. The contents of the seven chapters following this introductory chapter are described below:

In Chapter 2, the procedure of applying the K-means clustering technique to modify the standard TSA is elaborately illustrated. The objective function based on the modal data is formulated for structural damage identification. The finite element modeling errors and noise in the measurement data are considered. The results from numerical and experimental studies are compared with those obtained from several latest swarm intelligence techniques. The identification results demonstrate that the proposed approach is more competitive and robust for structural damage identification.

In Chapter 3, the Tree Seeds Algorithm is used for identifying three nonlinear models, including the Bouc-Wen model and two bilinear models. To enhance the performance of the standard Tree Seeds Algorithm, namely, the Lévy flight search mechanism is introduced for the best-so-far solution in each cycle while a new updating equation is introduced for the remaining solutions. Acceleration responses are used to formulate the objective function. Identification results are compared with those obtained from other swarm intelligence techniques and the enhanced sensitivity methods to demonstrate the improvement and superiority of the proposed approach.

In Chapter 4, the application of the Jaya algorithm in undetermined structural damage identification is investigated. The clustering strategy and a new updating equation are used to modify the Jaya algorithm. The objective function that is sensitive and robust for effective and reliable damage identification, is developed based on sparse regularization and Bayesian inference. Optimization analysis is conducted with the proposed improved Jaya algorithm. Numerical and experimental studies show that the proposed method can yield satisfactory identification results, although a limited quantity of modal data is used and significant measurement noise and modeling errors are assumed.

Chapter 5 demonstrates the application of the deep belief network (DBN) in undetermined structural damage identification with uncertainties. Natural frequencies and mode shapes are extracted as the input to the network, while the output are damage locations and severities of the structure. To enhance the performance of the DBN, the Arc-tan sparse constraint is introduced. The final identification results show that the proposed sparse DBN can be used to identify the damage effectively and its accuracy is better than those obtained by other swarm intelligence techniques.

Chapter 6 mainly illustrates the hybridization of the TSA and the Jaya algorithm. A hybrid algorithm along with the non-probabilistic method is applied to conduct the undetermined damage identification. The alteration of natural frequencies and the MAC (Modal Assurance Criteria) values as well as the $L_{0.5}$ sparse regularization norm are used to formulate the objective function. The simplified Guangzhou New TV Tower model is chosen as the numerical example and a simply-supported beam is selected for experimental verification. Structural identification results demonstrate that the hybrid algorithm with the non-probabilistic method can well quantify damages, even though high-level uncertainties are considered.

In Chapter 7, a hybridization of the K means Jaya and the ANN algorithm is illustrated. Vibration characteristics, as well as the acceleration responses are extracted as the input to the network while the output is the nonlinear parameters and structural damages. To make the standard ANN more powerful, the K means Jaya algorithm is applied to replace the back-propagation algorithm during the training process. Relatively high-level noise is introduced into the acceleration data. Final identification results for a benchmark show that the proposed hybrid approach can effectively identify both the nonlinear parameters and structural damages.

Chapter 8 briefly discusses and concludes the development and application of the above developed methods. Major findings are summarized in this chapter, and discussions and recommendations are provided for the possible future work.

It should be noted that this thesis is compiled by combining the technical papers prepared by the candidate during his PhD study. Therefore, Chapters 2 to 7 can be read independently. Furthermore, to make each technical paper complete, the introduction of the intelligence methods as well as their advantages towards the traditional methodologies are introduced in each independent chapter. These parts thus might be slightly repetitive with each other.

References

- Belbas, S.A., & Mayergoz, I.D. (2002) Optimal control of dynamical systems with Preisach hysteresis. *International Journal of Nonlinear Mechanics*, 37, 1351-1361.
- Berger, E.J., & Krousgrill, C.M. (2002) On friction damping modeling using bilinear hysteresis elements. *ASME Journal of Vibration and Acoustics*, 124, 367-375.
- Chang, C.C., & Shi, Y. (2010) Identification of time-varying hysteretic structures using wavelet multiresolution analysis. *International Journal of Nonlinear Mechanics*, 45, 737-756.
- Chen, Z.P., & Yu, L. (2017) A novel PSO-based algorithm for structural damage detection using Bayesian multi-sample objective function. *Structural Engineering & Mechanics*, 63(6), 825-835.
- Chinchalkar, S. (2001) Determination of crack location in beams using natural frequencies. *Journal of Sound and Vibration*, 247(3), 417-42.
- Corigliano, A., & Mariani, S. (2004) Parameter identification in explicit structural dynamics: performance of the extended Kalman filter. *Computer Methods in Applied Mechanics and Engineering*, 193, 3807-3835.
- Ding, Z.H., Huang, M. & Lu, Z.R. (2016) Structural damage detection using artificial bee colony algorithm with hybrid search strategy. *Swarm and Evolutionary Computation*, 28, 1-13.
- Ding, Z.H., Lu, Z.R., Huang, M. & Liu, J.K. (2017) Improved Artificial Bee Colony Algorithm for crack identification in beam using natural frequencies only. *Inverse Problems in Science & Engineering*, 25(2), 218-238.
- Ding, Z.H., Yao, R.Z., Li, J., & Lu, Z.R. (2018) Structural damage identification based on modified Artificial Bee Colony algorithm using modal data. *Inverse Problems in Science & Engineering*, 26(3), 422-442.
- Ding, Z.H., Li, J., Hao, H., & Lu, Z.R. (2019) Structural damage identification with uncertain modelling errors and measurement noise by clustering based tree seeds algorithm. *Engineering Structures*, 165, 301-314.
- EI-Fergany, A.A., & Hasnien, H.M. (2018) Tree-seed algorithm for solving optimal power flow problem in large-scale power systems incorporating validations and comparisons. *Applied Soft Computing*, 64, 307-316.
- Fan, W., & Qiao, P. (2011) Vibration-based damage identification methods: a review and comparative study. *Structural Health Monitoring*, 10(1), 83-111.
- Fan, W., & Qiao, P.Z. (2012) A strain energy-based damage severity correction factor method for damage identification in plate-type structures. *Mechanical Systems and Signal Processing*, 28, 660-678.
- Farrar, R.C., & Worden, K. (2007) An introduction to structural health monitoring. *Philosophical Transactions of the Royal Society A*, 365, 303-315.
- Geng, Z.Q., Li, Z.K., & Han, Y.M. (2018) A new deep belief network based on RBM with glial chains. *Information Science*, 463, 294-306.
- Guo, H.Y., & Li, Z.L., (2009) A two-stage method to identify structural damage sites and extents by using evidence theory and micro-search genetic algorithm. *Mechanical Systems and Signal Processing*, 23(3), 769-782.
- Guo, H.Y., & Li, Z.L., (2012) Structural damage identification based on Bayesian theory and improved immune genetic algorithm. *Expert Systems with Applications*, 39(7), 6426-6434.
- Guo, J., Jiao J., Fujita, K.H., & Takewaki, I. (2020) A spectrum-driven damage identification by minimum constitutive relation error and sparse regularization. *Mechanical Systems and Signal Processing*, 136, 106496.

- Hu, L., Huang, M. & Lu, Z.R. (2017) Crack identification of beam structures using homotopy continuation algorithm. *Inverse Problems in Science and Engineering*, 25(2), 169-187.
- Ikhoulane, F., & Rodellar, J. (2005) On the hysteretic Bouc-Wen model. Part I: Force limit cycle characterization. *Nonlinear Dynamics*, 42, 63-78.
- Jahangiri, M., Majafgholipour, M.A., Dehghan, S.M., & Hadianfard, M.A. (2019) The efficiency of a novel identification method for structural damage assessment using the vibration data. *Journal of Sound and Vibration*, 458, 1-16.
- Jiang, S.F., Zhang, C.M., & Koh, C.G. (2006) Structural damage detection by integrating data fusion and probabilistic neural network, *Advances in Structural Engineering*, 9, 445-458.
- Jian, X.Z., & Weng, Z.Y. (2020) A logistic chaotic Jaya algorithm for parameters identification of photovoltaic cell and module models. *Optik*, 203, 164041.
- Katsaras, C.P., Panagiotakos, T.B., & Kolias, B. (2008) Restoring capacity of bilinear hysteretic seismic isolation systems. *Earthquake Engineering and Structural Dynamics*, 37, 557-575.
- Kiran, M.S. (2015) TSA: Tree-seed algorithm for continuous optimization. *Expert Systems with Applications*, 42, 6686-6698.
- Khodabandehlou, H., Pekcan, G., & Fadali, M.S. (2019) Vibration-based structural condition assessment using convolution neural networks. *Structural Control & Health Monitoring*, 26(2), e2308.
- Kang, F., Li, J.J., & Xu, Q. (2012) Damage detection based on improved particle swarm optimization using vibration data. *Applied Soft Computing*, 12(8), 2329-2335.
- Lu, X.B., Liu, J.K., & Lu, Z.R. (2013) A two-step approach for crack identification in beam. *Journal of Sound and Vibration*, 332, 282-293.
- Lu, Z.R., & Law, S.S. (2007) Features of dynamic response sensitivity and its application in damage detection. *Journal of Sound and Vibration*, 303(1), 305-329.
- Lu, Z.R., & Liu, J.K. (2011) Identification of both structural damages in bridge deck and vehicular parameters using measured dynamic responses. *Computers & Structures*, 89, 1397-1405.
- Lu, Z.R., Yao, R.Z., Wang, L., & Liu, J.K. (2017) Identification of nonlinear hysteretic parameters by enhanced response sensitivity approach. *International Journal of Non-Linear Mechanics*, 96, 1-11.
- Lu, Z.R., & Wang, L. (2017) An enhanced response sensitivity approach for structural damage identification: Convergence and Performance. *International Journal for Numerical Methods in Engineering*, 111, 1231-1251.
- Modarres, C., Astorga, N., Droguett, E.L., & Meruane, V. (2018) Convolution neural networks for automated damage recognition and damage type identification. *Structural Control & Health monitoring*, 25(10), e2230.
- Morfidis, K., & Kostinakis, K. (2019) Comparative evaluation of MFP and RBF neural networks' ability for instant estimation of r/c buildings' seismic damage level, *Engineering Structures*, 197, 109436.
- Pedram, M., Esfandiari, A., & Khedmati, M.R. (2017) Damage detection by a FE model updating method using power spectral density: Numerical and experimental investigation. *Journal of Sound and Vibration*, 397, 51-76.
- Ramesh, L., & Rao, P.S. (2018) Damage Detection in Structural Beams Using Model Strain Energy Method and Wavelet Transform Approach. *Materialstoday Proceedings*, 5(9), 19565-19575.
- Rao, R.V. (2016) Jaya: a simple and new optimization algorithm for solving constrained and unconstrained optimization problems. *International Journal of Industry Engineering*

Computation, 7, 19-34.

Rao, R.V., & Saroj, A. (2017) A self-adaptive multi-population based Jaya algorithm for engineering optimization. *Swarm and Evolutionary Computation*, 37(4), 1-26.

Rizk, Y., Hajj, N., Mitri, N., & Awad, M. (2019) Deep belief networks and cortical algorithms: A comparative study for supervised classification. *Applied Computing and Informatics*, 15(2), 81-93.

Salawu, S. (1997) Detection of structural damage through changes in frequency: a review. *Engineering Structures*, 19(9), 718-723.

Sirca Jr, G.F., & Adeli, H. (2012) System identification in structural engineering. *Scientia Iranica*, 19(6), 1355-1364.

Shiki, S.B. Silva, S.D., & Todd, M.D. (2017) On the application of discrete-time Volterra series for the damage detection problem in initially nonlinear systems. *Structural Health Monitoring*, 16(1), 62-78.

Sun, H., Lus, H., & Betti, R. (2013) Identification of structural models using a modified Artificial Bee Colony algorithm. *Computers & Structures*, 116, 59-74.

Sun, H., & Betti, R. (2014) Simultaneous identification of structural parameters and dynamic input with incomplete output-only measurement. *Structural Control & Health Monitoring*, 21(6), 868-889.

Truong, T.T., Dinh-Cong, D., Lee, J., & Nguyen-Thoi, T. (2020) An effective deep feed-forward neural network (DFNN) method for damage identification of truss structures using noisy incomplete modal data. *Journal of Building Engineering*, 30, 101244.

Villani, L.G.G., Silva, S.D., & Cunha Jr, A. (2019) Damage detection in uncertain nonlinear systems based on stochastic Volterra series. *Mechanical Systems and Signal Processing*, 125, 288-310.

Wang, Z.C., Xin, Y., & Ren, W.X. (2016) Nonlinear joint model updating in shear type structures based on instantaneous characteristics of dynamic responses. *Mechanical system and signal processing*, 76-77, 476-496.

Warid, W. (2020) Optimal power flow using the AMTPG-Jaya algorithm. *Applied Soft Computing*, 91, 106252.

Wu, M. & Smyth, A. (2008) Real-time parameter estimation for degrading and pinching hysteretic models. *International Journal of Nonlinear Mechanics*, 43, 822-833.

Xia, Y., & Hao, H. (2003) Statistical damage identification of structures with frequency changes. *Journal of Sound and Vibration*, 263(4), 853-870.

Xie, Z.B., & Feng, J.C. (2012) Real-time nonlinear structural system identification via iterated unscented Kalman filter. *Mechanical Systems and Signal Processing*, 28, 309-322.

Xu, S.H., Wang, Y., & Wang, Z. (2019) Parameter estimation of proton exchange membrane fuels cells using eagle strategy based on Jaya algorithm and Nelder-Mead simplex method. *Energy*, 173, 457-467.

Xu, Y., Wei, S.Y., Bao Y.Q., & Li, H. (2019) Automatic seismic damage identification of reinforced concrete columns from images by a regional-based deep convolutional neural network. *Structural Control & Health Monitoring*, 26(3), e2313.

Yan, W.J., Ren, W.X., & Huang, T.L. (2012) Statistic structural damage detection based on the close-form of element modal strain energy sensitivity. *Mechanical Systems and Signal Processing*, 28, 183-194.

Yang, J.N., Lin, S.L., Huang, H.W., & Zhou, L. (2006) An adaptive extended Kalman filter for structural damage identification. *Structural Health Monitoring*, 13(4), 849-867.

Yang, Q.W., & Sun, B.X. (2011) Structural damage identification based on best achievable

flexibility change. *Applied Mathematical Modelling*, 35(10), 5217-5224.

Yu, L., & Li, C. (2014) A global artificial fish swarm algorithm for structural damage detection. *Advances in Structural Engineering*, 17(3), 331-346.

Zapico, J.J., González, M.P., Friswell, M.I., Taylor, C.A., & Crewe, A.J. (2003) Finite element model updating of a small scale bridge. *Journal of Sound and Vibration*, 268, 993–1012.

Zhang, J., Xu, J.C., Guo, S.L., & Wu, Z.S. (2013) Flexibility-based structural damage detection with unknown mass for IASC-ASCE benchmark studies. *Engineering Structures*, 48, 486-496.

Zhang, S., Dong, Q.L., Zhang, W., Huang, H., Zhu, D.J., & Liu, T.M. (2019) Discovering hierarchical common brain networks via multimodal deep belief network. *Medical Image Analysis*, 54, 238-252.

Zheng, Z.D., Lu, Z.R., Chen, W.H., & Liu, J.K. (2015) Structural damage identification based on power spectral density sensitivity analysis of dynamic responses. *Computers & Structures*, 146, 176-184.

Zhou, J.Z., Yang, Z., Xu, Y.H., Liu, H., & Chen, D.Y. (2018) A heuristic T-S fuzzy model for the pumped-storage generator-motor using variable-length Tree-Seeds Algorithm-based competitive agglomeration. *Energies*, 11(4), 944-964.

CHAPTER 2 STRUCTURAL DAMAGE IDENTIFICATION WITH UNCERTAIN MODELLING ERRORS AND MEASUREMENT NOISE BY CLUSTERING BASED TREE SEEDS ALGORITHM

ABSTRACT¹

This paper proposes a novel structural damage identification approach by using the clustering based Tree Seeds Algorithm, termed as C-TSA, taking into account of both the finite element modeling errors and measurement noise. In order to make the standard TSA more powerful and robust, K-means cluster technique is introduced into the standard TSA before starting the seeds search, which is beneficial to enhance the algorithm's global optimization performance. The objective function based on the modal data is formulated for structural damage identification. Numerical studies on benchmark functions and a 61-bar truss structure are conducted to investigate the accuracy and robustness of the proposed approach. The finite element modelling errors and noises in the measurement data are considered. Experimental verifications on a laboratory steel frame structure model is conducted to further validate the accuracy of the proposed approach. The results from the numerical and experimental studies are compared with those obtained from several latest evolutionary algorithms. The identification results demonstrate that the proposed approach is more competitive and robust for structural damage identification even considering the modelling errors and measurement noises.

2.1 Introduction

Structures may accumulate damage inevitably with time, due to the material degradation, fatigue, over loading, excess deformation and vibrations under extreme events, etc. It is essential to inspect structural damages at an early stage to ensure the safety of structures. To achieve this purpose, numerous methods have been developed to conduct structural damage identification (Fan & Qiao, 2011; Ng, 2014; Li et al., 2017). Vibration based damage identification methods by using dynamic responses or vibration characteristics, such as acceleration, natural frequencies, mode shapes, have gained a significant amount of attention.

¹This chapter was published in *Engineering Structures* with the full bibliographic citation as follows: Ding, Z., Li, J., Hao, H., & Lu, Z. (2019). Structural damage identification with uncertain modelling error and measurement noise by clustering based tree seeds algorithm. *Engineering Structures*, 185, 301-314. <https://doi.org/10.1016/j.engstruct.2019.01.118>.

Vibration based structural damage identification can be formulated as an inverse problem. An appropriate objective function related with structural parameters is defined, and mathematical optimization is conducted to identify the best-fit parameters with physical meanings. Swarm intelligence methods (Diptangshu et al. 2018) can be explored to achieve a better optimization performance. Compared with the traditional methods, such as sensitivity based method (Lu & Law, 2007; Lu et al. 2017), one noticeable advantage of the swarm intelligence methods is that a good initial value and gradient information may not be required. Furthermore, swarm intelligence methods are usually based on machine learning techniques to learn and make predictions via data instead of using the explicit formulations. This could not only avoid the shortcomings of many traditional methods, i.e. requiring good initial values, but also enable to perform the identification of relatively large-scale and complex structures. Lin et al. (2018) developed a multi-type sensor placement approach for structural damage identification, in which Genetic Algorithm (GA) is used to find out the optimal sensor placement locations. Numerical studies show that the obtained optimal multi-type sensor placement can effectively avoid redundant sensors. Yi et al. (2012) proposed a modified monkey algorithm (MA) for optimal sensor placement in structural health monitoring, where the Euclidean distance operator and the stochastic perturbation mechanism of the harmony search algorithm were used to enhance the standard algorithm's local and global search ability. Yi et al. (2017) proposed an innovative approach based on hierarchic wolf algorithm (HWA) to optimize tri-axial sensor placement locations. To enhance the standard algorithm's global optimization ability, five local search strategies are employed and the results show that the HWA can effectively determine the global optimal tri-axial sensor placement configuration so that the identified mode shapes have the excellent linear independence. Sun et al. (2013) formulated the model updating of structures as an inverse problem, and solved it by a modified Artificial Bee Colony (ABC) algorithm, in which a nonlinear factor for convergence control was introduced to enhance its performance. Zhu et al. (2017) used the Birds Mating Optimizer (BMO) to conduct the identification of local structural damage, in which a hybrid objective function was introduced by minimizing the discrepancies between the measured and calculated frequencies and correlation function vector of acceleration between damaged and intact structures. Ding et al. (2016) applied the ABC with hybrid search strategies to identify structural damage. Yu and Li (2014) utilized a global Artificial Fish Swarm (AFS) algorithm

for structural damage detection, in which the information of the best-so-far solution was added into other solutions' updating equation. Numerical and experimental results show that the modified AFS can acquire better identification results. Dinh-Cong et al. (2017) compared the capacities of using Cuckoo Search (CS) algorithm, Differential Evolutionary (DE) algorithm and Jaya algorithm to handle with structural damage identification problem and concluded the Jaya is the best choice among the mentioned three algorithms. It has been demonstrated that the Improved Nelder-Mead Particle Swarm Optimizer (INM-PSO) (Chen & Yu, 2017) and the Ant Lion Optimizer (ALO) algorithm (Chen et al., 2018) performed well in structural damage identification. In addition, some other intelligence optimization techniques, such as the non-probabilistic Artificial Neural Network (ANN) (Padil et al. 2017) and the fuzzy clustering method (Yu et al. 2013), have also been introduced for structural damage identification.

Although these state-of-the-art methods have achieved relatively satisfactory identified results, challenges still exist. For example, in the Refs. (Sun et al. 2013; Zhu et al., 2017; Ding et al., 2016; Yu & Li, 2014; Dinh-Cong et al., 2017; Chen & Yu, 2017; Chen et al., 2018) the modelling errors, which inevitably exist in the real structures, may not be considered thoroughly. The identification accuracy in boundary conditions may also need to be improved. The considered noise is a bit low and the structure used for investigating is relatively simple. For solving these deficiencies, it is necessary to investigate and develop more efficient and robust algorithms for structural damage identification considering modelling errors and significant measurement noise.

Lately, a novel swarm intelligence approach, named as Tree Seeds Algorithm (TSA), has been proposed (Kiran, 2015). It employs the trees propagation as a framework, which has been proven to equip a more competitive optimization capacity compared with GA, PSO and DE algorithm. TSA has already been applied to solve optimal power flow problem (EI-Fergany & Hasnien, 2018) and estimate parameters for pumped-storage generator motor (Zhou et al. 2018). In this study, it will be extended to the field of structural damage identification based on vibration data with modelling errors (Xia et al. 2018) and measurement noises.

TSA plays an important role in identifying local damages. If the TSA does not have a good robustness, the identified results will be significantly affected by the measurement noise. When TSA is trapped in the local minimal during the optimization process, the identification accuracy will be enormously weakened. Generally speaking, for the swarm intelligence

methods, exploration and exploitation are two essential cornerstones that lead an evolutionary process toward optimization and/or convergence. These two search modes are very necessary for search processes when utilizing any meta-heuristic algorithm. Exploration is defined as visiting the whole new regions of a search space, while exploitation is defined as visiting those regions of a search space within the neighborhood of previously visited points (Liu et al. 2013). This is a paradox behind these two search modes. If an algorithm focuses on the exploration, it would affect the convergence performance. However if an algorithm concentrates on the exploitation, it may be trapped in the local minimal. Therefore, it is essential for swarm intelligence methods to achieve a balanced capacity between the exploration and exploitation through some certain ways, i.e. by colony diversity maintaining, diversity control, diversity learning etc (Črepinšek et al. 2013). To achieve this purpose, the K-means clustering mechanism is applied and integrated into the standard TSA before performing the individuals' updating. This new approach is therefore termed as C-TSA. This mechanism serves as a crossover operator that can effectively utilize the colony information and achieve the purpose of balancing the exploration and exploitation (Imrani et al, 2000; Damavandi & Safavi-Naeini, 2005).

This paper proposes a novel structural damage identification approach by using C-TSA, taking into account of the uncertainties in the modelling and noise in the measurements. An objective function is established by minimizing the discrepancies between the measured natural frequencies and Model Assurance Criteria (MAC) values, and the calculated ones from the finite element model. K-means clustering technique is applied to improve the performance of the standard TSA. The performance of the proposed approach is investigated and tested on Benchmark test functions and compared with several latest methods. Numerical studies on classical benchmarks as well as CEC benchmarks are conducted to compare the global optimization ability between the C-TSA and other state-of-the-art swarm intelligence methods. Numerical studies on a 61-bar truss structure with and without uncertainties are conducted to verify the accuracy and effectiveness of the proposed approach. Errors in the finite element modelling and noise in the measurements are considered. Experimental validations on a laboratory steel frame structure are conducted to demonstrate the performance of the proposed approach.

2.2 Mathematical Model and Problem Formulation

2.2.1 Structural damage model

Alterations in the structural stiffness or other parameters will lead to change in the vibration properties of structures, and therefore damage identification in structures can be conducted based on this fact by using vibration data. The modal characteristics of an undamaged structure without considering the damping can be obtained by analyzing the eigenvalue problem

$$(\mathbf{K} - \omega_i^2 \mathbf{M}) \cdot \Phi_i = 0 \quad (2.1)$$

where \mathbf{K} and \mathbf{M} are the global stiffness and mass matrices, ω_i represents the i th natural frequency and Φ_i denotes the corresponding mode shape.

The mass change of a structure could be inspected visually (Zhu et al., 2017). In this study, structural damage is assumed only related to the stiffness reduction, i.e. in the elastic module of material. Structural damage can be expressed through a scalar stiffness reduction variable for each element $\alpha_i (i=1,2,\dots,nel)$ with the value between 0 and 1. This damage model can be described as

$$\mathbf{K}_d = \sum_{i=1}^{nel} (1 - \alpha_i) \cdot \mathbf{k}_{ei} \quad (2.2)$$

where \mathbf{k}_{ei} represents the i th elemental stiffness matrix under the intact state; nel denotes the total number of elements in a structure; and \mathbf{K}_d denotes the structural stiffness matrix under the damaged state; α_i is the elemental stiffness reduction to be identified. It shall be noted that $\alpha_i = 1$ means that this element is completely damaged, and $\alpha_i = 0$ means that the element is intact. It should be noted that this damage model can also be used to describe the damage in the boundary stiffness. When simultaneously identifying the elemental stiffness parameters and the boundary stiffness, both the elemental stiffness and boundary stiffness parameters are included in the optimization.

2.2.2 Objective function for damage identification

Condition monitoring of structures can be conducted based on the changes in the vibration modal characteristics, i.e. natural frequencies and mode shapes, which are related with system

parameters, i.e. stiffness. This is the foundation that the modal information are used for structural damage identification. The objective function based on both natural frequencies and MAC can be expressed as (Ding et al., 2016)

$$f(\alpha_i) = \sum_{i=1}^{NF} W_{\omega_i} \Delta \omega_i^2 + \sum_{i=1}^{NM} W_{\Phi_i} \cdot (1 - MAC_i) \quad (2.3)$$

in which

$$\Delta \omega_i = \frac{|\omega_i^c - \omega_i^m|}{\omega_i^m} \quad (2.4)$$

$$MAC_i = \frac{(\Phi_i^{cT} \cdot \Phi_i^m)^2}{\|\Phi_i^c\|^2 \|\Phi_i^m\|^2} \quad (2.5)$$

where W_{ω_i} and W_{Φ_i} are the weight factors for the i th natural frequency and MAC , respectively; It should be noted that the weight factors W_{ω_i} and W_{Φ_i} in this paper are defined as 1, which is the same as those used in Ref. (Ding et al., 2016). This indicates the equal importance of measured frequencies and mode shapes. ω_i^c and Φ_i^c are the i th calculated natural frequencies and mode shape from the finite element model, respectively; ω_i^m and Φ_i^m are the corresponding measured frequency and mode shape. The calculated modal data are obtained based on the stiffness reduction parameters $\alpha = [\alpha_1, \alpha_1, \dots, \alpha_{nel}]$ with the finite element analysis. If the estimated damage parameters match with the true values perfectly, the objective function value will achieve the minimum and be 0. The identified stiffness parameter vector α will reflect the structural damage. Generally speaking, structural damage identification is treated as an ill-posed problem with the searching parameters region that may have multiple local optimal points (Sun et al., 2013). In this case, the traditional optimization techniques could be stuck with the local minimum, which may result in the poor identification results. Therefore, just as mentioned above, it is necessary to investigate and develop robust and powerful algorithms, which could deal with the complex identification problems well.

2.3 Methodology

2.3.1 Standard TSA

TSA is a kind of swarm intelligence method, which is developed based on the natural phenomenon of trees propagation. In reality, trees usually spread to other places through their

seeds. These seeds will grow into the new trees over time. In the algorithm, these places for trees and seeds can be considered as searching spaces for the optimization problems. The specific locations of trees and seeds are considered as feasible solutions. In fact, the core of this algorithm is searching the seeds since it will update the new feasible solutions in this phase, which provides two search equations for this process as described below

$$S_{i,j} = T_{i,j} + \gamma_{i,j} \times (B_j - T_{r,j}) \quad (2.6)$$

$$S_{i,j} = T_{i,j} + \alpha_{i,j} \times (T_{i,j} - T_{r,j}) \quad (2.7)$$

where $S_{i,j}$ is the j th dimension of the i th seed that would be generated by the i th tree, $T_{i,j}$ is the j th dimension of the i th tree, B_j is the j th dimension of best-so-far solution in the colony, $T_{r,j}$ is the j th dimension of the r th solution randomly selected from the colony size; the coefficient $\alpha_{i,j}$ is a uniform random number, $\gamma_{i,j}$ is the scaling factor arbitrarily generated in the range of $[-1,1]$, and i and j are different indices. Based on the search equation as shown in Eq. (2.6), a new candidate is produced by removing the old solution towards the best-so-far solution in the colony, which enhances the exploitation ability of the algorithm to some extent. However, from Eq. (2.7), a new candidate is created by removing the old solution towards a randomly chosen one in population. The randomly selected solution could be a good one, which also has the same likelihood to be a bad one. Hence Eq. (2.7) has a strong exploration ability (Gao et al., 2015).

Afterwards, the key point is to create a new solution. This process is controlled by a parameter called search tendency (ST) in the range of $[0,1]$. Selecting a better equation between Eqs. (2.6) and (2.7) to update the solution relies on the comparison between a random number and ST. If the random number is larger than ST, Eq. (2.6) is chosen as the update equation. Otherwise Eq. (2.7) will be selected. Therefore, for every tree seed, a higher ST value makes it have a higher chance of exploitation whereas a lower ST value renders it possess likely for exploration. This is the reason why the exploration and exploitation capacities of the TSA is controlled by ST parameters.

When applying TSA, the initial possible solutions for the optimization problem are produced as

$$T_{i,j} = L_{j,\min} + r_{i,j} \times (H_{j,\max} - L_{j,\min}) \quad (2.8)$$

where $L_{j,\min}$ and $H_{j,\max}$ are the lower and upper bounds of the search space respectively, $r_{i,j}$ is a random number produced for every dimension and location, which is in the range of $[0,1]$. The seeds number can be determined approximately as 10% and 25% of the colony size. The exact number of the seed generation is random in TSA.

2.3.2 The proposed approach

Clustering-based TSA, termed as C-TSA in this paper, is proposed and the motivation behind this development is described in this section. As mentioned in Section 2.2.2, the objective function is difficult to be dealt with by using the traditional optimization algorithms due to its multimodal feature. To balance TSA's global and local search capacity through making full use of the colony information and render the proposed algorithm equipped with a more powerful optimization ability, an improved framework is developed based on clustering technique. For the original TSA, the updating operation as shown in Eqs. (2.6) and (2.7) is performed between randomly selected individuals from the entire colony, which allows any two individuals have a chance to create the new generation. The Greedy Selection Scheme (Ding et al., 2016) is also applied for the old solution and the new one. Therefore, the problem is that when dealing with a multimodal problem, it may suffer the slow-convergence problem or even trap in the local minimal at the final stage. This is because in the final iteration for the multimodal problem, the whole colony has a large likelihood to distribute around the different optimal regions. In this case, the distance in the parameter space between different optima is large, which leads to the slow convergence rate due to the relatively large magnitude of the vector generated from individuals with different optimal regions (Gao et al., 2014). Besides, the mutation mechanism in the original TSA cannot guarantee the full use of the colony information, since only two individuals are adopted to make further exploration in every cycle. To tackle these two challenges, that is, to enhance the convergence performance and to increase the utilization rate of the population information, K-means clustering is applied before updating the solutions.

2.3.2.1 Overview of the K-means clustering

Clustering is an important research topic in the field of machine learning, which aims to categorize a massive amount of data into several groups according to their patterns. It can be used to re-organize the database into a number of groups or clusters so that those data within a cluster have similar features. Clustering technique is a significant tool to discover the inherent patterns in any given database (Cai et al., 2011). The clustering centers can represent the whole clusters, since these centers' formations are the results of combining with the information of other individuals in this colony. Therefore, it is beneficial to utilize the information of the colony efficiently and enhance the algorithm's convergence performance (Gao et al., 2014), by introducing the K-means clustering mechanism.

The K-means clustering belongs to an unsupervised learning algorithm. Considering a set of n data points, i.e. $\mathbf{X} = \{X_1, X_2, \dots, X_n\}$ in the space \tilde{U} and an integer K , the K-means clustering is to determine a series of K cluster centers $C = \{c_1, c_2, \dots, c_k\}$ to minimize the sum of squared errors as $SSE = \sum_{X \in \mathbf{X}} \min_{i=1..k} \|X - c_i\|^2$. It usually consists of three steps, namely, selecting the initial clusters centers, assigning other data to these centers and re-estimating the new cluster centers (Hussain & Haris, 2019).

The specific procedure of the K-means clustering (Cai et al., 2011) is described as

Step 1: Select k initial cluster centers c_1, c_2, \dots, c_k randomly from the n points $\{X_1, X_2, \dots, X_n\}$

Step 2: Assign the point X_i , ($i=1, 2, \dots, n$) to a cluster $C_j, j=1, 2, \dots, k$, only if the distance satisfies, $\|X_i - c_j\| \leq \|X_i - c_p\|$ the point X_i belongs to the cluster with the center point c_j . Similarly, other clusters can be defined through the comparison with the distance generated from every center point.

Step 3: The criteria of determining which cluster the point belongs to is based on the distance between all the centers. In this study, the Euclidean distance is employed to calculate the distance, which is given as below

$$d(X_i, X_j) = \|X_i - X_j\| = \sqrt{\sum_{p=1}^D (X_{i,p} - X_{j,p})^2} \quad (2.9)$$

where X_i and X_j represent any two individuals from the colony and D denotes the dimension number of the individual.

Step 4: Calculate new cluster centers c'_1, c'_2, \dots, c'_k based on the following equation

$$c'_i = \frac{1}{n_i} \sum_{X_j \in c_i} X_j, i = 1, 2, \dots, k \quad (2.10)$$

where n_i is the number of elements within the cluster c_i .

Step 5: If the center points for the whole colony remain the same, it means the algorithm terminates and c_1, c_2, \dots, c_k are selected as the final center points. Otherwise, update each c_i with c'_i ($i = 1, 2, \dots, k$), and go back to Step 2 for the next iteration.

2.3.2.2 C-TSA

Recently, some researchers have employed the K-means clustering technique to improve the performance of swarm intelligence algorithms. For example, Imrani et al. (2000) integrated the sharing mechanism and a fuzzy clustering algorithm to modify the GA. It is found that the improved algorithm was good at dealing with the multiple model functions. Damavandi and Safavi-Naeini (2005) utilized a density clustering mechanism to preserve the diversity of the colony and the results showed that the hybrid method has greatly enhanced the robustness and convergence performance of the algorithm for tackling the complex multi-modal circuit optimization problem.

For the application in civil engineering, structural damage identification taking into account of uncertain modelling errors and measurement noise is an ill-posed and multi-modal complex optimization problem (Sun et al., 2013; Zhu et al., 2017; Ding et al., 2016; Yu & Li, 2014; Du et al., 2017; Chen & Yu, 2017; Chen et al., 2018). Besides, due to the simple mutation mechanism of the original TSA, it may suffer not making the full use of the colony information. Therefore, the K-means clustering technique is introduced in the proposed approach before updating the solutions, which is essential to balance the exploration and exploitation of TSA and accelerate the convergence speed. Figure 2-1 illustrates the framework of the proposed C-TSA. From observing its algorithmic structure, it is clear that C-TSA equips the feature of simplicity and easy-operation. On the other hand, C-TSA also possesses the

deconstruction mechanism (Hussain & Haris, 2019). When canceling the clustering operation, C-TSA will become the standard TSA. Therefore, it is convenient to investigate whether the K-means clustering mechanism improves the performance of TSA or not.

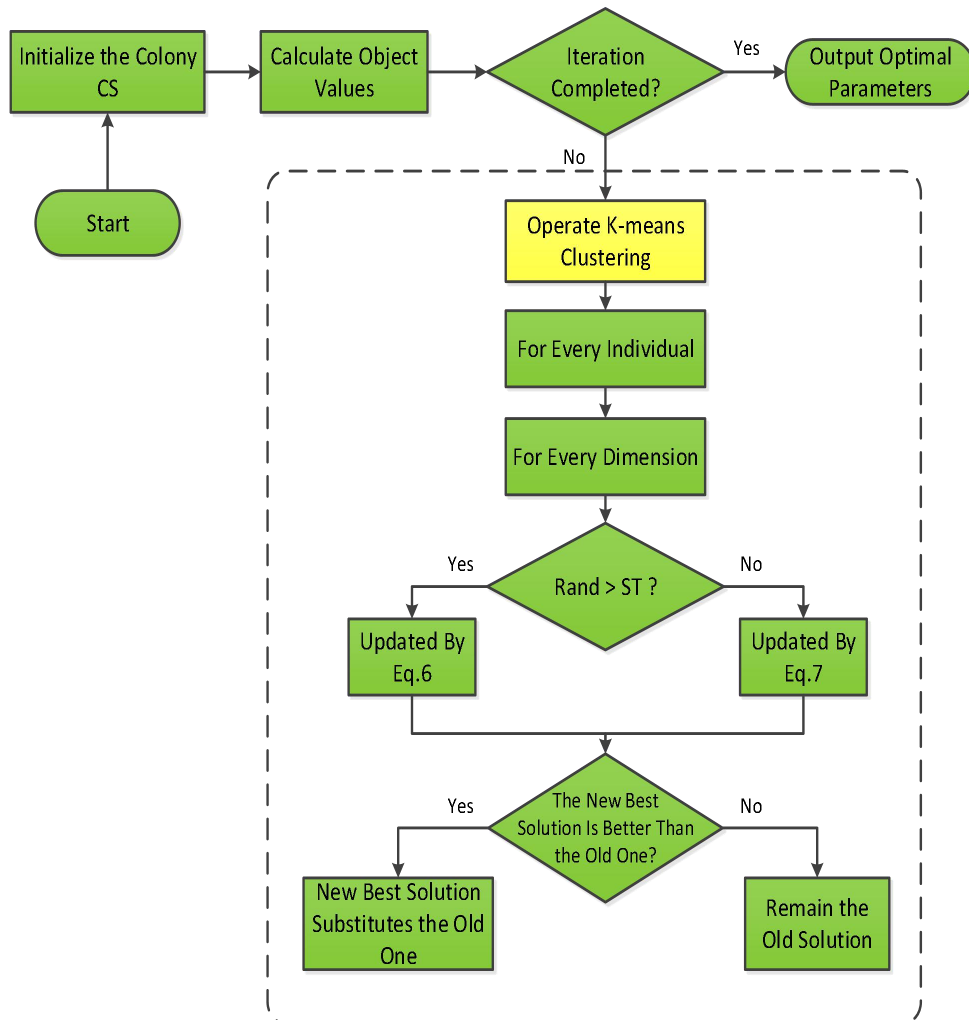


Figure 2-1 The flowchart of the proposed C-TSA.

As shown in Figure 2-1, the K-means clustering is performed before the individuals' updating. To present the process of the K-means clustering in a straightforward way, Figure 2-2 displays its diagram. From Figure 2-2, it is assumed that $K \in [2, \sqrt{CS}]$ clusters will be randomly generated and K individuals are selected from the colony as the initial clustering points. Afterwards, other individuals will be assigned to these cluster centers according to their Euclidean distances, which can be calculated by Eq. (2-9). Then the K new cluster centers are calculated by using Eq. (2-10). According to Ref. (Cai et al., 2011), the one step clustering is

simple, linear time complex but effective. Therefore, in the proposed C-TSA, one step clustering is also adopted. K individuals are randomly chosen from the colony, and these individuals with the new clustering centers are combined together as a sample P . The objective function values of the individuals in the sample P are calculated, and the best K individuals will be put into the colony again, which enables the elite preservation (Cai et al., 2011). When the conduction of the K-means clustering is finished, the seeds search is commenced. Figure 2-3 shows the pseudo-code of the proposed C-TSA. It is observed that the proposed C-TSA keeps a simple structure, which is easy to implement with a deconstruction mechanism and other advantages of the original TSA.

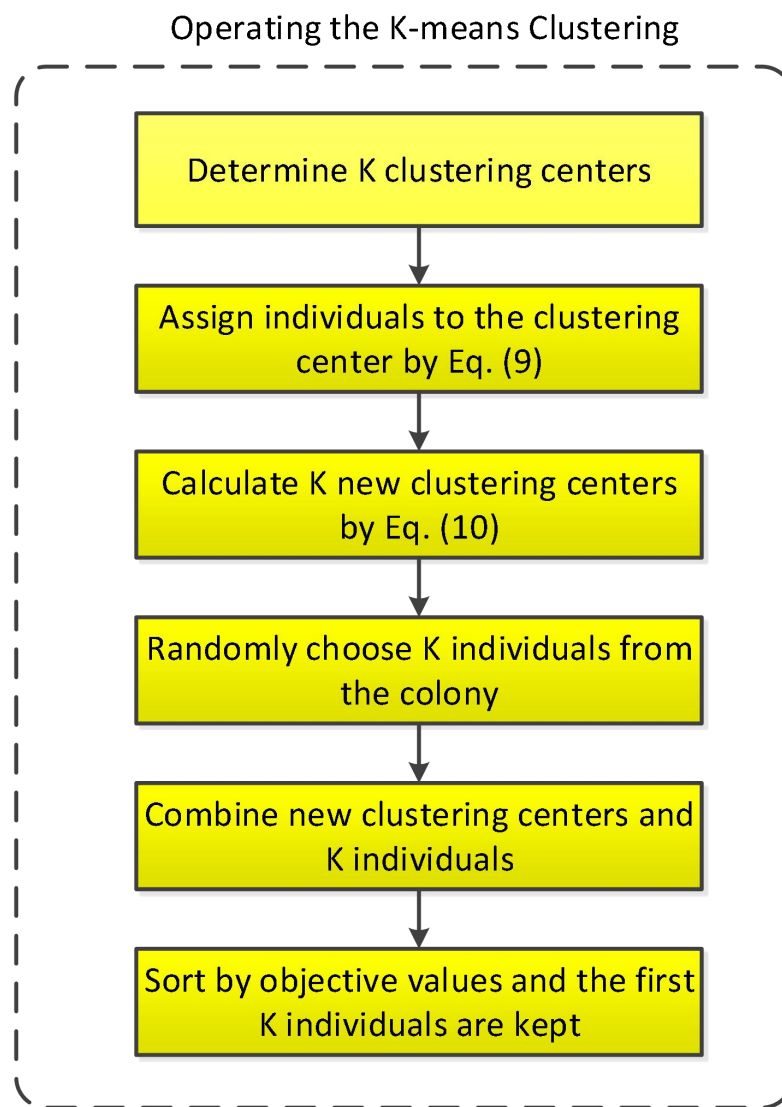


Figure 2-2 The diagram of operating the K-means clustering in the proposed C-TSA.

Step 1. Initialization of the proposed algorithm

Set the number of population size CS , parameter ST

Set the dimension of the problem D

Decide the termination condition

Generate CS random tree location with D dimension on search space using Eq. (2.8)

Evaluate the tree location using objective function based on Eq. (2.3)

Select the best-so-far solution **B**

Step 2. Operation of the K-means clustering**Step 3. Searching with seeds**

For all individuals in the colony

 Decide the number of seeds produced for this individual.

For all dimensions

If (rand<ST)

 Update this dimension using Eq. (2.6)

Else

 Update this dimension using Eq. (2.7)

End If

End For

End For

Select the best seed and compare it with the individual. If the seed location is better than the individual's, the seed replace this individual.

End For

Step 4. Selection of Best Solution

Select the best solution in every cycle. If the new best solution is better than the previous best one, the new best solution substitutes for the previous best solution.

Step 5 Check the termination condition and feedback

If the termination condition is not met, go to Step 2. Report the best solution.

Figure 2-3 The pseudo-code of the proposed C-TSA.

2.4 Numerical Simulations

In this section, the accuracy and performance of the proposed approach will be demonstrated with numerical simulations and compared with several existing state-of-the-art algorithms. Six mathematical benchmark functions in the literature (Ding et al., 2017), which are list in Table 2-1, are employed for conducting colony diversity analysis between the TSA and C-TSA. After that, C-TSA will be utilized to optimize CEC'05 benchmarks (Sunganthan et al., 2005) to compare its capacity with several state-of-the-art algorithms. The effectiveness and performance of using C-TSA for identifying the structure damage are also demonstrated with numerical studies on a truss structure.

Table 2-1 Classical mathematical benchmarks.

Number	Name	Definition	Range
F1	Sphere	$f_1(x) = \sum_{i=1}^D x_i^2$	[-100,100]
F2	Griewank	$f_2(x) = 1/4000 \sum_{i=1}^D x_i^2 - \prod_{i=1}^D \cos x_i / \sqrt{i} + 1$	[-600,600]
F3	Ackley	$f_3(x) = 20 + e - 20 \exp(-0.2 \sqrt{(1/D) \sum_{i=1}^D x_i^2}) + \exp((1/D) \sum_{i=1}^D \cos 2\pi x_i)$	[-32,32]
F4	Rastrigin	$f_4(x) = \sum_{i=1}^D [x_i - 10 \cos(2\pi x_i) + 10]$	[-5.12,5.12]
F5	Rosenbrock	$f_5(x) = \sum_{i=1}^{\frac{D}{2}} (100(x_{2i} - x_{2i-1}^2)^2 + (1 - x_{2i-1})^2)$	[-30,30]
F6	Schaffer	$f_6(x) = 0.5 + \sin^2(\sqrt{\sum_{i=1}^D x_i^2 - 0.5}) / (1 + 0.001(\sum_{i=1}^D x_i^2))^2$	[-100,100]

2.4.1 Colony diversity analysis between TSA and C-TSA on classical benchmark

In order to compare the performance of the proposed approach with the TSA, a series of classical mathematical benchmarks, as list in Table 2-1, are adopted for calculation. According to the literature (Kiran, 2015; EI-Abd, 2017), the colony size and the search tendency are set as $CS = 25$ and $ST = 0.4$ respectively. For C-TSA, one step clustering is conducted in each iteration. All benchmark tests are conducted on dimensions $D = 30$ for a maximum of $10000 \times D$. Each situation repeats 50 times, best results are highlighted in bold in Table 2-2.

To quantify the exploration and exploitation ability of these two algorithms, the standard deviation (std.) of individuals in each cycle is employed to illustrate the improvement of convergence performance. The colony diversity is measured by

$$Diversity = \sum_{i=1}^D \sqrt{\frac{1}{CS} \sum_{j=1}^{CS} (S_{ji} - \bar{S}_j)^2} \quad (2.11)$$

where \bar{S}_j is the mean position of the colony.

Table 2-2 Statistical results obtained by TSA and C-TSA on classical benchmarks.

Function	C-TSA				TSA			
	Objective values		Final diversity value		Objective values		Final diversity value	
	Mean	std	Mean	std	Mean	std	Mean	std
F1	4.47E-150	2.45E-149	1.03E-75	5.63E-75	1.28E-21	3.93E-21	1.84E-19	6.02E-19
F2	0.00E+00	0.00E+00	1.84E-07	8.63E-08	5.91E-03	7.54E-03	1.69E-05	2.42E-05
F3	1.78E-15	2.91E-15	4.67E-15	6.72E-15	3.33E-02	1.82E-01	6.38E-09	3.49E-08
F4	1.89E-15	1.04E-14	2.61E-08	1.91E-08	3.57E+01	3.60E+01	4.03E+00	9.89E+00
F5	2.70E+00	5.73E+00	3.70E-03	7.81E-03	2.68E+01	2.72E+01	2.68E-02	3.80E-02
F6	3.12E-04	9.54E-04	2.68E-07	2.85E-07	1.93E-02	7.97E-02	7.19E+00	2.07E+00

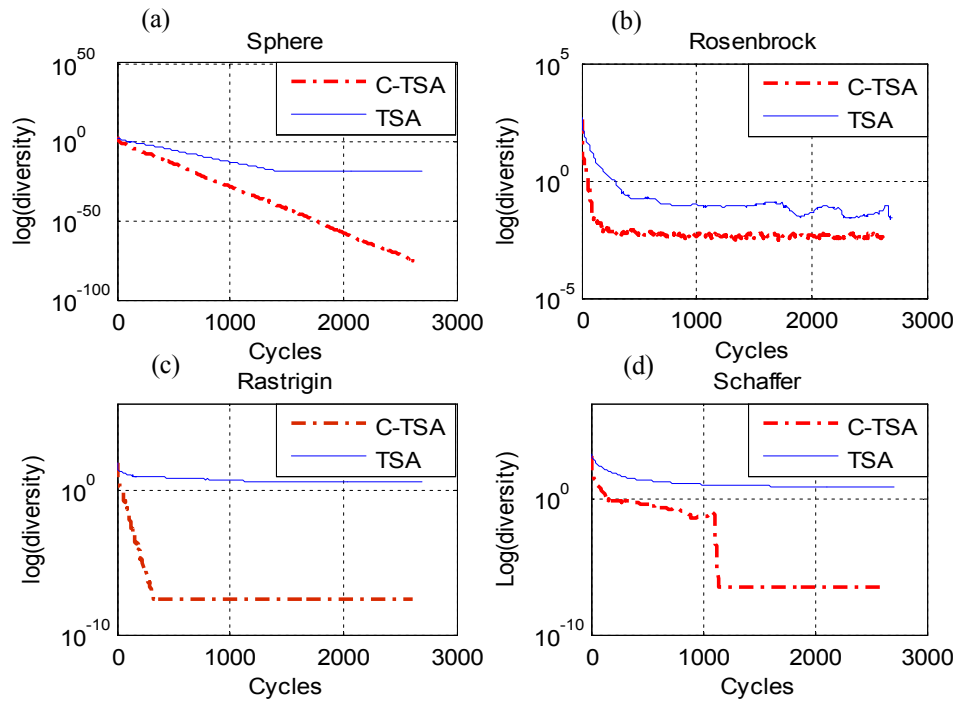


Figure 2-4 The diversity values on several benchmark functions by using TSA and C-TSA:

(a) Sphere; (b) Rosenbrock; (c) Rastrigin; (d) Schaffer.

Figure 2-4 has shown the colony diversity values of several test benchmarks from TSA and C-TSA. From the diversity values on several benchmark functions as shown in Figure 4, it can be observed that during the early iterations (before 500 cycles), the diversity values are relatively large, which denotes that the individuals scatter in the search space and focus on the exploration search. With iterations, especially after 2000 cycles, the diversity values remain at very low values until the end of iterations. This indicates that the individuals gradually gather together and concentrate on the exploitation search. Therefore, the diversity values could be

used as a criterion to quantify the algorithms' exploration and exploitation ability to some extent. Furthermore, as shown in Table 2-2 and Figure 2-4, it is clearly observed that in the later iterations (after 1000 iterations), the diversity values of the proposed C-TSA are significantly smaller, indicating that C-TSA achieves a better balance between the exploration and exploitation and has a quicker convergence rate. This is owing to the operation of the K-means clustering in the developed C-TSA.

2.4.2 Comparison with state-of-the-art algorithms on CEC benchmarks

In this section, several state-of-the-art algorithms including Global-best Artificial Bee Colony (GABC) (Zhu & Kwong, 2010), 2011 version of Standard Particle Swarm Optimizer (SPSO) (Zambrano-Bigiarini et al., 2011), the Improved Global-best Harmony Search (IGHS) (EI-Abd, 2013) and Global Brain Storm Optimization (GBSO) (EI-Abd, 2017) are employed to make comparison with the proposed C-TSA on CEC'05. The parameters setting for the C-TSA are the same as those in the section 4.1. All benchmark tests are conducted on dimensions $D = 10$, $D = 30$ and $D = 50$ for a maximum of $10000 \times D$ function evaluations. In Tables 2-3 to 2-5, best results are highlighted in bold. It is noted that the results of other algorithms are extracted from a previous study (EI-Abd, 2017). It is clear that the C-TSA can obtain the best identified results in most cases.

To assess these algorithms' global optimization capacities in a more rigorous and persuasive framework, the non-parametric Friedman test with a 5% confidence interval (EI-Abd, 2017) is employed as a criterion to assess these algorithms. The Friedman test is used to detect significant differences between the performances of different algorithms (Derrac et al., 2011). Mean errors of objective function values acquired by the mentioned algorithms are used for the test. This method first finds the rank of algorithms for the individual problems and then calculates the average rank to obtain the final rank of the each algorithm for the considered problems. Figure 2-5 shows the mean rank of the algorithms for the CEC'05 benchmarks. With calculations by the Friedman test, C-TSA has acquired the best rank among these algorithms, with the lowest score of 2.45. On the other hand, the p-value for the test is only $3.6 \cdot 10^{-4}$, which is far less than the 5% confidence interval. This confirms the outstanding performance of C-TSA for the CEC'05 over the considered algorithms, and lays foundations for the following identifications (EI-Abd, 2017; Derrac et al., 2011).

Table 2-3 Performance results of various algorithms on CEC05 functions: 10D.

Benchmark Function	GABC		SPSO		IGHS		GBSO		C-TSA	
	Mean	std.	Mean	std.	Mean	std.	Mean	std.	Mean	std.
1	0.00E+00	0.00E+00	0.00E+00	0.00E+00	8.18E-09	2.21E-09	0.00E+00	0.00E+00	0.00E+00	0.00E+00
2	6.71E+00	6.30E+00	9.47E-15	2.15E-14	1.13E-08	3.67E-09	9.39E-11	2.42E-10	7.03E-23	2.72E-22
3	6.23E+05	3.08E+05	3.85E+04	2.91E+04	7.54E+04	5.81E+04	4.97E+04	3.81E+04	5.91E+04	4.81E+04
4	6.64E+02	4.14E+02	1.71E-14	2.65E-14	1.34E-08	4.39E-09	2.97E-09	8.06E-09	2.75E-21	1.05E-20
5	2.03E+00	1.56E+00	0.00E+00	0.00E+00	2.75E-03	1.00E-03	1.42E-06	1.00E-06	1.50E-08	3.68E-08
6	7.63E-02	9.26E-02	4.11E+01	9.71E+01	3.19E+01	5.40E+01	6.21E+00	2.60E+00	2.90E-02	4.43E-02
7	7.95E-02	5.09E-02	9.46E-02	1.10E-01	1.64E-01	7.69E-02	8.46E-02	5.13E-02	1.15E-01	6.41E-02
9	0.00E+00	0.00E+00	5.24E+00	2.10E+00	1.63E-06	3.50E-07	0.00E+00	0.00E+00	0.00E+00	0.00E+00
10	1.35E+01	3.25E+00	4.57E+00	2.09E+00	9.68E+00	3.98E+00	4.61E+00	2.34E+00	9.88E+00	2.83E+00
11	5.23E+00	9.11E-01	3.27E+00	1.65E+00	9.92E-01	9.34E-01	2.57E-01	5.35E-01	0.00E+00	0.00E+00
12	1.96E+02	1.05E+02	2.00E+04	9.50E+03	1.78E+02	4.63E+02	5.44E+02	7.14E+02	1.92E+00	6.73E-01
13	1.36E-01	1.18E-01	7.93E-01	1.68E-01	4.39E-01	1.19E-01	4.84E-01	1.12E-01	7.21E-01	8.32E-02
14	3.21E+00	1.75E-01	2.30E+00	5.10E-01	3.28E+00	6.37E-01	1.94E+00	5.35E-01	3.04E+00	3.56E-01

Table 2-4 Performance results of various algorithms on CEC05 functions: 30D.

Benchmark Function	GABC		SPSO		IGHS		GBSO		C-TSA	
	Mean	std.	Mean	std.	Mean	std.	Mean	std.	Mean	std.
1	6.82E-14	2.31E-14	5.49E-14	1.04E-14	8.87E-08	1.25E-08	5.49E-14	1.04E-14	1.73E-27	1.88E-27
2	1.38E+03	8.51E+02	3.35E-13	1.07E-13	6.51E-07	1.68E-07	3.15E-04	2.10E+04	1.08E-04	3.40E-04
3	6.22E+06	3.21E+06	2.80E+05	1.37E+05	4.78E+05	2.36E+05	1.06E+06	3.61E+05	1.16E+05	4.96E+04
4	3.29E+04	5.04E+03	5.03E+01	3.27E+01	9.59E-03	1.89E-02	1.83E-01	1.66E-01	3.26E-05	1.03E-04
5	7.62E+03	1.46E+03	4.73E+03	7.93E+02	1.18E+03	5.32E+02	8.90E+01	7.94E+01	5.19E+02	2.68E+01
6	1.53E+01	2.67E+01	5.04E+02	1.06E+03	1.61E+02	1.71E+02	8.80E+01	1.47E+02	7.06E-02	1.19E-01
7	2.77E-02	1.84E-02	2.94E-02	2.43E-02	8.70E-03	1.06E-02	7.72E-03	7.91E-03	2.71E-02	7.43E-13
9	5.68E-14	2.57E-29	5.77E+01	2.71E+01	1.69E-05	1.70E-06	3.60E-01	6.30E-01	9.95E-01	2.25E-15
10	1.70E+02	2.45E+01	5.52E+01	1.31E+01	4.98E+01	1.41E+01	2.52E+01	7.85E+00	6.76E+01	2.56E-14
11	2.69E+01	1.50E+00	2.66E+01	4.48E+00	5.60E+00	2.25E+00	1.35E+00	1.74E+00	8.28E+00	2.32E+00
12	6.54E+03	2.60E+03	1.04E+06	1.51E+05	1.59E+03	1.74E+03	4.44E+03	5.34E+03	1.63E+03	8.75E+01
13	8.07E-01	1.56E-01	5.98E+00	3.30E+00	1.23E+00	2.43E-01	1.73E+00	2.73E-01	3.81E+00	8.53E-01
14	1.27E+01	2.36E-01	1.20E+01	6.68E-01	1.19E+01	5.73E-01	1.01E+01	8.59E-01	1.32E+01	2.83E-01

Table 2-5 Performance results of various algorithms on CEC05 functions: 50D.

Benchmark Function	GABC		SPSO		IGHS		GBSO		C-TSA	
	Mean	std.	Mean	std.	Mean	std.	Mean	std.	Mean	std.
1	1.63E-13	2.73E-14	9.47E-14	2.73E-14	2.74E-07	2.87E-08	1.00E-13	2.45E-14	1.55E-27	8.11E-28
2	1.39E+04	6.08E+03	1.38E-11	1.64E-11	9.63E-06	1.92E-06	1.07E-01	4.10E-02	1.15E-01	3.15E-01
3	1.18E+07	3.69E+06	4.33E+05	1.44E+05	9.07E+05	3.72E+05	2.06E+06	7.49E+05	2.94E+05	1.26E+05
4	9.28E+04	1.10E+04	3.92E+03	1.02E+03	3.18E+03	2.03E+03	8.46E+01	4.50E+01	3.02E-02	8.81E-02
5	2.13E+04	1.97E+03	1.24E+04	1.87E+03	3.29E+03	7.67E+02	6.61E+02	3.23E+02	1.11E+02	1.12E+01
6	3.32E+01	4.35E+01	6.77E+02	1.73E+03	1.45E+02	1.70E+02	1.44E+03	2.42E+03	3.99E+00	1.53E-03
7	1.02E-02	1.66E-02	1.12E-02	1.48E-02	1.07E-03	2.80E-03	1.48E-03	3.01E-03	6.20E-03	4.65E-09
9	1.04E-13	2.15E-14	1.31E+02	2.78E+01	5.12E-05	4.33E-06	2.85E+00	1.19E+00	1.42E-15	3.43E-15
10	5.25E+02	6.61E+01	1.52E+02	3.02E+01	8.94E+01	2.13E+01	5.13E+01	1.24E+01	2.06E+02	4.15E+01
11	5.33E+01	2.90E+00	5.72E+01	4.13E+00	1.20E+01	3.35E+00	3.56E+00	2.43E+00	5.90E+00	3.58E-01
12	2.96E+04	1.15E+04	5.16E+06	7.99E+05	1.22E+04	1.04E+04	1.79E+04	1.37E+04	7.83E+04	7.58E+03
13	1.45E+00	2.45E-01	1.38E+01	8.27E+00	2.01E+00	2.83E-01	3.19E+00	5.29E-01	7.71E+00	6.29E-01
14	2.24E+01	2.46E-01	2.16E+01	6.81E-01	2.11E+01	7.82E-01	2.11E+01	9.18E-01	2.30E+01	2.00E-01

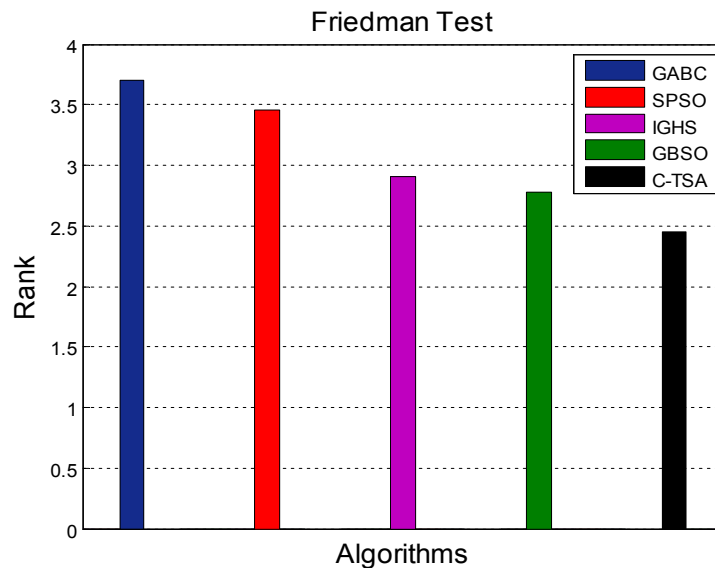


Figure 2-5 Friedman rank test for the CEC'05 benchmarks.

2.4.3 Numerical simulation on a truss structure

The above studies on benchmark functions demonstrate the improved accuracy and efficiency of the proposed algorithm compared with several latest methods and the standard

TSA. In this section, numerical studies on a planar truss structure (Ding et al., 2016) are conducted. The model of the simply supported truss structure and the locations of placed sensors are shown in Figure 2-6. The structure has 26 nodes and 61 elements. The Young's modulus, mass density and Poisson's ratio of the truss structure member are respectively $E = 70\text{Gpa}$, $\rho = 2.7 \times 10^3 \text{ kg/m}^3$ and $\mu = 0.33$. The boundary supports are modeled with three springs with a large stiffness of $2 \times 10^{10} \text{ N/m}$. The first six nature frequencies of the structure are obtained as 16.48 Hz, 54.96 Hz, 73.75 Hz, 132.15 Hz, 193.06 Hz and 222.25 Hz, respectively, based on the finite element model analysis. In terms of parameters setting for TSA and C-TSA, the colony size, the search tendency and the maximum iteration number are set as $CS = 50$, $ST = 0.4$ and 200, respectively. The first six frequencies and mode shapes are used for the identification. For every damage scenario, the identification is repeated 20 times with a different initialized random seed to obtain the statistical results. To investigate the effect of measurement noise on damage identification, natural frequencies and mode shapes are contaminated by adding a uniformly distributed noise (Dinh-Cong et al., 2017)

$$\omega_i^{noise} = (1 + (2 \cdot rand - 1) \cdot \eta_i) \cdot \omega_i , \quad \Phi_{ji}^{noise} = (1 + (2 \cdot rand - 1) \cdot \eta_j) \cdot \Phi_{ji} \quad (2.12)$$

where ω_i^{noise} and Φ_{ji}^{noise} are the i th natural frequency and the j th component of the i th mode shape vector polluted by noise; η_i and η_j are the noise levels in the frequency and mode shape, respectively.

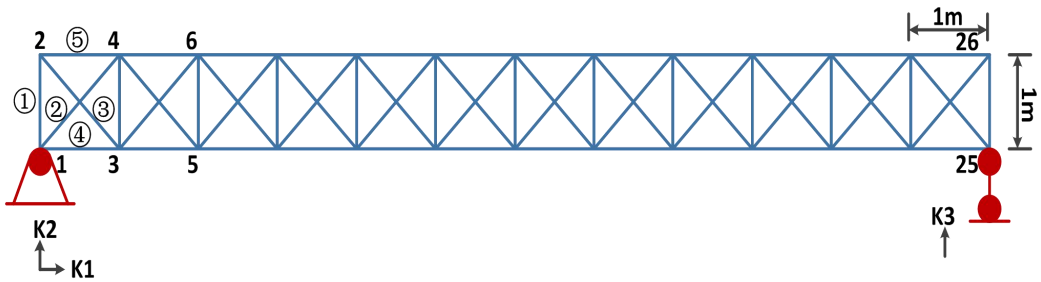


Figure 2-6 A planar truss structure in the numerical study.

2.4.4 Damage identification without modeling uncertainty

2.4.4.1 Scenario 1

The first damage scenario is assumed with 15% stiffness reduction introduced in the 3rd

element, that is, $\alpha_3 = 0.15$. The performance of the proposed approach is compared with those of ABC, quicker Artificial Bee Colony (QABC) algorithm, Artificial Bee Colony algorithm with hybrid search strategy (ABCHSS) and TSA. Figure 2-7(a) shows the evolutionary process of the objective function values by using TSA and C-TSA for structural damage identification. It can be seen that C-TSA has a quicker convergence speed and achieve a very small objective function value. When 1% noise is added into the frequencies and 10% noise is added into the mode shapes (Ding et al., 2016), Figure 2-7(b) shows the iterations of the identified damage index of the 3rd element. It is clearly observed that the iteration process by using C-TSA converges faster, indicating the proposed improvement based on K-means clustering technique enhances the performance of the original TSA.

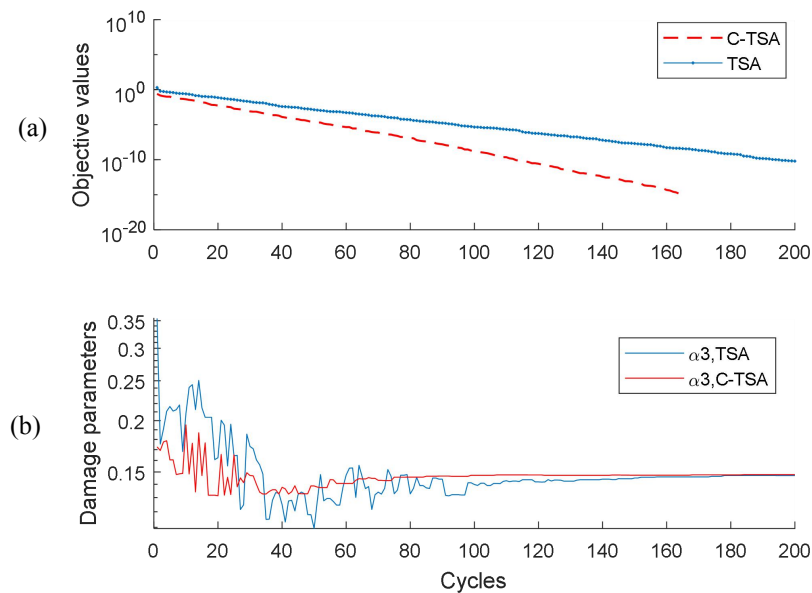


Figure 2-7 The evolutionary process of Scenario 1:

(a) Objective function (without noise); (b) Damage parameters (with noise).

The final structural damage identification results are shown in Figure 2-8. It is noted that less false identifications are observed from C-TSA, when the noise is included in the measurement. To compare with other methods, the statistical results of the identified damages without noise and with noise in the 3rd element are shown in Table 2-6. It can be found that ABCHSS, TSA and C-TSA can identify the damage correctly for the noise free situation. Generally TSA and C-TSA provide the better results than ABCHSS, QABC and ABC. When

noise is included in the measurement data, C-TSA outputs the best identification results with the maximum relative error of 0.09%, better than 0.3% and 1% from TSA and ABCHSS.

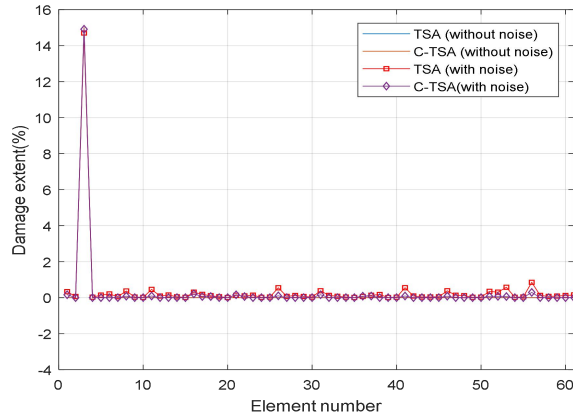


Figure 2-8 Damage identification results of Scenario 1.

2.4.4.2 Scenario 2

Three damages in the 5th, 15th and 25th elements with 10% stiffness reduction each are defined in Scenario 2. The same procedure is followed to identify the damage. Figure 2-9 shows the evolutionary process of the objective function and identified damage extents in Scenario 2. It is also observed that C-TSA converges quickly, which means that C-TSA is more competitive and efficient.

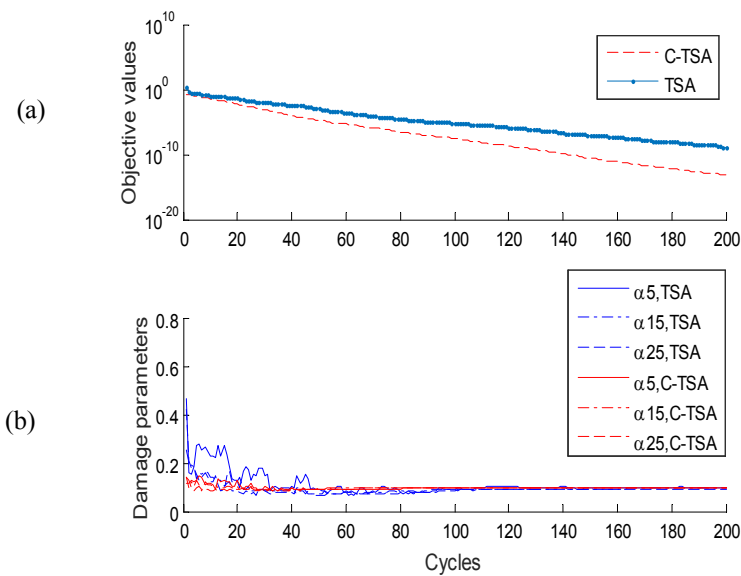


Figure 2-9 The evolutionary process of Scenario 2: (a) Objective function (without noise);
(b) Damage parameters (with noise).

Figure 2-10 shows the damage identification results in the truss structure. The simulated damages can be identified accurately, even when the noise is included. C-TSA outputs a less number of false identifications than TSA, indicating that the performance of the proposed approach is good and robust. The identified damage extents without noise and with noise are listed in Table 2-6. It can be seen that C-TSA can accurately identify the multiple damage with very small standard deviations, and outperforms the other three existing methods.

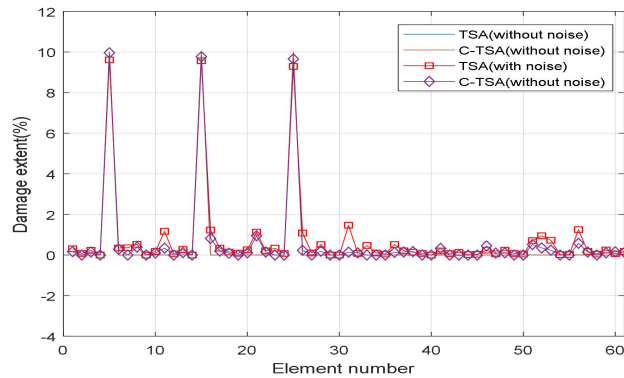


Figure 2-10 Damage identification results of Scenario 2.

2.4.4.3 Scenario 3

Scenario 3 is defined to investigate the effect of the boundary conditions on the structural identification. Damage is introduced into the 3rd element with a 15% stiffness reduction. The boundary stiffness K_3 as shown in Figure 2-6 is underestimated as 92.5% of the true value, which means that a 7.5% reduction is simulated in this boundary stiffness. Both the structural elemental stiffness parameters and boundary stiffness parameters are included in the identification. As mentioned in Section 2.1, damage in the boundary stiffness can also be identified by introducing three extra stiffness parameters into the optimization process. The final identified results of this scenario are shown in Figure 2-11 and Table 2-6. It can be seen that C-TSA can identify the element damage and boundary stiffness reduction accurately, even considering the noise effect. The results demonstrate that the accuracy and robustness of the proposed algorithm are better than QABC, ABCHSS and TSA.

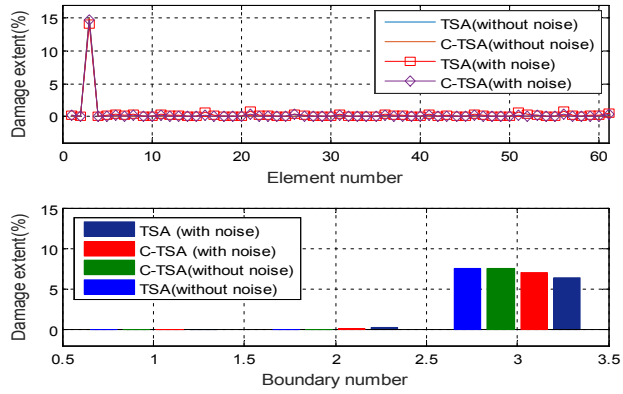


Figure 2-11 The identified damage and boundary condition of Scenario 3:

(a) Damage in elements; (b) Damage in boundary conditions.

Table 2-6 Damage identification results in numerical simulation.

Scenarios		Methods							
		QABC		ABCHSS		TSA		C-TSA	
		mean	std.	mean	std.	Mean	std.	mean	std.
Scenario 1									
α_3 (15%)	Without noise	13.98%	0.02	15%	0	15%	0	15%	0
	With noise	7.92%	0.06	13.89%	0.004	14.70%	0.004	14.91%	7.10E-04
Scenario 2									
α_5 (10%)	Without noise	6.76%	0.04	9.54%	0.009	10.00%	1.07E-04	10.00%	0
	With noise	6.84%	0.04	9.30%	0.02	9.61%	0.008	9.96%	0.005
α_{15} (10%)	Without noise	6.19%	0.04	9.45%	0.006	10.00%	6.81E-05	10.00%	1.30E-06
	With noise	5.97%	0.05	9.10%	0.008	9.57%	0.003	9.77%	8.57E-04
α_{25} (10%)	Without noise	4.11%	0.04	9.53%	0.006	9.95%	1.25E-04	10.00%	1.10E-06
	With noise	4.02%	0.03	8.43%	0.01	9.29%	0.03	9.66%	0.002
Scenario 3									
α_3 (15%)	Without noise	11.98%	0.05	14.95%	0.0003	15.00%	5.92E-05	15.00%	5.62E-07
	With noise	8.89%	0.04	12.75%	0.01	14.12%	0.004	14.68%	0.002
α_{k3} (7.5%)	Without noise	9.26%	0.22	7.21%	0.0124	7.49%	1.58E-04	7.50%	7.43E-07
	With noise	24.28%	0.22	11.47%	0.07	6.41%	0.006	7.00%	0.003

2.4.5 Damage identification with modeling uncertainty

In the above mentioned simulations, the modelling uncertainty is not considered and the

first six mode shapes of all the degrees of freedom (DOFs) are used for identification. However, uncertainties inevitably exist in the finite element modelling which affects the subsequent structural damage identification. Furthermore it is very difficult to acquire the modal data of those rotational DOFs, implying only incomplete modal data are available for damage identification analysis. To ensure that the conducted numerical simulations are more realistic with uncertainties and incomplete measurements, 1% uncertainty with Gaussian distributions (Xia et al., 2002; Pathirage et al. 2018) is introduced into all the elemental stiffness parameters to simulate the modelling errors. The first six natural frequencies and the mode shapes in the vertical direction of all the nodes are used for identification. It has been demonstrated in the last section that TSA and C-TSA provide the better results than other methods, therefore only these two algorithms are used in this section for damage identification.

When the modelling uncertainty is introduced, the damage can be determined from the statistical distributions of the stiffness parameters under the undamaged and damaged states. For example, if the stiffness parameter of the i th element follows a Gaussian distribution with a mean value of $E(1-\alpha_i)$ and a standard deviation of $\sigma(1-\alpha_i)$. The probability of damage existence is defined as that of $1-\alpha_i$ not within 95% confidence interval $\Omega(1-\alpha_i, 0.95)$ of the healthy stiffness parameter. Therefore, the probability of damage existence of the i th element can be calculated as

$$\begin{aligned} p_d^i &= 1 - \text{prob}(x_{\alpha_i} \in \Omega(1-\alpha_i, 0.95)) = 1 - \text{prob}(L_{\Omega} \leq x_{\alpha_i} < \infty) \\ &= \text{prob}(-\infty < x_{\alpha_i} \leq L_{\Omega}) \end{aligned} \quad (2.13)$$

where L_{Ω} is the lower bound of the interval $\Omega(1-\alpha_i, 0.95)$. When the confidence level is set to 95%, the lower bound can be decided by $L_{\Omega} = E(1-\alpha_i) - 1.645\sigma(1-\alpha_i)$, which indicates that there is a probability of 95% that the healthy stiffness parameter falls in the range of $[E(1-\alpha_i) - 1.645\sigma(1-\alpha_i), \infty]$ (Xia et al., 2002).

2.4.5.1 Scenario 4

15% stiffness reduction is assumed in the 3rd element in this scenario. The same damage identification procedure is followed, and only the above mentioned modeling uncertainty is considered. Figure 2-12(a) shows the evolutionary process of the objective function values. It is

demonstrated again that C-TSA converges quicker. Probability Density Functions (PDFs) of the ‘health’ stiffness parameters and the damaged stiffness parameters with the maximum error alarms in the intact elements obtained from TSA and C-TSA are shown in Figures 2-12(b) and (c), respectively. The lower bound L_{Ω} is also drawn in these two figures. As observed from the TSA result in Figure 2-12(b), a relatively large part of PDF is located on the left side of L_{Ω} , which means that the probability of damage existence is relatively high (87.6%) and a false identification may be obtained with a large likelihood. It can be observed that basically half of the PDF from C-TSA locates on the left side of the lower bound L_{Ω} , as shown in Figure 2-12(c), which means that the probability of damage existence is relatively low (59.3%) and the error in identification results stems from the uncertainty and noise effect with a large likelihood. This also demonstrates the superiority of the developed C-TSA for damage identification with uncertainties. The final structural damage identification results are shown in Figure 2-13. The specific identified damage in the 3rd elements are shown in Table 2-7. The relative errors in the results obtained from TSA and C-TSA are 1.19% and 0.24%, respectively. Due to the modelling uncertainty, the difficulty for identification is increased, but the superiority of the developed C-TSA can also be demonstrated.

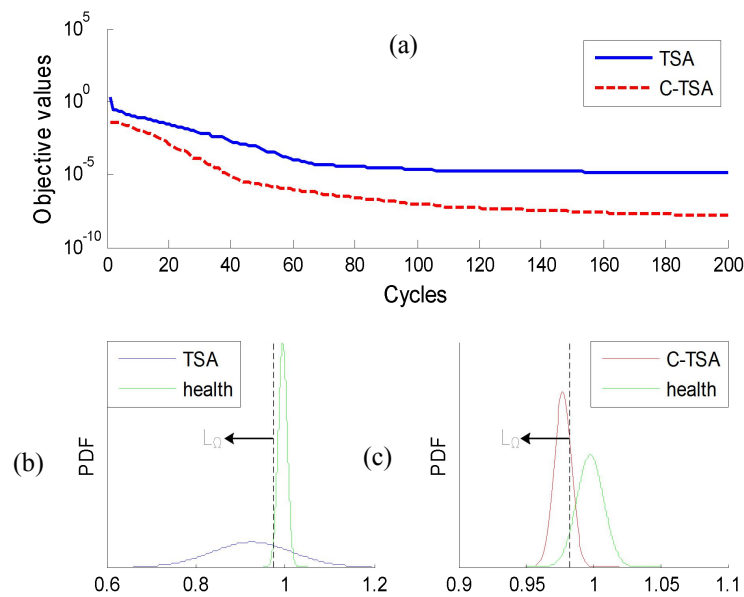


Figure 2-12 The identified results of Scenario 4; (a) The evolutionary process of the objective function value; (b) Distribution results from TSA; (c) Distribution results from C-TSA.

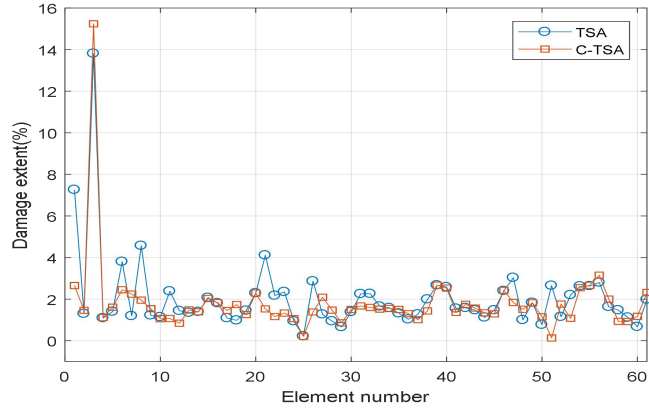


Figure 2-13 Damage identification results of Scenario 4.

2.4.5.2 Scenario 5

In this section, a multiple damage scenario with modeling uncertainty is defined to investigate the accuracy and effectiveness of the proposed algorithm. 25%, 20%, 13% and 18% stiffness reductions are introduced in the 4th, 8th, 18th and 45th elements. Figure 2-14 shows the iteration processes of the identified damages in those four elements. It is observed that C-TSA has a more stable and faster convergence than TSA. The final damage identification results are shown in Figure 2-15, and the specific damage extents are listed in Table 2-7. The maximum false identification obtained from TSA is observed in the 11th element with the mean value of 5.03% and standard deviation of 0.059. Such a large deviation indicates significant error in the 11th element, in contrast to the corresponding error of the results from C-TSA of only 2.67% with a standard deviation value of 2.91×10^{-4} . Furthermore, for the damaged elements, the maximum relative error in the identification by using TSA and C-TSA are 2.86% and 0.90%, respectively, indicating the superiority of C-TSA.

2.4.5.3 Scenario 6

In this damage scenario, both the measurement noise and modelling uncertainty are introduced to investigate the performance of the proposed approach. It is quite challenging to achieve an effective and reliable structural damage identification when significant measurement noise and modelling uncertainty effect are involved, since the coupling uncertainties generally have a significant influence on damage identification results. For the damage simulations, the same damages as Scenario 5 are introduced, that is, $\alpha_4 = 0.25$,

$\alpha_8 = 0.2$, $\alpha_{18} = 0.13$ and $\alpha_{45} = 0.18$. Figure 2-16 shows the identification results with uniformly distributed noise. False identifications are observed in the 6th, 11th, 16th, 21st, 26th, 31st, 51st and 56th elements when utilizing the TSA. However, there are no false identifications from the proposed C-TSA, which indicates again that the proposed approach can significantly improve the robustness against the measurement noise and uncertainty effects. Furthermore, in terms of the identified damage extents, the identification accuracy from the proposed C-TSA is generally more competitive. The performance evaluation results are shown in Table 2-7. The above numerical studies comprehensively demonstrate the accuracy and robustness of using the proposed approach in structural damage identification, even when the measurement noise and finite element modelling errors are considered.

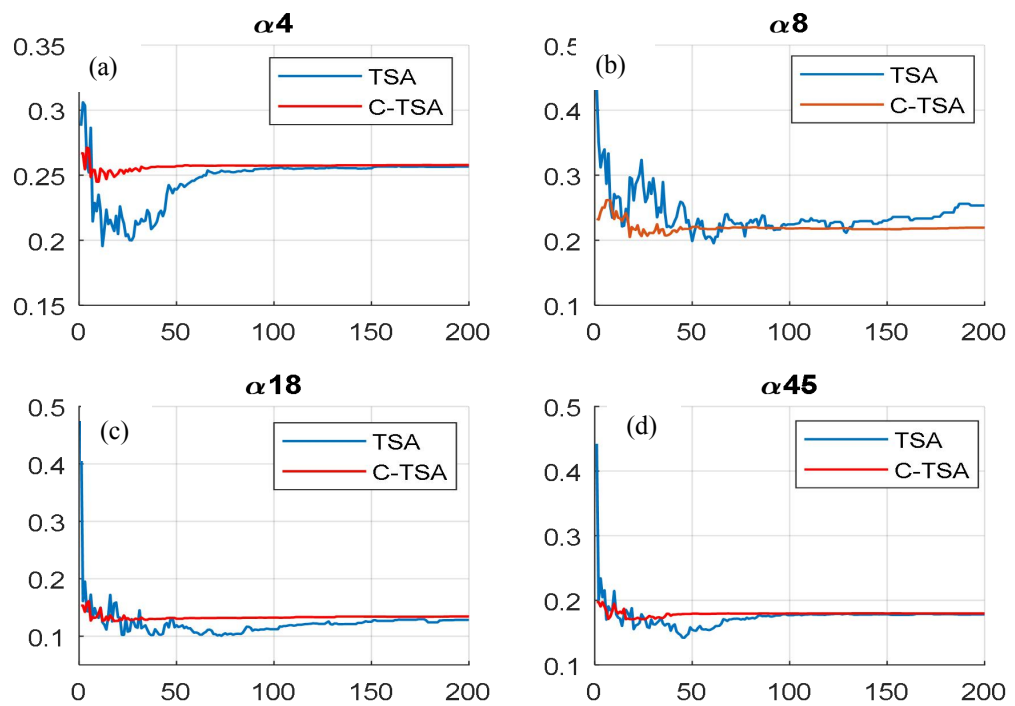


Figure 2-14 The evolutionary processes of the identified damage in Scenario 5 by using TSA and C-TSA: (a) α_4 ; (b) α_8 ; (c) α_{18} ; (d) α_{45} .

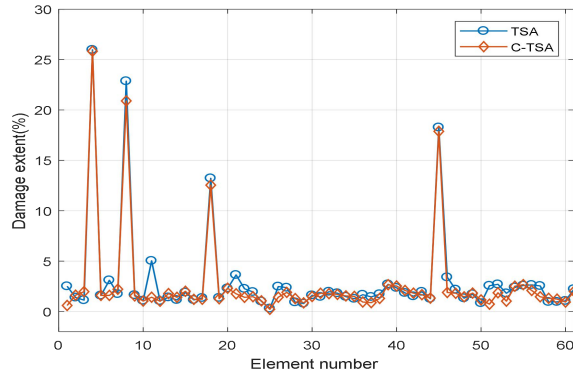


Figure 2-15 Damage identification results in Scenario 5.

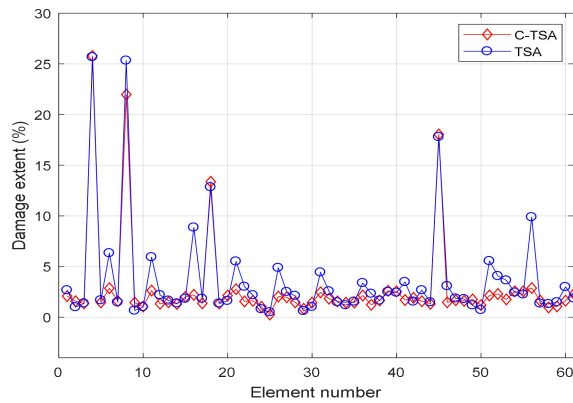


Figure 2-16 Damage identification results in Scenario 6.

Table 2-7 Damage identification results in numerical simulation with modelling uncertainty

Scenarios	Methods				Assumed value
	TSA		C-TSA		
	Mean	std.	Mean	std.	
Scenario 4					
α_3	13.81%	0.0442	15.24%	0.0126	15%
Scenario 5					
α_4	25.97%	0.0037	25.83%	2.2E-4	25%
α_8	22.86%	0.0167	20.90%	0.0032	20%
α_{18}	13.22%	0.0101	12.54%	0.0028	13%
α_{45}	18.27%	0.0039	17.88%	2.51E-4	18%
Scenario 6					
α_4	25.67%	0.0044	25.78%	6.5E-4	25%
α_8	25.33%	0.0319	21.97%	0.0094	20%
α_{18}	12.84%	0.0302	13.37%	0.0028	13%
α_{45}	17.79%	0.0081	18.03%	0.0011	18%

2.5 Experimental Verification

Experimental studies on an eight-story shear-type steel frame model are conducted to verify the accuracy and performance of the proposed approach. Figure 2-17 shows the fabricated shear type frame structure in the laboratory. The height and width of the frame structure are 2000mm and 600mm, respectively. Thick steel bars with dimension of 100mm×25mm are used as the floors of the frame model. Two flat bars of the same cross section with a width of 50mm and a thickness of 5mm are utilized as columns. The beams and columns are welded to form rigid beam-column joints. The bottom of the two columns is welded onto a thick and solid steel plate, which is fixed to a stronger floor. The detailed dimensions of the frame model are introduced in Ref. (Ni et al., 2018). The initial elastic modulus of the steel is estimated as 200Gpa and the mass density is 7850kg/m³. The dynamic tests are conducted to obtain the vibration characteristics of the frame structure. A modal hammer with a rubber tip is used to generate the impact excitation to this frame. Acceleration responses in the lateral direction of all the floors under the hamper impact are measured. The sampling rate is set as 1024 Hz and the cut-off frequency range for the band-pass filter is set from 1 Hz to 100 Hz for all the responses.



Figure 2-17 A steel frame model in the laboratory.

2.5.1 Initial finite element model

To identify the structural damage accurately, the modelling errors ought to be minimized through the initial model updating and the intact finite element model with updated parameters will be taken as the baseline for the damage identification. This procedure can also be considered as an inverse problem to adjust the parameters to be updated by minimizing the dynamic responses between the analytical model and the experimental tests (Ding et al., 2016). In this paper, the discrepancy between the measured frequencies and mode shapes and the calculated ones from the initial finite element model is used to build the objective function, which is given as below

$$f(\boldsymbol{\beta}) = \sum_{i=1}^8 \frac{|\omega_i^c - \omega_i^{real}|}{|\omega_i^{real}|} + \sum_{i=1}^8 \left(1 - \frac{(\boldsymbol{\Phi}_i^{cT} \cdot \boldsymbol{\Phi}_i^{real})^2}{\|\boldsymbol{\Phi}_i^c\|^2 \|\boldsymbol{\Phi}_i^{real}\|^2}\right), 0.7 \leq \boldsymbol{\beta} \leq 1.2 \quad (2.14)$$

where ω_i^c and $\boldsymbol{\Phi}_i^c$ represent the natural frequencies and mode shapes from the analytical finite element model; $\boldsymbol{\beta}$ denotes the parameter vector to be updated; ω_i^{real} and $\boldsymbol{\Phi}_i^{real}$ denote the measured frequency and mode shape values. In the model updating process, the updated parameters are the elemental stiffness parameters. The measured eight frequencies and mode shapes in the lateral direction are employed as input. The proposed C-TSA is used to optimize the objective function, and the natural frequencies before and after updating are shown in Table 2-8.

Table 2-8 Measured and analytical natural frequencies of the experimental model before and after updating

Mode	Measured (Hz)	Before updating		After updating		After updating	
		Analytical (Hz)	Error (%)	Analytical (Hz)	Error (%)	Analytical(Hz)	Error(%)
1	4.645	4.586	1.2602	4.645	0.0003	4.636	0.19
2	13.705	13.603	0.7428	13.705	0.0024	13.714	0.06
3	22.554	22.157	1.7615	22.552	0.0077	22.558	0.02
4	30.695	29.956	2.4086	30.698	0.0097	30.776	0.26
5	38.241	36.735	3.9393	38.239	0.0064	38.225	0.04
6	44.434	42.262	4.8871	44.434	0.0003	44.422	0.03
7	48.826	46.351	5.0686	48.828	0.0046	48.712	0.23
8	52.306	48.861	6.5853	52.302	0.0078	52.161	0.28

Furthermore, it also compares the updating results acquired by the first-order sensitivity method (Pathirage et al., 2018). The maximum error of the initial model is up to 6.5853%, and it is only 0.0097% after updating by the C-TSA in contrast to 0.28% by using the sensitivity method. This demonstrates the advantages of C-TSA to deal with modal updating problem, since the accuracy of the finite element model has been significantly improved. This baseline model is used in the subsequent damage identification analysis.

2.5.2 Damage identified results

Damages are introduced by reducing the cross sections of specific columns of the frame structure. Two damage cases, namely, Case 1 and Case 2, are defined in this structure. For Case 1, a single damage is introduced, which is introduced with a 20% reduction of the equivalent stiffness of the 2nd floor. For Case 2, multiple damages are considered, that is, besides the damage in Case 1, another damage is introduced with 10% stiffness reduction in the 7th floor. Figure 2-18 shows the details of the introduced damages in these two levels. The first eight natural frequencies and mode shapes in the lateral direction are used for structural damage identification by using TSA and C-TSA. The parameter settings are the same as the numerical simulations. In addition, ANN is used to identify the damages for comparison. For generating the training samples, in single element damage cases, the stiffness parameter of each damaged element varies from 1, 0.99, 0.98... to 0.7 while maintaining all other elements undamaged. 30 data is created for the scenario when a local damage is introduced in a specific element. With eight elements in the finite element model, 240 single element damage cases are simulated. In multiple element damage cases, the stiffness parameters for two random elements vary from 1, 0.99, 0.98, ... , to 0.7 while keeping the other elements undamaged, thus a total of 25200 multiple element damage scenarios are simulated. The input vector contains eight frequencies and 8×8 mode shape values, namely, 72 values in total. The final output vector has 8 elemental stiffness parameters.

Figure 2-19 shows the damage identification results for Cases 1 and 2. It is observed that the results from the proposed C-TSA are very close to the exact values with less and smaller false identifications. For Case 1, the relative errors in the identified damage extents of the 2nd level stiffness from ANN, TSA and the C-TSA are 5.80%, 2.17% and 0.42%, respectively. For Case 2, C-TSA also provides the best results. The relative errors in identified damage of the 2nd

and 7th floors are 4.89% and 4.34% by using ANN, 2.96% and 3.04% by TSA, and 0.58% and 1.08% by C-TSA. These experimental studies and results demonstrate that the proposed C-TSA can well identify the preset structural damages in the experimental model with testing data, which naturally include environmental noise and modeling uncertainties.

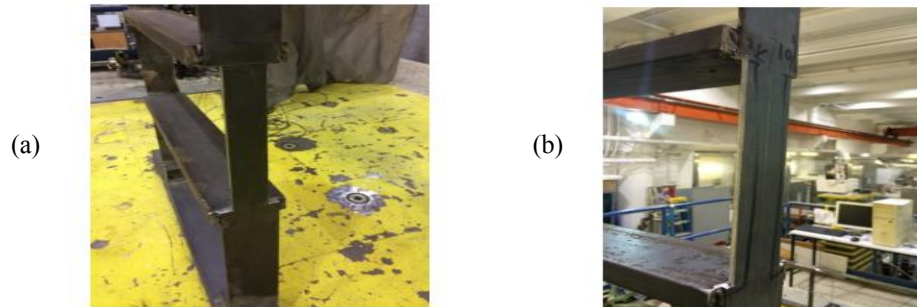


Figure 2-18 Introduced damages in the frame model;

(a) Introduced damage at the 2nd floor; (b) Introduced damage at the 7th floor.

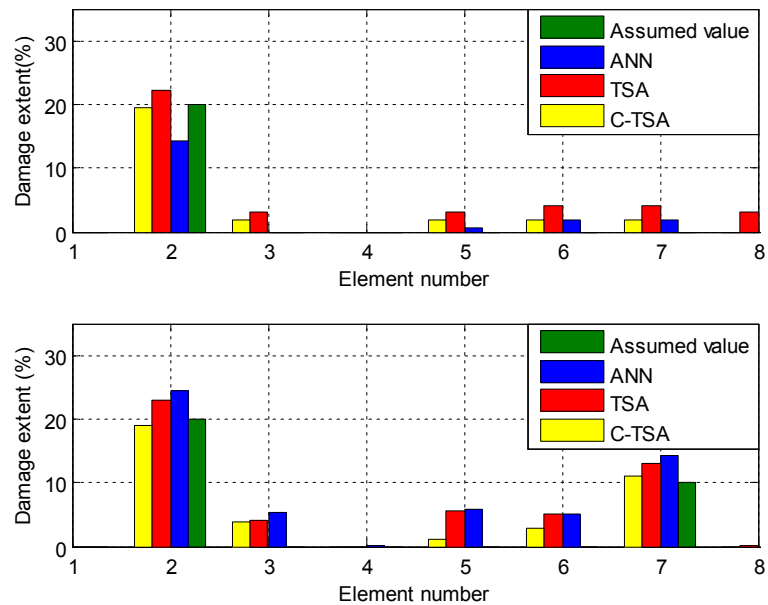


Figure 2-19 Identified damage results in the experimental tests; (a) Case 1; (b) Case 2.

2.6 Conclusions

A new type of swarm intelligence algorithm named TSA is presented for structural damage identification. To balance the algorithm's exploration and exploitation ability further, the K-means clustering is introduced before the seeds search phase. Benchmark functions and a

truss structure are utilized to investigate the accuracy and efficiency of the proposed approach in the numerical studies. Experimental studies are carried out on a shear type steel frame structure for further verification of the performance of the proposed approach. Some conclusions can be given as below:

- The proposed C-TSA is more efficient to deal with the benchmark test functions. The results show an improved performance and global optimization ability compared with the latest algorithms;
- Results in the numerical studies demonstrate that the proposed approach converges faster, and it is more robust to obtain good identification results with small variations in the parameter estimation across many damage cases. Uncertainties in the modelling and measurement noise are taken into account. The performance of the proposed approach is not sensitive to the measurement noise. When the modeling uncertainty is considered, C-TSA can still provide a good damage identification of structures. In contrast, when modeling uncertainty exists, TSA generates some false structural damage identifications.
- In the modal updating process for a real frame structure, it can be found the C-TSA also has superb advantages compared with the traditional sensitivity method.
- Experimental studies demonstrate that C-TSA can obtain better identification results, compared with the standard TSA and ANN.
- Results in the numerical and experimental studies demonstrate that C-TSA is a promising tool to perform structural damage identifications with data consisting of modelling errors and measurement noises.

References

- Cai, Z.H., Gong, W.Y., Ling, C.X., & Zhang, H. (2011) A clustering-based differential evolution for global optimization. *Applied Soft Computing*, 11, 1363-1397.
- Črepinšek, M., Liu, S.H., & Mernik, M. (2013) Exploration and exploitation in evolutionary algorithms: A survey. *ACM Computing Surveys*, 45(3), 35-42.
- Chen, C.B., Pan, C.D., Chen, Z.P., & Yu, L. (2019) Structural damage detection via combining weighted strategy with trace Lasso. *Advances in Structural Engineering*, 22(3), 597-612.
- Chen, Z.P., & Yu, L. (2017) A novel PSO-based algorithm for structural damage detection using Bayesian multi-sample objective function. *Structural Engineering & Mechanics*, 63(6), 825-835.
- Damavandi, N., & Safavi-Naeini, S. (2005) A hybrid evolutionary programming method for circuit optimization. *IEEE Transactions on Circuits and Systems-I*, 52(5), 902-910.
- Derrac, J. García, S., Molina, D., & Herrera, F. (2011) A practical tutorial on the use of nonparametric statistical tests as a methodology for comparing evolutionary and swarm intelligence algorithms. *Swarm and Evolutionary Computation*, 1, 3-18.
- Ding, Z.H., Huang, M., & Lu, Z.R. (2016) Structural damage detection using artificial bee colony algorithm with hybrid search strategy. *Swarm and Evolutionary Computation*, 28, 1-13.
- Ding, Z.H., Yao, R.Z., Li, J., & Lu, Z.R. (2018) Structural damage identification based on modified Artificial Bee Colony algorithm using modal data. *Inverse Problems in Science & Engineering*, 26(3), 422-442.
- Diptangshu, P., Li, Z., Samiran, C., Chee, P.L., & Liu, C.Y. (2018) A scattering and repulsive swarm intelligence algorithm for solving global optimization problems. *Knowledge-Based System*, 156, 12-24.
- Du, D.C., Vinh, H.H., Trung, V.D., Quyen, N.T.H., & Trung, N.T. (2017) Efficiency of Jaya algorithm for solving the optimization-based damage identification problem based on a hybrid objective function. *Engineering Optimization*, 50(8), 1233-1251.
- EI-Abd M. (2017) Global-best brain storm optimization algorithm. *Swarm and Evolutionary Computation*, 37, 27-44.
- EI-Abd M. (2013) An improved global-best harmony search algorithm. *Applied Mathematical Computation*, 222, 94-106.
- EI-Fergany, A.A., & Hasnien, H.M. (2018) Tree-seed algorithm for solving optimal power flow problem in large-scale power systems incorporating validations and comparisons. *Applied Soft Computing*, 64, 307-316.
- Fan, W., & Qiao, P. (2011) Vibration-based damage identification methods: a review and comparative study. *Structural Health Monitoring*, 10(1), 83-111.
- Gao, W.F., Chan, F.T.S., Huang, L.L., & Liu, S.Y. (2015) Bare bones artificial bee colony algorithm with parameter adaption and fitness-based neighborhood. *Information Science*, 316, 180-200.
- Gao, W.F., Yen, G.G., & Liu, S.Y. (2014) A cluster-based differential evolution with self-adaptive strategy for multimodal optimization. *IEEE Transactions on Cybernetics*, 44(8), 1314-1327.
- Hussain, S.F., & Haris, M. (2019) A K-means based co-clustering (KCC) algorithm for sparse, high dimensional data. *Expert Systems with Applications*, 118, 20-34.
- Imrani, A., Bouroumi, A., & Abidine, H. (2000) A fuzzy clustering-based niching approach to multimodal function optimization. *Journal of Cognitive Systems Research*, 1(2), 119-133.
- Kiran, M.S. (2015) TSA: Tree-seed algorithm for continuous optimization. *Expert Systems with*

Applications, 42, 6686-6698.

Li, J., Hao, H., & Chen, Z.W. (2017) Damage identification and optimal sensor placement for structures under unknown traffic-induced vibrations. *ASCE Journal of Aerospace Engineering*, 30(2), B4015001.

Lin, J.F., Xu, Y.L., & Law, S.S. (2018) Structural damage detection-oriented multi-type sensor placement with multi-objective optimization. *Journal of Sound and Vibration*, 422, 568-589.

Liu, S.H., Mernik, M., Hrnčič, D., & Črepinšek, M. (2013) A parameter control method of evolutionary algorithms using exploration and exploitation measures with a practical application for fitting Sovova's mass transfer model. *Applied Soft Computing*, 13, 3792-3805.

Lu, Z.R., & Law, S.S. (2007) Features of dynamic response sensitivity and its application in damage detection. *Journal of Sound and Vibration*, 303(1), 305-329.

Ng, C.T. (2014) On the selection of advanced signal processing techniques for guided wave damage identification using a statistical approach. *Engineering Structures*, 67, 50-60.

Ni, P.H., Xia, Y., Li, J. & Hao, H. (2018) Improved decentralized structural identification with output-only measurements. *Measurement*, 122, 597-610.

Padil, K.H., Bakhary, N., & Hao, H. (2017) The use of a non-probabilistic artificial neural network to consider uncertainties in vibration-based-damage detection. *Mechanical Systems & Signal Processing*, 83, 194-209.

Suganthan, P.N., Hansen, H., Liang, J.J., Deb, K., Chen, Y.P., Auger, A., & Tiwari, S. Problem definitions and evaluation criteria for the CEC 2005 special sessions on real-parameter optimization, *Technique Report*, ITT Kanpur, India.

Sun, H., Lus, H., & Betti, R. (2013) Identification of structural models using a modified Artificial Bee Colony algorithm. *Computers & Structures*, 116, 59-74.

Wang, L., Liu, J.K., & Lu, ZR. (2017) Incremental response sensitivity approach for parameter identification of chaotic and hyperchaotic systems. *Nonlinear Dynamics*, 89(1), 153-167.

Xia, Y., Hao, H., Brownjohn, J.M.W, & Xia, P.Q. (2002) Damage identification of structures with uncertain frequency and mode shape data. *Earthquake Engineering & Structural Dynamics*, 31, 1053-1066.

Yi, T.H., Li, H.N., & Zhang, X.D. (2012) A modified monkey algorithm for optimal sensor placement in structural health monitoring. *Smart Material and Structures*, 21(10), 105033.

Yi, T.H., Zhou G.D., Li, H.N., & Wang, C.W. (2017) Optimal placement of triaxial sensors for modal identification using hierarchic wolf algorithm. *Structural Control & Health Monitoring*, 24(8): e1958.

Yu, L., & Li, C. (2014) A global artificial fish swarm algorithm for structural damage detection. *Advances in Structural Engineering*, 17(3), 331-346.

Yu, L., Zhu, J.H., & Yu, L.L. (2013) Structural damage detection in a truss bridge model using fuzzy clustering and measured FRF data reduced by principle component Projection. *Advances in Structural Engineering*, 16(1), 207-217.

Zambrano-Bigiarini, M., Clerc, M., & Rojas, R. (2013) Standard Particle Swarm Optimisation 2011 at CEC-2013 : A baseline for future PSO improvements, in: *Proceedings of the IEEE Congress on Evolutionary Computation*, 2337-2334.

Zhou, J.Z., Yang, Z., Xu, Y.H., Liu, H., & Chen, D.Y. (2018) A heuristic T-S fuzzy model for the pumped-storage generator-motor using variable-length Tree-Seeds Algorithm-based competitive agglomeration. *Energies*, 11(4), 944-964.

Zhu, G.P., & Kwong, S. (2010) Gbest-guided artificial bee colony algorithm for numerical function optimization. *Applied Mathematical Computation*, 217, 3166-3173.

Zhu, J.J., Huang, M., & Lu, Z.R. (2017) Bird mating optimizer for structural damage

detection using a hybrid objective function. *Swarm and Evolution Computation*, 35, 41-52.

CHAPTER 3 NONLINEAR HYSTERETIC PARAMETER IDENTIFICATION USING AN IMPROVED TREE SEEDS ALGORITHM

ABSTRACT²

The tree seeds algorithm (TSA) is a new type of heuristic algorithms based on the simulation of trees propagation. It has been applied to solve continuous optimization problems effectively and efficiently. This paper proposes an improved TSA, termed as I-TSA, to solve the nonlinear hysteretic parameter identification problem with three typical hysteretic models, namely Bouc-Wen model, bilinear model with kinematic hardening and bilinear model with equal yielding force. In order to enhance the capability of the proposed approach to search for the best optimization results, the Lévy search mechanism and a new updating equation are introduced to improve the original TSA. Numerical studies on several mathematical benchmark test functions, a single degree-of-freedom system and a multi degree-of-freedom system are conducted to investigate the accuracy and performance of the proposed approach. The identification results are compared with those obtained from several existing widely used heuristic algorithms and the enhanced sensitivity method to demonstrate the improvement and superiority of the proposed approach.

3.1 Introduction

Nonlinear hysteretic effect has been observed in many physical systems, i.e. mechanical systems with nonlinear joints, structural dampers, seismic isolation systems and friction models (Katsaras et al., 2018; Berger & Krousgrill, 2002; Wang & Xin, 2015; Wang et al., 2016). Many mathematical models, such as Preisach, Ischlinskii, Bouc-Wen and bilinear models, have been used to describe the nonlinear hysteretic behavior of civil and mechanical systems. It is noted that the nonlinear hysteretic behavior usually has the memory function since its instantaneous input depends on its past history. Many conventional system identification methods may fail to solve the nonlinear hysteretic parameters identification problem due to their inherent non-linearity and memory nature, therefore it is essential to conduct researches on this kind of inverse problem. Many mathematical models, such as Preisach, Ischlinskii,

²This chapter was published in *Swarm and Evolutionary Computation* with the full bibliographic citation as follows: Ding, Z., Li, J., Hao, H., & Lu, Z. (2019). Nonlinear hysteretic parameter identification using an improved tree-seed algorithm. *Swarm and Evolutionary Computation*, 46, 69-83. <https://doi.org/10.1016/j.swevo.2019.02.006>.

Bouc-Wen and bilinear models, have been used to describe the nonlinear hysteretic behavior of civil and mechanical systems. It is noted that the nonlinear hysteretic behavior usually has the memory function since its instantaneous input depends on its past history. Many conventional system identification methods may fail to solve the nonlinear hysteretic parameters identification problem due to their inherent non-linearity and memory nature, therefore it is essential to conduct researches on this kind of inverse problems (Lu et al., 2017; Charalampakis & Dimou, 2010).

Two main categories of existing methods for the nonlinear hysteretic parameter identification can be summarized from the literature. The first category is to formulate it as a discrete state identification problem, which can be solved by using methods like Kalman filter and wavelet analysis techniques. Wu and Smyth (2008) proposed combining the extended Kalman filter and unscented transformation to estimate the nonlinear parameters. Khellat (2009) introduced the multi-wavelet basis function first, and then the problem can be converted as a time invariant system estimation problem which can be tackled by the optimal control method. Chang and Shi (2010) conducted the parameter identification of Bouc-Wen hysteretic systems via wavelet multiresolution analysis. More recently, Calabrese et al. (2018) used an adaptive constrained unscented Kalman filter to conduct the identification of real-time nonlinear structural systems. Wang and Ding (2017) presented a filtering based multi-innovation gradient estimation algorithm and applied to the nonlinear dynamical system identification. The above-mentioned studies acquired relatively good results, however, a high sampling rate is necessary since the discrete state equations shall be accurate enough to approximate the original differential equations.

The second category is to formulate the hysteretic parameter identification problem as an inverse problem through defining objective functions relevant to the systematic parameters, which can be solved with optimization techniques. The objective functions are usually defined as minimizing the difference between the measured and analytical data, which can be the modal information and/or the weighted time domain responses (Li & Hao, 2016). Ni et al. (1998) used the Levenberg-Marquardt algorithm integrated with the frequency-domain displacement data from periodic vibration tests to identify parameters of friction-type isolators. However, acquiring frequency-domain data for a nonlinear system is not as straightforward as a linear one, which requires a large amount of sample data. In contrast, the time-domain data is

much easier to be accessed. Therefore, various techniques have been developed by formulating the time domain responses in the objective functions. Loh and Chung (1993) proposed a three-stage scheme to solve the nonlinear parameter estimation problem by using acceleration responses. Yar and Hammond (1987) formulated the objective function based on the input force and output acceleration data, and then utilized Gauss-Newton method to identify these nonlinear parameters. Sues et al. (1988) and Roberts and Sadeghi (1990) used the restoring force data to deal with such identification problems. More recently, Waubke and Kassess (2016) proposed a Gaussian closure technique based on Kolmogorov equations and applied it to solve the Bouc-wen model with white noise excitation. A nonlinear state-space approach (2017) was proposed to tackle the hysteresis identification problem. Lu et al. (2017) proposed an enhanced response sensitivity approach to solve the nonlinear hysteretic parameters identification problem and obtained good parameter estimation results with accelerations.

Nevertheless, when using gradient-based methods (Lu et al., 2017; Los & Chung, 1993; Yar & Hammond, 1987; Sues et al., 1988; Roberts & Sadeghi, 1990; Waubke & Kassess, 2016; Noel et al., 2017) for solving this identification problem, good initial values and reliable sensitivity gradient calculations are required. In addition, difficulties will amplify when utilizing these methods for the identification of large systems with limited available measurement data. Heuristic algorithms that could overcome these shortcomings have gained significant attention.

Garg et al. (2016) used the evolutionary algorithm (EA) to solve identifying the characteristics problems of bone drilling operations based on three different output models. Garg et al. (2017) also utilized Genetic programming (GP) to determine wilting point for green infrastructure. Extending the applications to the nonlinear parameter identification problem, Charalampakis and Koumouisis (2008) adopted the sawtooth Genetic Algorithm (GA) combined with a new mutation operator to solve identification problem of a steel cantilever beam with Bouc-Wen model. Later, Charalampakis and Dimou (2010) employed two variants of the Particle Swarm Optimization (PSO) algorithm for the identification of Bouc-Wen hysteretic systems. Ortiz et al. (2013) used the discrepancy between the calculated and measured displacements of a nonlinear system with Bouc-Wen model as the objective function and then employed a fast multi-objective GA to identify the parameters. Sun et al. (2013) used the modified Artificial Bee Colony (ABC) algorithm to identify the parameters of nonlinear

systems with Bouc-Wen models. Besides, some other heuristic algorithms like Firefly Algorithm (FA) (Zaman & Sikder, 2015), Charged System Search (CSS) optimization (Talatahari et al., 2012) and Differential Evolutionary (DE) algorithm (Quaranta et al., 2014) have also been employed to solve such identification problem. Recently, Brewick et al. (2016) utilized Volterra/Wiener Neural Network (VWNN) to conduct probabilistic identification of nonlinear hysteric models. Shu and Li (2017) utilized a modified version of GA, in which the real-integer hybrid coding with adaptive crossover and mutation rates were used, to conduct the parametric identification of Bouc-Wen models. Ben Abdesslem et al. (2018) used sequential Monte-Carlo and Bayesian inference to estimate the nonlinear structural parameters. Nguyen et al. (2018) introduced a neural differential evolution identification approach to perform the nonlinear systems identification. However, when utilizing these heuristic algorithms to perform the identification of nonlinear systems, several challenges still remain, i.e., (a) Significant computational demand and time are required. For example, the maximum iteration step of the improved PSO algorithm is defined up to 5,000 (Charalampakis & Dimou, 2010); (b) The slow convergence speed or trapping in the local optima. When the algorithms are not able to balance their exploration and exploitation ability well, they easily encounter the problem of slow convergence or acquiring some local optimal values, especially when dealing with the complex nonlinear problem; (c) The robustness against the measurement noise effect. The accuracy of identification results may be greatly affected when the measured data are smeared with significant noise and uncertain effect. To this end, it is important to develop and apply new algorithms for nonlinear system identification to improve the efficiency and robustness.

Recently, a new heuristic algorithm called as Tree Seeds algorithm (TSA) has been proposed and proven to be more effective and efficient when dealing with the low-dimensional continuous optimization problems (Kiran, 2015). The most attractive feature of this algorithm is its way of producing new solution, since it can generate more offspring instead of one-dimensional perturbation compared with other traditional heuristic algorithms. Based on this characteristic, TSA has achieved a better performance to search for the global optima in some benchmark functions, particularly when dealing with the uniform functions (i.e. Sphere function). Nevertheless, it should be noted that TSA may also face the slow convergence issue or stuck with the local optima like other heuristic algorithms. This is a paradox behind these algorithms. When an algorithm more focuses on the exploitation (local search), the solution

will be likely trapped in the local optima. However when an algorithm concentrates more on the exploration (global search), it may suffer the slow convergence problem. Therefore, only when the exploration and exploitation abilities are balanced well, the algorithm can achieve a strong performance in optimization accuracy as well as the efficiency. To address this problem, this paper proposes an improved TSA, named as I-TSA, for the nonlinear hysteretic parameter identification. An improved framework integrated with the Lévy flight search mechanism and a new updating equation for every colony individual are developed to form the I-TSA. Numerical investigations on mathematical benchmark test functions and two nonlinear hysteretic systems are conducted to verify the accuracy and efficiency of the proposed approach. The identification results are compared with those from the enhanced sensitivity method and several existing heuristic algorithms to demonstrate the improvement and superiority of the proposed approach.

The rest of this paper is organized as follows. Section 2 describes the problem formulation for nonlinear hysteretic system identification and reviews the nonlinear hysteretic models, such as Bouc-Wen model and two bilinear models. Section 3 briefly presents the original TSA and describes the proposed I-TSA in detail with specific modifications. Section 4 mainly demonstrates the accuracy and efficiency of using the proposed algorithm in the benchmark tests and numerical simulations on nonlinear system identification. The results are compared with those obtained from the existing latest methods to demonstrate the improvement and superiority of the developed algorithm. Finally, conclusions will be drawn in Section 5.

3.2 Nonlinear Hysteretic Models and Parameter Identification

3.2.1 Nonlinear hysteretic models

This section briefly reviews the widely used Bouc-Wen hysteretic model and two kinds of bi-linear models with kinematic hardening and equal yielding force, respectively. The hysteretic behavior describes the memory-based relationship between the displacement u and the restoring force r , which can be generally defined as

$$\dot{r} = f(r, u, \dot{u}, \mathbf{p}) \quad (3.1)$$

where $f(\cdot)$ is the nonlinear function representing the hysteretic behavior, and \mathbf{p} denotes the effective model parameters. Bouc-Wen model is a versatile representation (Ismail et al., 2009;

Brewick & Masri, 2016) which can be used to simulate various nonlinear hysteretic systems, i.e. dampers, nonlinear joints and isolation devices. It can be described as

$$\dot{r} = \frac{1}{\eta} [A\dot{u} - \nu(\beta \cdot r |r|^{n-1} |\dot{u}| + \gamma |r|^n \dot{u})] \quad (3.2)$$

where $\eta, A, \nu, \beta, \gamma$ and n are the design parameters to represent the nonlinear hysteretic behavior. Specifically, the two parameters η and ν are respectively controlling the degrading and pinching behavior (Wu & Smyth, 2008), and could be defined as unity without loss of generality. The exponential coefficient n is usually set as $n \geq 1$ in order to meet the requirement of the thermodynamic admissibility (Erlicher & Point, 2004) requiring $|\gamma| \leq \beta$ and $A > 0$. To simplify Eq. (2) and build up the equivalence between the design and effective parameters, a vector \mathbf{P}_{BW} is defined as

$$\mathbf{P}_{BW} = [p_1 = \frac{A}{\eta}, p_2 = \frac{\nu\beta}{\eta}, p_3 = \frac{\nu\gamma}{\eta}, p_4 = n]^T \quad (3.3)$$

Besides, the definition domain for the vector is given as below

$$\mathbf{p} \in p^{BW} := \{p \in R^4 : p_1 > 0, |p_3| \leq p_2, p_4 \geq 1\} \quad (3.4)$$

The first bilinear model with kinematic hardening (Katsaras et al., 2018) is described as

$$\dot{r} = [\frac{k_1 + k_2}{2} - \frac{k_1 - k_2}{2} \text{sgn}((r - k_2 u) \text{sgn}(\dot{u}) - F_0)] \dot{u} \quad (3.5)$$

where k_1 and k_2 are the primal and degraded stiffness of the model, respectively, F_0 is the yielding force with zero displacement and $\text{sgn}(\cdot)$ represents the sign function as follows

$$\text{sgn}(x) = \begin{cases} -1, & \text{if } x < 0 \\ 1, & \text{if } x \geq 0 \end{cases} \quad (3.6)$$

The simplified form of this bilinear model can be rewritten as

$$\dot{r} = [p_1 + p_2 - p_1 \text{sgn}((r - p_2 u) \text{sgn}(\dot{u}) - p_3)] \dot{u} \quad (3.7)$$

with

$$\mathbf{P}_{B1} = [p_1 = \frac{k_1 - k_2}{2}, p_2 = k_2, p_3 = F_0]^T \quad (3.8)$$

The parameters shall be in the following domain for this bilinear model

$$\mathbf{p} \in p^{B1} := \{\mathbf{p} \in R^3 : p_1 > 0, p_2 \geq 0, p_3 > 0\} \quad (3.9)$$

The second bilinear model with equal yielding force (Yar & Hammond, 1987) can be expressed as

$$\dot{r} = \left[\frac{k_1 + k_2}{2} - \frac{k_1 - k_2}{2} \text{sgn}(r \text{sgn}(\dot{u}) - F_y) \right] \dot{u} \quad (3.10)$$

where k_1 and k_2 represent the stiffness parameters before and after yielding, and F_y denotes the yielding force. Likewise, it can be rewritten as

$$\dot{r} = [p_1 - p_2 \text{sgn}(r \text{sgn}(\dot{u}) - p_3)] \dot{u} \quad (3.11)$$

with

$$\mathbf{P}_{B2} = [p_1 = \frac{k_1 + k_2}{2}, p_2 = \frac{k_1 - k_2}{2}, p_3 = F_y]^T \quad (3.12)$$

The parameters shall be in the following domain in this case

$$\mathbf{p} \in p^{B2} := \{\mathbf{p} \in R^3 : p_1 \geq p_2, p_2 > 0, p_3 > 0\} \quad (3.13)$$

With the presented three nonlinear hysteretic models, a single degree-of-freedom (SDOF) system as shown in Figure 1 is taken as an example to demonstrate the dynamic response calculation of a nonlinear system. The equation of motion of the nonlinear system considering the hysteretic models can be expressed as (Charalampakis & Dimou, 2010)

$$\begin{cases} m\ddot{u} + c\dot{u} + ku + r = \mathbf{F}(t) \\ \dot{r} = f(r, u, \dot{u}, \mathbf{p}) \\ u(0) = u_0, \dot{u}(0) = \dot{u}_0, r(0) = r_0 \end{cases} \quad (3.14)$$

where u is the displacement; u_0, \dot{u}_0 and r_0 are respectively the initial displacement, velocity and restoring force of the nonlinear system; and m, c, k and \mathbf{F} denote the mass, damping, stiffness and excitation respectively. It should be noted that the restoring force r can be obtained based on any of the abovementioned three hysteretic models, such as Eqs. (5), (7) and (10). The Runge-Kutta method (Cash & Karp, 1990) is used to solve Eq. (14) to obtain the dynamic responses. Likewise, the equation of motion of a nonlinear multi degree-of-freedom (MDOF) can be built by defining a connection matrix T for those hysteretic components (Lu et al., 2017).

3.2.2 Nonlinear system identification formulation

Nonlinear system identification with hysteretic models can be formulated as an optimization problem with a suitable objective function relevant to the structural parameters,

for instance, the error between the measured and calculated response data (Lu et al., 2017; Sun et al., 2013). Optimization techniques can then be used to identify the system parameters by minimizing the objective function.

In this study, $F(t)$ and $u(t)$ are defined as two vectors containing the input and the output data, respectively; $\mathbf{t} = t_1, t_2, \dots, t_k$ denotes the time instant series and $u(t_k)$ represents the response at the time instant t_k . $\hat{\boldsymbol{\theta}} = \{\hat{\theta}_1, \hat{\theta}_2, \dots, \hat{\theta}_n\}$ is defined as a vector of structural parameters that could be stiffness, damping ratio, mass density or nonlinear hysteretic parameters. The dynamic response $\hat{u}(t_k)$ at the time instant t_k can be expressed as

$$\hat{u}(t_k) = f(\hat{\boldsymbol{\theta}}, t_k) \quad (3.15)$$

The dynamic response can be solved by using the Runge-Kutta method based on the equation of motion of the nonlinear system, and the difference between the calculated and measured responses can be obtained. The identification problem has been formulated as identifying the optimal parameters, which will minimize the difference between the measured and analytical responses as small as possible. The objective function is defined as follow

$$g(\hat{\boldsymbol{\theta}}) = \sum_{i=1}^{n_{res}} \sum_{k=1}^{n_{time}} (\hat{u}_i(t_k) - u_i(t_k)) \cdot (\hat{u}_i(t_k) - u_i(t_k))^T \quad (3.16a)$$

$$\hat{\lambda} = \{\hat{\boldsymbol{\theta}} \in R^n \mid \theta_j^{\min} \leq \hat{\theta}_j \leq \theta_j^{\max}, \forall j \in \{1, 2, \dots, n\}\} \quad (3.16b)$$

where n_{res} is the number of the available measurements that can be used for updating, which depends on the number of sensors available in the test; n_{time} is the number of sample points in each measured response. Eq. (3.16b) defines the lower and upper bounds of the parameters domain. $\hat{\theta}_j$ is defined as the j th parameter to be identified with the upper and lower bounds θ_j^{\max} and θ_j^{\min} , respectively; n represents the total number of the parameters to be optimized. Through Eqs. (3.15) and (3.16), the identification problem is mathematically formulated as a constrained nonlinear optimization problem (Sun et al., 2013). Generally the objective function may have multiple local minimum. In this case, the traditional optimization techniques could be stuck with the local minimum, which may result in the poor identification results. Therefore, it is necessary to investigate and develop robust and powerful algorithms, which could deal with the nonlinear identification problem well.

3.3 Improved Tree Seeds Algorithm (I-TSA)

3.3.1 Original TSA

TSA is a heuristic algorithm and has been proposed based on the natural phenomenon of trees propagation (Kiran, 2015). In reality, trees usually spread to other places through their seeds. These seeds will grow the new trees over time. In the algorithm, these places for trees and seeds can be considered as searching spaces for optimization problems. The specific locations of trees and seeds are regarded as feasible solutions. In fact, the core of this algorithm is the seeds searching since it will update the new feasible solution in this phase, which provides two search equations for this process given as

$$S_{z,j} = T_{i,j} + \alpha_{i,j} \times (B_j - T_{r,j}) \quad (3.17)$$

$$S_{z,j} = T_{i,j} + \alpha_{i,j} \times (T_{i,j} - T_{r,j}) \quad (3.18)$$

where $S_{z,j}$ is the j th dimension of the z th seed that would be generated by the i th tree. $T_{i,j}$ is the j th dimension of the i th tree, B_j is the j th dimension of best-so-far tree location, $T_{r,j}$ is the j th dimension of the r th tree randomly picked up from the colony size, $\alpha_{i,j}$ is uniformly distributed in the range of $[-1,1]$. The seeds number can be usually determined as 10% - 25% of the colony size. The exact number of the seed generation is random in TSA. As mentioned before, it is necessary for a heuristic algorithm to define a proper balance between the global and local searching performances. Based on the search equation as shown in Eq. (3.17), a new candidate is produced by the old solution towards the best-so-far solution in the colony, which enhances the algorithm's local searching ability to some extent. In contrast, from observing Eq. (3.18), a new candidate is created by moving the old solution towards a randomly chosen one in population. Meanwhile, the coefficient $\alpha_{i,j}$ is also a uniform random number, therefore Eq. (3.18) has a strong global search ability (Gao et al., 2015)

One of the key points of the algorithm is to decide whether Eq. (3.17) or Eq. (3.18) will be chosen to create a new seed location. This process is controlled by a parameter called as search tendency (ST) within the range of $[0, 1]$. Selecting the best equation for the updating relies on comparing a uniform random number and ST. If the random number is larger than ST, Eq.

(3.17) is chosen as the update equation. Otherwise Eq. (3.18) will be used. Therefore, for every individual, a higher ST value makes it have a higher chance to exploitation. This is the reason why the exploration and exploitation capacities of the TSA is controlled by ST parameters.

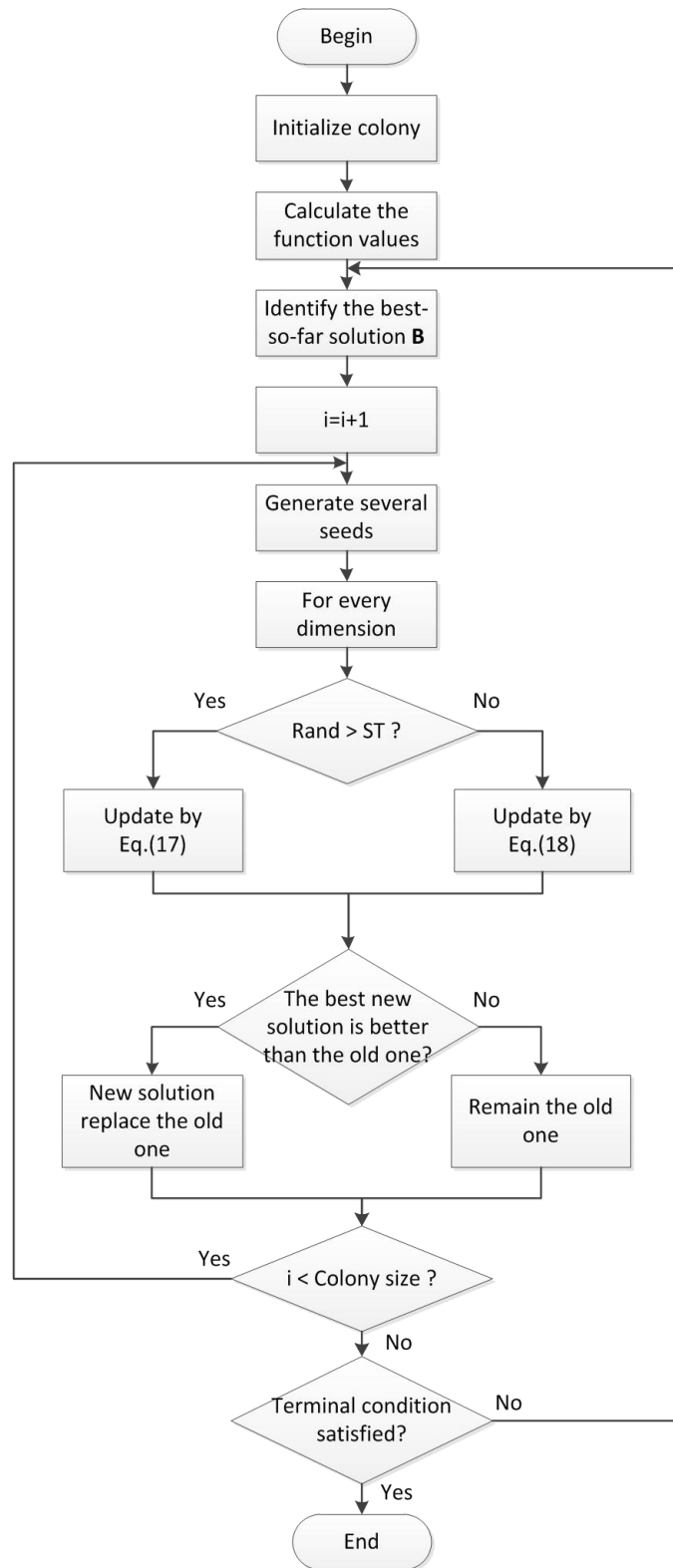


Figure 3-1 The flowchart of the TSA

When applying TSA, the initial tree locations, namely the possible solutions for the optimization problem, are produced as

$$T_{i,j} = L_{j,\min} + r_{i,j} \times (H_{j,\max} - L_{j,\min}) \quad (3.19)$$

where $L_{j,\min}$ is the lower bound of the search space and $H_{j,\max}$ is the upper bound, $r_{i,j}$ is a random number produced for every dimension and location, which is in the range of $[0, 1]$.

The flowchart of TSA is shown in Figure 3-1.

3.3.2 Proposed modifications

In this section, I-TSA is presented and the motivation behind this development is described. The Lévy search mechanism and a new updating equation that are used in I-TSA will be described. As mentioned in Section 3.2.2, the objective function in complex nonlinear problems is difficult to deal with due to its multimodal feature. To make the TSA more powerful and balance its exploration (global search) and exploitation (local search) capacities, two modifications are made. From observing the seeds search equation as shown in Eq. (3.17), TSA conducts its exploitation just around the current best solution, which may not make the full use of the information hidden in the other individuals, leading to a premature convergence in the multimodal cases. Unlike other heuristic algorithm, i.e. Artificial Bee Colony (ABC) (Karaboga, 2008; Sun et al., 2013), TSA is not equipped with the ‘Scout bee phase’, which is a negative feedback into the ABC. Due to this mechanism, ABC has an opportunity to discard the best solution trapped into the local optimal and cease the evolution, which is beneficial for escaping from local optima. Based on this motivation, a similar framework is introduced into the original TSA to improve the optimization performance.

Modification 1: Lévy flight mechanism

Lévy flight has a random moving direction with its step size following the power-law distribution. This turns out to be a quite beneficial way to escape from local minimum for optimization algorithms. It has been successfully applied in Cuckoo Search algorithm (Yang & Deh, 2009; Soneji & Sanghvi, 2014), Fruit algorithm (FA) (Miticet et al., 2015) for greatly enhancing their optimization performances. As shown in Eq. (3.17), the search in the original TSA is centered as the best solution (**B**) in the current iteration. If the best-so-far solution in

every cycle traps in the local optima, it will significantly affect the whole optimization process. Based on this motivation, the Lévy flight is applied for searching the best-so-far solution of every iteration. It will launch several random searches around the best solution in every iteration, which can be viewed as a good way to escape from the local optima (Sharma et al., 2016; Ding et al., 2016).

Aforementioned, the Lévy flight is actually a random walk where its steps are determined by the step lengths, which follow a certain probability distribution. The random step lengths s with the power-law distribution is given as

$$L(s) \sim |s|^{-1-\beta}, (0 < \beta \leq 2) \quad (3.20)$$

where $\beta (0 < \beta \leq 2)$ denotes an index, and s denotes the step length.

In this paper, similar with Refs. (Sharma et al., 2016; Ding et al., 2016), the Mantegna algorithm for a symmetric Lévy distribution is used to create random sizes. Herein, ‘symmetric’ means that the produced size may be positive or negative. Based on a Mantegna framework, the step length s can be calculated as

$$s = \frac{\omega}{|\mathbf{v}|^{1/\beta}}, \quad (3.21)$$

where ω and \mathbf{v} follow normal distributions and their expressions can be given as below

$$\omega \sim N(0, \sigma_u^2), \quad \mathbf{v} \sim N(0, \sigma_v^2) \quad (3.22)$$

with

$$\sigma_u = \left\{ \frac{\Gamma(1+\beta)\sin(\pi\beta/2)}{\beta \cdot \Gamma[(1+\beta)/2]2^{(\beta-1)/2}} \right\}^{1/\beta}, \quad \sigma_v = 1 \quad (3.23)$$

in which $\Gamma(\cdot)$ represents the Gamma function and can be calculated as

$$\Gamma(1+\beta) = \int_0^{\infty} t^{\beta} e^{-t} dt \quad (3.24)$$

Afterwards, $Step_size(t)$ that is generated based on the Lévy flight to make further exploitation can be expressed as

$$Step_size(t) = F_A \times s(t) \times (\mathbf{B}(t) - \mathbf{T}_r(t)) \quad (3.25)$$

where t is the time instant of the Lévy flight, $s(t)$ is obtained from Eq. (3.21). \mathbf{B} is the best solution in the current iteration cycle and \mathbf{T}_r is the randomly selected tree which is not

the same as \mathbf{B} in the colony, and F_A is the scaling factor. In this study, it equals to 0.001. Herein, the final solution updating equation to search around the best solution can be expressed as

$$\mathbf{B}(t+1) = \mathbf{B}(t) + \text{step_size}(t) \times U(0,1) \quad (3.26)$$

where \mathbf{B} is the best-so-far solution in the current cycle, which is going to be exploited. $U(0,1)$ is an uniform distribution within 0 and 1, $\text{step_size}(t) \times U(0,1)$ is the actual random flights for the solution, which is calculated from Lévy flight. After completing the Lévy flight once, the ‘Greedy Selection Mechanism’ (Karaboga & Basturk, 2008) will be applied and the solution with a better fitness will replace the previous one. Generally speaking, this means that the Lévy flight can assist the solution in escaping from the local optima and ceasing the evolution process in most cases.

Modification 2: A new updating equation for seeds search

In the original TSA, after selecting the best-so-far solution, it will conduct the seeds search by using Eqs. (3.17) or (3.18). It can be observed from Eq. (3.18) that a new candidate is created in the direction which is around the previous solution towards any individual chosen from the colony, whereas the coefficient $\alpha_{i,j}$ is a uniform random number within $[-1,1]$. Hence Eq. (3.18) can ensure the algorithm’s global search capacity because of randomly selecting the individual solution (Gao et al., 2015). However, as shown in Eq. (3.17), it is clear that when the original algorithm arrives at the seeds searching stage, its way of exploitation just simply centers on the current best solution, which may not make full use of the colony information and suffer the premature convergence problem to some extent.

To address this problem, a new updating equation (Cui et al., 2016) is introduced into the seeds search stage. This equation is described as

$$S_{z,j} = \frac{1}{2}(T_{i,j} + \mathbf{B}_j) + \alpha_{k,j}(\mathbf{B}_j - T_{k,j}) \quad (3.27)$$

where $T_{k,j}$ represents the j th dimension of another different tree from the colony, $\alpha_{k,j}$ denotes a random number within $[-1,1]$. In this equation, the first term is good at exploitation whereas the second one does well in exploration (Cui et al., 2016). To further improve the convergence performance, a nonlinear factor is also utilized. The final updating equation used

for the modified TSA is given as

$$S_{i,j} = \frac{1}{2}(T_{i,j} + \mathbf{B}_j) + \lambda_1 \alpha_{k,j} (\mathbf{B}_j - T_{k,j}) \quad (3.28)$$

$$\lambda_1 = 1 - \left(\frac{iter}{miter}\right)^4 \quad (3.29)$$

where *iter* denotes the current iteration number and *miter* is the maximum iteration number. Eqs. (3.28) and (3.29) are used for the I-TSA. When the number of iteration increases, λ_1 will decrease and the weight of the second term will reduce as well, which could make I-TSA concentrate on exploitation in the later stage and thus enhance the convergence performance of the algorithm. Figure 3-2 show the procedures of the developed I-TSA.

3.4 Numerical Studies

In this section, the accuracy and performance of using the proposed approach for nonlinear system identification will be demonstrated with numerical simulations and compared with several existing state-of-the-art methods. Since variables of nonlinear structures can continuously distribute in the feasible solution space, this is generally considered as a continuous function optimization problem. Firstly, comprehensive benchmark functions are utilized to verify and compare the accuracy and performance of the proposed approach against the latest methods. Secondly, a Single Degree Of Freedom (SDOF) system with three nonlinear hysteretic models respectively is taken as an example to validate the proposed approach, and compare the nonlinear model parameter identification results with the enhanced sensitivity method as presented in one of the latest studies (Lu et al., 2017). Finally, the proposed approach is applied to identify the system parameters of a seven-storey shear building. The system parameters to be identified in this structure include the external forces, stiffness, damping, and nonlinear parameters. The accuracy of identification results will be compared with several existing heuristic algorithms to demonstrate the superiority of the proposed approach.

Step 1. The initialization of the algorithm

Set the population size CS , ST parameter for the algorithm and the dimension of the problem D

Decide the termination condition

Generate CS random tree locations with D dimension in the search space using Eq. (3.19)

Evaluate the tree locations using objective function based on Eq. (3.16)

Select the best-so-far solution \mathbf{B}

Step 2. Lévy search mechanism for the Best-so-far solution

Randomly choose an individual T_i from the Colony

Initialize $t = 1, \sigma_v = 1$, and compute σ_u according to Eq. (3.23)

While ($t \leq t_{\max}$) %% t_{\max} denotes the times of operating Lévy flight

 Generate a new feasible solution according Eq. (3.20) to (3.25)

 Calculate the objective value, marked as $f(\mathbf{B}(t+1))$

 Apply the greedy selection between $f(\mathbf{B}(t))$ and $f(\mathbf{B}(t+1))$

End While

Step 3. Searching with seeds

For all trees

 Decide the number of seeds produced for this tree.

For all dimensions

If (rand > ST)

 Update this dimension using Eq. (3.28)

Else

 Update this dimension using Eq. (3.18)

End If

End For

End For

 Select the best seed and compare it with the tree. If the seed location is better than the tree's, the seed substitutes this tree.

End For

Step 4. Selection of Best Solution

 Select the best solution in every iteration. If new best solution is better than the previous best solution, new best solution substitutes the previous solution.

Step 5. Testing Termination condition and reporting

 If termination condition is not met, go to Step 2. Otherwise, report the best solution.

Figure 3-2 The pseudo code of I-TSA.

3.4.1 Benchmark Study

Independent contribution analysis of these two modifications

To justify the contributions of the proposed two modifications, the classical benchmark functions (Gao et al., 2015; Karaboga & Basturk, 2008) have been used for the first benchmark study. For the comparison purpose, the same maximum calculation time for the involved algorithms, i.e. TSA, TSA with modification 1 (TSA with M1), TSA with modification 2 (TSA with M2) and I-TSA are set as 60 seconds per run. The computer used for calculation is deployed with Intel-I5-Core. The parameters are defined as $CS = 40$, $ST = 0.45$, and the number of operating Lévy flight is set as 100. The used benchmark functions are listed in Table 3-1. 30 runs are conducted independently, and the mean values and standard deviation (Std) of identification results are obtained. The results are shown in Table 3-2. It can be observed that using TSA with M1 and TSA with M2 can improve the identification results over the original TSA. However better identification results with smaller errors can be obtained with I-TSA. Figure 3-3 shows the convergence processes of using different algorithms to optimize Griewank and Rastrigin functions. It is noted that for optimizing the Griewank function, the main improvement contribution comes from TSA with M2, which is beneficial to improve the convergence performance. When tackling the Rastrigin function, TSA with M1 plays a more significant role in escaping the local minimal. The results in Table 3-2 and Figure 3-3 demonstrate that both the modifications can be useful for improving the performance of TSA independently and the proposed I-TSA can provide the best identification results for most of benchmark functions.

Table 3-1 Classical benchmark functions employed for tests.

Function	Range	Dimension	Type
Sphere	[-100, 100]	30	Uni-modal, Separable
Schaffer	[-100, 100]	5	Multi-modal, Non-separable
Ackley	[-32, 32]	30	Multi-modal, Non-separable
Rastrigin	[-5.12, 5.12]	30	Multi-modal, Separable
Rosenbrock	[-30, 30]	15	Uni-modal, Non-separable
Griewank	[-600, 600]	15	Multi-modal, Non-separable

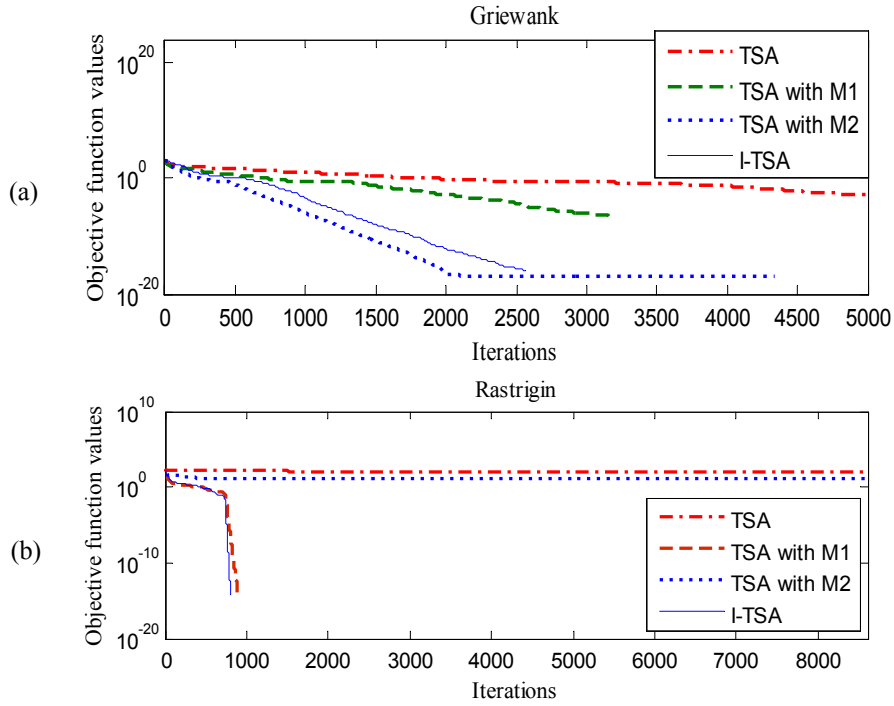


Figure 3-3 The iteration process of two benchmark functions: (a) Griewank; (b) Rastrigin.

Table 3-2 Classical benchmark tests results.

Function name	TSA		TSA with M1		TSA with M2		I-TSA	
	Mean	Std	Mean	Std	Mean	Std	Mean	Std
Sphere	0	0	0	0	0	0	0	0
Schaffer	3.12E-03	3.39E-14	7.76E-06	4.46E-15	1.82E-18	6.69E-18	0	0
Ackley	3.55E-15	0	3.13E-15	0	3.32E-15	0	3.13E-15	0
Rastrigin	85.56	9.36	0	0	13.37	5.57	0	0
Rosenbrock	5.18E-07	7.32E-07	3.88E-09	7.71E-09	4.65E-07	1.44E-07	1.32E-9	6.65E-9
Griewank	7.44E-03	1.66E-03	1.03E-05	2.19E-05	0	0	0	0

Note: The bold values denote the best identification results.

CEC benchmark tests

To verify the effectiveness of using I-TSA for the continuous function optimization, CEC 2014 benchmark functions (Liang et al., 2013) are used for tests. To compare with the results in the references, all experiments are conducted on dimensions $D = 10$, $D = 30$ and $D = 50$ for a maximum number of $10000 \times D$ function evaluations. These CEC benchmarks involve

Unimodal Functions ($F_1 \sim F_3$), Simple Multimodal Functions ($F_4 \sim F_{16}$), Hybrid Functions ($F_{17} \sim F_{22}$) and Composite Functions ($F_{23} \sim F_{30}$), which can be used to well demonstrate the capacity of the optimization algorithms. Several latest and powerful algorithms including the Gbest-guided artificial bee colony algorithm (GABC) (Zhu & Kwong, 2010), 2011-version Particle Swarm Optimization algorithm (SPSO) (Zambrano-Bigiarini et al., 2013), Global-best Brain Storm Optimization algorithm (GBSO) (EI-Abd, 2017), and winner algorithm for CEC 2014---an Adaptive DE with Linear Population Size Reduction Mechanism (LSHADE) (Tanabe & Fukunage, 2014) are employed for comparison in this benchmark study. Regarding the parameters setting for I-TSA, $CS = 40$, $ST = 0.45$, and the number of the Lévy flight is 100. Tables 3-3 to 3-5 show the errors in the final optimization results from these algorithms and the proposed approach for $10D$, $30D$ and $50D$, respectively.

Results demonstrate that no algorithm could outperform all the other competitors on all the benchmark functions. For example, for the optimization results of $10D$ as shown in Table 3-3, GABC offers better optimization results on F_8 , F_{23} and F_{26} ; GBSO performs well in functions F_{12} and F_{24} . LSHADE is the best performer for 17 functions, i.e. $F_1 \sim F_3$, F_6 , $F_8 \sim F_{11}$, F_{14} , F_{17} , F_{18} , $F_{20} \sim F_{22}$, F_{24} , F_{27} and F_{29} . The proposed I-TSA provides the best results on 10 functions, i.e., F_4 , F_5 , F_7 , F_{13} , F_{15} , F_{16} , F_{19} , F_{25} , F_{28} and F_{30} . This is because LSHADE utilizes several advanced mechanisms that are not integrated in the proposed I-TSA, including the success-history based adaption of its parameters, the use of an external archive and the linear reduction of the population size (EI-Abd, 2017; Tanabe & Fukunage, 2014). All these techniques could be the promising future research directions to further enhance the performance of the proposed I-TSA. Overall, even comparing with the state-of-the-art and winner algorithms on CEC14 benchmark functions, the results from the proposed I-TSA still demonstrates the superiority on a number of test functions, which lays the foundation for the following nonlinear system identification

Table 3-3 Performance of I-TSA on CEC14 Functions---Results of 10D.

Benchmark	GABC		SPSO		GBSO		LSHADE		I-TSA	
Function	Mean	std.	Mean	std.	Mean	std.	Mean	std.	Mean	std.
1	9.84E+04	7.41E+04	2.04E+04	1.08E+04	4.75E+04	4.85E+04	0.00E+00	0.00E+00	4.59E+04	1.76E+04
2	6.91E+01	1.32E+02	9.51E+02	1.06E+03	2.23E+03	2.15E+03	0.00E+00	0.00E+00	1.01E+03	7.93E+02
3	1.05E+02	1.08E+02	1.24E+03	7.08E+02	4.70E+02	7.70E+02	0.00E+00	0.00E+00	8.89E+01	7.06E+01
4	3.13E-03	4.18E-03	2.36E+01	1.61E+01	2.61E+01	1.49E+01	2.94E+01	1.26E+01	1.45E-03	1.18E-03
5	1.68E+01	7.35E+00	1.88E+01	5.11E+00	1.57E+01	8.32E+00	1.41E+01	8.76E+00	1.22E+01	7.68E-02
6	8.96E-01	4.99E-01	3.18E-01	6.19E-01	4.50E-01	8.71E-01	1.75E-02	1.25E-01	9.65E-02	7.33E-02
7	4.81E-03	6.78E-03	2.13E-02	1.76E-02	5.59E-02	2.93E-02	3.04E-03	6.51E-03	0.00E+00	0.00E+00
8	0.00E+00	0.00E+00	5.21E+00	2.32E+00	3.48E-02	1.61E-01	0.00E+00	0.00E+00	1.39E+00	1.71E+00
9	4.09E+00	1.37E+00	4.44E+00	2.10E+00	2.95E+00	1.21E+00	2.34E+00	8.40E-01	2.67E+00	1.20E+00
10	3.31E-02	3.46E-02	3.57E+02	1.81E+02	1.97E+00	2.40E+00	8.57E-03	2.17E-02	6.59E+01	5.50E+01
11	1.58E+02	1.06E+02	4.28E+02	2.76E+02	1.04E+02	8.01E+01	3.21E+01	3.83E+01	1.86E+02	2.36E+02
12	2.15E-01	6.48E-02	5.39E-01	1.59E-01	8.37E-03	1.37E-02	6.82E-02	1.92E-02	8.80E-03	4.69E-02
13	1.09E-01	1.83E-02	6.16E-02	2.72E-02	5.05E-02	2.12E-02	5.16E-02	1.51E-02	1.42E-02	0.00E+00
14	9.71E-02	2.42E-02	1.13E-01	5.30E-02	1.31E-01	6.04E-02	8.14E-02	2.55E-02	1.22E-01	5.02E-02
15	6.22E-01	1.25E-01	9.33E-01	1.97E-01	8.03E-01	2.54E-01	3.66E-01	6.92E-02	2.88E-01	1.50E-01
16	1.72E+00	3.48E-01	1.84E+00	4.35E-01	1.20E+00	5.79E-01	1.24E+00	3.03E-01	1.05E+00	5.28E-01
17	1.22E+05	1.02E+05	1.51E+03	1.51E+03	1.39E+03	1.66E+03	9.77E-01	1.08E+00	3.43E+03	3.03E+03
18	5.88E+02	5.42E+02	1.66E+03	2.63E+03	8.18E+03	6.48E+03	2.44E-01	3.14E-01	2.02E+00	1.66E-01
19	1.52E-01	6.33E-02	2.24E+00	5.71E-01	8.63E-01	3.31E-01	7.73E-02	6.40E-02	5.31E-02	6.44E-02
20	3.80E+02	5.84E+02	1.84E+02	2.48E+02	3.53E+02	8.12E+02	1.85E-01	1.80E-01	9.62E+01	2.25E+01
21	5.91E+03	5.89E+03	1.03E+03	1.06E+03	2.93E+02	3.18E+02	4.08E-01	3.09E-01	3.73E+01	5.38E+01
22	1.87E-01	1.18E-01	2.86E+01	7.29E+00	2.63E+01	4.49E+01	4.41E-02	2.82E-02	1.60E+01	1.03E+01
23	2.70E+02	1.22E+02	3.29E+02	0.00E+00	3.29E+02	2.30E-13	3.29E+02	2.87E-13	3.29E+02	3.93E-06
24	1.13E+02	2.71E+00	1.12E+02	4.32E+00	1.07E+02	3.99E+00	1.07E+02	2.28E+00	1.12E+02	2.12E+00
25	1.25E+02	4.75E+00	1.81E+02	2.74E+01	1.78E+02	3.17E+01	1.33E+02	4.04E+01	4.88E+01	2.56E+01
26	9.73E+01	1.56E+01	1.00E+02	2.56E-02	1.00E+02	1.97E-02	1.00E+02	1.63E-02	1.00E+02	2.89E-02
27	9.85E+01	1.58E+02	2.61E+02	1.49E+02	2.49E+02	1.14E+02	5.81E+01	1.34E+02	2.62E+02	1.76E+02
28	3.62E+02	5.84E+00	3.96E+02	5.39E+01	4.30E+02	6.51E+01	3.81E+02	3.17E+01	3.45E+02	1.04E+00
29	2.97E+02	4.02E+01	4.91E+02	1.39E+02	1.21E+05	4.11E+05	2.22E+02	4.43E-01	4.49E+02	2.21E+02
30	5.27E+02	6.75E+01	7.75E+02	3.02E+02	5.76E+02	1.16E+02	4.65E+02	1.33E+01	3.59E+02	5.91E+00

Note: The bold values denote the best identification results and the results of other algorithms are extracted from Refs (EI-Abd, 2017; Tanabe & Fukunage, 2014).

Table 3-4 Performance of I-TSA on CEC14 Functions---Results of 30D.

Benchmark	GABC		SPSO		GBSO		LSHADE		I-TSA	
Function	Mean	std.	Mean	std.	Mean	std.	Mean	std.	Mean	std.
1	4.95E+06	3.93E+06	2.74E+05	1.55E+05	8.38E+05	4.94E+05	0.00E+00	0.00E+00	5.42E+05	3.99E+05
2	4.70E+01	7.18E+01	7.48E+03	5.10E+03	8.55E+03	7.48E+03	0.00E+00	0.00E+00	3.91E+03	2.45E+03
3	5.61E+02	5.04E+02	4.51E+03	1.54E+03	2.22E+02	2.96E+02	0.00E+00	0.00E+00	1.59E+02	1.38E+01
4	3.94E+01	3.15E+01	2.39E+01	3.27E+01	6.15E+01	1.83E+01	0.00E+00	0.00E+00	2.05E+01	3.41E+01
5	2.02E+01	5.89E-02	2.07E+01	9.98E-02	2.03E+01	3.33E-01	2.01E+01	3.68E-02	2.01E+01	4.49E-02
6	1.30E+01	1.79E+00	1.21E+01	2.50E+00	9.84E-01	1.18E+00	1.38E-07	9.89E-07	3.79E-01	1.12E-01
7	1.81E-08	4.73E-08	1.06E-02	1.28E-02	9.17E-03	9.68E-03	0.00E+00	0.00E+00	0.00E+00	0.00E+00
8	1.14E-13	1.03E-28	4.35E+01	1.04E+01	1.70E-01	4.16E-01	0.00E+00	0.00E+00	1.67E+01	2.18E+00
9	5.38E+01	9.20E+00	4.66E+01	1.28E+01	2.31E+01	6.82E+00	6.78E+00	1.48E+00	4.96E+00	6.21E-01
10	8.86E-01	1.57E+00	2.68E+03	5.63E+02	3.80E+00	2.27E+00	1.63E-02	1.58E-02	1.70E+02	7.39E+01
11	1.70E+03	2.68E+02	3.59E+03	6.74E+02	4.37E+02	2.56E+02	1.23E+03	1.83E+02	1.15E+03	1.58E-12
12	1.90E-01	5.71E-02	1.39E+00	2.93E-01	1.86E-02	2.07E-02	1.61E-01	2.29E-02	2.59E-02	2.42E-02
13	2.08E-01	2.62E-02	1.88E-01	4.04E-02	1.57E-01	4.36E-02	1.24E-01	1.75E-22	2.32E-02	4.58E-03
14	1.82E-01	1.58E-02	2.21E-01	4.08E-02	2.21E-01	4.03E-02	2.42E-01	2.98E-02	2.08E-01	3.64E-02
15	4.69E+00	9.99E-01	6.92E+00	2.69E+00	3.38E+00	7.13E-01	2.15E+00	2.51E-01	1.51E+00	8.04E-02
16	9.16E+00	4.43E-01	1.10E+01	4.66E-01	8.66E+00	7.46E-01	8.50E+00	4.58E-01	8.11E+00	4.46E-01
17	2.03E+06	1.34E+06	2.12E+04	1.47E+04	7.28E+04	4.65E+04	1.88E+02	7.50E+01	1.12E+04	1.01E+04
18	5.24E+03	5.75E+03	1.44E+03	1.55E+03	2.39E+03	3.24E+03	5.91E+00	2.89E+00	3.52E+00	1.12E+00
19	7.09E+00	9.24E-01	1.36E+01	2.53E+00	4.72E+00	1.02E+00	3.68E+00	6.80E-01	2.36E+00	7.76E-01
20	5.56E+03	2.13E+03	8.33E+02	4.31E+02	8.80E+01	3.10E+01	3.08E+00	1.47E+00	1.31E+02	1.36E+02
21	2.44E+05	1.75E+05	2.01E+04	1.58E+04	2.32E+04	1.53E+04	8.68E+01	8.99E+01	2.65E+04	2.39E+04
22	2.39E+02	1.15E+02	2.79E+02	9.59E+01	2.24E+02	9.10E+01	2.76E+01	1.79E+01	3.03E+02	2.12E+01
23	3.16E+02	6.50E-01	3.15E+02	6.39E-05	3.15E+02	1.55E-04	3.15E+02	4.02E-13	3.15E+02	1.05E-03
24	2.19E+02	1.74E+01	2.34E+02	7.04E+00	2.00E+02	5.98E-02	2.24E+02	1.06E+00	2.32E+02	4.21E+00
25	2.08E+02	1.36E+00	2.14E+02	2.47E+00	2.03E+02	3.05E-01	2.03E+02	4.96E-02	8.87E+01	2.47E-01
26	1.00E+02	5.86E-02	1.27E+02	4.49E+01	1.00E+02	3.90E-02	1.00E+02	1.55E-02	1.00E+02	3.92E-02
27	4.08E+02	2.88E+00	6.09E+02	1.24E+02	3.96E+02	7.11E+01	3.00E+02	2.40E-13	5.09E+02	7.41E+01
28	8.40E+02	3.39E+01	1.23E+03	2.82E+02	7.94E+02	7.80E+01	8.40E+02	1.40E+01	9.80E+02	3.85E+01
29	1.18E+03	2.25E+02	3.08E+06	6.24E+06	1.71E+05	1.21E+06	7.17E+02	5.13E+00	1.18E+03	9.22E+02
30	3.02E+03	8.46E+02	5.84E+03	1.79E+03	2.03E+03	6.51E+02	1.25E+03	6.20E+02	1.05E+03	6.05E+02

Note: The bold values denote the best identification results and the results of other algorithms are extracted from Refs (EI-Abd, 2017; Tanabe & Fukunage, 2014).

Table 3-5 Performance of I-TSA on CEC14 Functions---Results of 50D.

Benchmark	GABC		SPSO		GBSO		LSHADE		I-TSA	
Function	Mean	std.	Mean	std.	Mean	std.	Mean	std.	Mean	std.
1	1.10E+07	3.89E+06	7.92E+05	2.51E+05	2.22E+06	7.45E+05	1.24E+03	1.52E+03	9.35E+05	5.09E+05
2	6.74E+03	8.87E+03	7.77E+03	7.89E+03	9.26E+03	8.21E+03	0.00E+00	0.00E+00	5.88E+03	3.19E+03
3	6.72E+03	2.82E+03	1.17E+03	3.34E+02	1.59E+03	8.57E+02	0.00E+00	0.00E+00	3.54E+02	9.59E+01
4	6.34E+01	2.98E+01	7.76E+01	3.35E+01	9.66E+01	2.90E+00	5.89E+01	4.56E+01	4.21E+01	3.56E+01
5	2.01E+01	7.40E-02	2.09E+01	9.24E-02	2.09E+01	3.73E-01	2.02E+01	4.59E-02	2.12E+01	6.54E-02
6	2.74E+01	2.10E+00	3.06E+01	3.13E+00	2.08E+00	1.65E+00	2.64E-01	5.23E-01	1.94E+00	4.23E-01
7	2.56E-04	8.99E-04	6.55E-03	1.31E-02	3.04E-03	4.34E-03	0.00E+00	0.00E+00	0.00E+00	0.00E+00
8	2.20E-13	2.88E-14	1.14E+02	2.23E+01	1.47E+00	1.30E+00	2.58E-09	7.48E-09	3.35E+01	1.03E+01
9	1.23E+02	1.43E+01	1.28E+02	2.53E+01	4.76E+01	1.06E+01	1.14E+01	2.13E+00	5.87E+00	2.72E-01
10	9.62E-01	1.25E+00	5.92E+03	9.42E+02	6.76E+00	6.01E+00	1.22E-01	4.13E-02	1.09E+03	2.71E+02
11	3.98E+03	4.50E+02	6.95E+03	1.09E+03	1.58E+03	5.25E+02	3.22E+03	3.30E+02	8.02E+03	4.75E+03
12	1.84E-01	3.90E-02	2.15E+00	3.93E-01	1.80E-02	1.30E-02	2.19E-01	2.82E-02	5.01E-02	2.70E-02
13	2.65E-01	3.86E-02	3.48E-01	7.08E-02	2.56E-01	4.56E-02	1.60E-01	1.83E-02	3.62E-02	6.04E-03
14	2.19E-01	1.40E-02	2.87E-01	3.33E-02	2.36E-01	6.71E-02	2.97E-01	2.47E-02	2.12E-01	2.06E-02
15	1.22E+01	1.79E+00	2.56E+01	7.36E+00	6.36E+00	1.25E+00	5.15E+00	5.08E-01	4.43E+00	1.01E-01
16	1.73E+01	5.65E-01	2.04E+01	5.29E-01	1.71E+01	8.47E-01	1.69E+01	4.81E-01	2.14E+01	2.99E-01
17	3.11E+06	1.59E+06	3.72E+04	2.02E+04	1.89E+05	1.51E+05	1.40E+03	5.13E+02	3.66E+04	2.75E+04
18	2.19E+03	1.45E+03	1.86E+03	1.06E+03	1.51E+03	1.45E+03	9.73E+01	1.38E+01	5.68E+01	4.78E+00
19	1.84E+01	2.56E+00	5.51E+01	1.94E+01	1.15E+01	1.37E+00	8.30E+00	1.81E+00	1.01E+01	7.74E+00
20	2.71E+04	6.94E+03	8.25E+02	2.55E+02	1.84E+02	4.61E+01	1.39E+01	4.56E+00	3.75E+02	7.45E+02
21	1.84E+06	8.64E+05	4.64E+04	2.22E+04	1.44E+05	7.87E+04	5.15E+02	1.49E+02	3.64E+04	2.02E+04
22	6.80E+02	1.98E+02	7.57E+02	2.50E+02	2.74E+02	1.40E+02	1.14E+02	7.50E+01	4.40E+02	2.97E+02
23	3.46E+02	2.28E+00	3.44E+02	3.59E-02	3.44E+02	1.60E-03	3.44E+02	4.44E-13	3.44E+02	2.34E-13
24	2.59E+02	2.49E+00	2.88E+02	6.81E+00	2.56E+02	2.51E+00	2.75E+02	6.62E-01	2.71E+02	4.27E+00
25	2.15E+02	1.64E+00	2.31E+02	4.46E+00	2.07E+02	8.45E-01	2.05E+02	3.65E-01	1.16E+02	9.50E-01
26	1.00E+02	7.85E-02	1.63E+02	4.89E+01	1.32E+02	4.68E+01	1.00E+02	7.85E-02	1.00E+02	5.35E-02
27	1.07E+03	1.83E+02	1.15E+03	1.22E+02	4.35E+02	5.76E+01	3.33E+02	3.03E+01	6.73E+02	2.48E+00
28	1.35E+03	1.33E+02	2.87E+03	7.01E+02	1.07E+03	7.14E+01	1.11E+03	2.91E+01	1.55E+03	8.74E-01
29	2.00E+03	6.43E+02	4.79E+07	7.40E+07	2.46E+03	6.22E+02	7.95E+02	2.40E+01	1.37E+03	2.56E+02
30	9.92E+03	7.28E+02	2.71E+04	5.73E+03	9.11E+03	6.40E+02	8.66E+03	4.13E+02	7.72E+03	4.01E+02

Note: The bold values denote the best identification results and the results of other algorithms are extracted from Refs (EI-Abd, 2017; Tanabe & Fukunage, 2014).

3.4.2 Nonlinear model parameter identification for a SDOF system

The first numerical example is a hysteretic Single Degree Of Freedom (SDOF) system (Lu et al., 2017), which is used to verify the proposed approach in identifying the nonlinear hysteretic parameters. The SDOF system is shown in Figure 3-4. The physical parameters are defined as: mass $m=1$, stiffness $k=1$ and damping $c=0.2$. The external loading is defined as $F(t)=2\cos(t)$, and the restoring force r is calculated from three nonlinear hysteretic models with parameters listed in Table 3-6. The initial displacement, velocity and restoring force of the system are all set as zero. For the parameters setting, the colony size, the search tendency, the number of the Lévy flight and the search range are defined as 40, 0.45, 100 and $[0, 5]$, respectively. The termination rule is set as the maximum evaluation time. For the nonlinear system identification in this study, considering that 100 iterations are sufficient for the proposed approach and the existing methods used for comparison, the computational time based on 100 iterations is used as the maximum evaluation time for the termination. Therefore 1335 seconds is used as the maximum function evaluation time for the identification of this SDOF system.

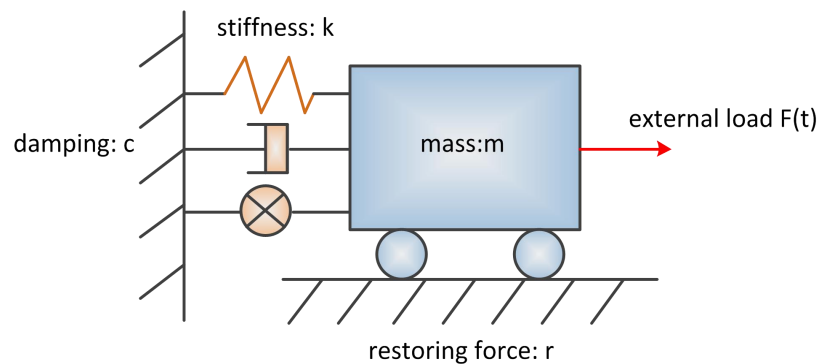


Figure 3-4 A nonlinear SDOF system with hysteretic effect.

Case 1: identification of the Bouc-Wen nonlinear model parameters

The proposed I-TSA is applied to identify the parameters of the Bouc-Wen nonlinear model. The objective is to identify the Bouc-Wen parameters $\mathbf{P}(p_1=2, p_2=1, p_3=0.5, p_4=2)$. To compare the accuracy of using the enhanced

sensitivity method (Lu et al., 2017), the original TSA and the proposed approach, with the same response data, namely 10s acceleration response with a sampling rate of 100Hz, are used. Figure 3-5 shows the evolutionary process of the objective function values. It can be observed that the objective function value by using I-TSA converges quickly to zero, however, the original TSA suffers the slow-convergence problem after a few iterations. The final identification results in this case are shown in Table 3-6. It shows that the proposed I-TSA can identify the Bouc-Wen nonlinear model parameters exactly, but the maximum errors of using the enhanced sensitivity method and TSA are 0.04% and 0.10%, respectively.

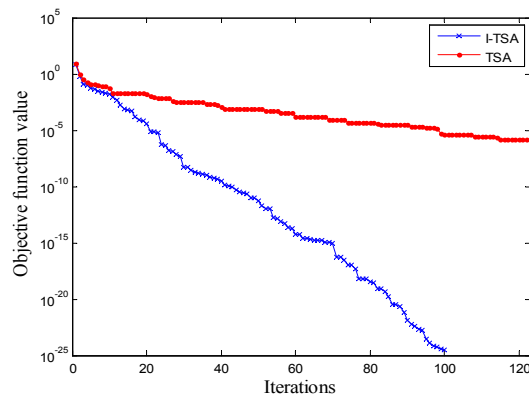


Figure 3-5 The evolution process of the objective function in Case 1 (without noise).

When 10% white noise is added into the acceleration response, the evolution processes of nonlinear parameter identification by using I-TSA are shown in Figure 3-6. It can be observed that the updating process based on I-TSA is more stable and converge quicker. It only takes around 48 iterations for the proposed approach to converge to the true values, with a better performance than the original TSA. The final results are also listed in Table 3-6. The maximum identification errors of using the standard TSA and I-TSA are 2.97% and 0.88%, respectively. Figure 3-7 presents the hysteresis loops calculated with true and identified nonlinear model parameters. It can be seen that a very good agreement between these two curves is obtained, indicating the nonlinear parameters are identified accurately.

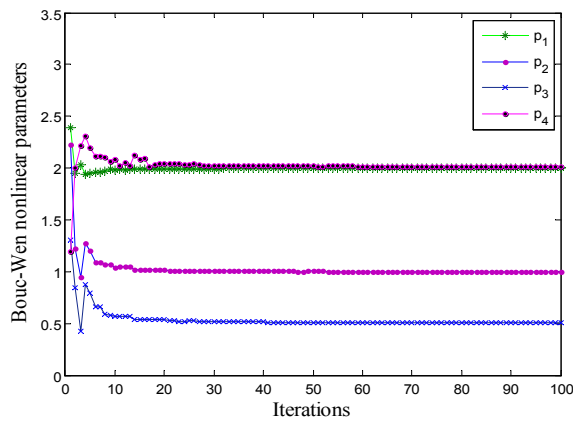


Figure 3-6 The evolution process of the nonlinear parameter identification in Case 1 with 10% noise effect by using I-TSA.

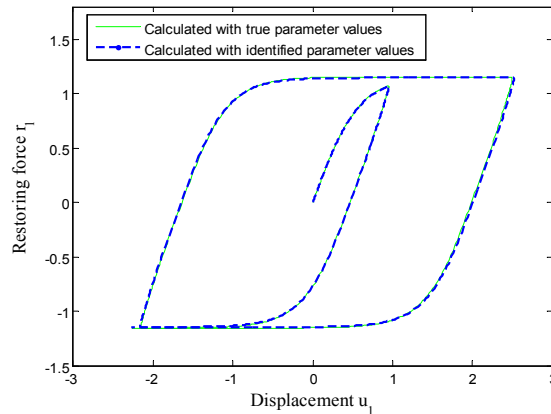


Figure 3-7 The true and identified hysteresis loop in Case 1 (with noise).

Case 2: identification of bilinear model with kinematic hardening considering noise effect

A bi-linear model with Kinematic hardening is used for further verification. The nonlinear model parameters are defined as $\mathbf{P}(p_1=1, p_2=2, p_3=1)$. 10% white noise is smeared into the 10s acceleration response, which will be used for identification. The identification results for this case are listed in Table 3-6, and the maximum error of using the I-TSA is only 0.53%, which is better than those acquired by using the standard TSA (1.80%) and enhanced sensitivity method (0.89%). The simulated response and calculated response with the identified parameters are shown in Figure 3-8. It is observed that a very good match is achieved.

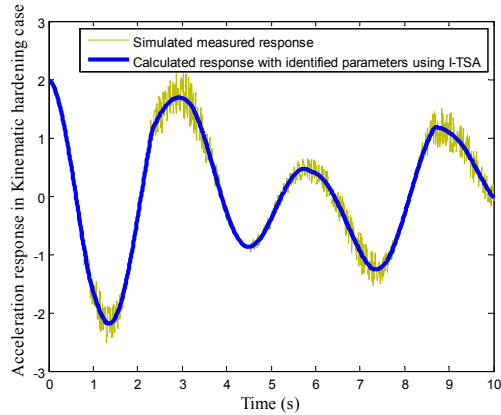


Figure 3-8 The simulated measured response and calculated response with identified parameters in Case 2.

Case 3: identification of the bilinear model with the equal yielding force considering noise

In this case, the bilinear model with the equal yielding force is used. Similar to Case 2, The parameters of this bilinear model are defined as $\mathbf{P}(p_1 = 3, p_2 = 1, p_3 = 1)$. 10s acceleration response with a 10% white noise are used for identification. The identified results of these parameters are shown in Table 3-6. It can be observed that the maximum error of using the I-TSA is only 0.18%, however, the errors from the standard TSA and enhanced sensitivity method are 0.67% and 0.49%, respectively. On the other hand, a smaller standard deviation is obtained from I-TSA than the original TSA, even with a significant noise effect in the measurements.

Figure 3-9 shows the colony distributions at the initialization and 381 seconds. Specifically, taking the identification of the first two variables as an example, the global optima shall be at $(p_1 = 3, p_2 = 1)$. It is observed from Figure 3-9 that at the initialization, the colonies from both the standard TSA and the proposed I-TSA are randomly distributed in the feasible solution space. After 381 seconds, the individuals from the I-TSA quickly converge to the true values. However when using TSA, the variance in the generated populations and the distance to the true values are larger than those from the proposed algorithm. This also well demonstrates that the convergence performance of the proposed I-TSA is significantly improved, and an accurate identification results can be obtained.

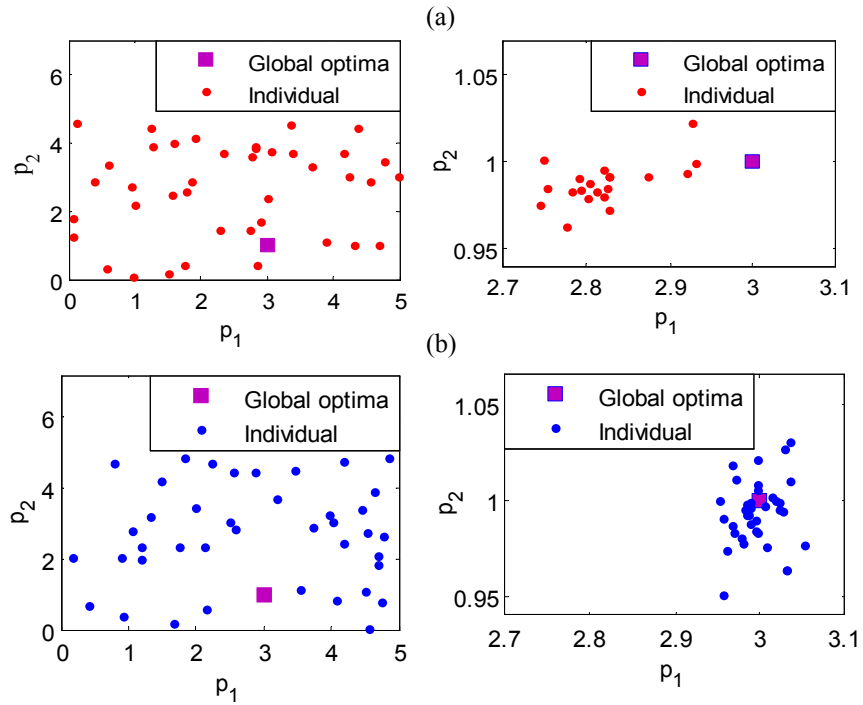


Figure 3-9 The colony distributions at the initial time instant and 381 seconds:

(a) TSA; (b) I-TSA.

Table 3-6 Identified results for a SDOF system with different nonlinear models.

Parameters	True values	Enhanced sensitivity	TSA		I-TSA		
		method	Mean	Std	Mean	Std	
Case 1	p1	2	1.9999	2.0002	0.0003	2.0000	0
	p2	1	1.0001	0.9997	0.0002	1.0000	0
	p3	0.5	0.4998	0.4995	0.0017	0.5000	0
	p4	2	2.0002	1.9991	0.0006	2.0000	0
	Maximum error		0.04%	0.10%		0	
Case 1 with 10% noise	p1	2	2.0559	2.0079	0.0159	1.9984	0.0065
	p2	1	1.0025	1.0011	0.0311	1.0022	0.0109
	p3	0.5	0.5758	0.4902	0.0489	0.5061	0.0145
	p4	2	1.8598	1.9405	0.0063	2.0175	0.0176
	Maximum error		16.60%	2.97%		0.88%	

Table 3-6 Identified results for a SDOF system with different nonlinear models (Continues)

Case 2	p1	1	1.0070	1.0191	0.0093	1.0043	0.0042
	p2	2	1.9874	1.9641	0.0172	1.9895	0.0019
	p3	1	1.0089	1.0130	0.0277	1.0053	0.0024
Maximum error			0.89%	1.80%		0.53%	
Case 3	p1	3	2.9935 ⁺	2.9982	0.0006	2.9998	0.0000
	p2	1	0.9962 ⁺	1.0067	0.0047	0.9982	0.0040
	p3	1	1.0049 ⁺	1.0043	0.0053	1.0003	0.0019
Maximum error			0.49%	0.67%		0.18%	

3.4.3 Nonlinear model parameter identification for a MDOF system

The above examples demonstrate that accurate identification results for a SDOF system with three different nonlinear models can be obtained by using I-TSA, which performs better than the original TSA and the enhanced sensitivity method. In this section, the performance and accuracy of the proposed approach will be compared with those of using several existing state-of-the-art heuristic algorithms for the nonlinear model parameter identification of a MDOF system. Based on the same reason explained at the beginning of Section 3.4.2, the maximum evaluation time is set as 7530 seconds for the nonlinear parameter identification of this MDOF system.

A seven-storey shear building (Lu et al., 2017) with nonlinearities is built as shown in Figure 2-10. Structural properties are defined as: mass of each storey $m=1$, stiffness $k=1$ and the linear damping $c=0.1$. To simulate the seismic isolation (Yar & Hammond, 1987), in this study, the bilinear hysteretic model with kinematic hardening is introduced in the first floor. Following the force used in previous studies (Lu et al., 2017), the external base excitation is assumed as a cosine function which is given as

$$a_g = A \cos(\omega \cdot t) v(t; t_0, t_n); \quad v(t; t_0, t_n) = \begin{cases} (t/t_0)^2, & t \leq t_0 \\ 1, & t_0 < t \leq t_n \\ e^{-0.2(t-t_n)}, & t > t_n \end{cases} \quad (2-30)$$

where A is the amplitude and its value is 2, ω represents the frequency of the external force and the value is 1, and $v(t; t_0, t_n)$ is a window function so that the excitation mainly occurs during $[t_0, t_n]$ and in this example, it is assumed that

$t_0 = 2, t_n = 6$. Figure 2-11 shows the hysteretic effect between the displacement and the restoring force with kinematic hardening.

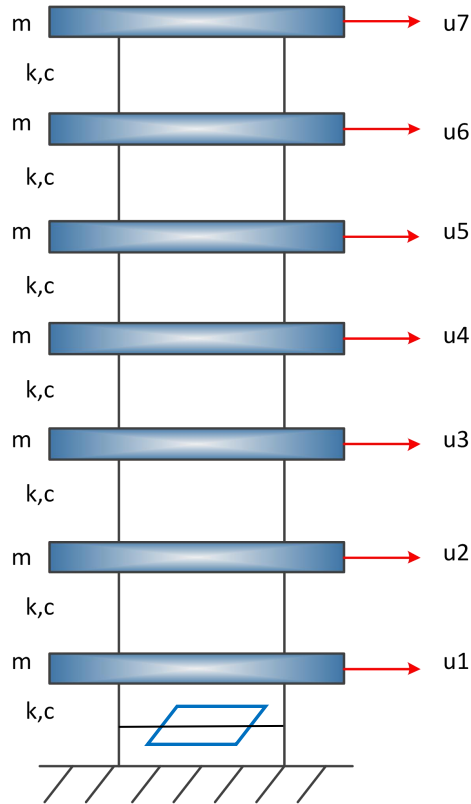


Figure 3-10 A seven-storey shear building with nonlinear hysteretic effect.

It shall be noted that a more complex identification problem is defined with more unknown parameters. The external force parameters, stiffness, damping and nonlinear model parameters are included in the parameter vector to be identified, which increases the difficulty of the identification problem, compared to existing studies only considering nonlinear model parameters (Sun et al., 2013). It should be noted that the parameters to be identified only include the amplitude A and frequency ω of the external force, the parameters of the bilinear model with kinematic hardening, stiffness and damping. Other parameters can also be identified similarly. To visualize the parameter identification results clearly, the normalized damping and stiffness values against the true values are presented. Therefore, the true objective parameter vector \mathbf{S} to be identified in this case includes $S_1 = 2$ (amplitude for the external force), $S_2 = 1$

(frequency of the external force), $S_3 = 1, S_4 = 2, S_5 = 1$ (nonlinear modal parameters), $S_6 = 1, S_7 = 1$ (normalized stiffness and damping parameters). It should be noted that these parameter values in this system are assumed, not based on the physical system dimensions or material properties. This is fine to use this system to demonstrate the effectiveness and performance of the proposed approach since the system parameters such as stiffness and mass, can be normalized against their initial values.

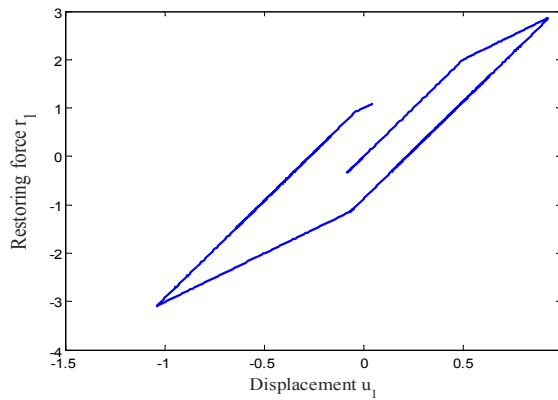


Figure 3-11 The hysteresis loop of a bilinear model in the shear building.

Case 4: Comparisons with existing heuristic algorithms

To compare the performance with other heuristic algorithms on the nonlinear identification of MDOF systems, the modified artificial bee colony algorithm (MABC) (Sun et al., 2013), differential evolutionary algorithm (DE) (Kyprianou et al., 2001), Genetic programme (GP) algorithm (Garg et al., 2016) and standard TSA are used for identification with the same data. For the setting of the common parameters, the colony size is set as 40 and the evaluation time is set as 7,530 seconds per run. The search range is defined as [0,5]. The acceleration responses from the 2nd to 5th floors with a duration of 30s and a sampling rate of 100Hz are used for the identification. Specifically, for TSA, ST is set as 0.45; for MABC, the parameter '*limit*' is set as 175 (Karaboga & Basturk, 2008). When using DE, the *rand/bin/1* operator is used to mutate, and the mutation rate is defined as 0.8. For the GP, the crossover, mutation and reproduction rate are 0.85, 0.1 and 0.05, respectively.

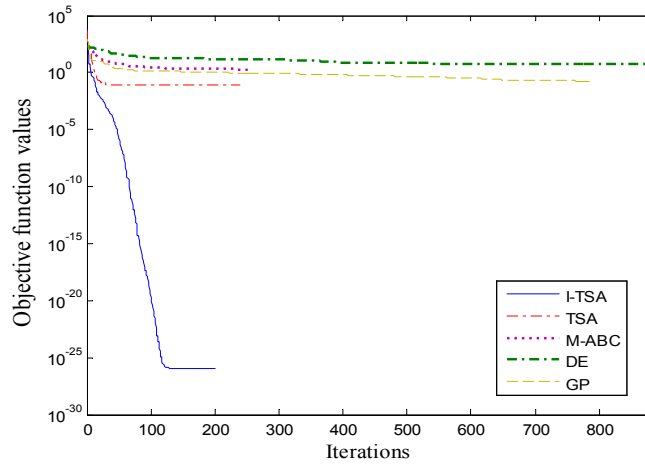


Figure 3-12 Comparison of the evolutionary processes in objective function values by using different approaches in Case 4.

Table 3-7 Comparisons between I-TSA and other heuristic algorithms on the identification of a nonlinear seven-storey shear building.

	True values	MABC		DE		GP		TSA		I-TSA	
		Mean	Std	Mean	Std	Mean	Std	Mean	Std	Mean	Std
s1	2	2.0124	0.0078	1.9987	0.0141	2.0841	0.0033	2.0031	0.0008	2.0000	0
s2	1	1.0068	0.0024	1.0079	0.0084	1.0042	0.0047	1.0000	0.0002	1.0000	0
s3	1	1.1782	0.3267	1.2641	0.2455	1.1134	0.2231	1.0482	0.0328	1.0000	0
s4	2	2.2464	0.5962	2.3766	0.6645	2.1766	0.3798	1.9275	0.0241	2.0000	0
s5	1	1.1896	0.2782	1.3793	0.6732	1.1277	0.1109	1.0591	0.0132	1.0001	8.1E-05
s6	1	0.9998	0.0075	1.0045	0.0517	1.0001	0.0017	0.9982	0.0009	1.0000	0
s7	1	0.9997	0.0098	0.9988	0.0159	0.9998	0.0026	0.9999	0.0004	1.0000	0
Maximum error		18.96%		37.66%		12.77%		5.91%		0.01%	

Figure 3-12 shows the evolutionary process of objective function values by using the proposed approach and the above-mentioned existing methods within the same evaluation time. It is clearly seen that the proposed algorithm achieves a very small error at a magnitude of 10^{-27} , with a much faster convergence speed than other methods. This also indicates that good identification results can be obtained. In contrast, GP, DE and MABC have been stuck with the local optima and the same situation can be observed in the original TSA, which confirms that the TSA easily ceases evolution

when facing more complex case, as mentioned in Section 3.3. When no noise effect is considered in the “simulated” acceleration responses, the identification results from all these different methods are listed in Table 3-7. It can be observed that errors in the identification results of using MABC, DE and GP are a little significant. Using TSA obtains a relatively good result with the maximum error equal to 5.91%. The obtained maximum error from the proposed approach is only 0.01%, demonstrating again the improvement in the identification accuracy of a complex nonlinear parameter identification problem.

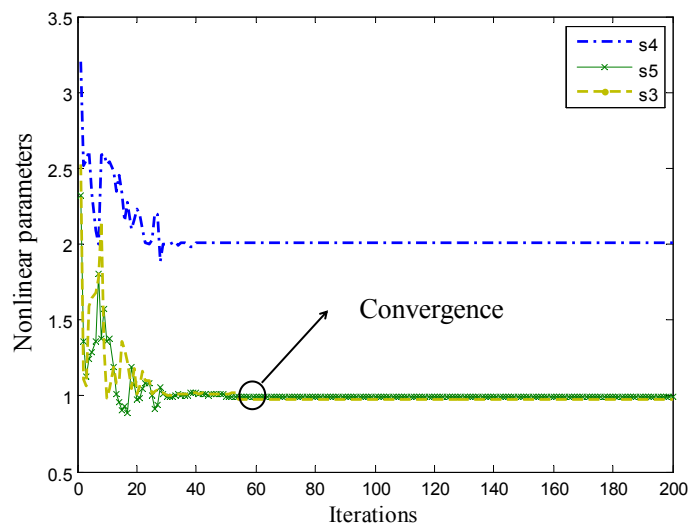


Figure 3-13 The identified system parameters by using responses with 5% noise.

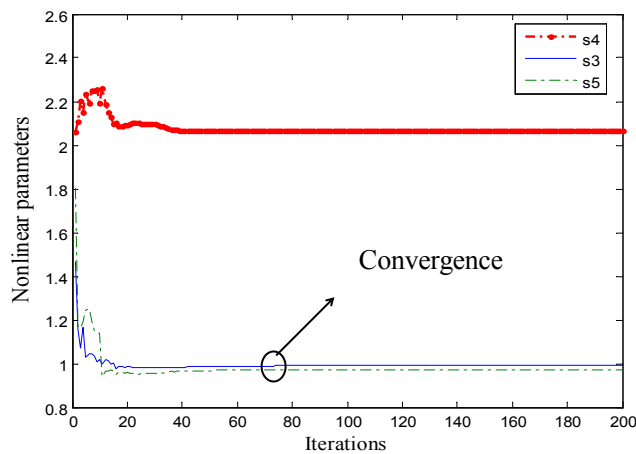


Figure 3-14 The identified system parameters by using responses with 10% noise.

To investigate the noise effect on the identification accuracy, two different noise levels, namely, 5% and 10%, are added into the original response data and then used for the identification. Since it has been demonstrated that I-TSA performs much better than MABC, DE and GP, only the proposed algorithm is used to conduct identification with noisy responses. Figure 3-13 presents the iteration process of the identified nonlinear parameters with the noisy response including 5% white noise. It can be seen that only after fifty iterations, all the parameters converge quickly to the preset true values and the evolutionary curves are quite stable. This demonstrates the good robustness of the proposed approach. Figure 3-14 shows the iteration process of the identified parameters by using acceleration responses with 10% noise. It can be seen that the evolutionary process is stable and the identified values converge quickly to the true values, although a high level noise is included in the acceleration responses. As can be observed from Table 3-8, the maximum errors in the identification of nonlinear parameters of 5% and 10% noise levels by using the proposed approach are 2.79% and 4.02%, respectively. This well demonstrate the robustness and superiority of using I-TSA for nonlinear system identification, even with noisy response data.

Table 3-8 Identification of a nonlinear seven-storey shear building under different noise.

Parameters	True values	Without noise		5% noise		10% noise	
		Mean	Std	Mean	Std	Mean	Std
s1	2	2.0000	0	2.0014	2.001E-06	2.0023	0.0030
s2	1	1.0000	0	1.0000	8.811E-07	1.0000	0.0001
s3	1	1.0000	0	0.9721	2.126E-04	0.9897	0.0113
s4	2	2.0000	0	2.0118	3.665E-04	2.0647	0.0129
s5	1	1.0001	8.11E-05	0.9923	2.076E-04	0.9598	0.0135
s6	1	1.0000	0	0.9998	3.921E-05	0.9974	0.0083
s7	1	1.0000	0	0.9999	2.812E-06	0.9996	0.0006
Maximum error		0.01%		2.79%		4.02%	

Case 5: identification of the nonlinear building model with different input data

Different input will be used to identify the nonlinear building model parameters and investigate the performance. The restoring force, which can be measured by a non-contacting capacitive probe and a force transducer in experimental tests (Yar & Hammond, 1987), and displacement data of the first floor are used to conduct the nonlinear system identification. Figure 3-15 shows the evolutionary processes of the objective function by using acceleration responses from the 2nd to 5th floors $\ddot{u}_2, \ddot{u}_3, \ddot{u}_4, \ddot{u}_5$, and both the restoring force and displacement data of the first floor, respectively. Overall, these two curves are converging to very small values quickly, indicating good identification results are obtained. In addition, using both the displacement and restoring force provides a quicker convergence speed with 85 iterations to reach the optimized results compared with 125 iterations by using acceleration responses. Table 3-9 shows the identification results. Good identification accuracy is achieved by using different input data, even with significant noise effect.

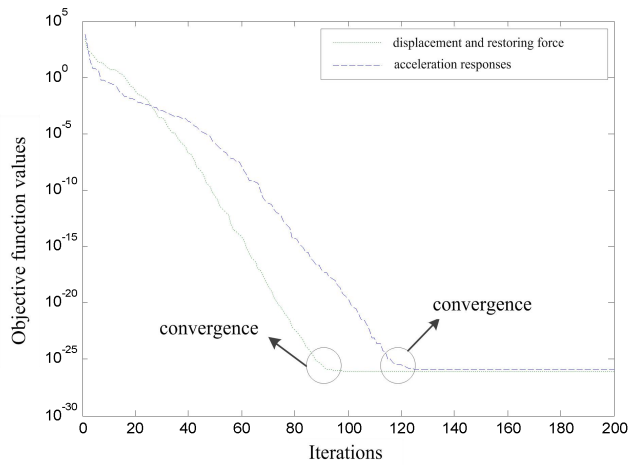


Figure 3-15 Comparison of the evolutionary processes in objective function values by using input data.

Table 3-9 Comparisons on using different input data for nonlinear system identification by using I-TSA.

Parameters	True values	Without noise		5% noise		10% noise	
		Mean	Std	Mean	Std	Mean	Std
s1	2	2.0000	0	1.9980	7.26E-06	2.0030	3.32E-07
s2	1	1.0000	0	1.0000	7.00E-07	1.0000	3.37E-07
s3	1	1.0000	0	1.0007	5.26E-06	0.9964	8.64E-07
s4	2	2.0000	0	1.9919	1.54E-07	1.9923	5.31E-06
s5	1	1.0001	2.92E-05	1.0016	7.20E-07	1.0004	2.89E-07
s6	1	1.0000	0	0.9980	1.23E-07	1.0059	1.19E-06
s7	1	1.0000	0	1.0003	9.30E-08	1.0009	1.31E-07
Maximum error		0.01%		0.40%		0.59%	

3.5 Conclusions

This paper proposes a new heuristic algorithm, named I-TSA, for nonlinear model parameter identification with three different hysteretic models. Two modifications, namely, Lévy flight mechanism and a new updating equation, are added to modify the standard TSA to improve the efficiency and capability for global optimization. The accuracy and performance of the proposed approach are verified by conducting the benchmark studies with benchmark test functions. The independent tests are conducted to investigate the contribution from these two modifications. Numerical studies on a nonlinear SDOF system and a nonlinear seven-storey shear building are conducted to demonstrate the effectiveness and superiority of the proposed approach over several existing methods. The noise effect on the identification accuracy is also investigated. Through the above studies, the following conclusions can be drawn:

- Both modifications are useful to improve the performance of TSA, however, the proposed I-TSA has the best performance in the optimizations of most benchmark function tests.
- When tackling CEC14 benchmarks, even though the winner algorithm is employed to conduct comparison, the proposed I-TSA still showcases its superiority on some specific functions.
- For the identification of a nonlinear SDOF system, it has been demonstrated that the proposed I-TSA can converge more quickly and obtain better identification

results compared with the original TSA and enhanced sensitivity method.

- For the identification of a nonlinear seven-storey shear building, the results demonstrate that the proposed approach has a good robustness even the responses used for identification analysis contain significant noises, and a better performance than several existing methods.

- The effectiveness of the proposed approach is independent of the type of input data used to excite the structure.

- However, there are still some limitations, i.e., uncertainties effect in the finite element modelling on the accuracy of using the proposed approach for nonlinear system identification has not been well investigated. These will be studied in the future.

References

- Abdessalem, A.B., Dervilis, N., Wagg, D., & Worden, K. (2018) Model selection and parameter estimation in structural dynamics using approximate Bayesian Computation. *Mechanical Systems and Signal Processing*, 99, 306-325.
- Berger, E.J., & Krousgrill, C.M. (2002) On friction damping modeling using bilinear hysteresis elements. *ASME Journal of Vibration and Acoustics*, 124, 367-375.
- Brewick, P.T., Masri, S.F., Chassiakos, A.G. & Kosmatopoulos, E.B. (2016) A probabilistic study of the robustness of an adaptive neural estimation method for hysteretic internal forces in nonlinear MSDOF systems. *Probabilistic Engineering Mechanics*, 45, 140-156.
- Brewick, P.T., & Masri, S.F. (2016) An evaluation of data-driven identification strategies for complex nonlinear dynamic systems. *Nonlinear Dynamics*, 85, 1297-1318.
- Cash, J.R., & Karp, A.H. (1990) A variable order Runge-Kutta method for initial value problems with rapid varying right-hand sides. *ACM Transactions on mathematical Software*, 16, 201-222.
- Calabrese, A., Strano, S., & Terzo, M. (2018) Adaptive constrained unscented kalman filtering for real-time nonlinear structural system identification. *Structural Control & Health Monitoring*, 25(2), 1-17.
- Chang, C.C., & Shi, Y. (2010) Identification of time-varying hysteretic structures using wavelet multiresolution analysis. *International Journal of Nonlinear Mechanics*, 45, 737-756.
- Charalampakis, A.E., & Dimou, C.K. (2010) Identification of Bouc-Wen hysteretic systems using particle swarm optimization. *Computers and Structures*, 88, 1197-1205.
- Charalampakis, A.E., & Koumoussis, V.K. (2008) Identification of Bouc-Wen hysteretic systems by a hybrid evolutionary algorithm. *Journal of Sound and Vibration*, 3-5, 571-585.
- Cui, L.Z., Li, G.H., Lin, Q.Z., Du, Z.H., Gao, W.F., Chen, J.Y., & Lu, N. (2016) A novel artificial bee colony algorithm with depth-first search framework and elite-guided search equation. *Information Sciences*, 367-368, 1012-1044.
- Ding, Z.H., Lu, Z.R., & Liu, J.K. (2018) Parameters identification of chaotic systems based on artificial bee colony algorithm combined with cuckoo search strategy. *Science China Technological Sciences*, 61, 417-426.
- EI-Abd, M. (2017) Global-best brain storm optimization algorithm. *Swarm and Evolutionary Computation*, 37, 27-44.
- Erlicher, S., & Point, N. (2004) Thermodynamic admissibility of Bouc-Wen type hysteresis models. *Comptes rendus mecanique*, 332, 51-57.
- Gao, W.F., Chan, F.T.S., Huang, L.L., & Liu, S.Y. (2015) Bare bones artificial bee colony algorithm with parameter adaption and fitness-based neighborhood. *Information Science*, 316, 180-200.
- Garg, A., Li, J.H., Hou, J.J., Berreta, C., & Garg, A. (2017) A new computational approach for estimation of wilting point for green infrastructure. *Measurement*, 111, 351-358.
- Garg, A., Shankhwar, K., Jiang, D., Vijayaraghavan, V., & Panda, B.N. (2016) An evolutionary framework in modelling of multi-output characteristics of the bone

- drilling process. *Neural Computing & Applications*, 102, 1-9.
- Ismail, M., Ikhoulane, F., & Rodellar, J. (2009) The hysteresis Bouc-Wen model, a survey. *Archives of computational methods in Engineering*, 16, 161-188.
- Karaboga, D., & Basturk, B. (2008) On the performance of artificial bee colony (ABC) algorithm. *Applied Soft Computing*, 8, 687-697.
- Katsaras, C.P., Panagiotakos, T.B., & Koulas, B. (2008) Restoring capacity of bilinear hysteretic seismic isolation systems. *Earthquake Engineering and Structural Dynamics*, 37, 557-575.
- Khellat, F. (2009) Optimal Control of Linear Time-delayed Systems by Linear Legendre Multiwavelets. *Journal of Optimization Theory and Applications*, 143(1), 107-121.
- Kiran, M.S. (2015) TSA: Tree-seed algorithm for continuous optimization. *Expert Systems with Applications*, 42, 6686-6698.
- Kyprianou, A., Worden, K., & Panet, M. (2001) Identification of hysteretic systems using the differential evolutionary algorithm. *Journal of Sound and Vibration*, 248(2), 289-314.
- Liang, J.J., Qu, B.Y., & Suganthan, P.N. (2013) Problem Definitions of Evaluation Criteria for the CEC 2014 Special Session and Competition and Single Objective Real-Parameter Numerical Optimization. *Technical Report 201311*, Computational Intelligence Laboratory, Zhengzhou University, Zhengzhou, China and Nanyang Technological University, Singapore.
- Loh, C.H., & Chung, S.T. (1993) A three-stage identification approach for hysteretic systems. *Earthquake engineering and structural dynamics*, 22, 129-150.
- Lu, Z.R., Yao, R.Z., Wang, L., & Liu, J.K. (2017) Identification of nonlinear hysteretic parameters by enhanced response sensitivity approach. *International Journal of Non-Linear Mechanics*, 96, 1-11.
- Mitić, M., Vuković, N., Petrović, M., & Miljković, Z. (2015) Chaotic fruit fly optimization algorithm. *Knowledge-Based Systems*, 89, 446-458.
- Nguyen, S.N., Vinh, H.H., & Ho, A.P.H. (2018) A neural differential evolution identification approach to nonlinear systems and modelling of shape memory alloy actuator. *Asian Journal of Control*, 20(1), 57-70.
- Ni, Y.Q., Ko, J.M., & Wong, C.W. (1998) Identification of nonlinear hysteretic isolators from periodic vibration tests. *Journal of Sound and Vibration*, 217(4), 737-756.
- Noel, J.P., Esfahani, A.F., Kerschen, G., & Schoukens, J. (2017) A nonlinear state-space approach to hysteresis identification. *Mechanical Systems and Signal Processing*, 84, 171-184.
- Ortiz, G.A., Alvarez, D.A., & Bedoya-Ruíz, D. (2013) Identification of Bouc-Wen type models using multi-objective optimization algorithms. *Computers & Structures*, 114-115, 121-132.
- Quaranta, G., Marano, G.C., Greco, R., & Monti, G. (2014) Parametric identification of seismic isolators using differential evolution and particle swarm optimization. *Applied Soft Computing*, 22(5), 458-464.
- Roberts, J.B., & Sadeghi, A.H. (1990) Sequential parameter identification and response of hysteretic oscillators with random excitation. *Structural safety*, 8, 45-68.
- Sharma, H., Bansal, J.C., & Arya, K.V. (2016) Lévy flight artificial bee colony algorithm. *International Journal of System Science*, 47, 2652-2670.

- Shu, G.P., & Li, Z.J. (2017) Parametric identification of the Bouc-Wen model by a modified GA: Application to evaluation of metallic dampers. *Earthquake and Structures*, 13(4), 397-407.
- Soneji, H., & Sanghvi, R.C. (2014) Towards the improvement of cuckoo search algorithm. *International Journal of Computer Information Systems and industrial Management Applications*, 6, 77-88.
- Sues, R.H., Mau, S.T., & Wen, Y.K. (1988) Systems identification of degrading hysteretic restoring forces. *ASCE Journal of the Engineering Mechanics*, 114, 833-846.
- Sun, H., Lus, H., & Betti, R. (2013) Identification of structural models using a modified Artificial Bee Colony algorithm. *Computers & Structures*, 116, 59-74.
- Talatahari, S., Kaveh, A., & Rahbari, N.M. (2012) Parameter identification of Bouc-Wen model for MR fluid dampers sing adaptive charged system search optimization. *Journal of Mechanical Science and Technology*, 26(8), 2523-2534.
- Tanabe, R., & Fukunage, A.S. (2014) Improving the search performance of shade using linear population size reduction, in: *Proceedings of the IEEE Congress on Evolutionary Congress on Evolutionary Computation*, 1658-1665.
- Wang, Y.J., & Ding, F. (2017) A filtering based multi-innovation gradient estimation algorithm and performance analysis for nonlinear dynamical systems. *Applied Mathematical Modelling*. *IMA Journal of Applied Mathematics*, 82(6), 1171-1191.
- Wang, Z.C., & Xin, Y. (2015) Nonlinear structural model updating based on instantaneous frequencies and amplitudes of the decomposed dynamic response. *Engineering Structures*, 100(1), 189-200.
- Wang, Z.C., Xin, Y., & Ren, W.X. (2016) Nonlinear joint model updating in shear type structures based on instantaneous characteristics of dynamic responses. *Mechanical system and signal processing*, 76-77, 476-496.
- Waubke, H., & Kassess, C.H. (2016) Gaussian closure technique applied to the hysteretic Bouc modal with non-zero mean white noise excitation. *Journal of Sound and Vibration*, 382, 258-273.
- Wu, M., & Smyth, A. (2008) Real-time parameter estimation for degrading and pinching hysteretic models. *International Journal of nonlinear mechanics*, 43, 822-833.
- Xue, S.T., Tang, H.S., & Zhou, J. (2009) Identification of structural systems using particle swarm optimization. *Journal of Asian Architecture Building Engineering*, 8(2), 517-524.
- Yang, X.S., & Deb, S. (2009) Cuckoo search via Lévy flights. In: *Proceedings of World Congress on Nature and Biologically Inspired Computing*. Coimbatore: IEEE, 210-214.
- Yar, M & Hammond, J.K. (1987) Parameter estimation for hysteretic systems. *Journal of Sound and Vibration*, 117, 161-172.
- Zaman, M.A., & Sikder, U. (2015) Bouc-Wen hysteresis model identification using modified firefly algorithm. *Journal of Magnetism and Magnetic Materials*, 395, 229-233.
- Zambrano-Bigiarini, M., Clerc, M., & Rojas, R. (2013) Standard Particle Swarm Optimisation 2011 at CEC-2013: A baseline for future PSO improvements, in: *Proceedings of the IEEE Congress on Evolutionary Congress on Evolutionary Computation*, 2337-2344.
- Zhu, G.P., & Kwong, S. (2010) Gbest-guided artificial bee colony algorithm for numerical function optimization. *Applied Mathematics and Computation*, 217(7),

3166-3173.

CHAPTER 4 STRUCTURAL DAMAGE IDENTIFICATION USING IMPROVED JAYA ALGORITHM BASED ON SPARSE REGULARIZATION AND BAYESIAN INFERENCE

ABSTRACT³

Structural damage identification can be considered as an optimization problem, by defining an appropriate objective function relevant to structural parameters to be identified with optimization techniques. This paper proposes a new heuristic algorithm, named improved Jaya (I-Jaya) algorithm, for structural damage identification with the modified objective function based on sparse regularization and Bayesian inference. To improve the global optimization capacity and robustness of the original Jaya algorithm, a clustering strategy is employed to replace solutions with low-quality objective values and a new updated equation is used for the best-so-far solution. The objective function that is sensitive and robust for effective and reliable damage identification is developed through sparse regularization and Bayesian inference and used for optimization analysis with the proposed I-Jaya algorithm. Benchmark tests are conducted to verify the improvement in the developed algorithm. Numerical studies on a truss structure and experimental validations on an experimental reinforced concrete bridge model are performed to verify the developed approach. A limited quantity of modal data, which is distinctively less than the number of unknown system parameters, are used for structural damage identification. Significant measurement noise effect and modelling errors are considered. Damage identification results demonstrate that the proposed method based on the I-Jaya algorithm and the modified objective function based on sparse regularization and Bayesian inference can provide accurate and reliable damage identification, indicating the proposed method is a promising approach for structural damage detection using data with significant uncertainties and limited measurement information.

³This chapter was published in *Mechanical Systems and Signal Processing* with the full bibliographic citation as follows: Ding, Z., Li, J., & Hao, H. (2019). Structural damage identification using improved Jaya algorithm based on sparse regularization and Bayesian inference. *Mechanical Systems and Signal Processing*, 132, 211-231. <https://doi.org/10.1016/j.ymssp.2019.06.029>.

4.1 Introduction

Conducting damage identification and quantification of structures based on measured vibration data is one of the most significant research topics in the area of structural health monitoring (SHM), because it is relevant to assessing the service performance and evaluating the integrity of structures (Farrar & Worden, 2007). When structures have damages, alternations are observed in the dynamic vibration characteristics. Therefore, numerous methods have been developed for structural damage identification based on the changes in structural vibration characteristics (Kerschen & Worden, 2006; Wan & Qiao, 2011).

Basically, these methods can be categorized into two types, relying on the fact that structural damage identification is performed in the frequency domain or the time domain. Frequency domain based methods are developed to identify damages by using structural modal information, such as natural frequencies, mode shapes, damping ratios and other frequency domain data. Pandey and Biswas (1994) used the flexibility matrices for damage identification. Shi and Law (1998) developed the modal strain energy ratio to locate the structural damages. Yan et al. (2015a; 2015b) used Principle Component Analysis (PCA) to analyze structural modal data for distinguishing the changes in vibration characteristics due to environmental variations or structural damage. Numerical and experimental studies illustrated that the proposed method can be effective for the linear and nonlinear structures. Furthermore, the spectral approach was also widely applied to address structural damage quantification, especially for nonlinear systems (Machado et al., 2017).

On the other hand, structural damage identification methods in the time domain have been developed rapidly in the recent years. Lu and Wang (2017) proposed an enhanced sensitivity method to perform damage identification, in which a trust-region restriction was introduced to improve the performance of the traditional sensitivity approach. Hu et al. (2017) developed a method using the homotopy continuation algorithm to identify the cracks in beam structures, in which acceleration responses were used to formulate the objective function. Li et al. (2017) developed a damage identification and optimal sensor placement method for structures under traffic-induced

vibrations, based on response reconstruction in the time domain. Recently, the time domain methods have been also developed to conduct the identification of nonlinear structures. Yang et al. (2006) developed an adaptive Extended Kalman Filter (EKF) approach to identify the damage in both the linear and nonlinear structures. Xie and Feng (2012) applied the Iterated Unscented Kalman Filter (IUKF) for highly nonlinear structures. Experimental results demonstrated that IUKF can be used to provide better state estimation and parameter identification results than Unscented Kalman Filter (UKF). For damage identification in initially nonlinear systems, Shiki et al. (2017) used a discrete Volterra model to separate the linear and nonlinear components of the dynamic responses of a system. Afterwards, hypothesis tests were introduced to detect variations in the statistical properties of the damage features. Villani et al (2019) adopted the stochastic Volterra series to conduct damage identification for uncertain nonlinear systems, in which the uncertainties were simulated by the variation posed in the linear stiffness and damping coefficient.

However, most of the above mentioned methods require a good guess of the initial system parameters and an accurate estimation of the gradients. Furthermore, difficulties arise when utilizing these methods for the identification of large scale structures when only few measurement data is available. Regularization in the solution would be essential to ensure that the identification results are physically meaningful. Considering that structural damage identification could be viewed as an optimization problem (Friswell, 2007), computational intelligence techniques are developed to perform the optimization in structural damage identification, such as the Genetic Algorithm (GA), the Particle Swarm Optimizer (PSO), the Artificial Bee Colony algorithms (ABCs), the Differential Evolution (DE) algorithms, the Artificial Neural Network (ANN), the Support Vector Machine (SVM) and other machine learning methods. These intelligence methods generally make predictions via data instead of the specific formulas. Therefore, they could not only avoid the mentioned shortcomings (requiring good initial values and gradient information), but also enable to perform identification of large-scale and complex structures (Ding et al., 2019). Wang (2009) developed using the hybrid GA with the Gaussian-Newton method to identify the parameters of both

linear and nonlinear structural systems. Guo and Li (2009) developed a two-stage damage identification method based on the evidence fusion along with the improved PSO. Later, Chen and Yu (2017) employed the PSO integrated with Nelder-Mead method to tackle the damage identification problem. Sun et al. (2013) constructed a modified ABC algorithm to perform the identification of structural parameters, in which a nonlinear factor used for improving the convergence performance was introduced to achieve the balance between the global and local searches. Ding et al. (2017; 2018) adopted ABC to identify structural damages and cracks by using the objective function based on natural frequencies and the modal assurance criteria (MAC). Tang et al. (2008) proposed DE to identify structural parameters with and without considering noise contamination in the measurement data. Padil et al. (2017) demonstrated that ANN is a good choice to solve the damage identification problem considering uncertainties. Bornn et al. (2010) developed an approach using the autoregressive SVM to detect the damage in initially nonlinear systems. Santos et al. (2016) presented four kernel-based algorithms for damage identification under varying operational and environmental conditions. From the above studies, it can be found that these computational intelligence approaches are promising tools for structural identification, however, challenges still exist, such as

(a) In some studies, the target structures used for investigation have a small number of elements. The uncertainty effect on the final identification results is rarely investigated; and

(b) The performance and robustness of algorithms for the scenarios when only a limited number of measurement data are available and at the same time the data contain significant noise, need to be improved.

Recently a new computational intelligence method, namely Jaya algorithm (Rao, 2016; Rao & Saroj, 2017), has been developed. Compared with the above-mentioned computational intelligence methods (Tang & Fan, 2008; Wang, 2009; Li & Guo, 2009; Sun et al., 2013; Chen & Yu, 2017; Ding et al., 2019), the distinct feature of the Jaya algorithm is that there are no special controlling parameters in the algorithm. In contrast for many other methods, GA needs a proper setting of crossover probability,

mutation rate and selection operator, and ABC needs proper quantities of onlooker bees, scout bees and parameter 'limit'. Furthermore, compared with other gradient-based algorithms (Pandey & Biswas, 1994; Shi & Law, 1998), the Jaya algorithm has the following superiorities: (i) It is free from sensitivity analysis and initial guess of the parameters; (ii) It does not require gradient information. When performing the damage identification of structures with a large number of elements, the gradient information may be difficult to obtain or the calculation is time consuming due to the significant computational demand with a large-scale system, which restricts the potential applications of these gradient-based methods. Therefore, it is interesting to develop and extend the Jaya algorithm for structural damage identification. Furthermore, to address the two challenges as mentioned above, modifications are introduced into the standard Jaya algorithm to enhance its global optimization ability and a better objective function that is more robust to identify structural parameters with limited measurement information is proposed. These are the two main contributions of this study.

For addressing the second challenge as mentioned, when developing and applying optimization methods for damage identification, studies on developing more reasonable objective functions that are more robust and stable in optimization analysis for damage identification are conducted. To achieve this purpose, one way is to introduce the regularization technique to reform the objective function. Recently, the sparse regularization techniques with the enforcement of the sparsity constraint on the damage locations have been widely investigated and promising results are obtained, since damages are often observed at a few locations while the majority of elements remain intact (Zhou et al., 2015; Hou et al., 2018). Furthermore, the traditional objective functions (Ding et al., 2017; Ding et al., 2018) are usually ill-posed, and introducing the sparse regularization constraint on the damage identification is beneficial to overcome the ill-posedness in the inverse problems (Titurus & Friswell, 2008). Another possible way to tackle this challenge is to employ the probabilistic analysis, i.e. based on the Bayesian inference. It considers the complete information relevant to the measured data for statistical inference with an appropriate likelihood function (Sun & Betti, 2015). Bayesian-based methods have been developed for damage identification.

For example, Beck et al. (1999) presented a Bayesian statistical framework for structural identification and adopted this theory to perform continuous online identification. Later, Bayesian spectral density approaches, Bayesian Fast Fourier Transform (FFT) methods (Yuen & Katafygiotis, 2003; Zhang et al., 2016), Bayesian-based Monte Carlo method (Figueiredo et al., 2014) have been further developed for structural damage identification. The results in previous studies (Chen & Yu, 2017; Sun & Betti, 2015) demonstrated that the Bayesian inference can be used to enhance the robustness of damage identification. Therefore, to improve the identification with a limited number of measurements of a significant noise effect, a new objective function is proposed by using incomplete modal data and the penalty items considering the sparse regularization and Bayesian inference.

This paper proposes an improved Jaya algorithm (I-Jaya) to conduct damage identification of structures by using vibration measurement data. To enhance the capacity of the developed methodology for the identification of large-scale structures, two modifications are developed based on the standard Jaya algorithm to enhance its global search ability. 1% variation (Xia et al., 2012) is introduced into the elemental stiffness parameters to simulate the uncertainties in the structure. To improve the identification with a limited number of measurements of a significant noise effect, a new objective function is proposed by using incomplete modal data and the penalty items considering the sparse regularization and Bayesian inference. Classical mathematical benchmarks are utilized to validate the accuracy and improvement of the proposed approach. Numerical investigations on a 121-bar truss structure are performed to demonstrate the accuracy of the developed algorithm with the use of the modified objective function. Experimental validations on a reinforced concrete bridge are conducted to demonstrate the performance of the proposed method.

4.2 Theoretical background

4.2.1 Damage identification of structures

Changes in structural system parameters, i.e. stiffness, mass and damping, would introduce the alterations in structural vibration properties. Hence SDI could be

conducted based on this fact by using vibration measurement data. Vibration characteristics, such as frequencies and mode shapes of a structure without considering the damping, could be obtained by solving the eigenvalue problem

$$(\mathbf{K} - \omega_i^2 \mathbf{M}) \cdot \Phi_i = 0 \quad (4.1)$$

where \mathbf{K} and \mathbf{M} represent the system stiffness and mass matrices, respectively; ω_i and Φ_i denote the i th natural frequency and the corresponding mode shape, respectively.

In this study, structural damage is assumed to be only related to the stiffness reduction, since the mass alteration of a structure could be easily inspected (Zhu et al., 2017). In this case, structural damage would be characterized via a scalar stiffness reduction variable for each element $\alpha_h (h=1,2,\dots,Nel)$ with the value between 0 and 1 as follows

$$\mathbf{K}_d = \sum_{h=1}^{Nel} (1 - \alpha_h) \cdot \mathbf{k}_{eh} \quad (4.2)$$

where \mathbf{k}_{eh} represents the h th elemental stiffness matrix under the undamaged state; Nel denotes the number of total elements of a structure; \mathbf{K}_d represents the structural stiffness matrix under the damaged state; α_h denotes the elemental stiffness reduction parameter to be identified. It shall be noted that $\alpha_h = 1$ implies that this element is totally damaged, and $\alpha_h = 0$ means that the element is intact.

The traditional objective function, denoted as f_{obj1} , is defined based on the alterations of natural frequencies and Modal Assurance Criterion (MAC), which can be given as (Ding et al, 2017; Chen & Yu, 2017)

$$\mathbf{\alpha}^* = \arg \min_{\mathbf{\alpha}} f_{obj1}(\mathbf{\alpha}) = \arg \min_{\mathbf{\alpha}} \left(\sum_{i=1}^{NF} \Delta \omega_i^2 + \sum_{i=1}^{NM} (1 - MAC_i) \right) \quad (4.3)$$

with

$$\Delta \omega_i = \frac{|\omega_i^c - \omega_i^m|}{\omega_i^m} \quad (4.4)$$

$$MAC_i = \frac{(\Phi_i^{cT} \cdot \Phi_i^m)^2}{\|\Phi_i^c\|^2 \|\Phi_i^m\|^2} \quad (4.5)$$

where ω_i^c and Φ_i^c represent the i th calculated natural frequency and mode shape from the finite element model analysis, respectively; ω_i^m and Φ_i^m are the corresponding measured natural frequency and mode shape, respectively. NF and NM represent the order numbers of natural frequencies and mode shapes, respectively. The calculated modal data are acquired by using the stiffness parameters $\boldsymbol{\alpha} = [\alpha_1, \alpha_2, \dots, \alpha_{Nel}]$ with the finite element analysis. Generally speaking, SDI is treated as an ill-posed problem with the searching parameters that may have multiple local optimal points (Ding et al., 2018). The optimization techniques can be used for identifying the optimal set of parameters that could minimize the objective function. When the input data is limited or even less than the number of unknown parameters to be identified and the data is contaminated with the significant measurement noise, the damage identification becomes much more difficult. To overcome these challenges, it is emerging to investigate and develop robust and powerful algorithms with proper objective functions, which may improve the identification of the complex structures.

4.2.2 Proposed objective function

4.2.2.1 The objective function based on sparse regularization

In real situations, structural damages happen usually at a few locations (Fan et al., 2018). Therefore the damage vector $\boldsymbol{\alpha} = [\alpha_1, \alpha_2, \dots, \alpha_{Nel}]$ should be a sparse vector with most of its items equal to zero or at least close to zero, except the damaged elements with non-zero entries. When the number of measured data is less than the total number of unknown parameters in the inverse identification, Eq. (4.3) is underdetermined and ill-posed. Therefore, the l_1 regularization technique (Hou et al., 2018) can be utilized to help solve the underdetermined inverse problem. The objective function based on sparse regularization, denoted as *obj2*, can be defined as

$$\boldsymbol{\alpha}^* = \arg \min_{\boldsymbol{\alpha}} f_{obj2}(\boldsymbol{\alpha}) = \arg \min_{\boldsymbol{\alpha}} \left(\sum_{i=1}^{NF} \Delta \omega_i^2 + \sum_{i=1}^{NM} (1 - MAC_i) + \lambda \|\boldsymbol{\alpha}\|_1 \right) \quad (4.6)$$

where $\lambda > 0$ is the regularization parameter and $\|\boldsymbol{\alpha}\|_1$ denotes the l_1 norm of the solution, namely, $\|\boldsymbol{\alpha}\|_1 = \sum_{h=1}^{Nel} |\alpha_h|$. It should be noted that a small λ would pose a

higher penalty on the residual term, resulting in an over-fitting solution. Conversely, for a large λ value, it would loss data fidelity. Therefore, the discrepancy principle (DP) rule (Hou et al., 2018) is employed here to select the optimal regularization parameter λ .

4.2.2.2 The objective function based on Bayesian inference

Vibration measurement data are usually polluted with the environmental noise, which could be considered as a zero-mean Gaussian white-noise in numerical simulations. The noisy response can be described as (Chen & Yu, 2017)

$$\mathbf{X}_{noise} = \mathbf{X}(1 + \varepsilon\mathbf{R}) \quad (4.7)$$

where \mathbf{X}_{noise} and \mathbf{X} are the noisy and original response vectors, respectively; ε denotes the noise level ranging from 0 to 100%, while \mathbf{R} is a random vector with the standard normal distribution $N(0,1)$.

To improve the capacity of the developed algorithm against the noise effect in the optimization process, the Bayesian inference is introduced to modify the objective function. The theoretical foundation of the Bayesian theory is the conditional probability, with the prior knowledge resulted from a certain event or hypothesis. This theory offers a rigorous process for uncertainty quantification. In Bayesian inference, the posterior Probability Density Function (PDF) of the model parameters ($\boldsymbol{\theta}$) can be obtained via Bayes' theorem

$$p(\boldsymbol{\theta}|\mathbf{D}) = c \cdot p(\mathbf{D}|\boldsymbol{\theta})p(\boldsymbol{\theta}) \quad (4.8)$$

where $p(\boldsymbol{\theta}|\mathbf{D})$ represents the PDF of model parameters $\boldsymbol{\theta}$ given the modal data \mathbf{D} , $p(\mathbf{D}|\boldsymbol{\theta})$ represents the likelihood function given the model parameter $\boldsymbol{\theta}$, and $p(\boldsymbol{\theta})$ denotes the prior PDF of model parameters $\boldsymbol{\theta}$ based on observations and/or modelling assumptions. Specifically, it ought to be noted that modal data \mathbf{D} means the real measured data, such as frequencies and mode shapes. In the Bayesian theory, these measured data are served to obtain the posterior probability density function of the model parameters $\boldsymbol{\theta}$. In this study for structural damage identification, the model

parameters denote the element stiffness parameters vector $\boldsymbol{\alpha} = [\alpha_1, \alpha_2, \dots, \alpha_{N_{el}}]$. Furthermore, the prior distribution of model parameters $\boldsymbol{\theta}$ is assumed as a uniform distribution, which means that their PDFs are a series of constants (Chen & Yu, 2017). c is a constant which enables the integral of $p(\boldsymbol{\theta} | \mathbf{D})$ to be 1. Supposing that the Bayesian inference is applied on natural frequencies and taking $\mathbf{D} = [\mathbf{D}_1, \mathbf{D}_2, \dots, \mathbf{D}_{N_s}]$ as observed modal data with N_s samples, and $\mathbf{D}_s = [\omega_{1,s}, \omega_{2,s}, \dots, \omega_{i,s}]$ denoting the natural frequencies in the s th observation or measurement. The likelihood functions of the modal data are assumed to be independent, and the principle of the maximum entropy is employed as a basis to assume Gaussian distributions for these modal data (Chen & Yu, 2017). Based on this assumption, the PDF of any frequency parameter ($\omega_{i,s}$) can be obtained as

$$p(\omega_{i,s} | \boldsymbol{\theta}) = c_1 \exp\left[-\frac{(\omega_{i,s} - \omega_i^c)^2}{2\sigma_i^2}\right] \quad (4.9)$$

where $\omega_{i,s}$ represents the i th frequency in the s th measurement, ω_i^c denotes the i th calculated frequency, and σ_i^2 represents the variance of the i th frequency and can be calculated as

$$\sigma_i^2 = \frac{1}{N_s - 1} \sum_{s=1}^{N_s} (\omega_{i,s} - \bar{\omega}_i)^2 \quad (4.10)$$

where $\bar{\omega}_i$ represents the mean value of the i th natural frequency.

Since it is assumed the testing obtained modal data are independent, the likelihood in Eq. (4.8) can be calculated as

$$p(\mathbf{D} | \boldsymbol{\theta}) = \prod_{s=1}^{N_s} p(\mathbf{D}_s | \boldsymbol{\theta}) = \prod_{s=1}^{N_s} \left(\prod_{i=1}^{NF} p(\omega_{i,s} | \boldsymbol{\theta}) \right) \quad (4.11)$$

When the prior distribution of natural frequencies is considered as the uniform distribution, substituting Eq. (4.11) to Eq. (4.8) can have the final form of $p(\boldsymbol{\theta} | \mathbf{D})$. It can be calculated as

$$p(\boldsymbol{\theta} | \mathbf{D}) = c \exp\left[-\sum_{s=1}^{N_s} \sum_{i=1}^{NF} \left[\frac{(\omega_{i,s} - \omega_i^c)^2}{2\sigma_i^2} \right] \right] \quad (4.12)$$

Eq. (4.12) represents the frequency-based Bayesian conditional probability function. The goal of Bayes analysis is to maximize the likelihood probability function $p(\boldsymbol{\theta} | \mathbf{D})$ based on the test data, which can be converted to minimize the exponent part in Eq. (4.12). Combining with the item related with the mode shapes in the objective function as described in Eq. (4.3), the third objective function, denoted as *obj3*, is given as

$$\boldsymbol{\alpha}^* = \underset{\boldsymbol{\alpha}}{\operatorname{argmin}} f_{obj3}(\boldsymbol{\alpha}) = \underset{\boldsymbol{\alpha}}{\operatorname{argmin}} \left(\sum_{s=1}^{N_s} \sum_{i=1}^{NF} \left[\frac{(\omega_{i,s} - \omega_i^c)^2}{2\sigma_i^2} \right] + \sum_{i=1}^{NM} (1 - MAC_i) \right) \quad (4.13)$$

Comparing with the first objective function defined in Eq. (3), the item relevant to minimizing the difference in natural frequencies is modified based on Bayesian inference. It should be noted that when involving the Bayesian inference in the objective function, significant computational time may be required to obtain the variances. Since natural frequencies are scalars, their covariance values are relatively straightforward to be obtained. However, for the mode shapes, obtaining the covariance matrices will be relatively complex and time-consuming, considering the modal shapes are vectors. To simplify the calculation and increase the efficiency, only the frequencies are considered in the objective function in Eq. (4.13).

4.2.2.3 The objective function based on Bayesian inference and sparse regularization

By considering the Bayesian inference and sparse regularization simultaneously, a hybrid objective function, defined as *obj4* expressed below is proposed in this study for SDI,

$$\boldsymbol{\alpha}^* = \underset{\boldsymbol{\alpha}}{\operatorname{argmin}} f_{obj4}(\boldsymbol{\alpha}) = \underset{\boldsymbol{\alpha}}{\operatorname{argmin}} \left(\sum_{s=1}^{N_s} \sum_{i=1}^{NF} \left[\frac{(\omega_{i,s} - \omega_i^c)^2}{2\sigma_i^2} \right] + \sum_{i=1}^{NM} (1 - MAC_i) + \lambda \|\boldsymbol{\alpha}\|_1 \right) \quad (4.14)$$

The Bayesian inference is included to improve the robustness (Chen & Yu, 2017), and the regularization term is applied to solve the underdetermined inverse problems (Sun & Betti, 2015). The effectiveness and improvement of these objective functions will be compared in this study.

4.3 Optimization algorithm

4.3.1 Jaya algorithm

The proposed I-Jaya algorithm in this study is developed and improved based on the standard Jaya algorithm. The standard Jaya algorithm is briefly reviewed here (Rao, 2016; Rao & Saroj, 2017) for the completeness of this paper. The Jaya algorithm is a new type of heuristic algorithms, inspired by the concept that the feasible solution acquired for a given problem ought to move towards the best solution and avoid the worst solution. Specifically, for every feasible solution, the way of generating its offspring is to move closer to the success (i.e. approaching the best solution) and avoid the failure (i.e. escaping from the worst solution). When generating the offspring, the objective function values are compared to decide whether the new solution (offspring) or the previous solution would be selected for the next iteration. Gradually, the algorithm endeavors to become victories by approaching the best solution and therefore it is named after Jaya (a Sanskrit word meaning victory). Compared with other computational intelligence methods, such as ABC, BMO and PSO etc., the distinct feature of the Jaya algorithm is that there are no special controlling parameters in the algorithm. The procedures of operating the Jaya algorithm includes three steps, namely, the initialization, the local search strategy and the greedy selection mechanism, which are briefly described in the following,

4.3.1.1 Initialization

An initial colony is generated randomly in the search space. This colony contains CS individuals. Each individual in the colony is marked with θ_j . Every individual (θ_j) contains n variables ($\theta_j = [\theta_1, \theta_2, \dots, \theta_q, \dots, \theta_n]$), which can be created as

$$\theta_{j,q} = \theta_{j,q}^l + rand(0,1) \cdot (\theta_{j,q}^u - \theta_{j,q}^l) \quad (4.15)$$

where $\theta_{j,q}$ denotes the q th variable of θ_j ; $\theta_{j,q}^u$ and $\theta_{j,q}^l$ are the upper bound and the lower bound of the variable $\theta_{j,q}$. $rand(0,1)$ represents a random number in the range within 0 to 1.

4.3.1.2 Local search strategy

After creating the initial colony, the local search for these individuals will be carried out. As mentioned before, the core of the Jaya is to pursue success but avoid failure, therefore, the best solution and the worst one in each iteration would be used to formulate the local search strategy for every individual. It is assumed that $\theta_{j,q,G}$ stands for the value of the q th dimension of the j th individual at the G th generation. The offspring $\theta'_{j,q,G}$ created by this value can be calculated as

$$\theta'_{j,q,G} = \theta_{j,q,G} + r_{1,q,G} \cdot (\theta_{best,q,G} - |\theta_{j,q,G}|) - r_{2,q,G} \cdot (\theta_{worst,q,G} - |\theta_{j,q,G}|) \quad (4.16)$$

where $r_{1,q,G}$ and $r_{2,q,G}$ are two random numbers located in the $[0,1]$. $\theta_{best,q,G}$ and $\theta_{worst,q,G}$ are the values of the q th variable for the best individual and the worst one, respectively. The second item in Eq. (4.16) denotes that the trend of the process towards the best solution while the third item represents the tendency of the solution to avoid the worst solution. Afterwards the judgement of boundary condition will be conducted by using

$$\theta'_{j,i,G} = \begin{cases} \theta'_{j,i,G}, & \text{if } \theta'_{j,i,G} < \theta^l_{j,i} \\ \theta^u_{j,i}, & \text{if } \theta'_{j,i,G} > \theta^u_{j,i} \\ \theta'_{j,i,G}, & \text{otherwise} \end{cases} \quad (4.17)$$

4.3.1.3 Greedy selection mechanism

Extending the above-mentioned local search strategy to all dimensions, it will acquire the new individual $\theta'_{j,G}$. The greedy selection mechanism (Zhu et al., 2017) is applied to determine whether the new individual or the previous one will be selected for the next iteration. Namely, the objective function values of the $\theta_{j,G}$ and $\theta'_{j,G}$ will be compared. The individual with a smaller function value will be kept to the next generation

$$\theta_{j,G+1} = \begin{cases} \theta'_{j,G}, & f(\theta'_{j,G}) \leq f(\theta_{j,G}) \\ \theta_{j,G}, & \text{otherwise} \end{cases} \quad (4.18)$$

where f denotes the objective function that requires to be minimized. The algorithm will be continually conducted until the termination condition is satisfied, i.e., the

maximum objective function evaluation number is reached.

4.3.2 Improved Jaya algorithm

In the standard Jaya algorithm, it can be found that every mutation as shown in Eq. (4.16) is relevant to the best-so-far solution and the worst one. Therefore, the whole colony will centralize into the best-so-far solution with iterations, and the colony information may not be fully used. In this case, if the best-so-far solution is trapped into the local minimal, the whole iteration of the algorithm would cease. Besides, from observing the updated strategy as shown in Eq. (4.16), it is clear that for the best-so-far solution, the second item trying to reach the best solution would make the optimization lose efficiency. Aiming at overcoming these drawbacks, two modifications are developed to enhance the algorithm's performance.

4.3.2.1 K-means clustering

The K-means clustering is a simple yet powerful tool that organizes a data set (pattern) into a number of groups or clusters. Within every group or cluster, these data or pattern are similar to each other. In other words, clustering technique is a useful tool to discover the inherent pattern in any given dataset (Jain et al., 1999). Besides, the clustering centers can be viewed as the representations of these clusters, since their formulations are based on the combinations of other individuals in these clusters. Therefore, to make full use of the colony information, it seems a smart choice to integrate the K-means clustering technique into the standard Jaya algorithm, since the information of the whole colony can be represented through these so-called 'clustering centers'. Furthermore, during early iterations, conducting the K-means clustering is straightforward and this works as a crossover operators that would effectively utilize the colony information, which is beneficial to improve the algorithm's convergence performance (Jain et al., 1999; Cai et al., 2011). The specific procedure of operating clustering mechanism is described as follow

Step 1: $K = 0.1 \cdot CS$ initial clustering centers C_1, C_2, \dots, C_k are produced randomly from the CS individuals $[\theta_1, \theta_2, \dots, \theta_{cs}]$.

Step 2: The remaining individuals are distributed to these clustering centers according to their distances to these centers. Specifically, θ_j is assumed to represent a remaining individual in the colony. If and only if it satisfies the distance condition $\|\theta_j - C_m\| \leq \|\theta_j - C_p\|$ (C_p denotes any other clustering centers), the individual θ_j will belong to the cluster with the clustering center C_m . Based on this rule, other individuals can find their clusters through the comparison with the distances generated from every clustering center. The distance between any two individuals (i.e., θ_j and θ_c) is determined by the Manhattan distance, given as follows

$$d(\theta_j, \theta_c) = \|\theta_j - \theta_c\| = \sum_{q=1}^n \text{abs}(\theta_{j,q} - \theta_{c,q}) \quad (4.19)$$

Step 3: After assigning other individuals to these clustering centers, the new clustering centers C'_1, C'_2, \dots, C'_k are calculated by using the following equation

$$C'_m = \frac{1}{u_m} \sum_{\theta_j \in C_m} \theta_j, j = 1, 2, \dots, CS \quad (4.20)$$

where u_m is the number of individuals belonging to the clustering center C_m .

Step 4: Finally, another K parents individuals from the colony will be selected and then combined with the newly-calculated clustering centers as a new set, marked with τ . The individuals' objective function values will be calculated in the set τ , and these values are sorted from the smallest to the largest. The first K individuals would be put in the colony. The clustering operation is demonstrated herein. The pseudo-code of operating the K-means clustering is shown in Figure 4-1.

Algorithm 1 Conducting K-means clustering before individuals' updating

1. Randomly select $K = rnd \text{ int}[0.1 \cdot CS]$ individuals from the colony
2. Calculate the distances between remaining individuals and clustering centers by Eq.(4.19)
3. Assign remaining individuals to clustering centers based on the nearest distance
4. Calculate the new clustering centers by Eq. (4.20)
5. Take away K parents individuals from the colony. Sort them together with the newly-calculated clustering centers in the τ
6. Calculate individuals' objective values in the τ and sort them from the smallest to the largest
7. The first K individuals are put in the colony

Figure 4-1 The pseudo-code of operating the K-means clustering.

4.3.2.2 A new updating equation for the best solution

In the Jaya algorithm, the best solution in every iteration plays a crucial role in the whole optimization process, because it guides and draws other individuals to its own region. To prevent best solutions from trapping in the local minimal to some extents, a new updating equation that focuses on the global search is introduced here (Gao et al., 2015)

$$\theta'_{best,q,G} = \theta_{best,q,G} + \varphi_{best,q,G} (\theta_{j,q,G} - \theta_{best,q,G}) \tag{4.21}$$

where $\theta_{best,q,G}$ denotes the value of the qth dimension of the best solution at the Gth generation and $\theta'_{best,q,G}$ represents its offspring value. $\varphi_{best,q,G}$ is a random number locating in the $[0,1]$. $\theta_{best,q,G}$ means the value of the qth dimension of an arbitrary individual in the colony. From Eq. (4.21), a new candidate is generated by removing the old solution towards a randomly chosen one in the colony. Such randomness can enable this search strategy's exploration ability.

The above two modifications for the standard Jaya algorithm are presented. These improvements are easy to operate and do not bring much complexity to the standard Jaya algorithm. The flowchart of the proposed I-Jaya algorithm is shown in Figure 4-2.

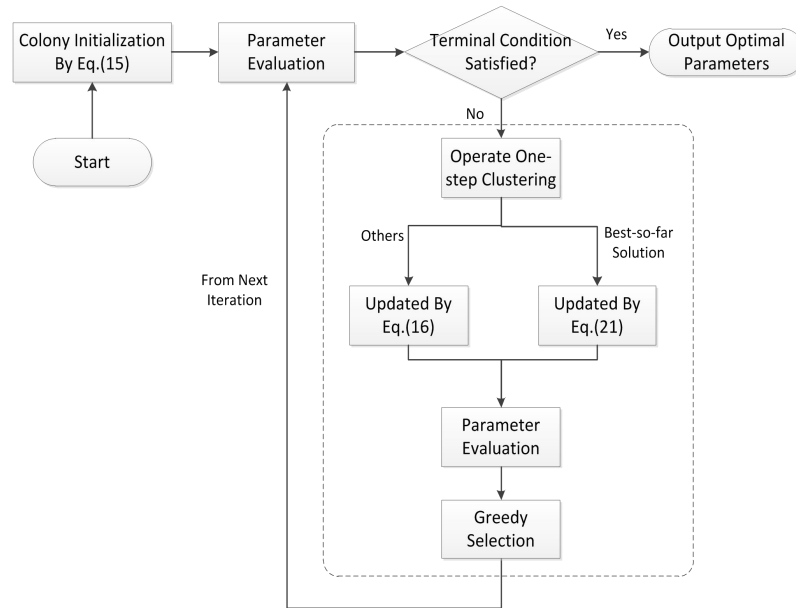


Figure 4-2 The flowchart of the proposed I-Jaya algorithm.

4.4 Numerical Studies

4.4.1 Benchmark tests

To investigate the accuracy of using the developed I-Jaya algorithm for tackling optimization problems against the standard Jaya algorithm, classical mathematical benchmark functions with 100 unknown variables (Ding et al., 2018) are tested here. These functions can be categorized into four types, that is, an uni-modal separable function (Sphere), three multi-modal and non-separable functions (Griewank, Schaffer and Ackley), an uni-modal and non-separable function (Rosenbrock) and a multi-modal separable function (Rastrigin). The global minimum of these test functions are zero. Regarding the parameters setting for algorithms, the colony size $CS = 100$ and the termination condition is set as when the total number of function evaluations reaches 10^5 . Each case is independently repeated 30 times and the means of objective function values are recorded.

Figure 4-3 shows the convergence progresses of the mentioned six benchmark functions. It can be clearly observed that the proposed I-Jaya algorithm has a more competitive convergence speed, and a much better accuracy in the solution than the standard Jaya algorithm as shown in Table 4-1. Because of its excellent performance in dealing with optimization problems, the I-Jaya algorithm will be used to tackle the

following SDI problem.

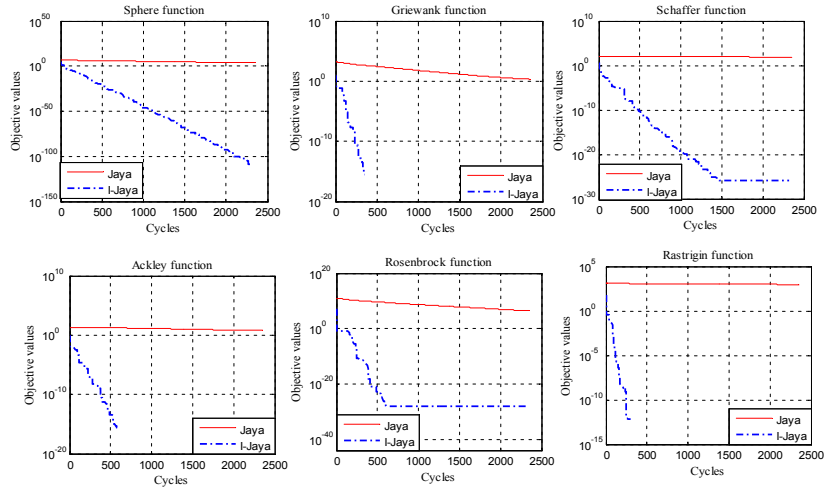


Figure 4-3 The convergence line for the classical benchmarks based on Jaya and the proposed I-Jaya algorithm.

Table 4-1 Statistic results obtained by the Jaya and I-Jaya algorithms for the classical benchmarks.

Algorithms		Function name					
		Sphere	Griewank	Schaffer	Ackley	Rosenbrock	Rastrigin
Jaya	Mean	3.91E+03	2.11E+00	8.22E+01	5.97E+00	2.62E+06	9.45E+02
	std.	6.67E+02	3.36E-01	4.33E+00	4.96E-01	7.78E+05	6.67E+01
I-Jaya	Mean	1.07E-109	0.00E+00	1.18E-26	0.00E+00	9.86E-29	0.00E+00
	std.	2.88E-110	0.00E+00	6.12E-27	0.00E+00	8.16E-30	0.00E+00

4.4.2 Numerical Simulations

The superiority of the proposed I-Jaya algorithm has been demonstrated in the above benchmark verifications. In this section, a 121-bar truss structure is employed as a numerical example to demonstrate the improvement by using the above-mentioned modified objective functions based on Bayesian inference and sparse regularization to identify the structural damage with a limited quantity of available measurement information. The truss model is shown in Figure 4-4. Young's modulus, density and Poisson's ratio are respectively defined as $E = 70\text{GPa}$, $\rho = 2700\text{kg/m}^3$ and $\mu = 0.33$. The boundary conditions of the truss are simulated by three springs with a large stiffness, i.e. $K_{1,1} = 2 \times 10^{10}\text{N/m}$; $K_{1,2} = 2 \times 10^{10}\text{N/m}$; $K_{49,2} = 2 \times 10^{10}\text{N/m}$. The first six

natural frequencies and the relevant incomplete mode shapes are used for identification. It should be noted that in the numerical studies, the number of available modal data is less than the number of unknowns. Therefore the damage identification of this structure is an underdetermined inverse problem. Random measurement noises are included in the natural frequencies and mode shapes, respectively, by using Eq. (4.7). 1% variation with Gaussian distributions is introduced into all the elemental stiffness parameters for simulating the uncertainties. In terms of the parameters setting for I-Jaya, the colony size is $CS=100$ and the maximum objective function evaluation number is set as 49000. For each damage case, 30 runs are independently conducted to acquire statistical results.

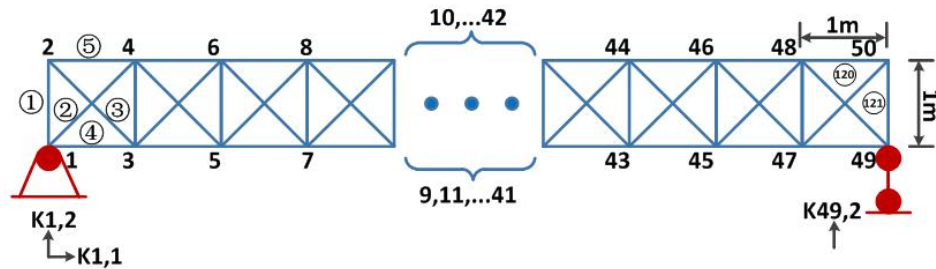


Figure 4-4 The model of the truss structure.

4.4.2.1 Performance comparison on different objective functions

The first damage case, denoted as Case 1, is assumed that there is a 15% stiffness reduction in the 10th element, which means $\alpha_{10} = 0.15$. The first six natural frequencies and mode shapes in the vertical direction of the 2nd, 7th, 12th, 17th, 22nd, 27th, 32nd, 37th, 42nd and 47th nodes are obtained for structural condition identification. There are six frequencies and sixty mode shape values in total. Significant measurement noises are assumed and added in natural frequencies and mode shapes with the noise levels of 3% and 5%, respectively. Furthermore, when calculating the Bayesian inference, it is assumed that the number of available measurement sets for *obj3* and *obj4* is 10 and the average frequencies and mode shapes are used for objective functions *obj1* and *obj2*. Similar to Ref (Chen & Yu, 2017), these data are generated with a 3% variance of their real values. It is noted that the DP rule is applied to

determine the regularization parameters (Hou et al., 2018), therefore the regularization parameter λ for the *obj2* and *obj4* are set as $2 \cdot 10^{-4}$ and $2 \cdot 10^{-6}$, respectively. The proposed algorithm is used for identification, with different objective functions.

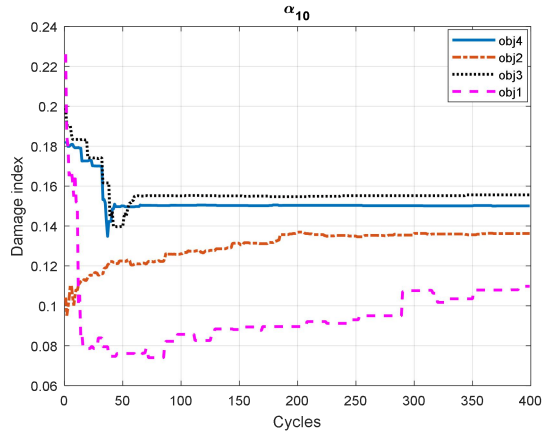


Figure 4-5 The convergence processes of the identified damage index α_{10} with different objective functions.

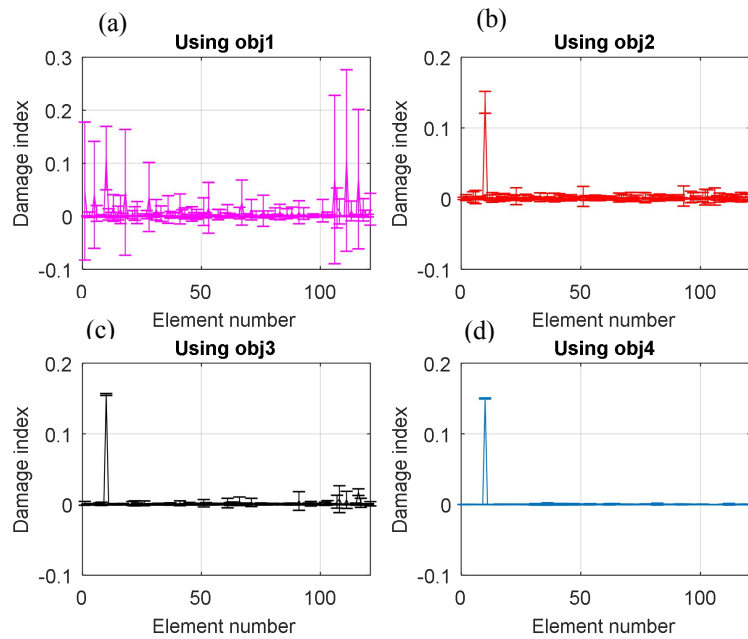


Figure 4-6 Damage identification results of Case 1 in the numerical study:

(a) using *obj1*; (b) using *obj2*; (c) using *obj3*; (d) using *obj4*.

Figure 4-5 shows the iteration processes of the identified damage index α_{10} by using different objective functions. It is observed that using *obj4* converges faster and

provides more accurate damage identification results. Figure 4-6 shows the final damage identification results in all the elements of the truss model by using four different objective functions. The mean values and the variation range with mean values plus and minus standard deviations are shown in Figure 4-6. The identified damage extents in the 10th element by using four objective functions are also given in Table 4-2. It can be observed from Figure 4-6 and Table 4-2 that the identification results by using *obj4* is the most accurate.

Table 4-2 Damage identification results in the numerical studies.

Damage case	Damage location	True value	<i>Obj1</i>		<i>Obj2</i>		<i>Obj3</i>		<i>Obj4</i>	
			Mean value	std.	Mean value	std.	Mean Value	std.	Mean value	std.
Case 1	α_{10}	0.15	0.1098	0.0598	0.1362	0.0154	0.1556	0.0014	0.1511	0.0006
	α_{10}	0.15	0.1351	0.0164	0.1388	0.0155	0.1440	0.0108	0.1486	0.0009
Case 2	α_{45}	0.15	0.1202	0.0475	0.1381	0.0132	0.1347	0.0399	0.1507	0.0007

The second damage case, denoted as “Case 2”, is assumed with 15% stiffness reductions in the 10th and the 45th element, namely, $\alpha_{10} = \alpha_{45} = 0.15$. The input modal data are the same as those in Case 1. The regularization parameters for the *obj2* and *obj4* are set as $5 \cdot 10^{-4}$ and 10^{-6} , respectively. Figure 4-7 shows the identification results of Case 2, and Table 4-2 lists the identified damage extents in the damaged elements. It is clearly observed that when using the *obj1*, a number of significant false identifications are generated. With the sparse regularization term, the false identification by using the *obj2* are greatly reduced. By including Bayesian inference in *obj3*, the identification can be improved as compared with using *obj1*. However, there are still a number of observed false identifications with considerable standard deviations. The identification accuracy by using *obj4* is significantly improved. The identification results from these two damage cases demonstrate the superiority of using both the sparse regularization and Bayesian learning. Using only sparse regularization in *obj2* or Bayesian inference in *obj3* can certainly improve the accuracy and

performance in damage identification. However, when sparse regularization and Bayesian inference are used simultaneously in *obj4*, a much more accurate identification is achieved. The identified damage extents are close to the true values with minor standard deviations, and almost no false identification is observed. These identification results verify that the new objective function based on Bayesian inference and sparse regularization can greatly enhance the accuracy and robustness of utilizing the I-Jaya algorithm for SDI.

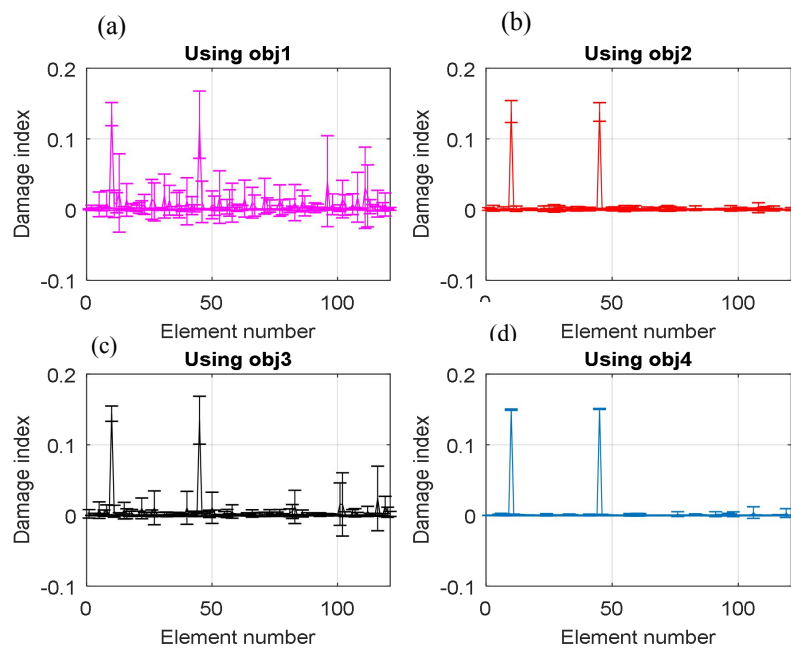


Figure 4-7 Damage identification results of Case 2 in the numerical study:
 using obj1; (b) using obj2; (c) using obj3; (d) using obj4.

4.4.2.2 Damage identification with limited modal data

The superiority of the proposed objective function *obj4* is demonstrated in the above examples. In this section, only the *obj4* is used to investigate the influence on damage identification by using limited modal data. The third damage case, denoted as Case 3, is assumed with 8% stiffness reductions in the 10th, 45th, and 100th element respectively, which means $\alpha_{10} = \alpha_{45} = \alpha_{100} = 0.08$. The first six natural frequencies and different numbers of mode shape values for these six modes are used for identification. Significant measurement noises are added in natural frequencies and mode shapes with

the noise levels of 3% and 5%, respectively. Four scenarios are considered and listed in Table 4-3.

Table 4-3 Used modal data in different scenarios and regularization parameters for Case 3.

Scenario	Number of the used modal data	Quantity of used modal data	λ
1	Six frequencies, and the corresponding mode shapes in the vertical direction at the 2 nd , 7 th , 12 th , ..., 47 th nodes	66	$2 \cdot 10^{-5}$
2	Six frequencies, and the corresponding mode shapes in the vertical direction at the 2 nd , 10 th , 18 th , ..., 50 th nodes	48	10^{-5}
3	Six frequencies, and the corresponding mode shapes in the vertical direction at the 2 nd , 11 th , 20 th , ..., 47 th nodes	42	10^{-5}
4	Six frequencies, and the corresponding mode shapes in the vertical direction at the 2 nd , 12 th , 23 th , 34 th , 45 th nodes	36	$1.2 \cdot 10^{-5}$

Table 4-4 Identified damage extents for Case 3 in the numerical studies.

Damage location	True value	Scenario 1		Scenario 2		Scenario 3		Scenario 4	
		Mean value	std.	Mean value	std.	Mean value	std.	Mean value	std.
α_{10}	0.08	0.0791	0.0008	0.0795	0.0014	0.0793	0.0009	0.0782	0.0021
α_{45}	0.08	0.0800	0.0012	0.0795	0.0013	0.0796	0.0016	0.0786	0.0015
α_{100}	0.08	0.0796	0.0013	0.0788	0.0006	0.0784	0.0010	0.0787	0.0013

It is noted that the number of available modal data used for identification in each scenario is always less than that of unknown system parameters to be identified. For Scenario 4, a much less number of modal data, that is 36, are used to identify 121 unknown elemental stiffness parameters in this study. The selected regularization parameters based on DP rule (Hou et al., 2018) as mentioned above are also listed in Table 4-3. Figure 4-8 shows the iteration processes of the damage index values on the damaged elements for these four scenarios with different numbers of used modal data.

It can be found that after around 200 iterations, all the damage index values converge to the neighborhood of preset values. Figure 4-9 shows the damage identification results of these four scenarios, and Table 4-4 lists the identified damage extents in the damaged elements. Accurate identification results are obtained for all the scenarios, indicating that the introduced damages can be well identified by using the proposed algorithm with the sparse regularization and Bayesian inference, even with a small number of available modal data.

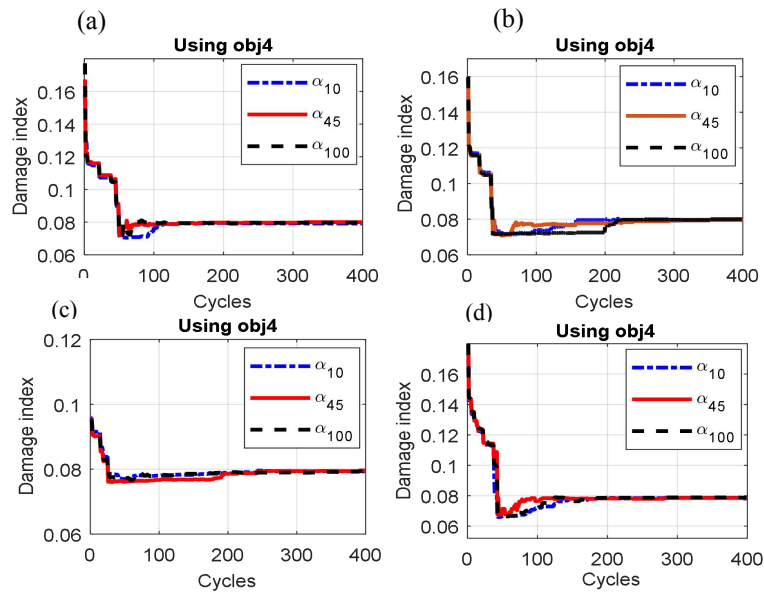


Figure 4-8 The iteration processes of the damage indices in damaged elements in Case 3:

(a) Scenario 1; (b) Scenario 2; (c) Scenario 3; (d) Scenario 4.

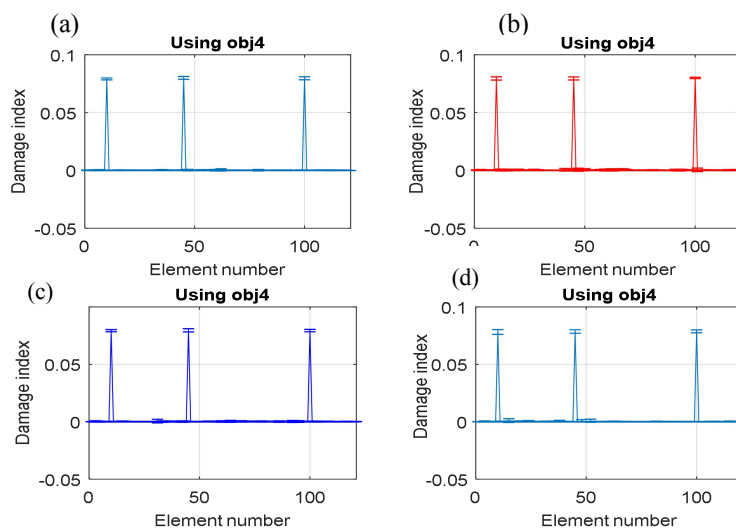


Figure 4-9 Damage identification results in Case 3 based on different inputs:

Scenario 1; (b) Scenario 2; (c) Scenario 3; (d) Scenario 4.

4.4.3 Comparison with other optimization techniques

In this section, other optimization techniques including GA, Nelder-Mead algorithm (Hassan et al., 2018), and Gaussian Bare-bones Artificial Bee Colony (GBABC) algorithm (Zhou et al., 2016) are employed to make comparisons. The fourth damage case, denoted as Case 4, is assumed with 5% stiffness reductions in the 10th, 45th and 100th elements, that is, $\alpha_{10} = \alpha_{45} = \alpha_{100} = 0.05$. This case is defined to simulate minor damage in structures. The used modal data are the same as those defined in Scenario 4 in Table 4-3, and the objective function *obj4* is used for identification with the regularization parameter defined as $1.8 \cdot 10^{-5}$. Significant measurement noises are added in natural frequencies and mode shapes with the noise levels of 3% and 8%, respectively. Regarding the parameters setting, for GA, the colony size is set as 100. The mutation rate and crossover rate are defined as 0.1 and 0.8, respectively. For the Nelder-Mead algorithm, the initial values are set as 0.1 for all the damage indices, which are quite close to the assumed values. For GBABC, the colony size, parameter ‘*limit*’ and the search tendency ‘*ST*’ are set as 100, 6050 and 0.3 respectively, which are the same as those in a previous study (Zhou et al., 2016). The maximum objective function evaluation number is set as 49000 for all these optimization methods.

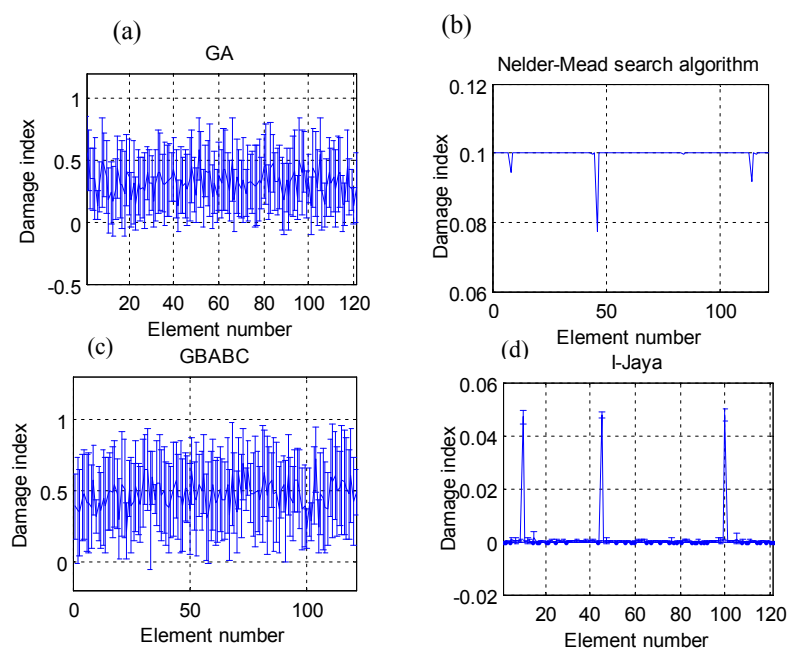


Figure 4-10 Damage identification results of Case 4 with different optimization

Methods; (a) GA; (b) Nelder-Mead algorithm; (c) GBABC; (d) I-Jaya.

Figure 4-10 shows the final damage identification results by using different optimization methods. It is clearly observed that even with the *obj4*, the state-of-the-art heuristic algorithm (GBABC) and the classical heuristic algorithm (GA) and the traditional optimization algorithm (Nelder-Mead) cannot provide accurate and reliable damage identification results. In contrast, the identified damage results from the proposed I-Jaya algorithm are accurate and reliable. The damage identification results on these three damaged elements are: $\alpha_{10} = 0.0469$ with a standard deviation of 0.0025, $\alpha_{45} = 0.0478$ with a standard deviation of 0.0011 and $\alpha_{100} = 0.0477$ with a standard deviation of 0.0025, respectively. The identified damage severities are very close to the assumed values. Besides, the false identifications from the proposed approach are minor. The results in this case demonstrate the superiority of the proposed approach to conduct the minor damage identification in structures with the measurement data of significant noise effect, compared with the latest optimization methods. This lays the foundation for the following experimental verification.

4.4.4 Comparison with the standard Jaya algorithm and other method

In this section, the standard Jaya algorithm and other two methods reported in the literature (Du et al., 2017; Wei et al., 2018) are employed to identify a new damage case. The results are compared with that obtained by the proposed approach to demonstrate the proposed method. The fifth damage case, denoted as Case 5, is assumed having a 50% stiffness reduction in the 10th element, that is, $\alpha_{10} = 0.5$, representing a single large damage in the structure.

Firstly, the standard Jaya and the developed I-Jaya algorithm associated with the *obj4* are used to identify the introduced damage in Case 5. The parameters setting for the Jaya and I-Jaya are the same as those in Cases 1 to 4. The regularization parameter is set as $2 \cdot 10^{-5}$. The used modal data are the same as those in Case 4. Significant measurement noises are assumed in natural frequencies and mode shapes with the noise levels of 3% and 8%, respectively. Figure 4-11(a) shows the evolutionary process of the mean values of the *obj4* with the two methods. It can be found that the values acquired

by the I-Jaya are significantly smaller than those obtained by the Jaya, which indicates the I-Jaya is able to achieve more satisfactory identification results. Figure 4-12 shows the evolutionary process of the identification damage index α_{10} from the I-Jaya algorithm. After around 320 cycles, the algorithm converges to the neighbourhood of the assumed true damage value. Figure 4-13 shows the final identification results in all the elements by using different methods. The Jaya algorithm is not able to identify the damages accurately, but the proposed I-Jaya algorithm is capable of identifying the single large damage effectively, with the mean value of 0.5004 and the standard deviation of 0.0002. The results demonstrate the improvement of the proposed modifications on the standard Jaya algorithm.

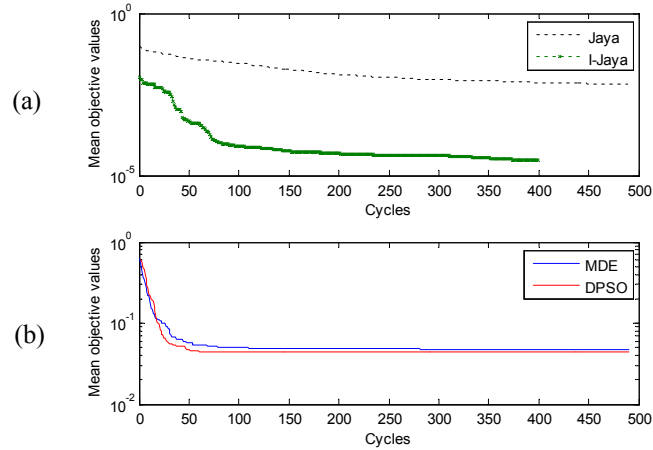


Figure 4-11 The evolutionary process of the objective values;
(a) Jaya and I-Jaya; (b) MDE and DPSO.

To further demonstrate the superiority of the proposed method, two methods for structural damage identification, named after the Modified Differential Evolutionary algorithm (MDE) (Du et al., 2017) and the Disturbed Particle Swarm Optimizer (DPSO) (Wei et al., 2018) are also employed to identify the damage in Case 5. According to Ref. (Du et al., 2017), the flexibility matrix is adopted to formulate the objective function for these two methodologies. For the general parameters setting, their colony size are set as $CS=100$ and their maximum evaluation times are 49000. For MDE, the threshold value is 0.1; the mutation rate is set as 0.4; the mutation constant is a random number locating in $[0.4,0.9]$. These special parameters setting are the same as those in

Reference. For DPSO, it touches the disturbance mechanism after 100 cycles, and two parameters relevant to the disturbance mechanism are $\varepsilon = 10^{-3}$ and $\Delta = 10^{-4}$, respectively. Figure 4-11(b) shows the evolutionary process of the objective values from these two methods. It can be found that their objective function values basically maintain at an order of 10^{-2} after around 100 cycles, which indicates both these two methods would not acquire good identification results for Case 5. The final results obtained from MDE and DPSO are shown in Figure 4-13. Similar to the standard Jaya algorithm, MDE and DPSO cannot provide accurate damage identification results.

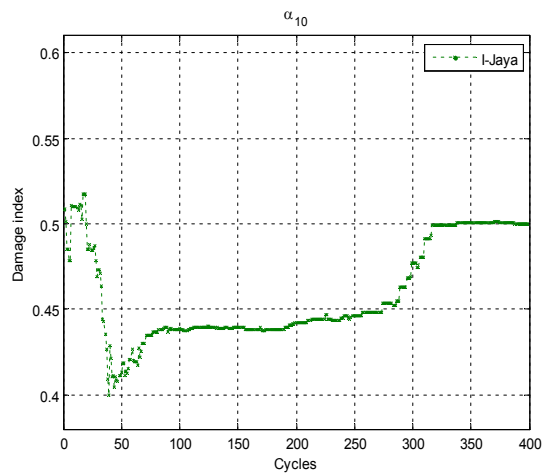


Figure 4-12 The evolutionary process of the identified damage index in the damaged element based on I-Jaya.

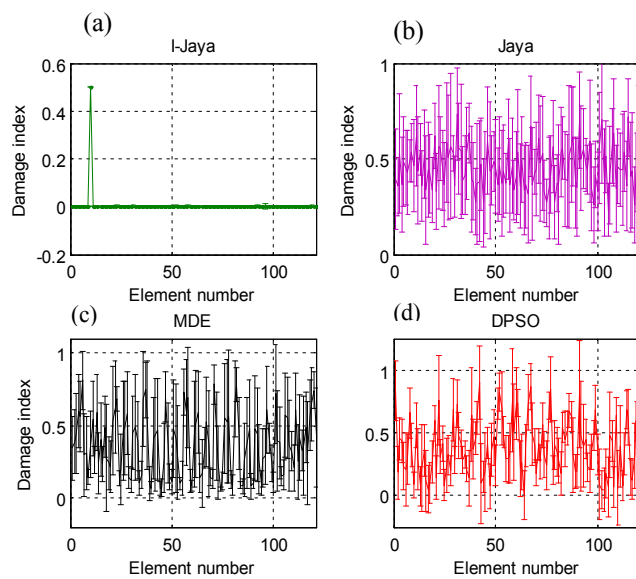


Figure 4-13 Identification results for Case 5: (a) I-Jaya; (b) Jaya; (c) MDE; (d) DPSO.

4.5 Experimental verification

Laboratory studies on a reinforced bridge model are performed to verify the performance of using the developed approach for structural damage detection with experimental testing data.

4.5.1 Experimental setup and initial model updating

Figure 4-14 shows the testing structure, which is a simply supported T-type prestressed concrete bridge model, used for validating the effectiveness of using the proposed algorithm and the objective function including sparse regularization and Bayesian inference for damage identification. Figure 4-15 shows the dimensions of the laboratory model and the placed accelerometer locations for collecting dynamic vibration testing data. The experimental model is 5 meters long. The widths of the slab and web elements, and the height of the bridge model are 0.65m, 0.15m and 0.415m, respectively. The initial Young's modulus and density of the bridge model are respectively 2.6×10^4 Mpa and 2.7×10^3 kg/m³. More details of the bridge model can be referred to (Li et al., 2013). Seven accelerometers are located on the top of the bridge model for acquiring the accelerations in the vertical direction, during the hammer impact tests for modal identification.

An initial model updating based on modal information from the intact structure is conducted to generate a baseline for the subsequent damage identification. An initial finite element model of the bridge is built by using flat shell elements, as shown in Figure 4-16. The finite element model includes 90 elements and 114 nodes with 6 Degrees-of-Freedom (DOFs) at each node. The boundary constraints are simulated by the linear springs. The initial model updating is conducted to adjust the stiffness parameters of the built finite element model by minimizing the difference between the first three natural frequencies acquired from the finite element model analysis and measured from the test. In the initial model updating, the Young's modulus of slab and web of the bridge as well as the support stiffness, that is three parameters in total, are chosen as the parameters to be updated. The proposed I-Jaya algorithm is used to update the initial finite element model. In terms of the parameters setting, CS is set as 30 and the maximum objective function evaluation number is set as 5000. It runs 30

times and the mean values are selected as the final updated parameters. It can be observed from Figure 4-17 that there are discrepancies between the analytical frequencies and the measured one. After updating, the calculated natural frequencies from the updated model match very well with the measured ones. The baseline model is used for the following damage identification.



Figure 4-14 The experimental testing model.

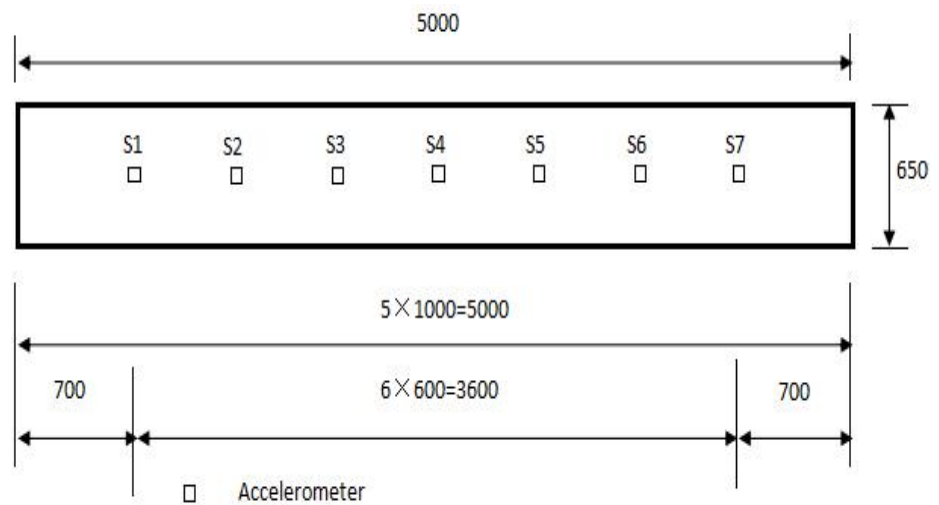


Figure 4-15 Dimensions (unit: mm) of the experimental concrete bridge model and the placed sensor location.

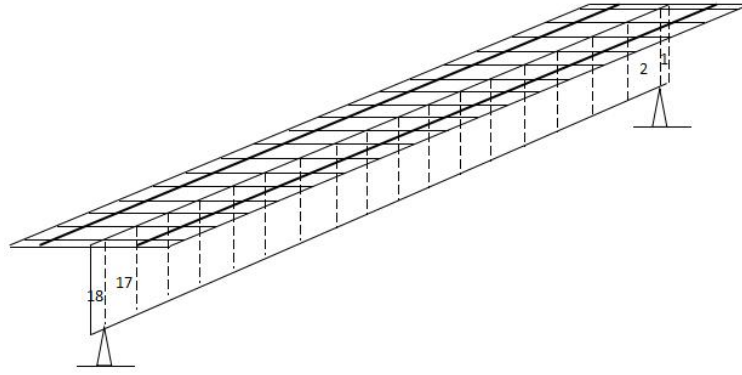


Figure 4-16 The finite element model of the experimental bridge model.

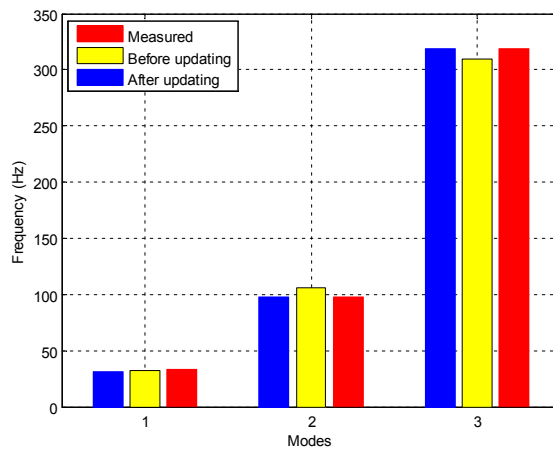


Figure 4-17 The measured and updated frequencies in the experimental studies.

4.5.2 Damage identification for the testing model

The cracks are introduced by applying the two-point loads at the center of the bridge model. Figure 4-18 shows the cracks observed in the web elements, under the static loads of 180KN . This is considered as the damaged state, and the stiffness reductions in web elements are to be identified. Specifically, 24 major cracks are observed in the web elements, which are from the 4th element to the 15th element. Table 4-5 lists the information about the observed typical cracks in the testing model, which are mainly distributed from the 8th element to the 13th element. Modal tests are conducted to obtain the natural frequencies and mode shapes at the sensor locations under the damaged state, as shown in Figure 4-15. These modal data are used as the input for the damage identification. The damages mainly occur in the web elements of the bridge model, and thus only the web elements are included for the identification. Elements 1 and 18 are however not included as they are outside the supports.

The proposed I-Jaya algorithm and the *obj4* are used to conduct the damage identification. The colony size is $CS=50$ and the maximum objective function evaluation number is set as 12250. Multiple measurements are required for the *obj4*, when introducing Bayesian inference. Therefore, similar as Ref. (Chen & Yu, 2017), natural frequencies are assumed to vary within $\pm 3\%$ of their real values. Limited number of modal data, which is less than the total number of the web elements of the structure, are used to identify the damage. The input data include the first natural frequency and the corresponding mode shape values at the placed sensor locations. Therefore totally 8 measured modal data are used to conduct damage identification in web elements. The regularization parameter is set as $\lambda = 5 \cdot 10^{-6}$, based on DP rule. The damage identification will be independently run 30 times to obtain the statistic results.

Figure 4-19 shows the final damage identification result. Since there is no analytical formula to relate a number of observed cracks in a reinforced concrete bridge model with the flexural stiffness of elements, it is difficult if not impossible to obtain the accurate damage extents according to the observed cracks, which are shown in Figure 4-18 and Table 4-5. Therefore the identified damage pattern in Figure 4-19 is compared with the observed crack pattern to validate the effectiveness of the proposed approach for damage identification. The identification results demonstrate that the main damage pattern, with the main damage distributed from the 8th element to the 13th element (Li et al, 2013), can be identified. Considering that only the first frequency and mode shape are used for identification and the main damage pattern can be identified, the results indicate that the proposed approach has the capacity to identify the damages in the experimental model with limited measurement data.



Figure 4-18 Observed cracks in the web elements of the concrete bridge model.

Table 4-5 Reported typical cracks in the tested structure (Li et al.,2018).

Distance from left support of beam (mm)	1800	1950	2125	2260	2340	2540	2680
Web element number	8	8	9	9	9	10	10
Crack height(mm)	280	248	273	286	243	244	261
Distance from left support of beam (mm)	2800	2900	3030	3130	3220	3330	3510
Web element number	11	11	12	12	12	13	13
Crack height(mm)	251	120	260	118	274	220	220

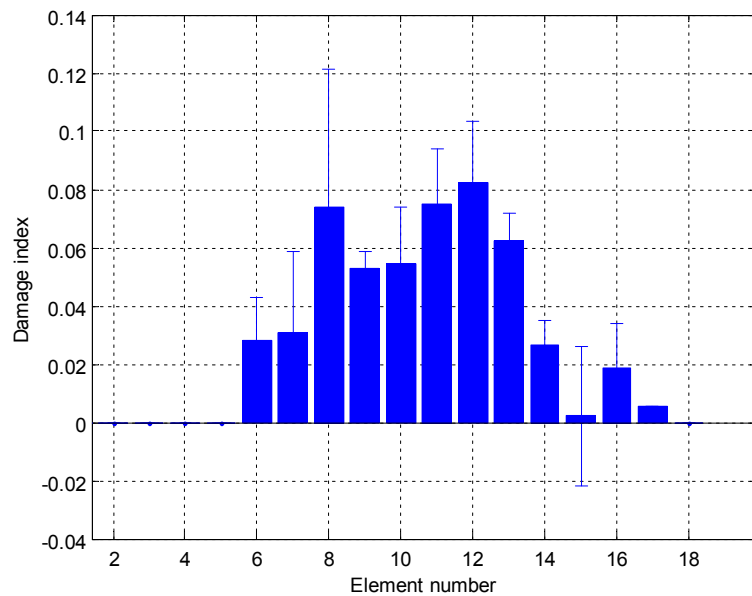


Figure 4-19 Damage identification results of the testing bridge model in the experimental study with limited input data.

4.6 Conclusions

This paper proposes a new approach for damage identification of structures based on I-Jaya algorithm. Since the objective function is important in the damage identification, the sparse regularization and Bayesian inference are added in the traditional objective function based on modal data to perform the damage identification and improve the robustness. Numerical studies on a truss structure are conducted to investigate the accuracy and efficiency of the proposed approach and demonstrate the improvement by using different objective functions for damage identification. Experimental studies on a reinforced concrete bridge model are carried out to verify the

performance and effectiveness of the proposed approach for damage identification with real experimental testing data. Some conclusions can be drawn as follows

- The proposed I-Jaya algorithm is more efficient to deal with the classical benchmark test functions. The results show an improved performance and global optimization ability compared with the original Jaya algorithm;

- Results in the numerical truss example demonstrate that the modified objective function based on the sparse regularization and Bayesian inference yields more reliable and accurate identification results, compared with the traditional objective functions or traditional objective functions with either sparse regularization or Bayesian inference only;

- Compared with other widely used optimization techniques, such as the Nelder-Mead algorithm, GA and GBABC algorithm, results from the proposed approach demonstrate the superiority in identifying the minor damages under the significant noise effect;

- In the experimental verifications, the proposed approach can be used to perform the initial model updating accurately. For the following damage identification, the developed I-Jaya algorithm and the modified objective function based on sparse regularization and Bayesian inference can well identify the damage pattern of a reinforced concrete bridge model with few modal data;

- The damage identification results in the numerical and experimental studies well demonstrate that the proposed approach can effectively and accurately identify the damages in the structures, even when the uncertainty effect is significant.

References

- Beck, J.L., Au, S.K., Vanik, M.W. (1999) Bayesian probabilistic approach to structural health monitoring. *Journal of Engineering Mechanics*, 126(7), 738-745.
- Bornn, L., Farrar, C.R., & Park. G. (2010) Damage detection in initially nonlinear systems. *International Journal of Engineering Science*, 48, 909-920.
- Cai, Z.H., Gong, W.Y., Ling, C.X., & Zhang, H. (2011) A clustering-based differential evolution for global optimization. *Applied Soft Computing*, 11, 1363-1379.
- Chen, Z.P., & Yu, L. (2017) A novel PSO-based algorithm for structural damage detection using Bayesian multi-sample objective function. *Structural Engineering & Mechanics*, 63(6), 825-835.
- Ding, Z.H., Li, J., Hao, H., & Lu, Z.R. (2019) Structural damage identification with uncertain modelling errors and measurement noise by clustering based tree seeds algorithm. *Engineering Structures*, 165, 301-314.
- Ding, Z.H., Lu, Z.R., Huang, M. & Liu, J.K. (2017) Improved Artificial Bee Colony Algorithm for crack identification in beam using natural frequencies only. *Inverse Problems in Science & Engineering*, 25(2), 218-238.
- Ding, Z.H., Yao, R.Z., Li, J., & Lu, Z.R. (2018) Structural damage identification based on modified Artificial Bee Colony algorithm using modal data. *Inverse Problems in Science & Engineering*, 26(3), 422-442.
- Du, D.C., Vinh, H.H., Trung, V.D., Quyen, N.T.H., & Trung, N.T. (2017) An efficient multi-stage optimization approach for damage detection in plate structures. *Advances in Engineering Software*, 112, 76-87.
- Farrar, R.C., & Worden, K. (2007) An introduction to structural health monitoring. *Philosophical Transactions of the Royal Society A*, 365, 303-315.
- Fan, W., & Qiao, P. (2011) Vibration-based damage identification methods: a review and comparative study. *Structural Health Monitoring*, 10(1), 83-111.
- Fan, X.Y., Li, J., Hao, H., & Ma, S.L. (2018) Identification of minor structural damage based on electromechanical impedance sensitivity and sparse regularization. *Journal of Aerospace Engineering*, 31(5), 04018061.
- Figueiredo, E., Radu, L., Worden, K., & Farrar, C.R. (2014) A Bayesian approach based on a Markov-chain Monte Carlo method for damage detection under unknown sources of variability. *Engineering Structures*, 80, 1-10.
- Frishwell, M.I. (2007) Damage identification using inverse methods. *Philosophical Transactions of the Royal Society A*, 365, 393-410.
- Gao, W.F., Chan, F.T.S., Huang, L.L., & Liu, S.Y. (2015) Bare bones artificial bee colony algorithm with parameter adaption and fitness-based neighborhood. *Information Science*, 316, 180-200.
- Guo, H.Y., & Li, Z.L., (2009) A two-stage method to identify structural damage sites and extents by using evidence theory and micro-search genetic algorithm. *Mechanical Systems and Signal Processing*, 23(3), 769-782.
- Hassan, A.K., Moinuddin, M, Al-Saggaf, U.M., Shaikh, M.S. (2018) On the Kernel Optimization of Radial Basis Function using Nelder Mead Simplex. *Arabian Journal for Science & Engineering*, 43(6), 2805-2816.
- Hu, L., Huang, M. & Lu, Z.R. (2017) Crack identification of beam structures using homotopy continuation algorithm. *Inverse Problems in Science and Engineering*, 25(2),

169-187.

Hou, R.R., Xia, Y., Bao, Y.Q., & Zhou, X.Q. (2018) Selection of regularization parameter for L_1 regularized damage detection. *Journal of Sound and Vibration*, 423, 141-160.

Jain, A., Murty, M., & Flynn, P. (1999) Data clustering: a review. *ACM Computing Surveys*, 31(3), 264-323.

Kerschen, G., Worden, K., Vakakis, A.F., & Golinval, J.C. (2006) Past, Present and future of nonlinear system identification in structural dynamics. *Mechanical Systems and Signal Processing*, 20, 505-592.

Li, J., Hao, H., & Chen, Z. (2017) Damage identification and optimal sensor placement for structures under unknown traffic-induced vibrations. *Journal of Aerospace Engineering*, 30(2), B4015001.

Li, J., Law, S.S. & Hao, H. (2013) Improved damage identification in a bridge structure subject to moving vehicular loads: numerical and experimental studies. *International Journal of Mechanical Sciences*, 74, 99-111.

Lu, Z.R., & Wang, L. (2017) An enhanced response sensitivity approach for structural damage identification: Convergence and Performance. *International Journal for Numerical Methods in Engineering*, 111, 1231-1251.

Machado, M.R., Adhikari, S., & Santos, Dos. J.M.C. (2017) A spectral approach for damage quantification in stochastic dynamic systems. *Mechanical Systems and Signal Processing*, 88, 253-273.

Padil, K.H., Bakhary, N., & Hao, H. (2017) The use of a non-probabilistic artificial neural network to consider uncertainties in vibration-based-damage detection. *Mechanical Systems and Signal Processing*, 83, 194-209.

Pandey, A.K., & Biswas, M. (1994) Damage detection in structures using changes in flexibility. *Journal of Sound and Vibration*, 169(1), 3-17.

Rao, R.V. (2016) Jaya: a simple and new optimization algorithm for solving constrained and unconstrained optimization problems. *International Journal of Industry Engineering Computation*, 7, 19-34.

Rao, R.V., & Saroj, A. (2017) A self-adaptive multi-population based Jaya algorithm for engineering optimization. *Swarm and Evolutionary Computation*, 37(4), 1-26.

Santos, A., Figueiredo, E., Silva, M.F.M., Sales, C.S., & Costa, J.C.W.A. (2016) Machine learning algorithms for damage detection: Kernel-based approaches. *Journal of Sound and Vibration*, 363, 584-599.

Shiki, S.B. Silva, S.D., & Todd, M.D. (2017) On the application of discrete-time Volterra series for the damage detection problem in initially nonlinear systems. *Structural Health Monitoring*, 16(1), 62-78.

Shi, Z.Y., & Law, S.S. (1998) Structural damage localization from modal strain energy change. *Journal of Sound and Vibration*, 218, 825-844.

Soize, C. (2013) Stochastic modelling of uncertainties in computational structural dynamics---Recent theoretical advances. *Journal of Sound and Vibration*, 332, 2379-2395.

Soize, C. (2017) Uncertainty quantification. *Interdisciplinary Applied Mathematics*, 47, 1-22.

Sun, H., Lus, H., & Betti, R. (2013) Identification of structural models using a modified Artificial Bee Colony algorithm. *Computers & Structures*, 116, 59-74.

- Sun, H & Betti, R. (2015) A Hybrid Optimization Algorithm with Bayesian inference for probabilistic model updating. *Computer-Aided Civil and Infrastructure Engineering*, 30(8), 602-619.
- Tang, H., Xue, S., & Fan, C. (2008) Differential evolution strategy for structural system identification. *Computer & Engineering*, 86(21-22), 2004-2012.
- Titurus, B., & Friswell, M.I. (2008) Regularization in model updating. *International Journal for Numerical Methods in Engineering*, 75, 440-478.
- Villani, L.G.G., Silva, S.D., & Cunha Jr, A. (2019) Damage detection in uncertain nonlinear systems based on stochastic Volterra series. *Mechanical Systems and Signal Processing*, 125, 288-310.
- Wang, G.S. (2009) Applications of hybrid genetic algorithm to system identification. *Structural Control & Health Monitoring*, 16(2), 125-153.
- Wei, Z.T., Liu, J.K., & Lu, Z.R. (2018) Structural damage detection using improved particle swarm optimization. *Inverse Problems in Science & Engineering*, 26(6), 792-810.
- Xia, Y., Hao, H., Brownjohn, J.M.W, & Xia, P.Q. (2002) Damage identification of structures with uncertain frequency and mode shape data. *Earthquake Engineering & Structural Dynamics*, 31, 1053-1066.
- Xie, Z.B., & Feng, J.C. (2012) Real-time nonlinear structural system identification via iterated unscented Kalman filter. *Mechanical Systems and Signal Processing*, 28, 309-322.
- Yan, A.M., Kerschen, G., Boe, P.D., & Golinval, J.C. (2005a) Structural damage diagnosis under varying environmental conditions---Part I: A linear Analysis. *Mechanical Systems and Signal Processing*, 19, 847-864.
- Yan, A.M., Kerschen, G., Boe, P.D., & Golinval, J.C. (2005b) Structural damage diagnosis under varying environmental conditions---Part II: local PCA for nonlinear cases, *Mechanical Systems and Signal Processing*, 19, 865-880.
- Yang, J.N., Lin, S.L., Huang, H.W., & Zhou, L. (2006) An adaptive extended Kalman filter for structural damage identification. *Structural Health Monitoring*, 13(4), 849-867.
- Yuen, K.Y., & Katafygiotis, L.S. (2003) Bayesian fast Fourier transform approach for modal updating using ambient data. *Advances in Structural Engineering*, 6(2), 81-95.
- Zhang, F.L., Xiong, H.B., Shi, W.X., & Ou, X. (2016) Structural health monitoring of Shanghai Tower during different stages using a Bayesian approach. *Structural Control & Health Monitoring*, 23, 1366-1384.
- Zhou, X.Q., Xia, Y., & Weng, S. (2015) L_1 regularization approach to structural damage detection using frequency data. *Structural Health Monitoring*, 14(6), 571-582.
- Zhou, X.Y., Wu, Z.J., Wang, H., & Rahnamayan, S. (2016) Gaussian bare-bones artificial bee colony algorithm. *Soft Computing*, 20(3), 907-924.
- Zhu, J.J., Huang, M., & Lu, Z.R. (2017) Bird mating optimizer for structural damage detection using a hybrid objective function. *Swarm and Evolution Computation*, 35, 41-52.

CHAPTER 5 STRUCTURAL DAMAGE IDENTIFICATION BY SPARSE DEEP BELIEF NEURAL NETWORK USING UNCERTAIN AND LIMITED DATA

ABSTRACT⁴

The accuracy of structural damage identification is affected by the uncertainties in the vibration measurements and the finite element modelling. This paper proposes a novel approach based on sparse deep belief network (DBN) for structural damage identification with uncertain and limited data. Vibration characteristics, i.e. natural frequencies and mode shapes are extracted as the input to the network, while the output are the damage locations and severities of the structure. DBN is chosen to train the generated datasets and identify structural damages. Restricted Boltzmann Machines (RBMs) are used as building blocks to composite a DBN. To further enhance the capacity of the RBMs, an Arc-tan based sparse constraint is utilized to enable the hidden units to become sparse. This is achieved by adding an Arc-tan norm constraint on the whole of the hidden units' activation probabilities. Numerical and experimental studies are conducted to verify the accuracy and performance of the proposed method. Undetermined damage identification is conducted, in which the quantity of input modal data is less than that of the system parameters to be identified. The identification results show that the proposed sparse DBN based on Arc-tan can identify the damage effectively and its accuracy is better than those obtained by other methods, even when the modelling uncertainty and the measurement noise exist, and only limited data is available.

5.1 Introduction

Structures could accumulate damage during the ongoing in-service period, due to various reasons, such as unexpected extreme loading scenarios such as earthquake,

⁴This chapter was published in Structural Control & Health Monitoring with the full bibliographic citation as follows: Ding, Z., Li, J., & Hao, H. (2020). Structural damage identification by sparse deep belief neural network using uncertain and limited data. *Structural Control & Health Monitoring*, 27(5), e2522. <https://doi.org/10.1002/stc.2522>.

blast and impact, material strength deterioration and fatigue, etc. If these structural damages cannot be inspected and quantified timely, it might lead to catastrophic failures of structures. Therefore, detecting structural damage at an early stage is necessary and important for infrastructure condition monitoring, maintenance planning and asset management. Numerous vibration-based methods have been developed in the past several decades for structural health monitoring and damage detection (Farrar & Worden, 2007; Fan & Qiao, 2011).

Beskhyroun et al. (2010) used a wavelet-based technique to extract representative vibration signals and then these signals were applied for damage identification. Yuen et al. (2004) utilized the modal data and the Markov chain Monte Carlo simulation algorithm to identify damages for the ASCE-IASC four storey benchmark structure. Later, Chatziefttheriou and Lagaros (2017) proposed a new two-loop trajectory method to conduct damage identification. Furthermore, the spectral density method (Pedram et al., 2016), the Bayesian method (Yuen & Ortiz, 2018; Uzun et al., 2019; Zhang et al., 2016, Yuen et al., 2002; Yuen et al., 2006; Hu et al., 2018) and the Kalman filter (Yan et al., 2017) have been respectively employed in the vibration-based structural identification.

From the prospective of mathematics, structural damage identification can be formulated as a pattern recognition problem. Therefore, optimization methods have gained a significant amount of attention in this field. Farshadi et al. (2017) utilized the least square method for damage identification, in which the objective function was formulated based on the incomplete frequency response function. Esfandiari (2017) developed an innovative sensitivity-based method for structural model updating using the modal data. Then this method was successfully applied to a plane truss and a frame structure. Hu et al. (2017) developed an extended constitutive relative error (ECRE) based method for damage identification and the efficiency of this method was demonstrated on a scaled two-story steel frame. More recently, Lu and Wang (2017) developed the enhanced response sensitivity method by using the trust-region algorithm, in which the concrete convergence analysis was conducted to ensure the performance of the enhanced sensitivity method. Other optimization techniques, such

as the Homotopy algorithm (Hu et al., 2017), the minimum constitutive error method (Guo et al., 2018) and the gradient-based method (Aquino et al., 2019), have been developed for structural damage identification. However, the above-mentioned methods usually require a good initial value and the gradient information. Difficulties also arise when using these methods for the identification of large-scale structures with few available measurement data. In addition, uncertainties inevitably exist in the finite element modelling and damage identification process, i.e. finite element modelling errors, measurement noises and uncertain environmental effects, which restricts the practical applications of these traditional optimization methods for civil engineering problems.

On the other hand, Artificial Intelligence (AI) and swarm intelligence methods can be used to overcome the abovementioned drawbacks, since they can learn and make predictions via data instead of the explicit formulations. These methods have the potentials to perform well in identifying structural parameters, even when uncertainties are considered. Many studies by using heuristic algorithms and Artificial Neural Networks (ANN), have been conducted for structural damage identification. Ding et al. (2019a) adopted Tree Seeds Algorithm (TSA) to identify structural damages with uncertainties based on frequency-domain data. Later, Ding et al. (2019b) used Jaya algorithm to conduct damage identification, in which the objective function is modified by using sparse regularization technique and Bayesian inference. Kang et al. (2012) proposed an improved Particle Swarm Optimizer (PSO) to identify structural parameters with and without considering noise contamination in the measurement data. In addition, Ni et al. (1999) proposed a structural damage identification approach by utilizing the Back-propagate (BP) neural network and concluded that using the noise-polluted samples to train the experimental data would acquire better identification results. Jiang et al. (2011) developed a two-stage structural damage identification method based on fuzzy neural networks, in which structural dynamic responses were used as the input to complete the rough assessment. Then the fusion center data was employed as the input and the final decision was obtained by filtering the result with a threshold function. Hence a refined structural damage assessment with a superior reliability was achieved. Xu et al. (2019) proposed an improved Faster

Region-based Convolutional Neural Network (Faster R-CNN) for the multi-type seismic damage identification and localization of reinforced concrete columns from images. Khodabandehlou et al. (2019) used a two-dimensional CNN combined with time domain data to conduct damage identification of a highway bridge. In addition, Modarres et al. (2018) also utilized CNN and images to identify damage types and demonstrated that CNN outperformed several other machine learning methods in identifying damage type. Furthermore, Padil et al. (2017) developed a non-probabilistic ANN to perform structural damage identification considering system uncertainties. Pathirage et al. (2018) proposed the deep auto-encoder neural networks to identify structural damage, in which the first several natural frequencies and mode shapes were employed as the input and structural damage locations and severities were identified as the output.

Although successful identifications and applications have been achieved by using the abovementioned methods, challenges still exist. The modelling uncertainties are not considered in the studies (Kang et al., 2012; Ni et al, 1999; Jiang et al., 2011; Xu et al., 2019) , however, they inevitably exist in real applications. Furthermore, when the input data (frequencies and mode shapes) are polluted by the white noise, the identification accuracy is greatly affected (Kang et al., 2012). For the ANN methods (Ni et al., 1999; Jiang et al., 2011; Padil et al., 2017), their weights relevant to the mapping functions act as a critical role in determining the accuracy and performance of the networks, but these weighting parameters are difficult to obtain accurately for the real applications when significant measurement noise and uncertainties are included in the data. It is well-known that the gradient descent algorithm is one of the most commonly used algorithms for training the neural networks. Nevertheless, when using these algorithms to train the samples, it might suffer gradient vanishing problem, especially when the number of the network's hidden layers is large. Therefore, an auto-encoder based framework was proposed (Pathirage et al., 2018) to improve the networks with deep architecture and more hidden layers. It should be noted that when using this method to conduct damage identification, a sufficient number of input modal data are used. In practice, it could be difficult to obtain a large number of modal parameters for the damage identification of large-scale structures. Therefore, investigating new approaches that require a limited number of modal data for effective identification is of

significant importance. It is noted that, when the number of the input modal data is less than the number of parameters to be identified, the identification becomes a more complex undetermined inverse problem.

Aiming at addressing drawbacks existed in the abovementioned methods, the Deep Belief Network (DBN), a type of new networks in the deep learning field, is employed to conduct the undetermined structural damage identification, by considering uncertainties and using a limited number of modal data less than the parameters to be identified. Based on the DBN's algorithmic structure, it is equipped with the potential to overcome the shortcomings mentioned in the general ANN. This is because the DBN contains several Restricted Boltzmann Machines (RBMs), which is a probabilistic generative model and can be used to extract the features of training samples effectively, providing reliable initial weights and bias for the following training.

To enhance the performance of the DBN, this study mainly concentrates on introducing the sparse technique to improve the standard network. The principle behind this modification is to simulate the humans' visionary system. When a person uses his eyes to recognize images, sparse visionary neurons are activated (Wu et al., 1992). Some existing results in the image process field demonstrate that the sparse technique is capable of eliminating redundant information and noise (Ji et al., 2014). Inspired by this feature, the sparse technique is applied to modify the standard DBN. In order to stimulate the network's sparseness better than that in an existing study (Ji et al., 2014), a more reasonable function, that is Arctangent (termed as Arc-tan) (Luo, 2017), is applied to achieve this goal. Specifically, it explicitly encourages the hidden units in the RBMs to be sparse via adding a sparse constraint on the totality of the hidden units' activation probabilities, forming a modified version of the DBN. The modified DBN could show more sparseness when referring to hidden units' activation. Furthermore, the modification is based on the Arctangent function, therefore the modified DBN is also termed as Arc-tan DBN in this article.

To validate the performance of using the proposed Act-tan DBN for structural damage identification, a three-dimensional truss and a steel frame structure are employed as the numerical example and the laboratory model for verifications. In the numerical studies, 1%

stiffness variations are introduced into the elemental stiffness parameters to simulate the uncertainty in the finite element modelling (Pathirage et al., 2018). A limited number of modal data, which is less than that of system parameters to be identified, are used as the input to the networks. Final identification results show that the proposed Arc-tan DBN has a good robustness and can obtain better results of undetermined structural damage identification than other existing methods.

5.2 Structural damage model

Alterations in structural system parameters, i.e. stiffness, mass and damping, introduce the changes in structural vibration characteristics. Conversely, these changes can be used to identify the structural damages. Vibration properties, such as natural frequencies and mode shapes, etc., of a structure without considering the damping are obtained through conducting the eigenvalue analysis

$$(\mathbf{K} - \omega_i^2 \mathbf{M}) \cdot \Phi_i = 0 \quad (5.1)$$

where \mathbf{K} and \mathbf{M} denote the system stiffness and mass matrices, respectively. ω_i and Φ_i represent the i th natural frequency and the corresponding mode shape.

In this article, structural damage is assumed to be only related to the stiffness reduction. Therefore, the damage of a structure can be expressed by a series of scalar variables for every element $\alpha_i (i=1,2,\dots,nel)$ with the value ranged from 0 to 1,

$$\mathbf{K}_d = \sum_{i=1}^{nel} (1 - \alpha_i) \mathbf{k}_{ei} \quad (5.2)$$

where \mathbf{k}_{ei} denotes the i th elemental stiffness matrix under the undamaged state; nel is the total number of elements of a structure; \mathbf{K}_d means the structural stiffness matrix under the damaged state; α_i denotes the elemental stiffness reduction parameter (also termed as ‘damage index’) to be identified. It shall be noted that $\alpha_i=1$ implies that this element is totally damaged, and $\alpha_i=0$ means that the element is intact.

5.3 Sparse Deep Belief Network

5.3.1 Restricted Boltzmann Machine

Restricted Boltzmann Machine (RBM) is a generative stochastic artificial neural network that can learn a probability distribution over its set of inputs. Its probability distribution is controlled by an energy function E , with the parameter setting $\lambda = \{\mathbf{W}, \mathbf{b}, \mathbf{c}\}$

$$E(\mathbf{v}, \mathbf{h}; \lambda) = -\sum_{i=1}^m c_i v_i - \sum_{j=1}^n b_j h_j - \sum_{i=1}^m \sum_{j=1}^n v_i h_j w_{ij} \quad (5.3)$$

where v_i denotes the binary state of the visible unit i ; h_j represents the binary state of the hidden unit j ; c_i represents the bias weight of v_i ; b_j denotes the corresponding bias weight of h_j ; w_{ij} is the collection weight of the hidden layer h_j and the visionary layer v_i ; m and n denote the total number of the visible and hidden units, respectively; and λ represents the model parameter of the RBM.

Based on the energy function in Eq. (5.3), the joint probability of the state (v, h) can be calculated as

$$p(v, h; \lambda) = e^{-E(v, h; \lambda)} / z(\lambda) \quad (5.4)$$

$$z(\lambda) = \sum_{(v, h)} e^{-E(v, h; \lambda)} \quad (5.5)$$

where z denotes a partition function defined in Eq. (5.5), which enables that the sum of probability distribution in Eq. (5.4) equals to 1. Given the training samples, training the RBM means adjusting the model parameter λ . Specifically, it can be found from Eq. (5.5) that the decrease or increase of the likelihood of the data v can be achieved by changing the model parameter λ .

Due to RBM's feature that there is no intra-layer collections, the activation probability of the hidden unit h_j can be calculated based on the visible units as follows,

$$p(h_j = 1 | \mathbf{v}; \lambda) = \sigma(b_j + \sum_{i=1}^m v_i w_{ij}) \quad (5.6)$$

where $\sigma(x) = \frac{1}{1 + e^{-x}}$. In Eq. (5.6), the activation probability of h_j is determined by the transvection of training data v_i and the weight w_{ij} . The bigger the transvection is,

the larger the activation probability of the h_j is.

Since the structure of RBM is symmetric, the activation probability of the visible unit v_i is decided by the hidden units as follow

$$p(v_i = 1 | \mathbf{h}; \lambda) = \sigma(c_i + \sum_{j=1}^n h_j w_{ij}) \quad (5.7)$$

From Eqs. (5.6) and (5.7), with the visible unit \mathbf{v} , $p(h_j | \mathbf{v})$ can be calculated and used to determine the state of the hidden units. Then new visible states \mathbf{v}^* are obtained through Eq. (5.7). If \mathbf{v}^* is similar as or equal to \mathbf{v} , the hidden units could be viewed as a “reconstruction” of the visible units. Therefore the RBM has the feature-selection ability.

The log probability of the training data, given the model parameter λ , is expressed as

$$\log p(\mathbf{v}; \lambda) = \log \sum_{\mathbf{h}} p(\mathbf{v}, \mathbf{h}; \lambda) \quad (5.8)$$

The purpose of training the RBM is to fit the training samples by adjusting the model parameter λ , as mentioned above. In order to acquire the best λ , it is feasible to apply the gradient method. Conducting the partial derivative of $\log p(\mathbf{v}; \lambda)$ with respect to system parameter set λ yields

$$\frac{\partial \log p(\mathbf{v}; \lambda)}{\partial \lambda} = - \sum_{\mathbf{h}} p(\mathbf{h} | \mathbf{v}) \frac{\partial E(\mathbf{v}, \mathbf{h}; \lambda)}{\partial \lambda} + \sum_{\mathbf{v}, \mathbf{h}} p(\mathbf{v} | \mathbf{h}) \frac{\partial E(\mathbf{v}, \mathbf{h}; \lambda)}{\partial \lambda} \quad (5.9)$$

From Eq. (5.9), it can be found that the second term is difficult to obtain, since it is relevant to the joint probability of the visible and hidden units. To obtain the joint probability, the specific distribution of $z(\lambda)$ ought to be known in advance, which is however fairly tough to obtain. To overcome this drawback, the Contrastive Divergence (CD) method (Luo, 2017; Lin et al., 2016) has been introduced. When using CD method, only several Gibbs sampling steps are required to approximate the gradient information. Therefore, based on the CD method, the complex derivation process in Eq. (5.9) could be replaced by Eq. (5.10) and it has been demonstrated in previous studies that such operation is reasonable and effective (Hinton et al., 2016).

$$\begin{cases} w'_{ij} = w_{ij}^{t-1} + \eta \cdot (\langle v_i h_j \rangle_{\text{data}} - \langle v_i h_j \rangle_{\text{recon}}) \\ c'_i = c_i^{t-1} + \eta \cdot (\langle v_i \rangle_{\text{data}} - \langle v_i \rangle_{\text{recon}}) \\ b'_j = b_j^{t-1} + \eta \cdot (\langle h_j \rangle_{\text{data}} - \langle h_j \rangle_{\text{recon}}) \end{cases} \quad (5.10)$$

where η denotes the step-size; $\langle \cdot \rangle_{\text{data}}$ represents that the probability distribution of $p(\mathbf{h} | \mathbf{v}; \lambda)$ and $\langle \cdot \rangle_{\text{recon}}$ denotes the expectation with respect to the model distribution.

5.3.2 Deep Belief Network

DBN is a probabilistic generative graphical model, or can be called as a class of deep neural networks, which includes several hidden layers. DBN can be considered as a stack of RBM networks, where the hidden layer of each subnetwork is severed as the visible layer for the next. Therefore, as shown in Figure 1, there are l layers in a DBN, which are trained by l RBMs. The parameters of the first RBM, which are composed by \mathbf{x}_0 and \mathbf{h}_1 in Figure 5-1, are trained based on the observed data \mathbf{x}_0 . For the following layers, the greedy learning algorithm is employed to train the network, with the corresponding input defined as the activation of the hidden layer in the previous subnetwork.

A composite model is developed by using the stacked RBMs, as shown in Figure 5-1. The top two layers are defined as the RBM, and the lower one a direct belief net (Hinton et al., 2016). This hybrid model is named after DBN, with the probability function calculated as

$$p(\mathbf{x}_0, \mathbf{h}_1, \mathbf{h}_2, \dots, \mathbf{h}_L) = p(\mathbf{h}_{L-1}, \mathbf{h}_L) p(\mathbf{v} | \mathbf{h}_1) \prod_{L=2}^{L-1} p(\mathbf{h}_{L-1} | \mathbf{h}_L) \quad (5-11)$$

where \mathbf{x}_0 denotes the observed data and $p(\mathbf{h}_{L-1} | \mathbf{h}_L)$ denotes the conditional probability of \mathbf{h}_{L-1} given \mathbf{h}_L . $p(\mathbf{h}_{L-1}, \mathbf{h}_L)$ is the joint probabilistic distribution, which can also be viewed as a RBM's probability distribution with the visible unit \mathbf{h}_{L-1} and the hidden unit \mathbf{h}_L .

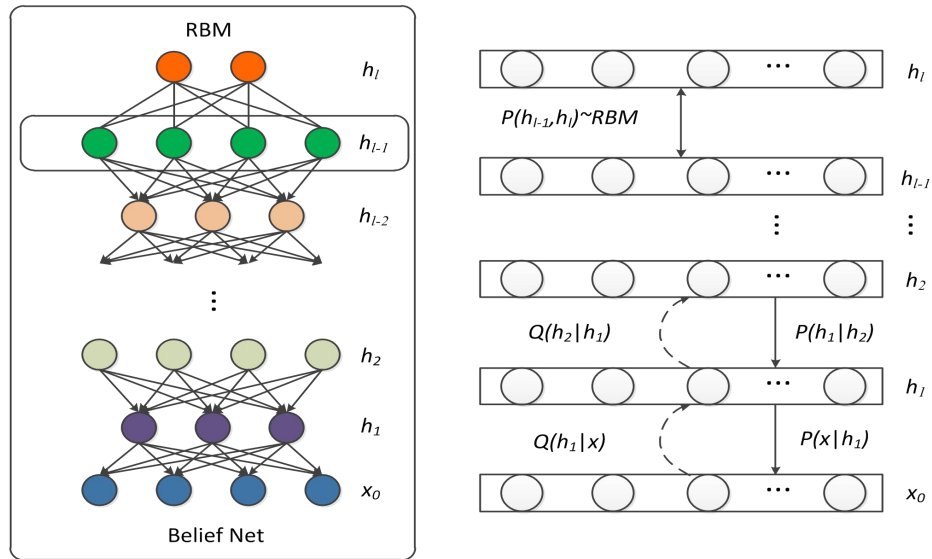


Figure 5-1 The architecture of the proposed DBN.

The training process for DBN is to learn the joint probabilistic distribution $p(\mathbf{x}, \mathbf{h}_1, \mathbf{h}_2, \dots, \mathbf{h}_L)$. However, the difficulty of this model lays on the post model probability $p(\mathbf{h}_{l-1} | \mathbf{h}_l)$, which is unable to calculate. According to reference (Hinton et al., 2016), this post probability can be approximated as $Q(\mathbf{h}_l | \mathbf{h}_{l-1})$, which is defined in the RBM and can be calculated by using Eq. (5-7). The whole training process contains two stages. The first stage, namely ‘pre-training’, is based on the greedy algorithm to obtain the initial value. The second stage is called ‘Fine-tuning’, which generally utilizes the supervised algorithm to obtain the final network parameters. The greedy algorithm is a type of unsupervised algorithm, which uses the sampling data to train the first RBM (data \mathbf{x} and \mathbf{h}_1 composed in the first RBM). Then the parameters of the first RBM are utilized to initialize the first layer’s parameters of the DBN. The input for the first RBM is calculated for the DBN based on $Q(\mathbf{h}_1 | \mathbf{x}_0)$. The newly calculated output will be employed as the input for the next layer until completing L layers. Then a fine-tuning mechanism is introduced, in which the BP network is employed to obtain the final systematic parameters. Therefore, it can be found out that, compared with the random initialization of the traditional ANN, the RBM enables the DBN with a good initial value and thus guarantees a better performance.

5.3.3 Sparse RBM based on Arc-tan

It has been reported in existing studies on the mammalian brain that only few neurons were activated when given a stimulation (Ji et al., 2014). Namely, an event could be encoded by a few neurons. Based on this evidence, extending the sparsity into machine learning algorithms becomes popular. In the sparse encoding (Hinton et al., 2006; Donoho, 2006), the L_0 norm as the quantity of non-zero elements in a vector is usually used to achieve the sparsity. However, the L_0 norm is non-convex and the optimization belongs to a Non-deterministic Polynomial-time (NP)-hard problem, that is, directly optimizing the L_0 norm is very difficult (Lee et al., 2007). To overcome this issue, in this study, a smooth function, that is Arc-tan (Salehani et al., 2014), is used to approach the L_0 norm, which is given as

$$f(\varepsilon, x) = \sum_{i=1}^n \frac{2}{\pi} \arctan\left(\frac{x_i}{\varepsilon}\right) \quad (5.12)$$

where n denotes the dimension number of x with $0 < \varepsilon < 1$, $0 \leq x_i \leq 1$. It is obvious that when ε approaches zero, the proposed Arc-tan function is the closest to the L_0 norm, as shown in Figure 5-2. Compared with using the L_1 norm and the Log-sum norm (Ji et al., 2014), the used Arc-tan norm is more reasonable and rational, since the shape of Arc-tan function is more similar to the L_0 norm. It is relatively easy to compute the gradient information of the Arc-tan function. Furthermore, the Arc-tan norm is directly utilized to control the activation probability of the hidden units. The specific Arc-tan based penalty item is defined as

$$R = \sum_{l=1}^m \sum_{j=1}^k \frac{2}{\pi} \arctan(|Ex(\mathbf{h}_l^j | \mathbf{v}_l)| / \varepsilon) \quad (5.13)$$

where $Ex(\cdot)$ represents the conditional expectations given m training samples, k denotes the total number of the hidden units, ε is the hyper-parameter that controls the similarity between the Arc-tan norm and the L_0 norm.

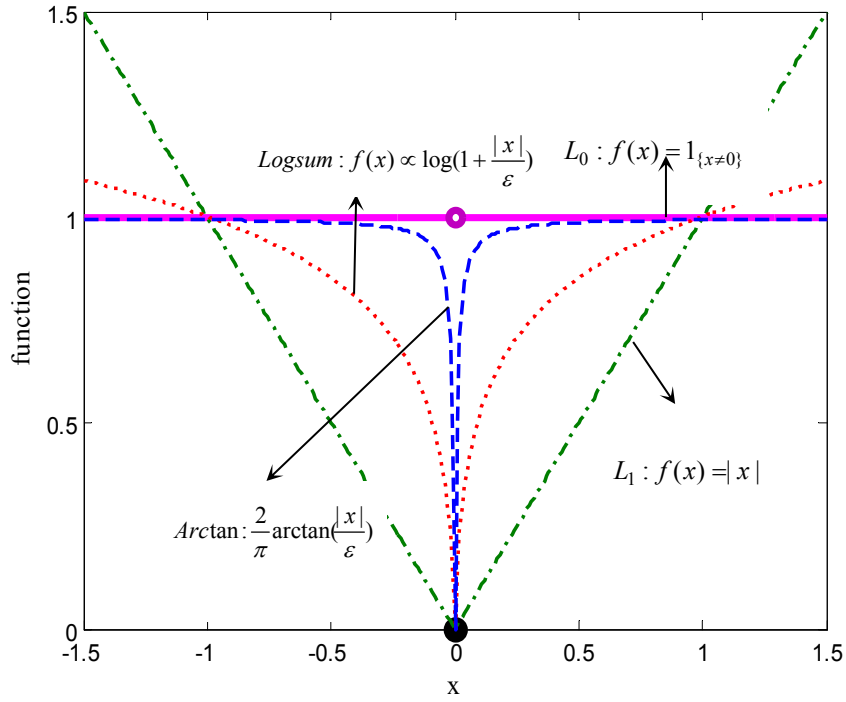


Figure 5-2 Demonstration of the functions used for approximating the L_0 norm, the Log-sum norm and the proposed Arc-tan norm with a hyper-parameter $\varepsilon = 0.01$.

In order to achieve the sparse representation, it ought to maximize the log likelihood function as well as the Arc-tan norm. Therefore, given the m sample data, the objective function to be optimized in the Arc-tan based RBM is given as below

$$\lambda^* = \arg \max_{\lambda} \sum_{i=1}^m \log(\mathbf{v}_i, \lambda) - \tau \sum_{i=1}^m \sum_{j=1}^k \frac{2}{\pi} \arctan(|E(\mathbf{h}_i^j | \mathbf{v}_i)| / \varepsilon) \quad (5.14)$$

in which

$$E(\mathbf{h}_i^j | \mathbf{v}_i) = p(\mathbf{h}_i^j = 0 | \mathbf{v}_i) \cdot 0 + p(\mathbf{h}_i^j = 1 | \mathbf{v}_i) = p(\mathbf{h}_i^j = 1 | \mathbf{v}_i) \quad (5.15)$$

$$p(\mathbf{h}_i^j = 1 | \mathbf{v}_i) = \sigma(c_j + \sum_i v_i^j w_{ij}) \quad (5.16)$$

where τ is a regularization parameter, reflecting the important relationship between the data distribution and the regularization (penalty) term. From Eq. (5.14), it is clear that the learning process for the Arc-tan based RBM is to maximize the likelihood and minimize the penalty term. With the introduced penalty term, the structure of the standard RBM is not altered. Therefore it is still effective to use the previous CDs method to optimize the likelihood part in the objective function, as shown in Eq. (5.14).

Algorithm 1 CD algorithm of parameters updating for the Arc-tan RBM for one epoch and one

sample

1. Update the parameters using CDs learning scheme as below

$$w_{ij} \leftarrow w_{ij} + \eta \cdot (\langle v_i h_j \rangle_{\text{data}} - \langle v_i h_j \rangle_{\text{recon}})$$

$$b_i \leftarrow b_i + \eta \cdot (\langle v_i \rangle_{\text{data}} - \langle v_i \rangle_{\text{recon}})$$

$$c_j \leftarrow c_j + \eta \cdot (\langle h_j \rangle_{\text{data}} - \langle h_j \rangle_{\text{recon}})$$

where η is a learning rate, and $\langle \cdot \rangle_{\text{recon}}$ is an expectation over the reconstructive data, which is estimated with one iteration of Gibbs sampling.

2. Update the parameter c_j via using Eq. (5-16).

3. Repeat Step 1 and Step 2 until the maximum epoch is reached.

The specific procedure of solving Eq. (5.14) is described as follows: Firstly, the CDs method is used to update the model parameters. Secondly, the gradient descent algorithm is used to calculate the penalty term. The gradient of the penalty term is calculated as

$$\frac{\partial}{\partial w_{ij}} R = \frac{1}{\varepsilon} \frac{2}{\pi} \sum_{i=1}^m \frac{1}{1 + (p_i^j / \varepsilon)^2} p_i^j (1 - p_i^j) \mathbf{v}_i \quad (5.17)$$

$$\frac{\partial}{\partial c_j} R = \frac{1}{\varepsilon} \frac{2}{\pi} \sum_{i=1}^m \frac{1}{1 + (p_i^j / \varepsilon)^2} p_i^j (1 - p_i^j) \quad (5.18)$$

To increase the computational efficiency, when using the gradient descent algorithm to update the penalty term, it would only need to update the bias c_j , since c_j is directly related to activate the hidden units (Salehani et al., 2014). The learning process for the parameters updating of the Arc-tan RBM is summarized in Algorithm 1.

5.3.4 Sparse DBN based on the Arc-tan RBM

As s mentioned above, stacking several RBMs to constitute a DBN is able to extract more abstract and meaningful characteristics. The proposed novel sparse DBN consists of several Arc-tan RBMs. Therefore, the proposed DBN in this article is marked as Arc-tan DBN, as mentioned in introduction. A greedy layer-by-layer training can also be used in the proposed Arc-tan DBN. Equally, while the bottom Arc-tan RBM is trained, the parameters w_{ij} , c_i and b_j are fixed and the probability of every hidden unit given the data is

calculated by Eq. (5.6). Then these probabilities are employed as the ‘data’ to train the next layer in the network. This operation could be repeated several times to learn a deep, hierarchical and sparse model. Once finishing the calculation of several stacked Arc-tan RBMs, the generated weight coefficients and bias parameters are applied to initialize the following fine-tune network. The fine-tune network is a BP network with G layers and is trained via using the conjugate gradient method. In the fine-tune stage, the Mean Squared Error (MSE) is used to measure the training accuracy of each epoch. Assuming that there are NoS samples in total in the observed and trained datasets denoted as **observed** and **trained**, the MSE is expressed as

$$MSE = \frac{1}{NoS} \sum_{i=1}^{NoS} (\mathbf{observed}_i - \mathbf{trained}_i)^2 \quad (5.19)$$

5.4 Numerical studies

In this section, the accuracy by using the proposed approach for structural damage identification is demonstrated with the simulation data generated from a spatial building frame structure. Two types of uncertainties, including the modeling errors and the measurement noise are considered in the following numerical studies.

5.4.1 Numerical Model

A 72-element building frame structure as shown in Figure 5-3 is used in numerical study. The Young’s modulus and mass density of this structure are defined as 210 GPa and 7800 kg/m³, respectively. Each node has three degrees-of-freedom (DOFs). The 1st, 2nd, 3rd and 4th nodes are constrained by a large stiffness. The cross-section area of each element is $2.5 \times 10^{-3} \text{ m}^2$. The first five frequencies and mode shapes are utilized as the input for the training of the network, while the output is the structural element-level damage indices. The mode shapes are measured at the 5th, 7th, 9th, 11th, 13th, 15th, 17th and 19th nodes, along the x -axial direction. Considering the data normalization, therefore the quantity of modal data is 40 in total, which is less than the total number of structural elements, which is 72. That is, the proposed algorithm will be used to perform the undetermined inverse identification. 1% stiffness variations with Gaussian distribution are introduced into the elemental stiffness parameters to simulate the uncertainties in the finite element

modelling (Pathirage et al., 2018). The standard DBN and the Log-sum DBN are also used to perform structural damage identification for comparison.

5.4.2 Data generation for training

For the training samples, it is assumed that the damage index for two specific elements are changed from 0.01, 0.02,..., to 0.3, while the other elements remain intact. 230,040 samples are generated in this example. The input data for the networks are the first five incomplete modal data while the output is a series of elemental damage indices α . Regarding the parameter setting for the above-mentioned three networks, namely, standard DBN, Log-sum DBN and the proposed Arc-tan DBN, these models are trained with 100 visible units and 100 hidden units. All the training samples in the numerical studies are executed by using CD training algorithm for Arc-tan RBM based on mini-batches of sizes 20 with two iterations. For the following fine-tuning training, a four layer BP network is introduced. The mini-batches size is set as 36 and the epoch is set as 2×10^5 . Particularly, according to Ref. (Jin et al., 2014), for the Log-sum DBN and the proposed Arc-tan DBN, the regularization parameter τ and the hyper parameter ε are set as 0.05 and 0.1, respectively. The numerical computations are conducted on a desktop computer with an Intel i7 8700k processor, 32 GB RAM for parallel computing. The training time of the DBN, Log-sum DBN, and the proposed Arc-tan DBN last around 7.8 hours, 7.6 hours, and 7.5 hours, respectively. Basically, the computation time of these three DBNs are similar and the proposed Arc-tan DBN is slightly fast.

Figure 5-4 shows the activation probabilities of hidden units over the generated 230,040 samples. The quantity of the hidden units of the DBN, the Log-sum DBN and the proposed Arc-tan DBN, with an activation probability exceeding 0.5, are 30, 26 and 18, respectively. Furthermore, the proposed Arc-tan DBN has the most hidden units, with an activation probability lower than 0.1, among the three approaches. Therefore, the proposed Arc-tan DBN exhibits the sparsity well.

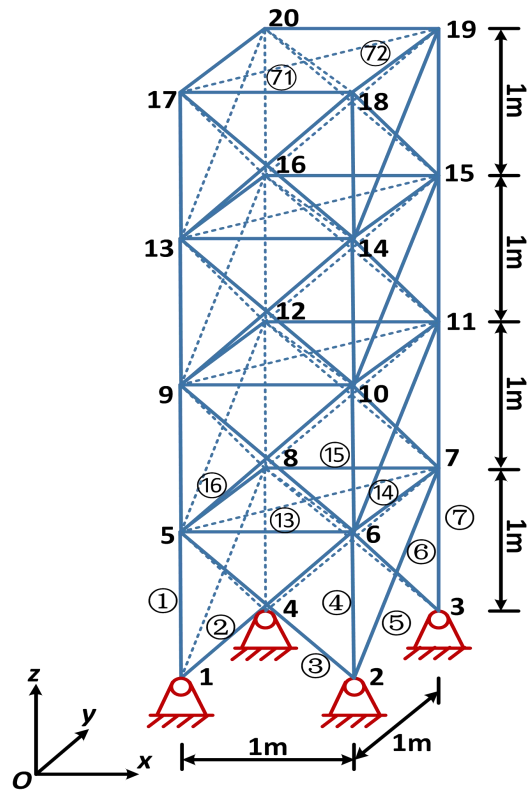


Figure 5-3 The building structure model used in numerical study.

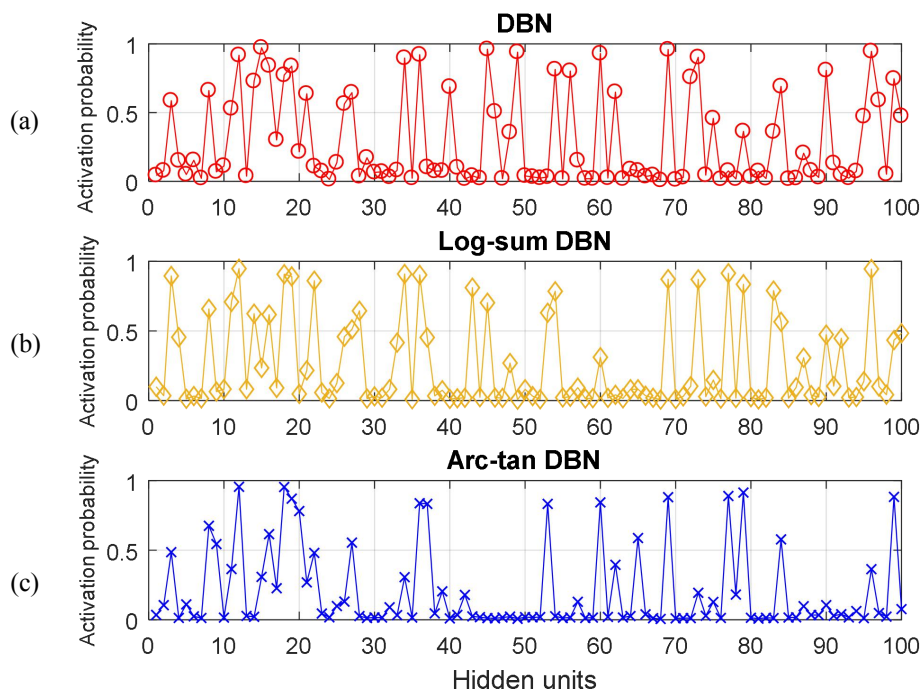


Figure 5-4 The activation probability of hidden units for the trained samples:

(a) DBN; (b) Log-sum DBN; (c) Arc-tan DBN.

To further illustrate the sparsity of the used three networks for training data samples, Figure 5-5 is provided, in which the vertical axis is the number of activation times on training samples for every hidden unit. It is observed that when training the data samples, the number of activated hidden units based on the proposed Act-tan DBN is significantly less than those of the standard DBN and the Log-sum DBN. The majority of hidden units are activated when using the standard DBN, in contrast, a significant less number of hidden units are activated while utilizing the proposed Arc-tan DBN. That is to say, nearly all hidden units of the standard DBN act as an important role in the representation of the data, but only a minority of hidden units in the proposed Arc-tan DBN are important for the data representation and network training to achieve a good performance. This further demonstrates that with the assistance of the introduced modifications, the sparsity of the proposed network has been greatly enhanced. As mentioned in Section 5.3.3, the principle of introducing the sparsity is to simulate human's visionary system, which requires to activate several neurons while the majority of neurons keep sleep when eyes work (Ji et al., 2012). Therefore, the Arc-tan DBN would achieve a better network training efficiency and accuracy, due to its good sparsity feature.

MSE is employed to present the training accuracy. MSE acquired by the standard DBN, the Log-sum DBN and the proposed Arc-tan DBN are 5.64×10^{-4} , 4.33×10^{-4} and 2.87×10^{-4} , respectively. This indicates that with the assistance of using the Arc-tan norm, the fitting performance of the standard DBN has been obviously enhanced. This also lays the foundation for the following damage identification. To test the generalization ability of the mentioned three approaches, a variety of damage cases, including the single damage, two damages and three damages, will be tested. Furthermore, in order to investigate the influence of noise levels on the identification results, 2% white noise is added into the frequency and 6% white noise is added into the mode shapes.

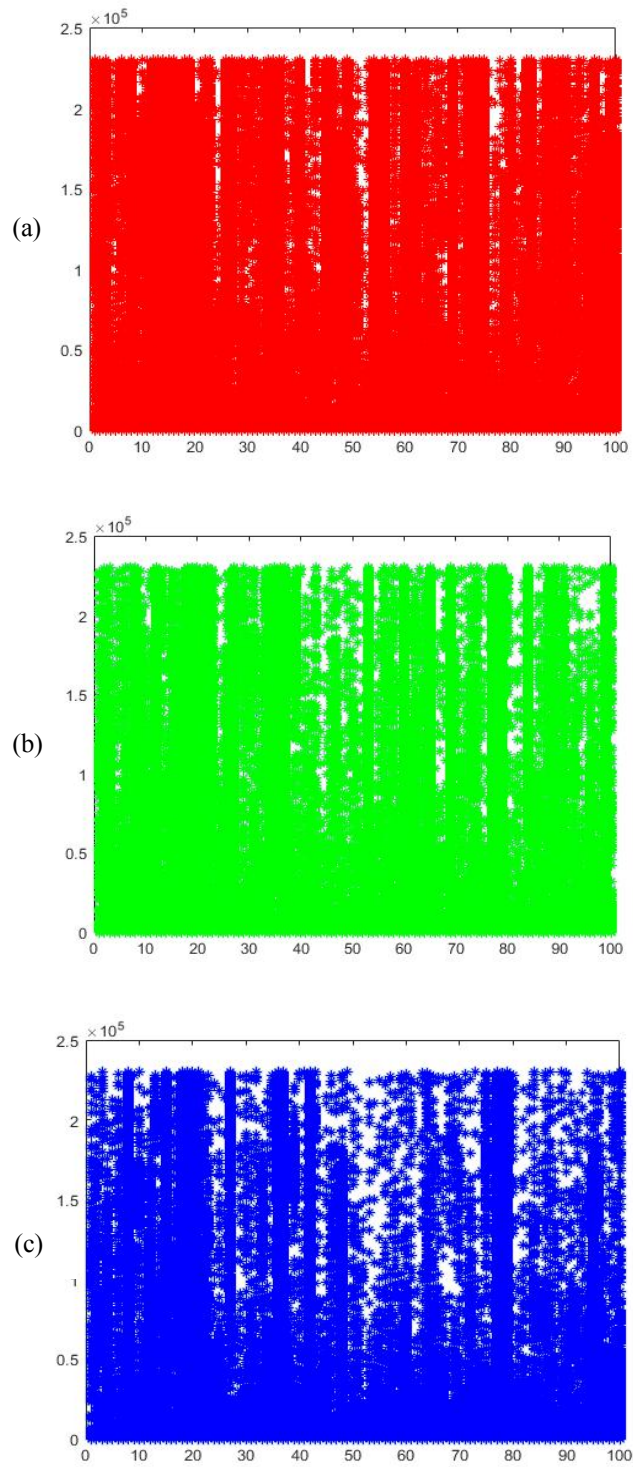


Figure 5-5 The activation times of each hidden unit on training samples:

(a) Standard DBN; (b) Log-sum DBN; (c) Arc-tan DBN.

5.4.3 Damage identification results

First, a single minor damage case is considered. It is assumed that there is an 8% stiffness reduction in the 15th element, which means $\alpha_{15} = 0.08$. This damage scenario is not within the training data set. Figure 5-6 displays the final identification result and it is clearly observed that these three approaches can locate the damage, but the results obtained by the proposed Arc-tan DBN are the most accurate. The absolute identification errors of the 15th element for the DBN, Log-sum DBN and the Arc-tan DBN are 0.0107, 0.0157 and 0.0021, respectively. Through comparing these identification results, the accuracy and robustness of utilizing the proposed Arc-tan DBN for minor single structural damage detection with uncertainty effects (modelling errors and measurement noises) are illustrated.

Second, a case with two minor damages is considered. It is assumed that there is a 5% stiffness reduction in the 1st element and a 10% stiffness reduction in the 50th element, which means $\alpha_1 = 0.05$ and $\alpha_{50} = 0.1$. The final identification results based on these three trained networks are shown in Figure 5-7. It is clear that the proposed Arc-tan DBN is capable of identifying both locations and extents of preset double small damages accurately, even the measurement noise and modelling errors are introduced in the data. The maximum identification absolute errors of the damaged elements based on the Arc-tan DBN is 0.0071, better than those acquired by the Log-sum DBN (0.0105) and the standard DBN (0.0201).

The third damage case is that there are a 5% damage in the 1st element and a 45% damage in the 20th element, which means, $\alpha_1 = 0.05$ and $\alpha_{20} = 0.45$. This damage scenario is defined to investigate the performance of identifying a minor damage and a large damage, which is not within the training data set. The input data are the same as the previous case. Figure 5-8 shows the final identification results. These three networks could localize the damages but the proposed Arc-tan DBN is able to obtain the best identification accuracy. For the damaged elements, the maximum identification error by using the proposed Arc-tan DBN is 0.0256, better than those obtained by the Log-sum DBN (0.0356) and the standard DBN (0.0480).

The fourth case includes three damage locations, i.e., a 20% stiffness reduction in the 1st element, a 30% stiffness reduction in the 25th element, and a 30% stiffness reduction in the 27th element, which means $\alpha_1 = 0.2$, $\alpha_{25} = 0.3$, and $\alpha_{27} = 0.3$. This damage scenario is defined to investigate the performance of identifying three damages, which is not within the training data set. Figure 5-9 shows the final identification results. Similar with the previous three cases, these three networks could localize the damages but the proposed Arc-tan DBN can obtain the best identification accuracy. For the damaged elements, the maximum identification error by using the proposed Arc-tan DBN is 0.0164, again better than those obtained by the Log-sum DBN (0.0211) and the standard DBN (0.0321).

The above numerical studies and results demonstrate that the proposed Arc-tan DBN performs better than the standard DBN and the Log-sum DBN in damage identification, even when the incomplete and uncertain modal data are used.

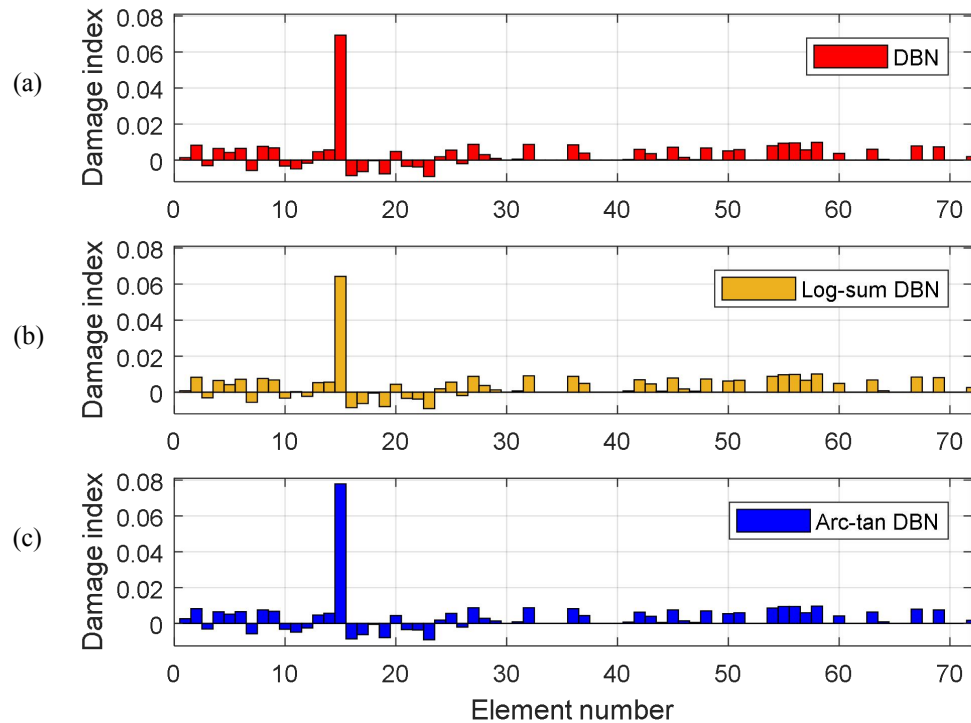


Figure 5-6 Identification results for a single minor damage case by using:

(a) Standard DBN; (b) Log-sum DBN; (c) Arc-tan DBN.

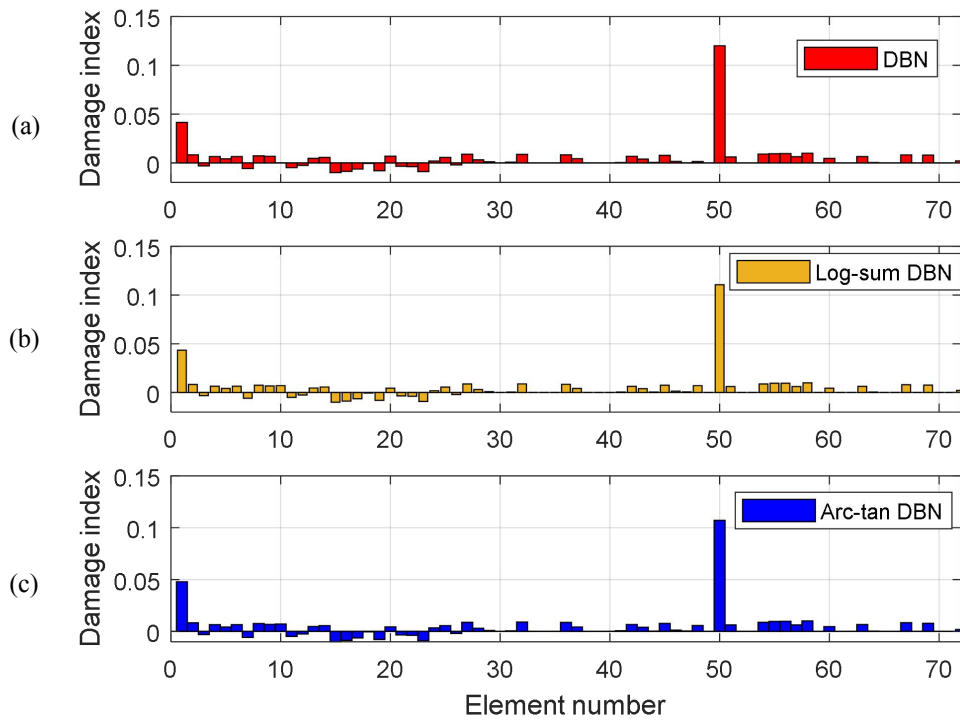


Figure 5-7 Identification results for a case with two minor damages by using: (a) DBN; (b) Log-sum DBN; (c) Arc-tan DBN.

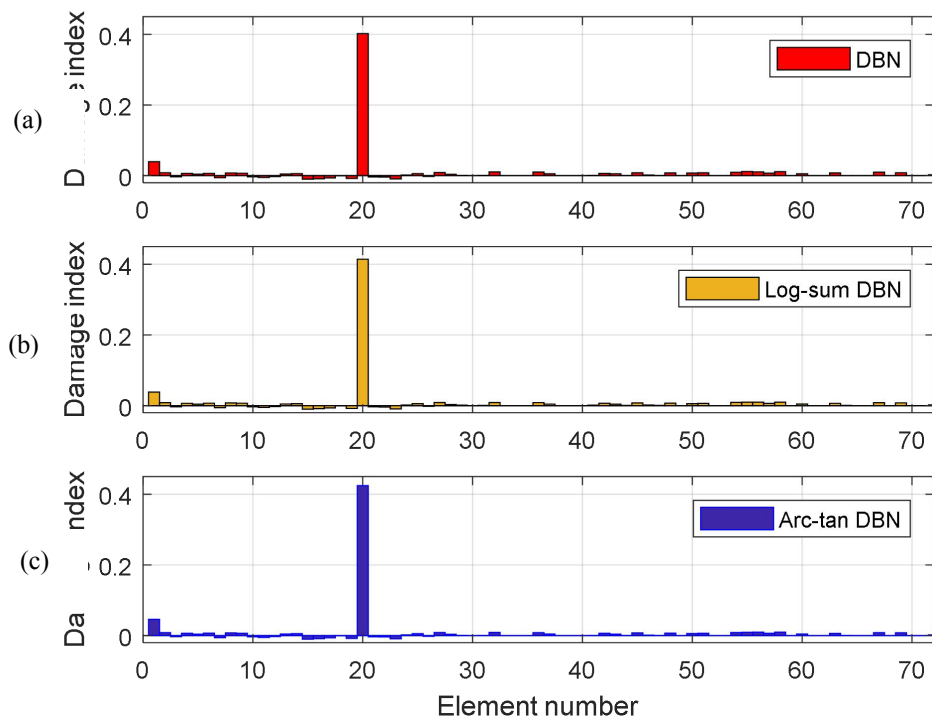


Figure 5-8 Identification results for a minor damage and a large damage case by using: (a) DBN; (b) Log-sum DBN; (c) Arc-tan DBN.

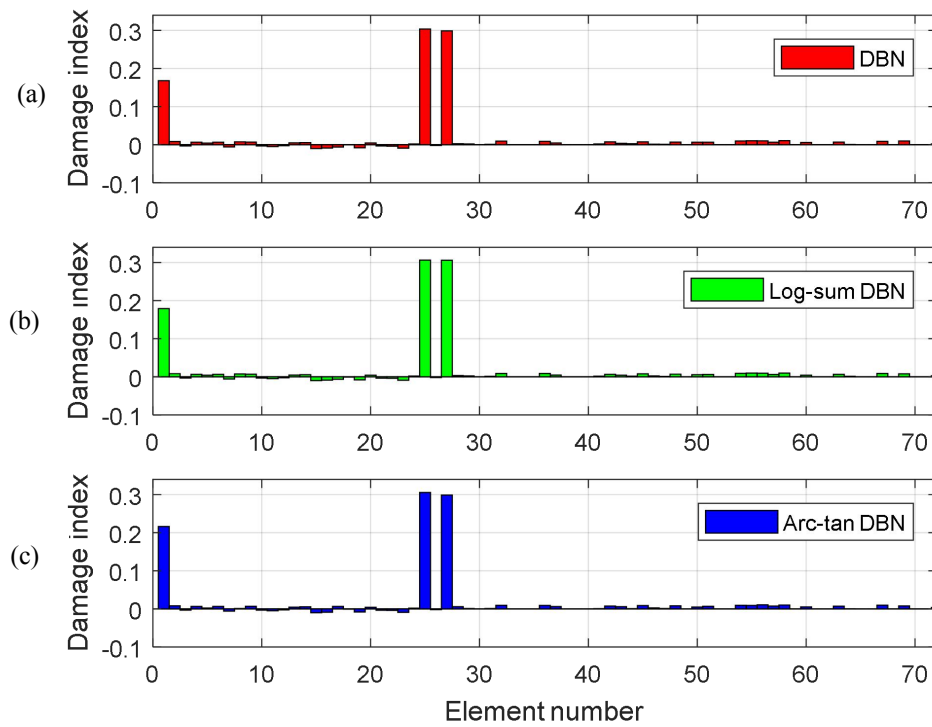


Figure 5-9 Identification results for the case with three damages by using: (a)DBN; (b) Log-sum DBN; (c) Arc-tan DBN.

5.5 Experimental verification

Laboratory studies on an eight-story shear-type steel frame model are conducted to verify the performance of the proposed approach. The detailed finite element model is described in reference (Ni et al., 2018). Figure 5-10 shows the fabricated shear type steel frame structure. The height and width of the frame structure are 2000 mm and 600 mm, respectively. The floors of this model are simulated by several thick steel bars with a dimension of 100 mm × 25 mm. Two flat bars of the same cross-section with a width of 50 mm and a thickness of 5 mm are used as columns. The beams and columns are welded. The bottom of the frame structural model is welded onto a thick plate. As regards the material properties, the initial elastic modulus and mass density of the steel are respectively 200 GPa and 7850 kg/m³.



Figure 5-10 A eight-storey steel frame model.

Dynamic responses of the structure under a modal hammer impact with a rubber tip are obtained. Acceleration responses in the lateral direction of all the floors under the hammer impact are measured. The sampling rate is set as 1024 Hz and the cut-off frequency range for the band-pass filter is set from 1 Hz to 100 Hz for all the responses. The initial finite element model is built with eight lumped mass and the abovementioned material properties.

5.5.1 Initial finite element model updating

To identify structural damage accurately, the initial model updating should be performed and the updated model is used as the baseline for the following damage identification. Vibration data from the experimental model under the undamaged state are used to conduct the model updating by minimizing the discrepancy of some dynamic properties, such as natural frequencies and mode shapes. In this study, the first-order sensitivity based method is utilized for modal updating (Lu & Wang, 2017;

Pathirage et al., 2018). Figure 5-11 presents the first eight measured natural frequencies, and analytical frequencies before and after updating. The updated frequencies are very close to the measured ones, indicating that an accurate finite element model is obtained as the baseline.

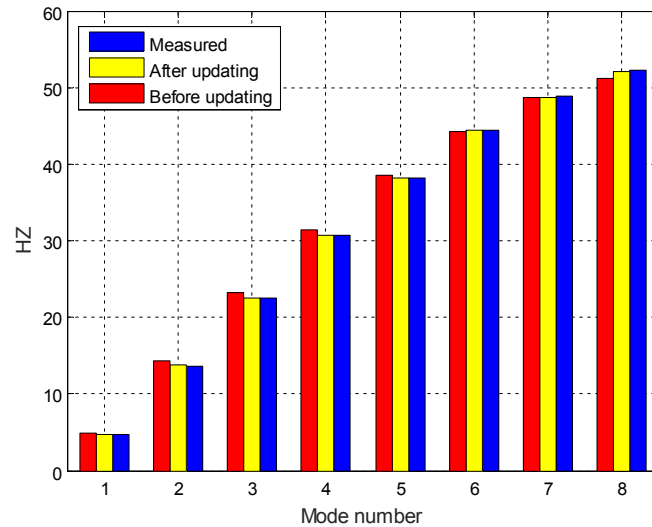


Figure 5-11 Measured and analytical frequencies of the laboratory model before and after updating.

5.5.2 Data generation for training

Similar as the numerical studies, experimental verification on undetermined inverse identification is also conducted. Therefore, only the first seven natural frequencies are applied as the input to the networks, in contrast to the scenario with a number of modal data used in an existing study (Pathirage et al., 2018). For convenience, the element is defined to describe the floor/beam of the frame structure. That is, the 1st element means the first floor/beam of the frame. Multiple damages are simulated to generate the training datasets based on the above baseline model. Specifically, the stiffness parameters for arbitrary two elements change from 1, 0.99, ..., to 0.4, while maintaining the remaining elements undamaged. A total of 100,800 multiple damage cases are generated.

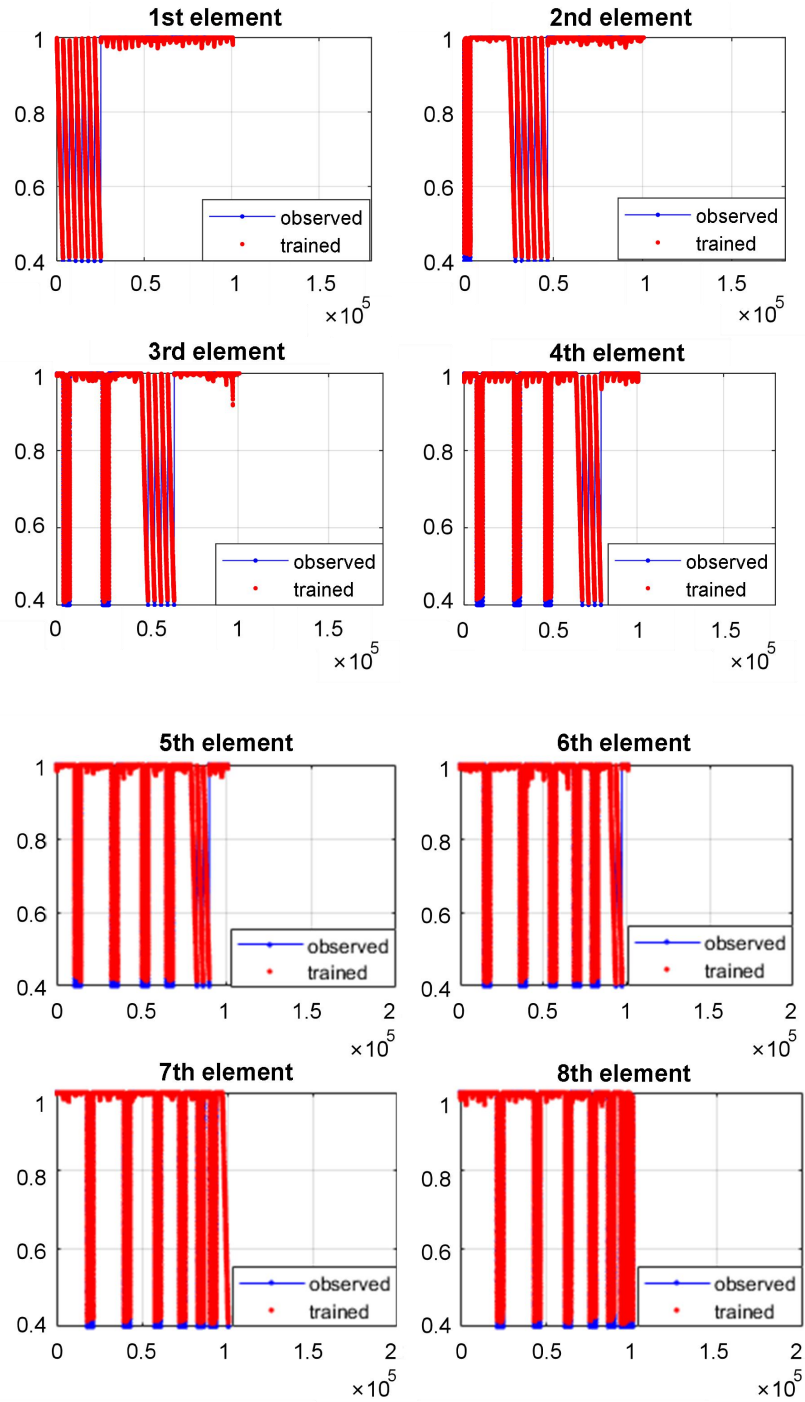


Figure 5-12 The fitting results on all the elements of the trained and observed samples based on the proposed Act-tan DBN.

The superiority of the proposed Arc-tan DBN over the standard DBN and the Log-sum DBN has been illustrated in the numerical studies, therefore only the proposed Arc-tan DBN is used for the experimental verifications. However, three

state-of-the-art swarm intelligence algorithms are introduced for the comparison purpose. Regarding the parameter setting for the proposed Arc-tan DBN, the network model is trained with 100 visible units and 100 hidden units. All the training sample datasets in the experimental verification are executed by using CD training algorithm for the RBM based on mini-batches of sizes 20 with one iteration. After training the RBMs, the weighting parameters would be transmitted to initialize the following used four layers BP network. The batch-size is set as 56 and the epoch is set as 5000. The regularization constant τ and the sparse constant ε are set as 0.01 and 0.1, respectively, based on studies on optimal parameter selection in sparse regularization (Ji et al., 2014). The computations for experimental verifications are conducted on a desktop computer with an Intel i7 8700k processor, 32 GB RAM for parallel computing. The whole training time lasts around 1.5 hours.

MSE value obtained by the proposed Arc-tan DBN in this experimental study is 3.53×10^{-4} . Figure 5-12 shows the fitted results from the 1st element to the 8th element of the observed and trained samples based on the proposed Arc-tan DBN. It is clearly observed that the trained samples are close to the observed ones. Such good agreements indicate the satisfactory training process by using the Arc-tan DBN is achieved. Then the trained networks are used for the following single and multiple damage identification. However, it ought to be noted that in reference (Pathirage et al., 2018), single damage scenarios are particularly designed to train the networks for identifying the single damage.

5.5.3 Damage identification results

Two realistic damage cases are introduced to the laboratory steel frame model and vibration tests are conducted. The measured natural frequencies are used as the input to the trained networks to test the accuracy of the proposed approach. In Case 1, a single damage is considered, which is introduced with a 20% reduction of the equivalent stiffness in the 2nd element. In Case 2, multiple damages are introduced, that is, besides the damage in Case 1, another damage is introduced with 10% stiffness reduction in the 7th element (Ni et al., 2018).

After training and validating the designed Arc-tan DBN, the first seven

frequencies from the above two damage cases are employed as the input to identify structural damages. Figures 5-13(a) and (b) present the final identification results. It should be noted that the single damage case is not included in the training datasets. For Case 1, the developed Arc-tan DBN can localize and quantify the damage accurately, although only one very minor error alarm is observed in the 7th element with the damage index value less than 0.01. The absolute identification error for the 2nd element is 0.0023. For Case 2, two introduced damages are identified accurately and the absolute identification errors for the 2nd and 7th elements are 0.0051 and 0.0137, respectively.

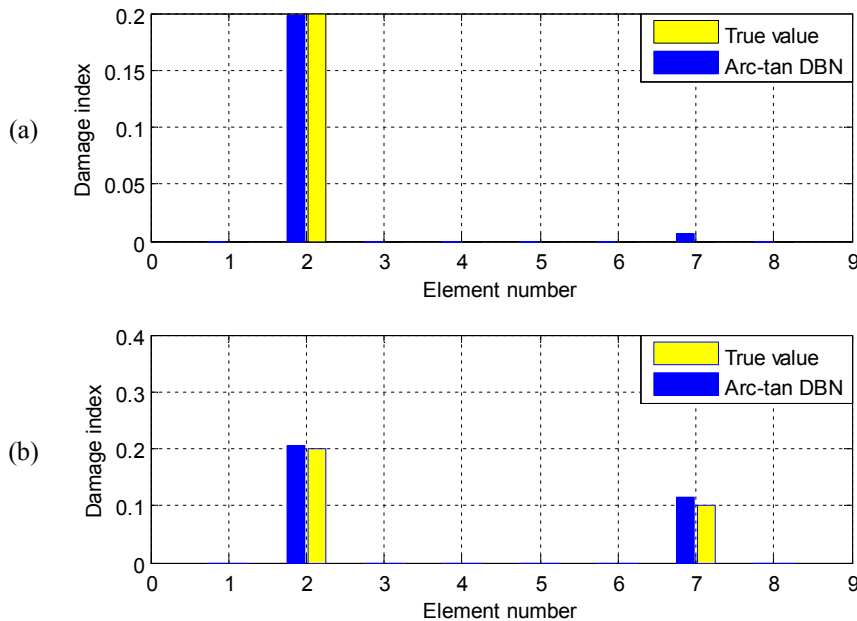


Figure 5-13 Identification results based on the Arc-tan DBN: (a) Single damage case; (b) Multiple damages case.

5.5.4 Comparisons with swarm intelligence methods

Three state-of-the-art swarm intelligence methods, including the Gbest-guided Artificial Bee Colony algorithm (GABC) (Zhu & Kwong, 2010), the Modified Differential Evolutionary algorithm (MDE) (Du et al., 2017) and the Jaya algorithm (Du et al., 2018), are used for structural damage identification with the same measurement data, for demonstration of the effectiveness of the proposed method. To

ensure the fair comparison between different methods, only the first seven natural frequencies are used to build up the objective function, which is expressed as

$$f(\mathbf{a}) = \sum_{l=1}^7 \frac{|\omega_l^c - \omega_l^{measured}|}{|\omega_l^{measured}|} \quad (5.20)$$

where ω_l^c represents the l th calculated natural frequency and $\omega_l^{measured}$ denotes the l th measured frequency. The abovementioned swarm intelligence methods are used to optimize the objective function.

Regarding the common parameters setting, the colony size is $CS = 50$ and the maximum iteration number is 200. Specifically, for GABC, the controlling parameter 'limit' is set as 200 according to reference (Karaboga & Gorkemi, 2014). For MDE, the threshold value and mutation rate are set as 0.1 and 0.4, respectively, and the mutation constant is a random number locating between $[0.4, 0.9]$. These special parameter settings are the same as those in previous studies (Du et al., 2017). Each damage case is identified with 20 independent runs, and the mean values are employed as the final identification results.

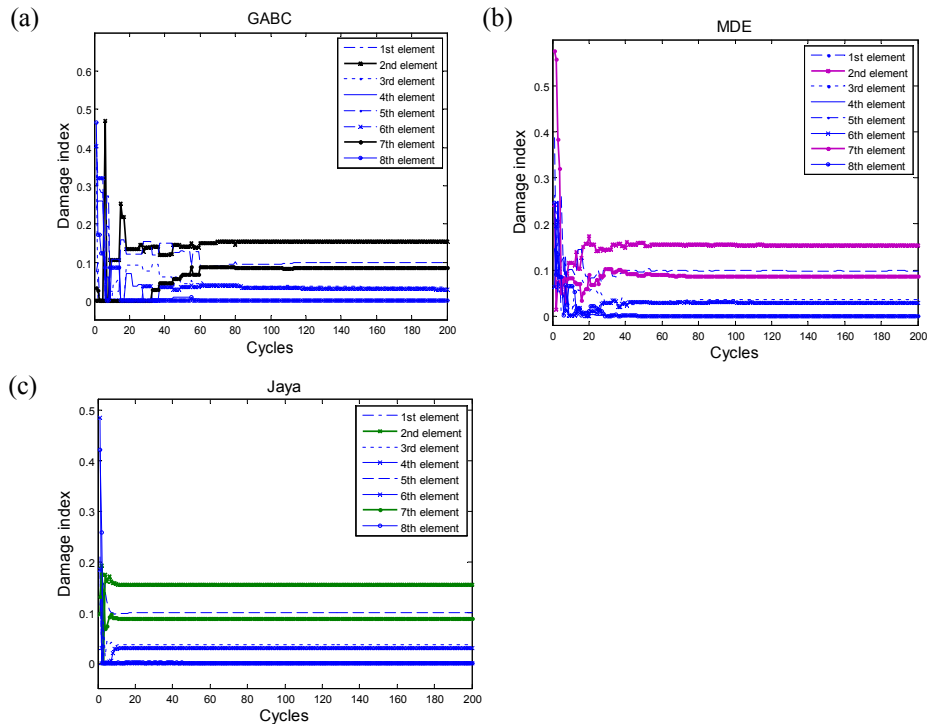


Figure 5-14 The iteration processes of all damage indices based on swarm intelligence methods for Case 2: (a) GABC; (b) MDE; (c) Jaya.

Figures 5-14(a), (b) and (c) provide the iteration process of all damage indices of Case 2, by using GABC, MDE and Jaya algorithm respectively. It is observed that when the maximum iteration number is reached, all the damage indices obtained by using these three algorithms almost acquire the same identification results. The difference is reflected through their different convergence rates.

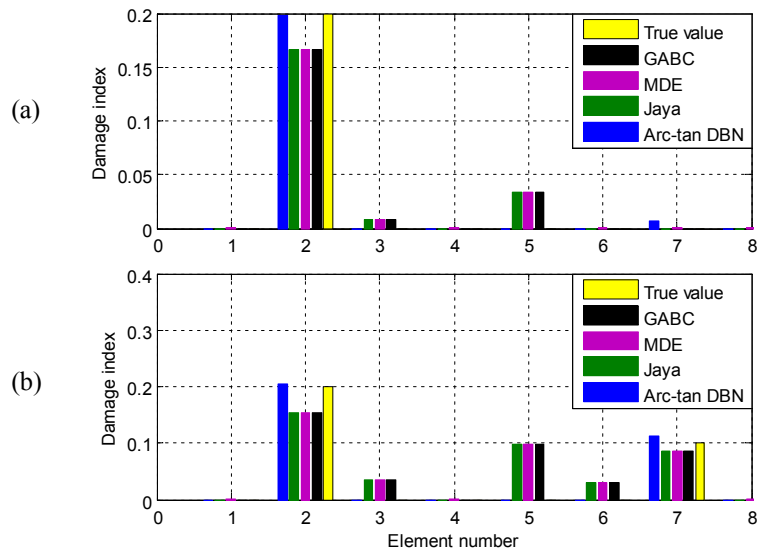


Figure 5-15 Identification results by using three swarm intelligence methods and the Arc-tan DBN: (a) Single damage case; (b) Multiple damages case.

The final identification results for Cases 1 and 2 based on the three algorithms are shown in Figures 5-15(a) and (b). It should be noted that only seven natural frequencies are used as input, and this is an undetermined inverse problem. It is clearly observed that, for the single damage case, these three algorithms obtain more significant false identifications, i.e. around 3% in the 5th element. Furthermore, for Case 2 with multiple damages, these three algorithms could not localize the damages accurately, since three false positives are observed in the 3rd, 5th and 6th elements. Comparing the results in Figure 5-15, the proposed approach based on Arc-tan DBN provides a better identification accuracy than using these three algorithms. The potential reason can be explained from the difference of principle between the DBN and swarm intelligence methods. Generally speaking, when using the swarm intelligence methods to optimize

the objective function built by the natural frequencies, several obvious false alarms would occur. This is because the objective function to be optimized is an ill-posed problem and limited measurement information is provided, which means that small perturbation would cause significant fluctuations in final identification results (Pan et al., 2016). There are several ways to address this drawback, such as, introducing the regularization technique to convert the ill-posed objective function to well-posed one. It is commonly accepted that structural damages are usually observed at a few locations (Hou et al., 2018), therefore the damage index should be a sparse vector with most of its items equal to zero or at least close to zero, except the damaged elements with non-zero entries. Based on this prior knowledge, regularization technique has been widely applied in the area of structural damage identification to improve the accuracy and stability of the solution, especially when performing some relatively difficult identification problems (Hou et al., 2019; Wang et al., 2020). Or combining the information of mode shape to formulate the objective function (Ding et al., 2016). In contrast, the DBN basically trains its ‘inference ability’ through learning the data samples. Therefore, the DBN could achieve better identification results with the training data and the well-designed networks and used sparse constraints.

In summary, these results demonstrate the superiority of the proposed Arc-tan DBN, compared with the three state-of-the-art swarm intelligence methods for solving the undetermined damage identification problem. Meanwhile, these results further illustrate that the proposed Arc-tan DBN can well identify the structural damages with uncertainties, since the testing data measured from the experimental model already include environmental noise and testing uncertainties.

5.6 Conclusions

A new type of deep learning method named Arc-tan DBN is presented for structural damage identification. To enhance its performance, a sparse penalty term based on Arc-tan norm is introduced. The undetermined inverse identification is conducted. The number of input modal data is less than that of the system parameters to be identified, which increases the complexity and difficulties of structural damage identification. Numerical simulations on a building structure model and experimental

studies on a shear-type steel frame structure are carried out to validate the proposed approach. The conclusions can be given as below:

- With the assistance of the Arc-tan norm, the sparsity representation of the samples could be clearly observed. The sparsity presentation is beneficial to improve the fitting performance of the developed networks. The standard DBN, Log-sum DBN and the proposed Arc-tan DBN can be applied to locate damages, even when the incomplete modal data with uncertainties are used. It is noted that the accuracy of the proposed Arc-tan DBN is the best.

- When performing the damage identification of example structures, the proposed Arc-tan DBN can identify structural damages by using several natural frequencies only, give better identification results than the swarm intelligence methods, especially when using them to identify multiple damages.

- In summary, results in the numerical and experimental studies demonstrate that the proposed Arc-tan DBN is a promising tool to perform structural damage identification with incomplete modal data.

References

- Aquino, W., Bunting, G., Miller, S.T., & Walsh, T.F. (2019) A gradient-based optimization approach for the detection of partially collected surfaces using vibration tests. *Computer Methods in Applied Mechanics and Engineering*, 345, 323-335.
- Beskhyroun, S., Oshima, T., & Mikami, S. (2010) Wavelet-based technique for structural damage detection. *Structural Control & Health Monitoring*, 17(5), 473-494.
- Chatzieleftheriou, S., & Lagaros, N.D. (2017) A trajectory method for vibration based damage identification of undetermined problems. *Structural Control & Health Monitoring*, 24(3), e1883.
- Ding, Z.H., Li, J., Hao, H., & Lu, Z.R. (2019a) Structural damage identification with uncertain modelling errors and measurement noise by clustering based tree seeds algorithm. *Engineering Structures*, 165, 301-314.
- Ding, Z.H., Li, J., & Hao, H. (2019b) Structural damage identification using improved Jaya algorithm based on sparse regularization and Bayesian inference. *Mechanical Systems and Signal Processing*, 132, 211-231.
- Ding, Z.H., Huang, M., & Lu, Z.R. (2016) Structural damage detection using artificial bee colony algorithm. *Swarm and Evolutionary Computation*, 28, 1-13.
- Donoho, D.L. (2006) Compressed sensing. *IEEE Transaction on Information Theory*, 52(4), 1289-1306.
- Du, D.C., Vinh, H.H., Trung, V.D., Quyen, N.T.H., & Trung, N.T. (2017) An efficient multi-stage optimization approach for damage detection in plate structures. *Advances in Engineering Software*, 112, 76-87.
- Du, D.C., Vinh, H.H., Trung, V.D., Quyen, N.T.H., & Trung, N.T. (2018) Efficiency of Jaya algorithm for solving the optimization-based structural damage identification problem based on a hybrid objective function. *Engineering Optimization*, 50(8), 1233-1251.
- Esfandiari, A. (2017) An innovative sensitivity-based method for structural model updating using incomplete modal data. *Structural Control & Health Monitoring*, 24(4), e1905.
- Fan, W., & Qiao, P. (2011) Vibration-based damage identification methods: a review and comparative study. *Structural Health Monitoring*, 10(1), 83-111.
- Farrar, R.C., & Worden, K. (2007) An introduction to structural health monitoring. *Philosophical Transactions of the Royal Society A*, 365, 303-315
- Farshadi, M., Esfandiari, A., & Vahedi, M. (2017) Structural model updating using incomplete transfer function and modal data. *Structural Control & Health Monitoring*, 24(7), e1932.
- Guo, J., Wang, L., & Takewaki, I. (2018) Modal-based structural damage identification by minimum constitutive relation error and sparse regularization. *Structural Control & Health Monitoring*, 25(12), e2255.
- Hinton, G.E., Osindero, S., & Teh, Y.W. (2016) A fast learning algorithm for deep belief nets. *Neuralcomputing*, 18, 1527-1554.
- Hinton, G.E., & Salakhutdinov, R.R. (2016) Reducing the dimensionality of data with neural networks. *Science*, 313(5768), 504-507.
- Hou, R.R., Xia, Y., Xia, Q., & Zhou, X.Q. (2019) Genetic algorithm based optimal sensor placement for L_1 regularized damage detection. *Structural Control & Health*

Monitoring, 26(1), e2274.

Hou, R.R., Xia, Y., & Zhou, X.Q. (2018) Structural damage detection based on L_1 regularization using natural frequencies and mode shapes. *Structural Control & Health Monitoring*, 25(3), e2107.

Hu, J., Lam, H.F., & Yang, J.H. (2018) Operational modal identification and finite element model updating of a coupled building following Bayesian approach. *Structural Control & Health Monitoring*, 25(2), e2089.

Hu, L., Huang, M. & Lu, Z.R. (2017) Crack identification of beam structures using homotopy continuation algorithm. *Inverse Problems in Science and Engineering*, 25(2), 169-187.

Hu, X., Prabhu, S., Atamturktur, S., & Cogan, S. (2017) Mechanistically informed damage detection using dynamic measurements: Extended constitutive relation error. *Mechanical Systems and Signal Processing*, 85, 312-328.

Jiang, S.F., Zhang, C.M., & Zhang, S. (2011) Two-stage structural damage detection using fuzzy neural networks neural networks and data fusion techniques. *Expert Systems with Applications*, 38, 511-519.

Ji, N.N., Zhang, J.S., Zhang, C.X. & Yin, Q.Y. (2014) Enhancing performance of restricted Boltzmann machines via log-sum regularization. *Knowledge-based Systems*, 63, 82-96.

Kang, F., Li, J.J., & Xu, Q. (2012) Damage detection based on improved particle swarm optimization using vibration data. *Applied Soft Computing*, 12, 2329-2335.

Karaboga, D., & Basturk, B. (2008) On the performance of artificial bee colony (ABC) algorithm. *Applied Soft Computing*, 8, 687-697.

Khodabandehlou, H., Pekcan, G., & Fadali, M.S. (2019) Vibration-based structural condition assessment using convolution neural networks. *Structural Control & Health Monitoring*, 26(2), e2308.

Lee, H., Ekanadham, C., & Ng, A. (2007) Sparse deep belief net model for visual area V2. In: *Proceedings of Advances in Neural Information Processing Systems*, 1416-1423.

Lin, P.T., Fu, S.W., Wang, S.S., Lai, Y.H., & Tsao, Y. (2016) Maximum entropy learning with deep belief neural network. *Entropy*, 18(7), 251-269.

Lu, Z.R., & Wang, L. (2017) An enhanced response sensitivity approach for structural damage identification: Convergence and Performance. *International Journal for Numerical Methods in Engineering*, 111, 1231-1251.

Luo, J.J. (2017) The improvement of Restricted Boltzmann Machine and its application. Dissertation for the master degree, *Guangdong University of Technology*.

Modarres, C., Astorga, N., Droguett, E.L., & Meruane, V. (2018) Convolution neural networks for automated damage recognition and damage type identification. *Structural Control & Health Monitoring*, 25(10), e2230.

Ni, Y.Q., Wang, B.S., & Ko, J.M. (1999) Selection of input to neural networks for structural damage identification. *Smart System and Bridge*, 3671, 270-280.

Ni, P.H., Xia, Y., Li, J., & Hao, H. (2018) Improved decentralized structural identification with output-only measurements. *Measurement*, 122, 597-610.

Padil, K.H., Bakhary, N., & Hao, H. (2017) The use of a non-probabilistic artificial neural network to consider uncertainties in vibration-based-damage detection. *Mechanical Systems and Signal Processing*, 83, 194-209.

- Pan, C.D., Yu, L., Chen, Z.P., Luo, W.F., & Liu, H.L. (2016) A hybrid self-adaptive Firefly-Nelder-Mead algorithm for structural damage detection. *Smart Structural & Systems*, 17(6), 957-980.
- Pathirage, C.S.N., Li, J., Li, L., Hao, H., Liu, W.Q., & Ni, P.H. (2018) Structural damage identification based on autoencoder neural networks and deep learning. *Engineering Structures*, 172, 13-28.
- Pedram, M. & Esfandiari, A. Khedmati. (2016) Finite element model updating using strain-based power spectral density for damage detection. *Structural Control & Health Monitoring*, 23(11), 1314-1333.
- Salehani, Y.E., Gazor, S., & Kim, I.M. (2014) Sparse hyperspectral unmixing via arc-tan approximation of L_0 norm. *Geoscience and Remote Sensing Symposium, IEEE International Quebec City*, 2930-2933.
- Uzun, M., Sun, H., Smit, D., & Buyukozturk, O. (2019) Structural damage detection using Bayesian inference and seismic interferometry. *Structural Control & Health Monitoring*, 26(11), e2445.
- Wang, Li., Zhou, J.X., & Lu, Z.R. (2020) A fast friction-model-inspired sparse regularization approach for damage identification with modal data. *Computers & Structures*, 227, 106142.
- Wu, X., Ghaboussi, J., & Garrett, J.H. (1992) Use of neural networks in detection of structural damage. *Computers & Structures*, 42, 649-659.
- Xu, Y., Wei, S.Y., Bao, Y.Q., & Li, H. (2019) Automatic seismic damage identification of reinforced concrete columns from images by a regional-based deep convolutional neural network. *Structural Control & Health Monitoring*, 26(3), e2313.
- Yan, G., Sun, H., & Buyukozturk, O. (2017). Impact load identification for composite structures using Bayesian regularization and unscented Kalman filter. *Structural Control & Health Monitoring*, 24(5), e1910.
- Yuen, K.V., Beck, J.L., & Au, S.K. (2004) Structural damage detection and assessment by adaptive Markov chain Monte Carlo simulation. *Structural Control & Health Monitoring*, 11(4), 327-347.
- Yuen, K.V., Beck, J.L., & Katafygiotis, L.S. (2002) Probabilistic approach for modal identification using non-stationary noisy response measurements only. *Structural Control & Health Monitoring*, 31(4), 1007-1023.
- Yuen, K.V., Beck, J.L., & Katafygiotis, L.S. (2006) Efficient model updating and health monitoring methodology using incomplete modal data without mode matching. *Structural Control & Health Monitoring*, 13(1), 91-107.
- Yuen, K.V., & Ortiz, G.A. (2018) Multiresolution Bayesian nonparametric general regression for structural model updating. *Structural Control & Health Monitoring*, 25(2), e2077.
- Zhang, F.L., Xiong, H.B., Shi, W.X., & Ou, X. (2016) Structural health monitoring of Shanghai Tower during different stages using a Bayesian approach. *Structural Control & Health Monitoring*, 23(11), 1366-1384.
- Zhu, G.P., & Kwong, S. (2010) Gbest-guided artificial bee colony algorithm for numerical function optimization. *Applied Mathematical Computation*, 217, 3166-3173.

CHAPTER 6 NON-PROBABILISTIC METHOD TO CONSIDER UNCERTAINTIES IN STRUCTURAL DAMAGE IDENTIFICATION BASED ON HYBRID JAYA AND TREE SEEDS ALGORITHM

ABSTRACT⁵

This paper proposes a novel non-probabilistic structural damage identification approach by developing a hybrid swarm intelligence technique based on Jaya and Tree Seeds Algorithm (TSA), taking into account the high-level uncertainties in the measurements and finite element modelling. The damage in structure is simulated as reduction of elemental stiffness, and structural damage identification is formulated as an optimization problem. To overcome the challenge for structural damage identification with a limited number of measurement data, an objective function based on the modal data and sparse regularization technique is defined. To make the optimization algorithm more powerful and robust, a hybridization of the K-means clustering based Jaya and TSA is proposed. Jaya algorithm is taken as the core in the hybridization. The clustering strategy is employed to replace solutions with low-quality objective values in the Jaya algorithm. Then the search strategy of the TSA is introduced into the best-so-far solution of each cycle. The proposed hybridization algorithm is termed as “C-Jaya-TSA”. To enhance the capacity of the proposed algorithm to consider uncertainties, a non-probabilistic method is also integrated to calculate the interval bound (lower and upper bounds) of the elemental stiffness changes by using the interval analysis method. To better quantify the structural damage extents, Damage Measure Index (DMI) values are introduced for representing structural damage states. The DMI value can be viewed as a combination of deterministic stiffness reduction and the Possibility of Damage Existence (PoDE). Numerical benchmark functions, numerical studies and experimental investigations are conducted to verify the accuracy and performance of the proposed method. The identification results show that the developed C-Jaya-TSA integrated with the non-probabilistic interval analysis method is a promising tool to accurately identify the structural damage, even high-level uncertainties exist.

⁵Ding, Z., Li, J., & Hao, H. (2020). Non-probabilistic method to uncertainty in structural damage identification based on Hybrid Jaya and Tree Seeds algorithm, *Engineering Structures*, 220, 110925. <https://doi.org/10.1016/j.engstruct.2020.110925>.

6.1 Introduction

Structures might accumulate damage inevitably with the increasing service time, due to a number of unforeseen reasons, such as material degradation, corrosion, overloading and fatigue, etc. Therefore, it is necessary to conduct structural health monitoring at an early stage, which is important to ensure the safety of the structures. Many scholars have presented numerous methods (Fan & Qiao, 2011; Li & Hao, 2016; Feng et al. 2018) to perform structural health monitoring by using the vibration response data and vibration characteristics, such as the acceleration responses, natural frequencies, mode shapes and flexibility etc. However, these modal data might be affected by environmental effects. Therefore, removing environmental or operational effects from identified modal data is also an important research topic in the field of structural health monitoring (Tsogka et al., 2017; Ubertini et al., 2018). Obtaining a relatively accurate finite element model and vibration data is usually the premise of conducting reliable vibration based structural damage identification. It is noted that the calibration of finite element model of civil engineering structures is not always straightforward because data measured from in-service structures, especially in the early stage of these structures are often no available. On the other hand, model updating analysis could be computationally very demanding, especially when the number of parameters that are updated is large. Thus reducing computational effort for model updating is also studied (Garcia-Macias et al., 2019).

Structural damage identification can be formulated as an optimization problem by defining an objective function that is related to structural dynamic properties, which creates the likelihood to apply classical optimization theories and swarm intelligence methods for the identification. Lu et al. (2013) used the curvature mode shapes to localize structural cracks and then applied the sensitivity based method to obtain the crack locations and depth, respectively. Lin et al. (2017) proposed a novel hybrid sensitivity method for the parameter identification of axially functionally graded beams, in which the method only required several natural frequencies and a few number of acceleration responses. However, when using these traditional optimization methods, good guess of initial values and gradient information are required. Furthermore, difficulties arise when applying these methods for the identification of large-scale structures (Pathirage et al., 2018). More recently,

swarm intelligence methods are developed to perform optimization in damage identification. The global optimization mechanism of these methods is based on the data comparison instead of the specific mathematical function. Therefore, these methods could not only avoid the abovementioned shortcomings in traditional optimization methods (requiring good initial values and gradient information), but also enable conducting the damage identification of some complex and large-scale structures (Ding et al., 2019a). For example, Kang et al. (2012) proposed artificial immunity mechanism to enhance Particle Swarm Optimization algorithm to conduct damage identification of a beam and a truss structure. Yu and Li (2014) developed a novel Global Artificial Fish Swarm (GAFS) algorithm to detect structural damages, in which the information of best-so-far solution in each cycle is integrated into other fishes' updating equation. Alkayem et al. (2019) proposed a Sine-Cosine (SC) algorithm to identify damages of three-dimensional irregular structures, in which the objective function was established by using modal strain energy and mode shape curvature. Tran-Ngoc et al. (2018) compared the performance of using Genetic Algorithm (GA) and Particle Swarm Optimizer (PSO) for model updating of a real bridge and concluded that PSO not only offers a better accuracy between the numerical model and measurements, but also reduces the computational cost compared to GA. Jahangiri et al. (2019) proposed using the Most Valuable Player (MVP) algorithm to perform structural damage identification, in which the objective function, termed as 'Relative Discrepancy Function', is built by the first natural frequency and mode shape. In addition, the Jaya algorithm (Ding et al., 2019b), the Monkey algorithm (MA) (Yi et al., 2012), the Modified Differential Evolutionary (MDE) algorithm (Du et al., 2017) and the Tree Seeds Algorithm (TSA) (Ding et al., 2019) are demonstrated to perform well in structural damage identification. Through the above studies, it is demonstrated that the swarm intelligence methods are promising tools in performing damage identification, however, challenges still exist, such as, A): In some studies (Lu et al., 2013; Lin et al., 2017; Pathirage et al., 2018; Ding et al., 2019a; Kang et al., 2012; Yu & Li, 2014; Alkayem et al., 2019; Jahangiri et al., 2019; Ding et al., 2019b), the structures used for numerical investigations are relatively simple, namely, the condition

number of the global stiffness matrix is maintained at a relatively low level. This means that dynamic properties of the structure are relatively not easily affected by alterations of stiffness and numerical calculation errors, therefore identifying damages of the simple structures might be relatively easy. Furthermore, numerical examples on beams and plates are quite common while identifying the damage of large scale civil structures is more challenging; B): In many previous studies (Ding et al., 2019a; Kang et al., 2012; Yu & Li, 2014; Alkayem et al., 2019; Du et al., 2017), damage identification is commonly considered as an over-determined inverse problem with a sufficient amount of measurement information, even with full modal data, for identification of some extreme cases. In practice, only a limited number of sensors are usually installed on large-scale structures and it is a common issue that the number of available measurements, such as natural frequencies and mode shapes, is less than that of the unknown parameters to be identified; C): Uncertainties in measurements and finite element models inevitably exist. However, when considering distinct uncertainties in vibration data, the identification accuracy would be greatly affected. Furthermore, in most studies (Lu et al., 2013; Lin et al., 2017; Pathirage et al., 2018; Ding et al., 2019a; Kang et al., 2012; Yu & Li, 2014; Alkayem et al., 2019; Tran-Ngoc et al., 2018; Jahangiri et al., 2019; Ding et al., 2019b; Yi et al., 2012; Du et al., 2017) the way of modelling uncertainties is realized through assuming certain distributions (i.e. uniform or Gaussian distributions).

For addressing the above mentioned challenge A, in this study, the Guangzhou new TV tower is modelled as an example in numerical investigations. Compared with some relatively traditional numerical example structures, including beams and plates, the Guangzhou new TV tower is more complex and the inverse problem is more difficult, since the condition number of the global stiffness matrix of the Guangzhou new TV is significantly larger than that of some simple structures, e.g. beam structures in existing studies (Lu et al., 2013; Lin et al., 2017). The large condition number of the inverse problem of the Guangzhou new TV tower stems from its finite element modeling process, which is based on many assumptions that may not well represent the realistic conditions. The larger the condition number is, the more difficult of the

inverse problem is to certain extent. Therefore, it is desirable to develop more powerful evolutionary algorithms to perform the identification of complex civil engineering structures. Developing hybrid evolutionary algorithms is one of promising ways to overcome this challenge. The hybridization algorithms are developed to improve the global optimization performance by integrating at least two different swarm intelligence methods. A good combination would generate the cooperative effect and enhance the algorithm's global optimization ability. Ding et al. (2018) introduced the search strategy of the Cuckoo Search Algorithm into the onlooker bee phase of the standard Artificial Bee Colony (ABC) algorithm and then applied the hybrid algorithm to identify the chaotic systems' parameters. Ghanem and Janta (2018) proposed a hybridization of ABC and Dragonfly Algorithm (DA), in which the first stage is performed for the global search (DA phase), the second stage for the local search (onlooker bee phase of the ABC) and the third stage with a modified scout bee phase implemented. Jadon et al. (2017) constructed a hybrid algorithm of the ABC and Differential Evolutionary (DE), in which the onlooker bee phase of the ABC was modified by the DE search mechanism. Şenel et al. (2019) developed a new hybrid algorithm based on the PSO and Grey Wolf Optimizer (GWO). These two methods are combined by replacing a particle of the PSO of a low-quality objective value with a particle that is partially modified by the GWO. In addition, the hybridizations of the Cuckoo Search and the Gravitation Search Algorithm (GSA) (Naik et al., 2015), the ABC and the Bat Algorithm (BA) (Ghosh et al., 2019) and the ABC and the GA (Pramanik & Malti, 2019) are respectively presented. Basically, these hybrid algorithms show better global optimization ability compared with using the single algorithm. However, using the hybrid algorithm would introduce more controlling parameters, which could increase the complexity of the algorithm. Therefore, two emerging swarm intelligence algorithms, named as Jaya (Rao, 2016; Ding et al., 2019b) and TSA (Ding et al., 2019a), would be smart choices for conducting hybridization. Jaya and TSA have simple algorithmic structures but relatively strong optimization ability, which have been successfully applied for damage identification of some simple structures, i.e. beam and truss structures. It ought to be noted that there is no

controlling parameters in the Jaya algorithm. Therefore, conducting hybridization of these two algorithms has some advantages in terms of the algorithm's complexity.

For addressing the challenge B, namely, using incomplete modal data to perform the identification of relatively complex structures, one approach is to formulate an objective function based on sparse regularization technique. A sparse penalty constraint is introduced in the objective function with the sparse regularization technique. The principle of applying the sparse regularization for damage identification is based on the fact that damages are often observed at a few locations while the majority of elements remain intact (Zhou et al., 2015). In addition, the traditional modal data based objective function (Ding et al., 2019a; Kang et al., 2012; Yu & Li, 2014; Alkayem et al., 2019; Tran-Ngoc et al., 2018; Jahangiri et al. 2019) are usually ill-posed, and the inverse problem could be undetermined with a limited number of measured modal information. The sparse regularization constraint on the structural damage identification can be applied to overcome the ill-posedness in the undetermined inverse problems.

For addressing the challenge C, a new way of generating the uncertainties is introduced (Padil et al., 2017). Specifically, the measurement noises in the frequencies and mode shapes as well as the finite element modeling errors are considered to be coupled instead of statistically independent. To make the whole identification process more robust to uncertainties, one traditional method is to assume the uncertainties as normally distributed random variables (Beck et al., 1999; Yuen & Katafygiotis, 2003). In reality, however, the probabilistic approaches are less straightforward since it is very difficult and unrealistic to acquire unbiased probabilistic distributions of uncertainties (Padil et al., 2017). Furthermore, if introducing probabilistic models into the swarm intelligence methods, the method would need significant computational demand. Therefore, a non-probabilistic method is used to model the effect of uncertainties. Specifically, a non-probabilistic method based on interval analysis is applied to calculate the interval bound (lower and upper bounds) of the modal data, which can be used as the input to obtain each elemental stiffness's upper and lower bounds (Wang et al., 2008). To establish the relationship between the input parameters (modal data with uncertainties) and the output parameters (stiffness reductions), an indicator called

Damage Measure Index (DMI) is defined for the undamaged and damaged status. Introducing the DMI values to quantify structural damages would greatly enhance the robustness of the proposed method to uncertainties (Wang et al., 2014).

Aiming at solving the above-mentioned three challenges, this paper proposes a hybrid algorithm based on Jaya and TSA, termed as Hybrid C-Jaya-TSA, to conduct structural damage identification by using vibration measurement data. To enhance the identification performance with incomplete modal data, a new objective function is proposed by using the penalty items with the sparse regularization. To enhance the robustness of the hybrid algorithm to uncertainties, DMI is introduced. Classical mathematical benchmarks are used to verify the accuracy and effectiveness of the proposed hybrid algorithm. Numerical investigations on the Guangzhou new TV tower and a benchmark structure are performed to demonstrate the identification accuracy of the developed algorithm with the use of the non-probabilistic method to consider the uncertainty effect. Experimental validations on a cantilever beam are also conducted to show the effectiveness and performance of the proposed method.

6.2 Theoretical background

Alterations of structural physical parameters, such as stiffness and damping, will introduce the change in vibration properties. Conversely, such change can be used to conduct damage identification of structures. The frequencies and mode shapes of a structure without considering the damping, could be obtained by conducting the eigenvalue analysis,

$$(\mathbf{K} - \omega_i^2 \mathbf{M}) \cdot \Phi_i = 0 \quad (6.1)$$

where \mathbf{K} and \mathbf{M} represent the global stiffness and mass matrices, respectively; ω_i and Φ_i denote the i th natural frequency and the corresponding mode shape, respectively.

In this study, structural damage is assumed to be only related to the stiffness reduction, since the mass alteration of a structure could be easily inspected (Ding et al., 2019a). Therefore, structural damages could be featured by a series of scalar variables

for all the element $\alpha_h (h=1,2,\dots,Nel)$ (also called as the element stiffness parameter) with a value between 0 and 1. The stiffness matrix of the damaged structure is expressed as follows

$$\mathbf{K}_d = \sum_{h=1}^{Nel} \alpha_h \cdot \mathbf{k}_{eh} \quad (6.2)$$

where \mathbf{k}_{eh} denotes the h th elemental stiffness matrix under the undamaged status; Nel is the total number of elements; \mathbf{K}_d denotes the structural stiffness matrix under the damaged status; α_h is the element stiffness parameter to be identified. It is noted that $\alpha_h=1$ means that this element is intact, and $\alpha_h=0$ means that the element is completely damaged. The element Stiffness Reduction Factor (**SRF**) is calculated as

$$SRF_h = 1 - \alpha_h \quad (6.3)$$

SRF is used to characterize structural damages.

The objective function is defined based on the changes of natural frequencies and Modal Assurance Criterion (MAC) as well as the $L_{0.5}$ sparse regularization norm (Xu et al., 2010), which can be given as

$$\boldsymbol{\alpha}^* = \arg \min_{\boldsymbol{\alpha}} f(\boldsymbol{\alpha}) = \arg \min_{\boldsymbol{\alpha}} \left(\sum_{i=1}^{NF} \Delta \omega_i^2 + \sum_{i=1}^{NM} (1 - MAC_i) + \lambda \|\mathbf{1} - \boldsymbol{\alpha}\|_{0.5} \right) \quad (6.4)$$

with

$$\Delta \omega_i = \frac{|\omega_i^c - \omega_i^m|}{\omega_i^m} \quad (6.5)$$

$$MAC_i = \frac{(\boldsymbol{\Phi}_i^{cT} \cdot \boldsymbol{\Phi}_i^m)^2}{\|\boldsymbol{\Phi}_i^c\|^2 \|\boldsymbol{\Phi}_i^m\|^2} \quad (6.6)$$

where $\boldsymbol{\alpha}$ denotes a vector that contains all damage parameters and must be identified; ω_i^c and $\boldsymbol{\Phi}_i^c$ represent the i th calculated natural frequency and mode shape from the finite element analysis, respectively; ω_i^m and $\boldsymbol{\Phi}_i^m$ are the corresponding measured natural frequency and mode shape; NF and NM represent the order numbers of natural frequencies and mode shapes, respectively. Regarding the sparse regularization term, as mentioned above, this is because the damage identification could be treated as an ill-posed problem with the searching parameter space that may have multiple local

optimal points (Titurus & Friswell, 2008). Using the sparse regularization technique can make the ill-posed problem a well-conditioned one (Sun & Betti, 2015). Furthermore, the $L_{0.5}$ norm is introduced in the study. Compared with the L_1 norm, this type of norm is closer to the L_0 norm and is more suitable to simulate the sparseness (Xu et al., 2010). λ is termed as the regularization parameter, which plays an important role in determining the participation extent of the $L_{0.5}$ norm in the objective function. When the input modal data is not polluted by the artificial noise, it ought to be noted that by using the regularization term, the global objective function value will not be zero and should be a value that is related with the regularization term. With the above objective function, evolutionary algorithms can be used to perform the optimization and damage identification results are obtained.

6.3 Hybrid algorithm: Hybrid C-Jaya-TSA

In this section, the proposed hybrid algorithm, namely Hybrid C-Jaya-TSA, is elaborated in details. Jaya and TSA are briefly introduced first. Then the development of the proposed hybrid algorithm will be described, and the innovations will be highlighted.

6.3.1 Jaya algorithm

The Jaya algorithm (Rao, 2016) is an emerging heuristic algorithm, inspired by the concept that the feasible solution acquired for a given problem should move towards the best solution while avoid the worst solution. That is, the way of creating the offspring of a solution is relevant to the best-so-far solution and the worst-so-far solution in each cycle. Afterwards, comparisons will be made between the offspring and the previous solution. The solution with a better objective function value will be survived, which is called as ‘Greedy Selection Mechanism’. Gradually, the whole colony will become victories via approaching to the best solution and therefore it is named after Jaya (a Sanskrit word meaning victory). The procedure of the Jaya algorithm mainly involves three steps, namely, the initialization, the local search

strategy and the greedy selection mechanism, which are briefly introduced herein.

6.3.1.1 Initialization

An initial colony is created randomly in the search space. This colony contains CS individuals. Each individual in the colony is marked with θ_j . Each individual (θ_j) has n variables ($\theta_j = [\theta_1, \theta_2, \dots, \theta_q, \dots, \theta_n]$), which could be generated as below,

$$\theta_{j,q} = \theta_{j,q}^l + \text{rand}(0,1) \cdot (\theta_{j,q}^u - \theta_{j,q}^l) \quad (6.7)$$

where $\theta_{j,q}$ denotes the q th variable of θ_j ; $\theta_{j,q}^u$ and $\theta_{j,q}^l$ represent the upper bound and the lower bound of the variable $\theta_{j,q}$. $\text{rand}(0,1)$ is a random number between 0 and 1.

6.3.1.2 Local search strategy

It is assumed that $\theta_{j,q,G}$ represents the value of the q th dimension of the j th individual at the G th generation. The offspring $\theta'_{j,q,G}$ generated by this value can be calculated as

$$\theta'_{j,q,G} = \theta_{j,q,G} + r_{1,q,G} \cdot (\theta_{best,q,G} - |\theta_{j,q,G}|) - r_{2,q,G} \cdot (\theta_{worst,q,G} - |\theta_{j,q,G}|) \quad (6.8)$$

where $r_{1,q,G}$ and $r_{2,q,G}$ are two random numbers within the range $[0,1]$. $\theta_{best,q,G}$ and $\theta_{worst,q,G}$ are the values of the q th variable for the best solution and the worst one, respectively. The second item in Eq. (6.8) shows that the trend of the process towards the best solution while the third item means the tendency of the solution to avoid the worst solution.

6.3.1.3 Greedy selection mechanism

Using the above-mentioned local search strategy to all dimensions, the offspring $\theta'_{j,G}$ would be acquired. The solution with a better objective function value would be survived, which can be described as follows

$$\boldsymbol{\theta}_{j,G+1} = \begin{cases} \boldsymbol{\theta}'_{j,G}, & f(\boldsymbol{\theta}'_{j,G}) \leq f(\boldsymbol{\theta}_{j,G}) \\ \boldsymbol{\theta}_{j,G}, & \text{otherwise} \end{cases} \quad (6.9)$$

where f denotes the objective function that requires to be optimized. The procedure of the proposed algorithm will be continually conducted until the termination condition is satisfied, i.e., the maximum iteration cycle is reached.

6.3.2 Clustering-based Jaya algorithm

Applying the clustering technique for modifying the swarm intelligence methods is one of effective ways to enhance the algorithms' optimization performance (Cai et al., 2011). In this study, the K-means clustering technique is applied before commencing the local search stage. Conducting this procedure is straightforward, and this acts as a crossover operators that would utilize the colony information effectively. This is useful to improve the algorithm's convergence performance. The specific step of conducting the K-means clustering is described as follows

1. Randomly choosing $K = 0.1 \cdot CS$ individuals from the colony as the initial clustering centers. The centers are marked as C_1, C_2, \dots, C_k and the individuals from the colony are marked as $[\boldsymbol{\theta}_1, \boldsymbol{\theta}_2, \dots, \boldsymbol{\theta}_{cs}]$.

2. The remaining individuals are assigned to this colony centers based on their shortest Manhattan distance. The distance between any two individuals (i.e. $\boldsymbol{\theta}_j$ and $\boldsymbol{\theta}_c$) is calculated as,

$$d(\boldsymbol{\theta}_j, \boldsymbol{\theta}_c) = \|\boldsymbol{\theta}_j - \boldsymbol{\theta}_c\| = \sum_{q=1}^n \text{abs}(\theta_{j,q} - \theta_{c,q}) \quad (6.10)$$

3. After assigning the remaining individuals to the initial clustering centers, the new clustering centers C'_1, C'_2, \dots, C'_k are calculated as,

$$C'_m = \frac{1}{u_m} \sum_{\boldsymbol{\theta}_j \in c_m} \boldsymbol{\theta}_j, j = 1, 2, \dots, CS \quad (6.11)$$

where u_m is the total quantity of individuals belonging to the clustering center C_m .

From Eq. (6.11), it is noted that the newly-created clustering centers are the combinations of other individuals in the colony.

Finally, another K individuals from the colony are randomly selected and integrated with the K newly-created clustering centers as the set ε . Calculating the objective function values with the set ε , and the results are sorted from the smallest to the largest. The first K individuals are put into the colony again. Afterwards, the procedure of the Jaya algorithm will be conducted. Hence, the Clustering-based Jaya algorithm is illustrated.

6.3.3 Tree Seeds Algorithm

TSA is also a newly-developed swarm intelligence method (Ding et al., 2019a), which is inspired based on the natural phenomenon of trees propagation. In the real world, trees generally spread to other locations via their seeds. These seeds will grow up over time. In general, the seeds quantity could be decided approximately as 10% and 25% of the colony size. In the algorithm, the specific locations of trees and seeds could be viewed as feasible solutions for the optimization problem. The key to this algorithm is the local search mode of the seeds. Two search modes can be designed at this phase. Assuming that $\theta_{q,G}$ is an arbitrary tree (feasible solution) in the colony at the G th generation and $\theta_{q,y,G}$ is the y th seed, the updating equation for the j th variable could be provided as,

$$\theta_{q,y,j,G} = \theta_{q,j,G} + r_{q,y,j,G} \cdot (\theta_{best,j,G} - \theta_{m,j,G}) \quad (6.12)$$

$$\theta_{q,y,j,G} = \theta_{q,j,G} + r_{q,y,j,G} \cdot (\theta_{v,j,G} - \theta_{m,j,G}) \quad (6.13)$$

where $\theta_{q,y,j,G}$ is the j th dimension of the y th seed that will be created by the q th tree at the G th generation; $\theta_{m,j,G}$ and $\theta_{v,j,G}$ are the j th dimension of the m th tree and v th at the G th generation, which are randomly selected from the remaining individuals in the colony; $\theta_{best,j,G}$ is the j th dimension of best-so-far solution in the colony at the G th generation; the coefficient $r_{q,y,j,G}$ is a uniform random number, which is arbitrarily generated in the range of $[-1,1]$. Selecting whether Eq. (6.12) or Eq. (6.13) to perform the updating is controlled by a parameter called search tendency

(ST). Specifically, choosing a better equation between Eqs. (6.12) and (6.13) to update the solution depends on the comparison between a random number and ST. If the random number is larger than ST, Eq. (6.13) is chosen as the updating equation. Otherwise Eq. (6.12) will be selected.

6.3.4 The proposed Hybrid C-Jaya-TSA

From observing the updated mechanism of the Jaya algorithm, a good exploitation search ability could be observed since other individuals in the colony are attracted by the best-so-far solution. However, when dealing with complex optimization problem, the best-so-far solution might have a large likelihood to be trapped in the local minimal. To address this issue, one remedy is to introduce the clustering mechanism, since this can be helpful to use the colony information more effectively and avoid early-maturing to some extent (Ding et al., 2019a; Ding et al., 2019b; Cai et al., 2011).

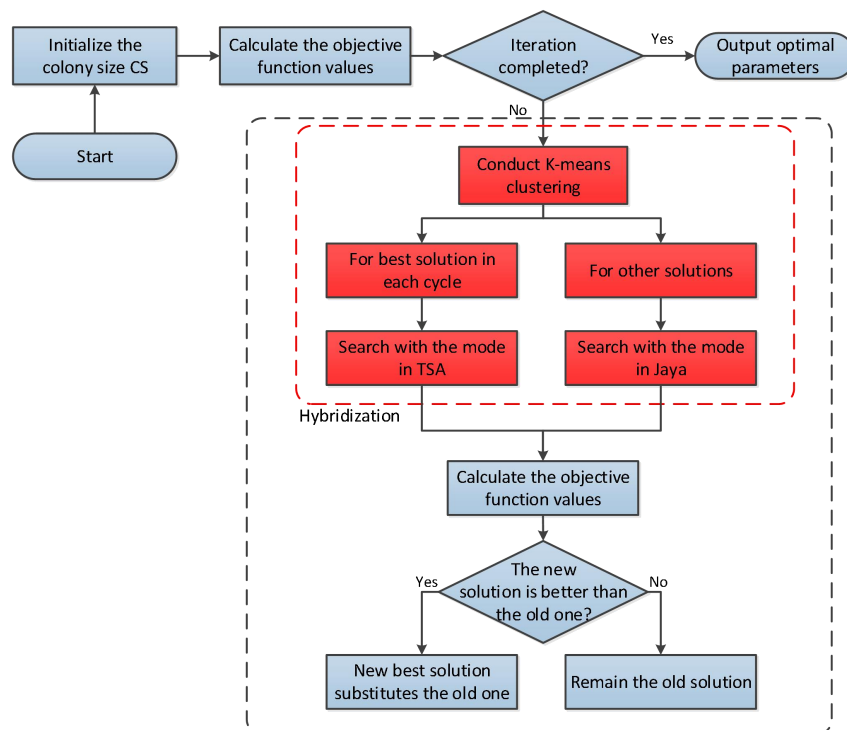


Figure 6-1 The flowchart of the proposed Hybrid C-Jaya-TSA.

Furthermore, considering that the updated strategy of the Jaya algorithm is not sufficient to approach the best-so-far solution, therefore the updated strategy of the

TSA will be used to update the best-so-far solution. Compared with the search mode of the Jaya algorithm, using the updated strategy of the TSA is more beneficial to enhance the algorithm's exploration ability, which could be further profitable to prevent the best-so-far solution trapping in the local minimal. Hence, the hybridization of the clustering technique, Jaya algorithm and TSA have been demonstrated. The flowchart of conducting the Hybrid C-Jaya-TSA algorithm is shown in Figure 6-1. The effectiveness and improvement of the applied modifications and developed hybrid algorithm will be demonstrated in the numerical simulations and experimental studies.

6.3.5 Non-probabilistic method to consider uncertainties

Considering that the uncertainties, including the measurement noise and the finite element modelling errors, inevitably exist in the damage identification process and aiming to providing reliable damage identification results, it is essential to take these uncertainties into account. However, when the input modal data is submerged with the effect of various sources of uncertainties, the performance of optimization algorithms will be affected (Kang et al., 2012). In this case, several measures can be taken to address this challenge, i.e. using a more robust objective function (Alkayem et al., 2019; Ding et al., 2019b) for the optimization. In this study, to mitigate the influence on the identification accuracy owing to the uncertainties, a non-probabilistic method based on interval analysis is employed. The interval analysis requires the upper and lower bounds of the input modal parameters (ω^m and Φ^m) (Padil et al., 2017; Wang et al., 2008; Wang et al., 2014). Therefore, assuming that the uncertainties are the coupling effects of the finite element model errors and the measurement noise, these uncertainties could be described by providing the upper and lower bounds of the input modal parameters (ω^m and Φ^m). Through this non-probabilistic method (Padil et al., 2017; Wang et al., 2008; Wang et al., 2014), the developed Hybrid C-Jaya-TSA could provide the upper and lower bounds of the element stiffness parameters (α_h) via optimizing the modal data with upper bounds and the data with lower bounds. Specifically, the modal data with upper and lower bounds are described as,

$$\underline{\omega}_i^m = \omega_i^m - \omega_i^m \cdot X_{\omega, \text{uncertain}} \quad (6.14)$$

$$\overline{\omega_i^m} = \omega_i^m + \omega_i^m \cdot X_{\omega, \text{uncertain}} \quad (6.15)$$

$$\underline{\Phi_{iz}^m} = \Phi_{iz}^m - \Phi_{iz}^m \cdot X_{\Phi, \text{uncertain}} \quad (6.16)$$

$$\overline{\Phi_{iz}^m} = \Phi_{iz}^m + \Phi_{iz}^m \cdot X_{\Phi, \text{uncertain}} \quad (6.17)$$

where $\underline{\omega_i^m}$ and $\overline{\omega_i^m}$ denote the lower and upper bounds of the i th measured frequency; $X_{\omega, \text{uncertain}}$ and $X_{\omega, \text{uncertain}}$ are the uncertainty levels for the natural frequencies; $\underline{\Phi_{iz}^m}$ and $\overline{\Phi_{iz}^m}$ represent the lower and upper bounds of the data at the z th degree of freedom (DOF) of the i th mode shape; $X_{\Phi, \text{uncertain}}$ and $X_{\Phi, \text{uncertain}}$ are the uncertainty levels for the mode shapes. Through using these uncertain data, the upper and lower bounds of the element stiffness parameters $[\underline{\alpha_1}, \overline{\alpha_1}; \underline{\alpha_2}, \overline{\alpha_2}, \dots, \underline{\alpha_h}, \overline{\alpha_h}; \dots; \underline{\alpha_{Nel}}, \overline{\alpha_{Nel}}]$ can be obtained. The middle value of these damage indices is calculated as,

$$SRF_h^{\text{middle}} = 1 - \frac{\alpha_h + \overline{\alpha_h}}{2} \quad (6.18)$$

When the lower and upper bounds of the element stiffness parameter α_h is acquired, the Possibility of Damage Existence (PoDE) of each element can be calculated. To differentiate the damaged and undamaged states of each element, two marks are introduced. α_{uh} denotes that the h th element is undamaged, and α_{dh} means that the h th element is damaged. It should be noted that when using the modal data of structures under the intact state, it is straightforward to obtain $[\underline{\alpha_{uh}}, \overline{\alpha_{uh}}]$. Figure 6-2 shows the schematic regions of the damaged and undamaged states on two different axes. A solid rectangle represents the variation of both intervals. The damaged and undamaged regions are also shown in this figure. In this regard, the PoDE is defined as the possibility that the identified element stiffness parameter α_{dh} is smaller than the threshold of the undamaged state α_{uh} (Wang et al., 2014).

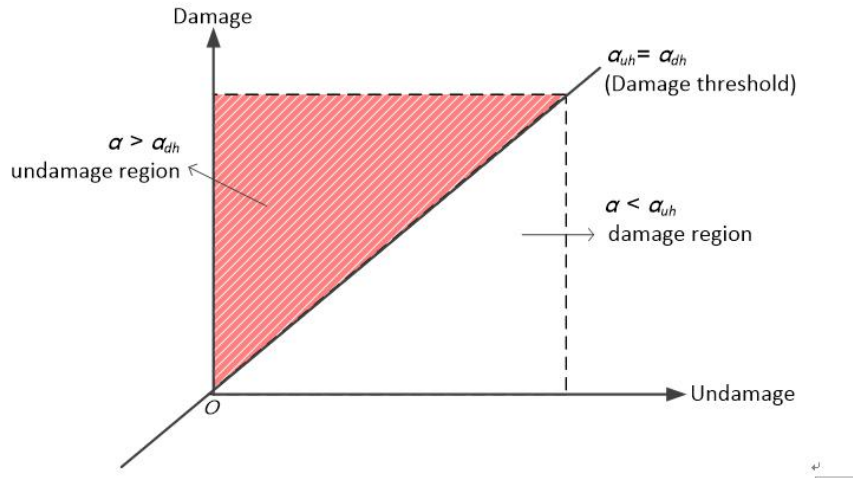


Figure 6-2 Damaged and undamaged regions of the *hth* element.

Then the PoDE is defined as the proportion between the area of the damaged region and the area of the entire region as follows (Padil et al., 2017; Wang et al., 2008; Wang et al., 2014)

$$PoDE = possibility(\alpha_{dh} < \alpha_{uh}) = \frac{A_{damage}}{A_{total}} \times 100\% \quad (6.19)$$

The PoDE value for each element is in a range from 0 and 100%, with 100% representing a large likelihood of damage and 0% indicating that no damage occurred in this element. The $PoDE = 100\%$ occurs when the interference between α_{uh} and α_{dh} does not exist, which also means that the upper bound of the damage index ($\overline{\alpha_{dh}}$) equals to or is less than the lower bound of the undamaged status ($\underline{\alpha_{uh}}$). To make the judgement more clear, Figures 6-3(a) and (b) provide two situations of $PoDE = 100\%$ on one axis. The first situation is related with the condition $\overline{\alpha_{dh}} \approx \underline{\alpha_{uh}}$, where the distance between two middle values is quite small. This also means that this damage index is a small value. The second situation means that these two intervals separate completely, which indicates that the stiffness reduction of this element is relatively large. Figure 6-3(c) shows the scenario where the PoDE is between 100% and 0%, where an overlapping is observed between these two intervals with an observed stiffness reduction.

With PoDE introduced to describe the likelihood of damage for each element and stiffness reduction factor used to represent the damage severity, similar as the existing studies (Padil et al., 2017; Wang et al., 2008; Wang et al., 2014), this study also uses the DMI developed by Wang et al. (2014) to provide a further reasonable quantification of damage extent. The DMI value is calculated as the product of stiffness reduction factor and PoDE. The formula of obtaining DMI for the h th element is given as

$$DMI_h = SRF_h^{middle} \times PoDE_h \quad (6-20)$$

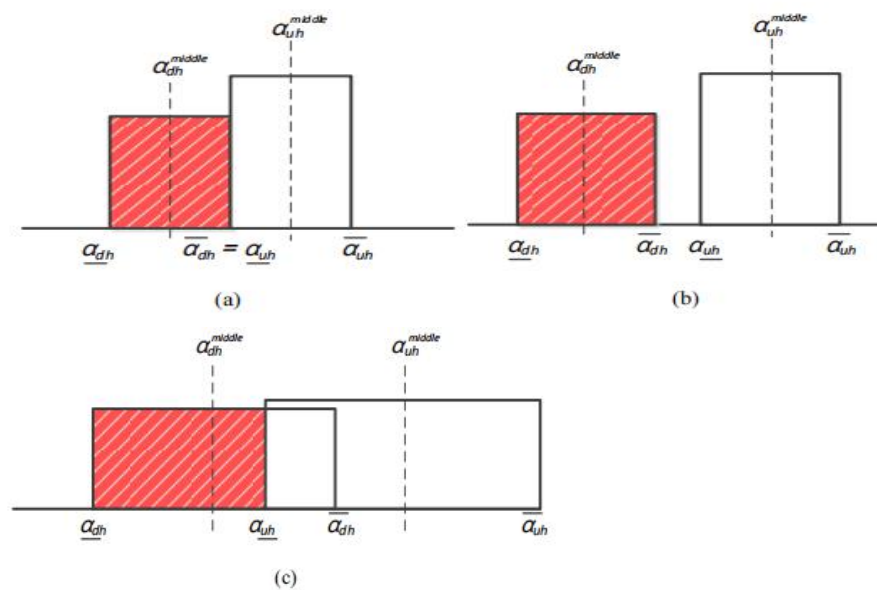


Figure 6-3 Situation of uncertain α_h : (a) PoDE=100% with a small damage index; PoDE=100% with large damage index; (c) PoDE is between 100% and 0%.

6.4 Numerical Studies

In this section, numerical studies are carried out to verify the accuracy and effectiveness of the proposed algorithm with the defined objective function. Numerical studies will be divided into two parts. The first part is based on the classical mathematical benchmarks, which can be used to verify the generality of the proposed algorithm. The second part are on the Guangzhou New TV tower and a benchmark study, which are utilized to verify the effectiveness and efficiency of the proposed

algorithm and objective function on structural damage identification with a limited quantity of measurement information.

6.4.1 Optimization for the classical benchmark

To compare the performance of using the proposed approach for structural damage identification with other evolutionary algorithms, a series of classical mathematical benchmarks (Ding et al., 2018), as listed in Table 6-1, are adopted for comparison. The global optima of these test functions are all 0. To make the mathematical benchmarks more difficult, compared with Ref. (Ding et al., 2018), the dimension number of each problem is greatly increased, as shown in Table 6-1. It is noted that these functions are categorized into four different types according to their geometric appearances. Optimizing different types of benchmarks is important to validate the general applicability of the proposed algorithm. For the comparison purpose, three evolutionary algorithms, which are more or less related with the proposed Hybrid C-Jaya-TSA, are applied to optimize the above-mentioned benchmarks as well. These three algorithms are the Jaya, TSA and the clustering based TSA (C-TSA) (Ding et al., 2019a). Specifically, in the C-TSA, the K-means clustering mechanism is also applied before its seeds search stage. Employing these algorithms for comparison is important to investigate the necessity of the modifications and demonstrate the improvement.

As regards the parameters setting, the common parameters Colony Size (CS) and the maximum iteration number are 100 and 5000, respectively. For the TSA, C-TSA and Hybrid C-Jaya-TSA, the parameter ST is set as 0.4. 30 independent runs are conducted for each test function, and the mean values and standard deviations (std.) are recorded for comparison. Table 6-2 presents the final optimization results based on the abovementioned four methods. The best optimization value for each test function is in bold. It is clearly observed that the proposed algorithm converges to zero, however, the Jaya and TSA have some difficulties to handle these high-dimensional functions, since the majority of optimization results acquired by these two algorithms maintain relatively large magnitudes. In contrast, the C-TSA has some difficulties in dealing with the Rosenbrock and Schaffer functions. Overall, the proposed algorithm reveals a

competitive optimization capacity in representative benchmark test functions, which fully illustrates the improvement due to the hybridization and lays the foundation for the following structural damage identification in numerical and experimental studies.

Table 6-1 Classical mathematical benchmarks.

Number	Name	Dimension number	Range	Function type
F1	Sphere	100	[-500,500]	Uni-modal, Separable
F2	Griewank	200	[-600,600]	Multiple-modal, Non-Separable
F3	Rosenbrock	300	[-32,32]	Uni-modal, Non-Separable
F4	Rastrigin	400	[-32,32]	Multiple-modal, Separable
F5	Ackley	500	[-32,32]	Multiple-modal, Non-Separable
F6	Schaffer	1000	[-100,100]	Multiple-modal, Non-Separable

Table 6-2 Statistical results obtained by TSA, C-TSA, Jaya and C-Jaya-TSA on benchmarks.

Function	TSA		C-TSA		Jaya		C-Jaya-TSA	
	Mean	std	Mean	std	Mean	std	Mean	std
F1	2.51e-06	5.61e-06	8.71e-204	0.00e+00	9.63e-01	3.58e-01	0.00e+00	0.00e+00
F2	4.73e+02	2.26e+02	2.44e-16	1.49e-16	3.15e+00	6.59e-01	0.00e+00	0.00e+00
F3	1.72e+09	1.03e+09	4.01e+02	1.05e+02	1.83e+06	4.99e+05	0.00e+00	0.00e+00
F4	6.85e+09	7.90e+08	4.95e-19	2.71e-18	1.08e+04	8.44e+02	0.00e+00	0.00e+00
F5	2.09e+01	1.21e-02	1.37e-13	1.96e-14	1.82e+01	1.84e+00	0.00e+00	0.00e+00
F6	5.00e-01	2.68e-08	1.46e-02	8.19e-03	4.99e-01	1.34e-06	0.00e+00	0.00e+00

Note: The best optimization value is in bold.

6.4.2 Damage identification for the Guangzhou New TV tower

The Guangzhou New TV tower is the landmark of the Guangzhou city, which is located in the Haizhu district. It is a super high tube-in-tube structure with a height of 610 m, which has 37 layers, connecting the inner and outer layers mainly used for office, entertainment, transmission television signals and tourism. In the sophisticated finite element modeling, the model contains 122,476 elements, 84,370 nodes and 505,104 DOFs (Chen et al., 2011). However, directly using this complex model to conduct structural damage identification is complicated and not practical. Therefore, according to the assumptions and simplifications presented in Ref. (Chen et al., 2011),

a reduced finite element model is developed from the full model. Specifically the simplified model has 37 beam elements, the axis of the beam element aligns with the centroid axis of the tower mast, and the horizontal coordinate of the center of the reduced model is kept at the same location of the full model. The mass of the structure is lumped at nodes in both the full and reduced model. The equivalent rotational inertia of the segment with respect to the nodes along the central axis of the reduced model is calculated to form rotational terms of the equivalent element mass matrix of the reduced model. The corresponding segment between two horizontal sections is selected from the full model, which is included in the beam element. There are five DOFs at each node, namely, the lateral translational displacements in the x and y directions, and rotations about x , y and z directions. Eventually the finite element model of the Guangzhou New TV tower is simplified as a structure with 37 elements and 38 nodes (Chen et al., 2011), as shown in Figure 6-4. The number of nodes is numbered from the bottom to the free top end. Each node has five degrees of freedom (DOFs), including two horizontal translations and three rotational displacements. The total DOFs of the finite element model is 185. The dynamic properties including frequencies and mode shapes of the simplified finite element model of Guangzhou New TV tower are close to those obtained from the detail full finite element model, therefore the simplified finite element model of Guangzhou New TV tower is viewed as the replacement of the sophisticated model to conduct the following damage identification analysis. Although the structure is significantly simplified, the difficulty of using this reduced model for system identification shall be noted. The condition number of the global stiffness matrix is up to the magnitude of 10^{10} and is far larger than that of those numerical structures in existing studies (Lu et al., 2013; Lin et al., 2017; Pathirage et al., 2018; Ding et al., 2019a; Kang et al., 2012; Yu & Li, 2014; Alkayem et al., 2019; Tran-Ngoc et al, 2018; Jahangiri et al., 2019; Ding et al., 2019b;, Yi et al., 2012; Du et al., 2017), which means small perturbation of the stiffness parameters would result in significant changes in modal parameters of the structure. Therefore, the difficulties of identification would arise to certain extent. The first five natural frequencies of the intact structure are 0.1104, 0.1587, 0.3463, 0.3688 and 0.3994HZ, respectively. The

damage identification of this structure is considered as an underdetermined inverse problem with limited measurement information, namely, the used input data will be less than the total number of system parameters to be updated. The first five natural frequencies and the mode shape data along the x direction of the 1st node, 9th node, 17th node, 25th node and 33rd node, are used for identification. Totally 30 modal data are used for identifying the parameters of 37 elements. It should be noted that these modal data in the following numerical examples are obtained by modal analysis of the numerical model.

6.4.2.1 Damage identification with incomplete modal data without considering uncertainty

For the comparison purpose, the Jaya (Rao, 2016), C-TSA (Ding et al., 2019a) and the MDE algorithm (Du et al., 2017) are used for the damage identification as well. It should be noted that MDE is an effective method for identification of some basic structures. In terms of the parameters setting for these algorithms, the common parameters CS and the maximum iteration number are set as 100 and 500, respectively. Specifically, for the C-TSA and the proposed C-Jaya-TSA, the parameter ST is defined as 0.4. For MDE, the threshold value is set as 0.1, the mutation rate is set as 0.4, and the mutation constant is a random number within $[0.4, 0.9]$. These parameters are set the same as those in Ref.(Du et al., 2017). The purpose of this section is to investigate the feasibility and applicability of using these algorithms for identifying the assumed damages in the finite element model of Guangzhou New TV tower, therefore the input modal data are not polluted by the uncertainties.

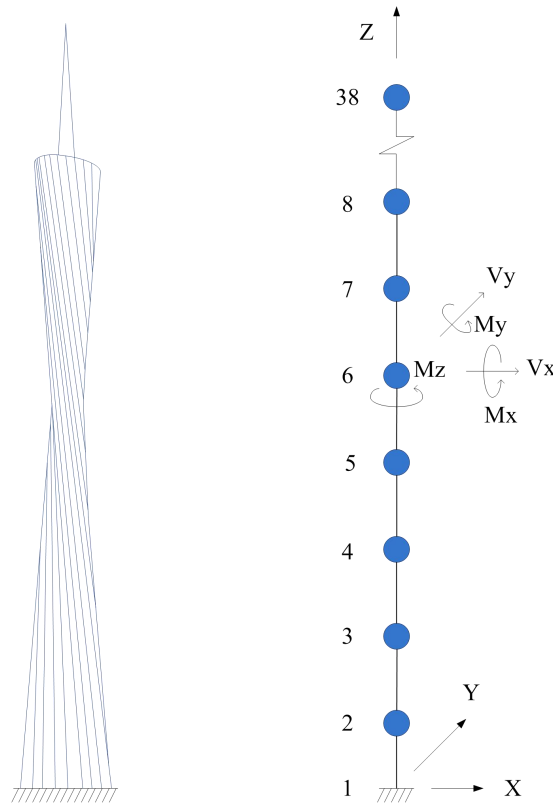


Figure 6-4 The Guangzhou New TV tower and its simplified finite element model.

Single damage case

The first damage case is assumed that there is a 15% stiffness reduction in the 37th element, which means $\mathbf{SRF}_{37} = 0.15$. The Discrepancy Principle (DP) rule (Hou et al., 2018) is used for selecting the optimal regularization parameter. In this case, the optimal regularization parameter used in the objective function is selected as $\lambda = 5 \cdot 10^{-4}$. With the regularization term, the global optimum in this case is $7.5 \cdot 10^{-6}$. The above mentioned four algorithms are used to optimize the proposed objective function as shown in Eq. (6.3), based on the incomplete modal data. Figure 6-5 provides the evolutionary process of the objective function values based on the four algorithms. It is clearly observed that the iteration process of the proposed algorithm is the most stable and takes only less than 50 cycles for the proposed algorithm to converge, indicating that the proposed algorithm's convergence speed is much faster. Other three algorithms take significantly more cycles to converge. Furthermore, the objective function value acquired by the developed Hybrid C-Jaya-TSA is closer to the

preset global optimum, which indicates that the Hybrid C-Jaya-TSA can obtain better identification results.

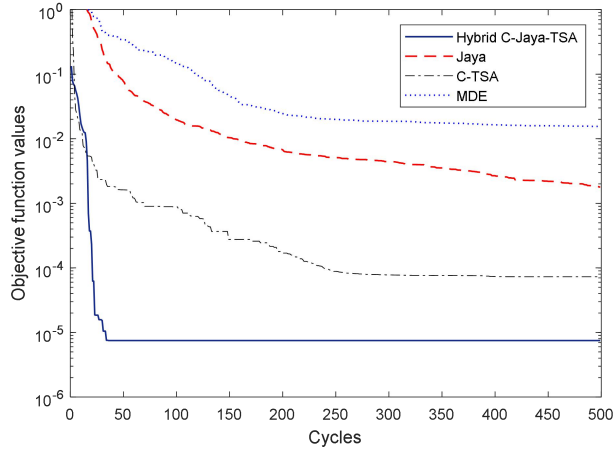


Figure 6-5 The evolutionary processes of the objective function values by using different methods.

Table 6-3 and Figure 6-6 present the damage identification results of the single damage case without uncertainties. The proposed Hybrid C-Jaya-TSA yields the best competitive results with the best accurate mean value of the damage extend and smallest standard deviation, demonstrating the stable and strong global optimization ability of the proposed algorithm. C-TSA is able to identify the damage but there are three false alarms at the 8th, 9th, and 12th elements. The Jaya and MDE methods could not provide accurate identification results in this case. This is because the objective function values obtained by the Jaya and MDE algorithms are far away from the preset global optimum.

Table 6-3 Identification results of single damage case without uncertainties.

Methods	Objective function value		Damage index at the 37 th element	
	Mean	Std.	Mean	Std.
MDE	1.551e-02	2.084e-03	0.4911	0.2967
Jaya	1.793e-03	3.127e-03	0.1798	0.2376
C-TSA	7.282e-05	1.735e-04	0.1282	0.0565
C-Jaya-TSA	7.489e-06	1.241e-16	0.1496	3.290e-08
True value	7.50e-06		0.15	

(The best identification value is in bold)

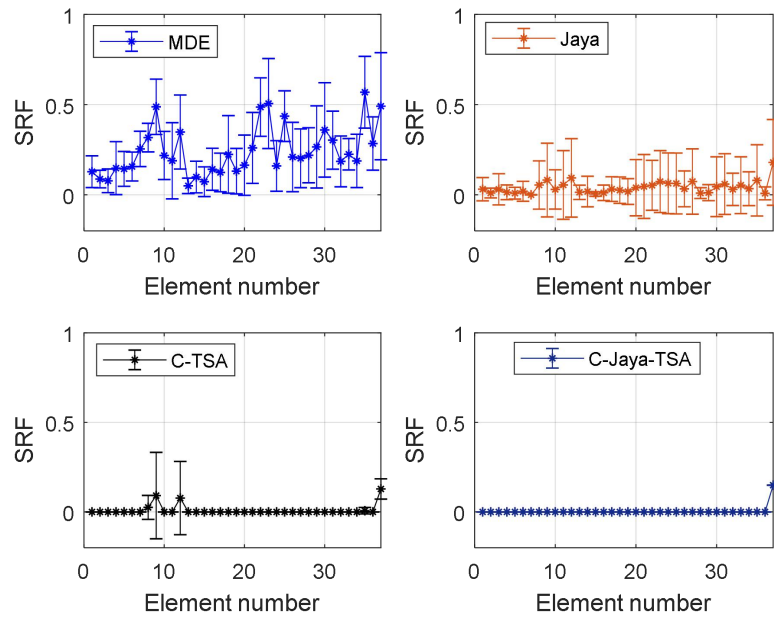


Figure 6-6 Identification results for the single damage case without uncertainties.

Multiple damages case

The second damage case is assumed with 20% stiffness reduction in the 16th and 23rd elements respectively, which means that $\mathbf{SRF}_{16} = \mathbf{SRF}_{23} = 0.2$. The regularization parameter in the objective function is set as $\lambda = 5 \cdot 10^{-4}$, and the global optimum in this case is $4.00 \cdot 10^{-5}$. These four methods are used for optimization. Figure 6-7 provides the evolutionary process based on the proposed Hybrid C-Jaya-TSA. Similar as the single damage case, the evolutionary process in this case is also stable. It needs around 150 iterations for the developed algorithm to achieve the convergence to the preset values.

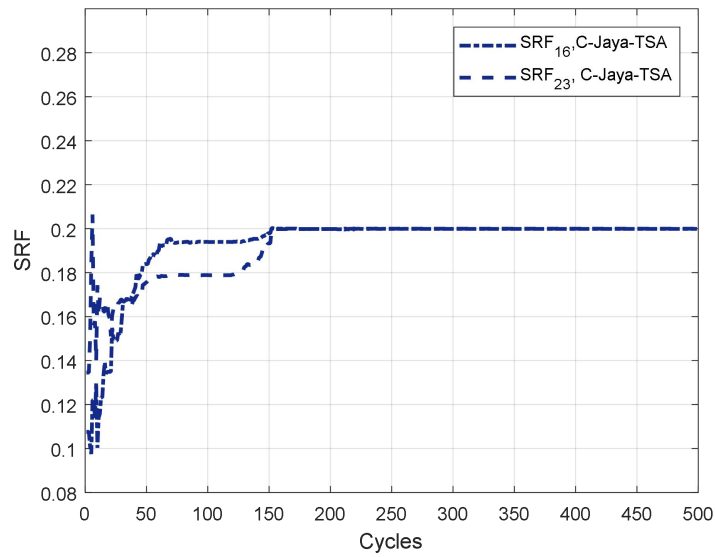


Figure 6-7 The evolutionary process of the damage indices based on the proposed method.

The final identification results based on the four methods are presented in Table 6-4 and Figure 6-8. It is clearly observed that MDE and the Jaya fail to provide significant identification again in the multiple case. In contrast, the C-TSA is capable to identify these two simulated damages but several error alarms are observed as well. The performance of the developed Hybrid C-Jaya-TSA is the best. The identified damage index values and objective function value are very close to the true values.

These two cases demonstrate that when uncertainties are not considered, the standard Jaya and MDE algorithms are not capable of tackling underdetermined identification for the Guangzhou New TV tower while the developed Hybrid C-Jaya-TSA can perform well.

Table 6-4 Identification results of multiple damage case without uncertainties.

Methods	Objective function value		Damage index at the 16 th element		Damage index at the 23 rd element	
	Mean	Std.	Mean	Std.	Mean	Std.
MDE	2.270e-02	7.972e-03	0.1932	0.0803	0.4587	0.2498
Jaya	6.018e-03	5.270e-03	0.0975	0.1190	0.2148	0.2535
C-TSA	2.830e-04	6.861e-04	0.1893	0.0302	0.2041	0.0116
C-Jaya-TSA	3.999e-05	1.333e-16	0.1999	1.43e-08	0.2000	4.43e-08
True value	4.00e-05		0.20		0.20	

Note: The best identification results are in bold.

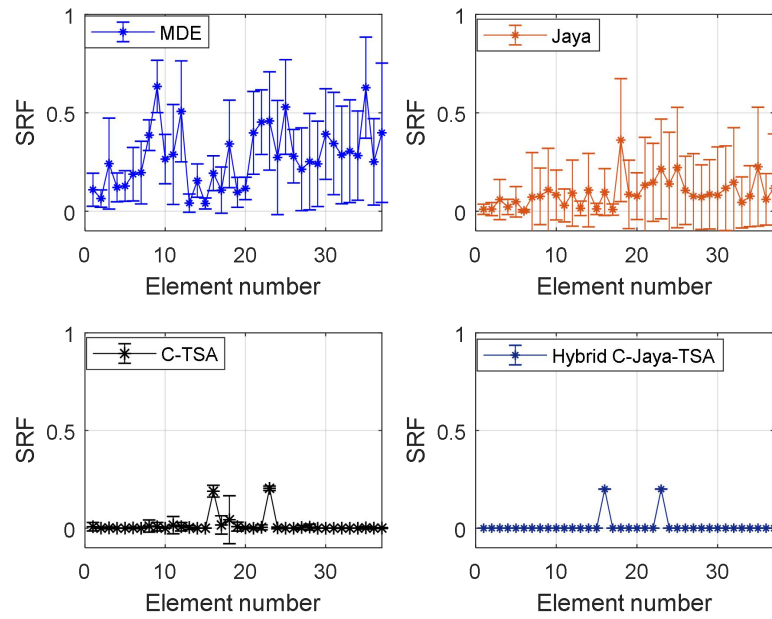


Figure 6-8 Identification result for the multiple damage case without uncertainties.

6.4.4.2 Damage identification with incomplete and uncertain modal data

The uncertainties are considered as the coupling effect of the finite element model errors and measurement noise. Eqs. (6.14) - (6.17) are used to generate the bounds of the modal data with uncertainties. Both uncertainty levels for the natural frequencies $X_{\omega, \text{uncertain}}$ and $X_{\omega, \text{uncertain}}$ are set as 1%, and the uncertainty levels for the mode shapes $X_{\Phi, \text{uncertain}}$ and $X_{\Phi, \text{uncertain}}$ are set as 10%. This is because compared with mode shapes, the acquisition of natural frequencies is more accurate in the real applications. It is elaborately demonstrated in Ref. (Padil et al., 2017) that applying the interval analysis method to analyze the uncertainty effect is reliable and accurate than directly using the deterministic method for damage identification. That is to say, using the DMI values for quantifying structural damages is more reliable than using the deterministic damage index, when the incomplete and uncertain data are used. Therefore, the Hybrid C-Jaya-TSA combined with the interval analysis method is introduced to conduct structural damage identification by using uncertain modal data. It has been demonstrated in the above studies that the developed Hybrid C-Jaya-TSA has the best performance. The Hybrid C-Jaya-TSA is used only in this section. The

parameters setting for the algorithm and regularization parameter are the same as the former cases. The same simulated measurement data are also used.

Single damage case

15% stiffness reduction is assumed in the 37th element. To conduct the interval analysis method, the first step is to acquire the upper and lower bounds of each element under the intact state. When performing the optimization with the modal data including the uncertainties by Eqs. (6.14) and (6.16), the lower bound of the element under the intact state can be obtained. For optimization by using the modal data with Eqs. (6.15) and (6.17), the corresponding upper bound values are obtained. Similarly, the proposed algorithm is used to perform the optimization by using the modal data with uncertainties under the damaged state. The upper and lower bounds of the damage indices are then obtained, and the middle value and PoDE are obtained accordingly. Figure 6-9 shows the evolutionary process of the middle value of the damage index at the damaged element $\text{SRF}_{37}^{\text{middle}}$, by the developed Hybrid C-Jaya-TSA. It is clearly observed that since the uncertainties are considered, around 330 iterations are needed for the algorithm to converge to the neighborhood of the preset value. The PoDE and DMI values of all the element are also calculated.

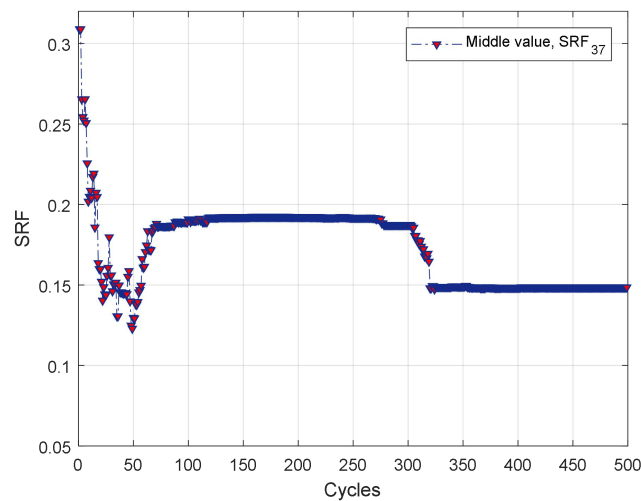


Figure 6-9 The evolutionary process of the damage index at the 37th element by the proposed method with uncertain modal data.

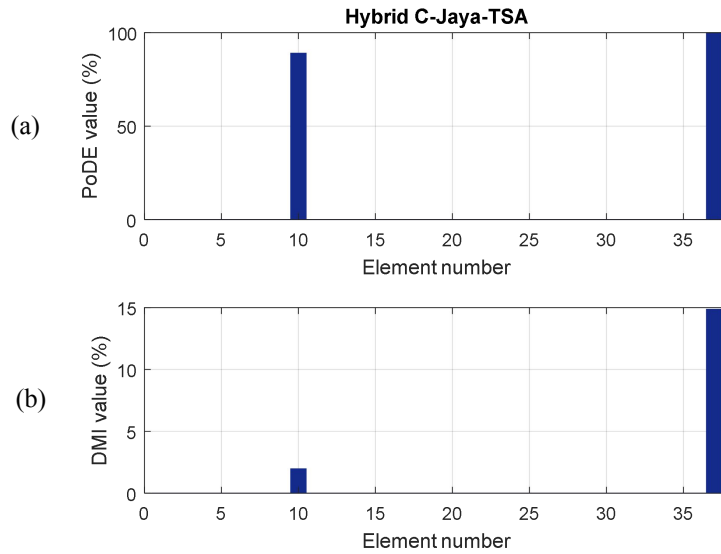


Figure 6-10 PoDE and DMI value of each element in the single damage case with uncertain modal data:(a) PoDE; (b) DMI.

The PoDE and DMI value for each element are shown in the Figure 6-10. It is found that the PoDE value for the 10th element is around 90%, due to the effect of uncertainties in the modal data. However, if using the DMI value to quantify damages, the DMI value at the 10th element is only 1.97%, while the corresponding value at the 37th element is 14.86%, which is very close to the preset damage extent of 15%. This indicates that DMI by considering the uncertainty effect is more reliable than the deterministic damage index, i.e. stiffness reduction factors.

Multiple damages case

20% stiffness reductions are assumed in the 16th and 23rd element. The same procedure as the single damage case is followed to conduct the interval analysis and obtain the upper and lower bounds of the identification results by using the non-probabilistic method to consider the effect of uncertainties. Figure 6-11 presents the PoDE and DMI values for all the elements, respectively. As mentioned, these two damaged locations are accurately identified. Due to the significant effect of uncertainties, the damage probability of the 10th, 14th and 37th elements are also large. However, when using the DMI to quantify damages, similar as the single damage case, the DMI values of these three false identified elements are minor and the damage

extents of the 16th and 23rd elements are close to the assumed true values. The multiple damage case further illustrates the effectiveness of using the proposed method to conduct structural damage identification, even uncertainties are considered.

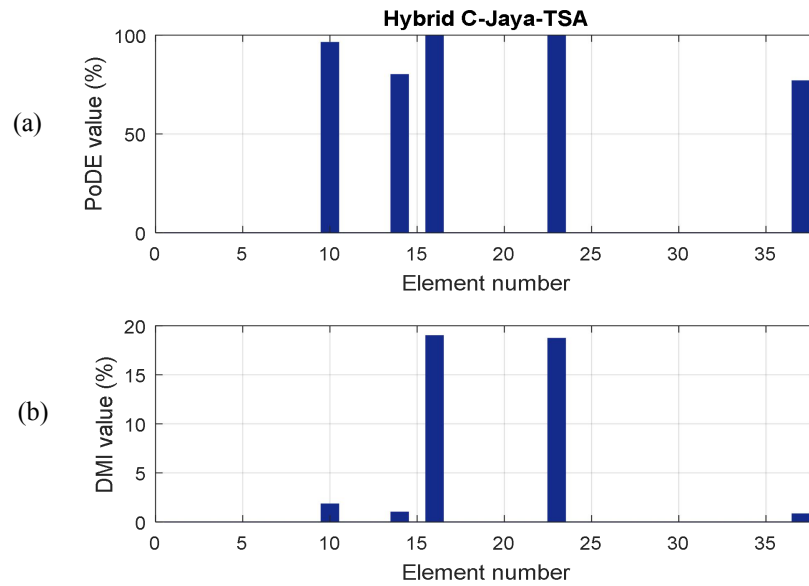


Figure 6-11 PoDE and DMI values for the multiple damages case with uncertain modal data: (a) PoDE; (b) DMI.

Minor structural damage case

In the previous cases, the damage extents are relatively large. In this section, identification of a minor structural damage case is performed. 6% stiffness reduction is assumed in the 9th element. The regularization parameter is selected as $\lambda = 4 \cdot 10^{-3}$, and the other parameters for the algorithm are defined as the same as those in the previous cases. 1% and 10% uncertainties are respectively introduced into the natural frequencies and mode shapes. By using the upper and lower bounds of uncertain modal data, the upper and lower bounds and the middle value of damage index of every element are obtained for the calculation of PoDE and DMI. Figure 6-12 presents the iteration processes of the upper bound, lower bound and middle value of the 9th element. It only needs around 50 iterations to achieve the convergence. Figure 6-13 shows the lower bound, upper bound, PoDE and DMI values of all the 37 elements. The location of the minor damage is accurately identified, and the DMI value for the 9th element is

5.67%, which is very close to the true value of 6%. No false identification is observed in the identification results. This case demonstrates the effectiveness of using the proposed approach for identifying the minor structural damage, even with 1% and 10% uncertainties in the natural frequencies and mode shapes respectively.

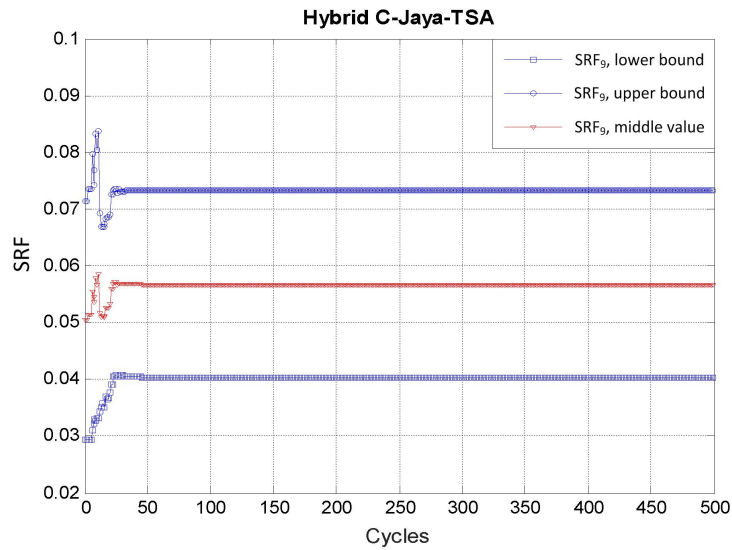


Figure 6-12 The evolutionary processes of the upper bound, lower bound and middle value of the damage index of the 9th element in the minor structural damage case.

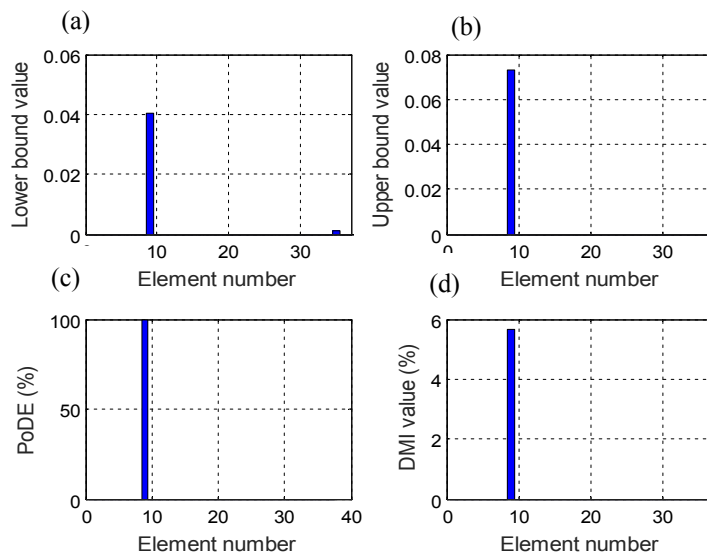


Figure 6-13 Identification results for the minor structural damage case:

(a) Lower bound; (b) Upper bound; (c) PoDE; (d) DMI value.

6.4.3 Verification with a benchmark structure

In this section, a benchmark truss model (Kim et al., 2019; Tam et al., 2020) is used as an example for further verification. Numerical studies on a simply supported truss, as shown in Figure 6-14, are conducted. The Young's modulus and density of this truss model are 2770kg/m^3 and 70GPa , respectively. The area of cross-section is 0.01m^2 . The first three natural frequencies and the mode shape data along the vertical direction of the 2nd, 4th, 5th, 8th, 12th and 13th nodes are employed as the input for the proposed Hybrid C-Jaya-TSA. Namely, the total 21 modal data are used to identify 31 stiffness parameters of this truss model. The C-TSA is also utilized for the comparison purpose. The parameter setting for these two algorithms are set as the same as those in the previous numerical example.

Case 1 is a minor damage case, and 8% stiffness reduction is assumed in the 10th element, which means that the stiffness reduction of the 10th element is 8%. Case 2 is a multiple damage case, in which 10% and 20% stiffness reductions are assumed in the 10th and 19th elements, respectively. Equally, both uncertainty levels for the natural frequencies $X_{\omega, \text{uncertain}}$ and $X_{\omega, \overline{\text{uncertain}}}$ are set as 1% while the uncertainty levels for the mode shapes $X_{\Phi, \text{uncertain}}$ and $X_{\Phi, \overline{\text{uncertain}}}$ are set as 10%. The regularization parameter for Case 1 and Case 2 are set as 10^{-4} and $8 \cdot 10^{-5}$.

Figure 6-15 shows the final identification results based on the proposed algorithm and the C-TSA. Both the algorithms can localize the damages correctly. The proposed algorithm has advantage in terms of the identification accuracy. For example, in Case 1, three false alarms are observed by using C-TSA, however, the proposed C-Jaya-TSA only outputs one. Furthermore, for Case 1, the DMI value of the 10th element acquired by the proposed algorithm is 7.87%, which is more accurate than using C-TSA. For Case 2, the obtained DMI value of the 10th and 19th elements are respectively 9.66% and 19.65%, which are close to the true values, even when the uncertain and limited modal data are used. The above results demonstrate that the proposed approach can provide accurate damage identification results for this benchmark truss structure.

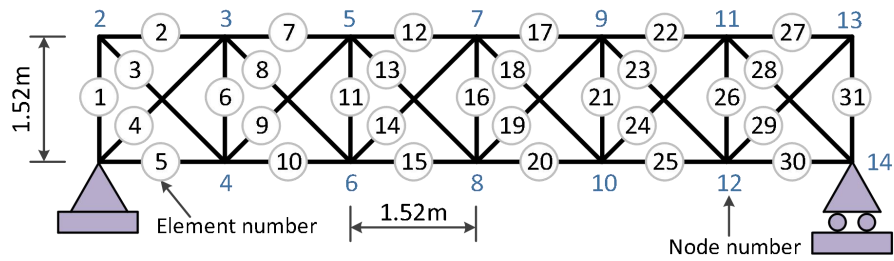


Figure 6-14 A truss model.

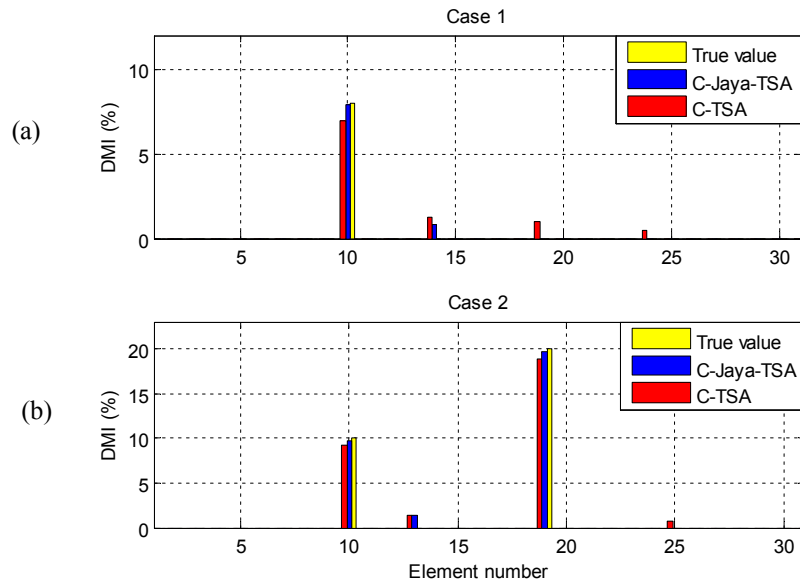


Figure 6-15 Identification results of the truss model; (a) Case 1, (b) Case 2.

The Guangzhou New TV tower and a benchmark truss structure are used as numerical examples in this section to investigate the effectiveness and accuracy of using the proposed method for conducting structural damage identification with significant uncertainties and a limited number of measurement data. With the simplifications made for modelling this complex Guangzhou New TV tower, the condition number of the global stiffness matrix is large, which introduce additional errors in the eigenvalue analysis to obtain the analytical natural frequencies and mode shapes. The damage identification with a limited number of measurement data which is less than the system parameters to be identified, is considered as an undetermined inverse problem. This further increases the difficulties in damage identification. By using the proposed Hybrid C-Jaya-TSA and the non-probabilistic method based on the interval analysis to consider the uncertainty effect, structural damage identification is

performed effectively and accurate results are obtained, indicating the superiority of the proposed algorithm.

6.5 Experimental validations

An experimental cantilever beam (Hou et al., 2018) is taken as an example for the experimental investigations in this section to verify the effectiveness and accuracy of the proposed method in structural damage identification. Eleven accelerometers are used in the vibration testing, and the sensor placement of the beam model is shown in Figure 6-16. The total length of the beam is 1000mm with a cross section of 49.60mm×5.00mm. The Young's modulus and density of this beam model are $7.67 \times 10^3 \text{ kg/m}^3$ and 144GPa, respectively. Considering that the ratio of the height to the length of this beam model is very small, Euler beam elements are used to build the finite element model. The beam is uniformly divided into 100 elements with two DOFs at each node. The elements are numbered from 1 to 100, from the left support to the right free end. Each element has a length of 10mm. The introduced damage locations and extents are listed in Table 6-5.

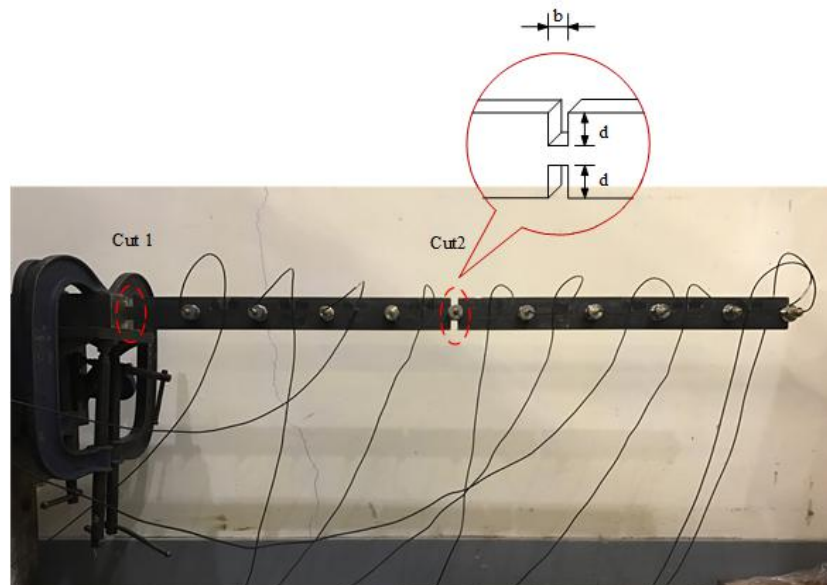


Figure 6-16 The cantilever beam structure and the locations of accelerometers (Hou et al., 2018).

It should be noted that even though the damage extent for a single element is relatively large, with the fine mesh of 10mm for each element, the damage effect is not significant. This is evident with the minor changes in the vibration characteristics. From previous studies on the modal identification results from hammer impact tests by using an instrumented hammer to apply excitations at a location near the fixed end (Hou et al., 2018).

Table 6-5 Damage locations and extents for the experimental verifications.

Case number	Damage locations	SRF	DMI (%)
Case 1	1 st element	0.4	40
Case 2	1 st element	0.6	60
Case 3	1 st element	0.6	60
	50 th element	0.6	60

The first six natural frequencies within the range of 0-300 Hz and the associated mode shapes were identified from vibration acceleration measurements by using rational fraction polynomial method (Hou et al., 2018). Model updating is conducted to calibrate the initial finite element model and make the initial finite element model as close as possible to the real undamaged structure (Ding et al., 2019a; Ding et al., 2019b). It is conducted by using the first six natural frequencies and the corresponding mode shape data along vertical direction of the 11th, 21st, 31st, 41st, 51st, 61st, 71st, 81st, 91st and 101st nodes and the proposed Hybrid C-Jaya-TSA. The first six mode shapes under the undamaged state used for the initial model updating are shown in Figure 6-17. Regarding the parameters setting, Colony Size is set as $CS=100$, the maximum iteration number is 500 and parameter $ST=0.4$. Table 6-6 lists the modal data of the initial finite element model and the updated one. It is clearly observed that the modal data of the updated model have a good agreement with the experimental measurements. Table 6-7 summarizes the identified first six natural frequencies and the corresponding MAC values of the beam under the undamaged and damaged states. Very minor changes in the natural frequencies and MAC values are obtained between the undamaged and damaged states. This indicates that minor damage is introduced in the structure.

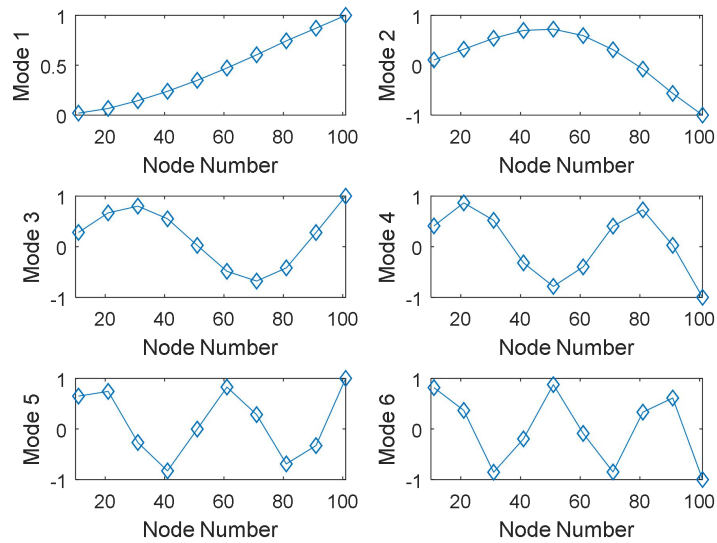


Figure 6-17 The first six measured mode shapes of the undamaged model.

Table 6-6 The first six natural frequencies of the initial and updated finite element models

Mode no.	Undamaged	Initial model		Updated model	
	Freq.(Hz)	Freq.(Hz)	MAC	Freq.(Hz)	MAC
1	3.53	3.50	0.9998	3.53	0.9998
2	21.77	21.90	0.9989	21.77	0.9991
3	60.78	61.18	0.9956	60.78	0.9965
4	119.46	119.46	0.9968	119.45	0.9969
5	194.78	196.50	0.9963	194.78	0.9972
6	292.82	291.51	0.9927	292.82	0.9929

Table 6-7 Measured modal data of the beam under the undamaged and damaged states

Mode no.	Undamaged	Damage case 1		Damage case 2		Damage case 3	
	Freq.(Hz)	Freq.(Hz)	MAC	Freq.(Hz)	MAC	Freq.(Hz)	MAC
1	3.53	3.49 (-1.24)	0.9999	3.38 (-4.41)	0.9997	3.33 (-5.91)	0.9998
2	21.77	21.39 (-1.72)	0.9995	20.85 (-4.26)	0.9984	20.29 (-6.81)	0.9986
3	60.78	59.46 (-2.16)	0.9988	58.93 (-3.04)	0.9983	58.38 (-3.95)	0.9957
4	119.46	118.31 (-0.96)	0.9988	116.01 (-2.88)	0.9951	113.35 (-5.12)	0.9923
5	194.78	191.98 (-1.44)	0.9978	188.74 (-3.10)	0.9917	188.46 (-3.25)	0.9887
6	292.82	281.56 (-3.84)	0.9807	286.76 (-2.07)	0.9495	275.08 (-6.06)	0.9826

Notes: Values in the brackets are the relative changes (%) in natural frequencies

Based on the updated cantilever beam and the measured modal data, the proposed Hybrid C-Jaya-TSA with the non-probabilistic method is used to conduct damage identification for this beam. The first six natural frequencies and the mode shape values at the vertical direction of the 11th, 21st, 31st, 41st, 51st, 61st, 71st, 81st, 91st and 101st nodes, where are the locations of the installed sensors, as shown in Figure 6-16, are used as the input. Namely, totally 66 modal data are applied to identify the stiffness parameters of 100 elements. Regarding the parameters setting, $CS=100$ and the maximum iteration number of 500 and parameter $ST=0.4$ are also used. The regularization parameter in Case 1 is set as $\lambda=0.01$. Similar to Ref. (Padil et al., 2017), uncertainties for the natural frequencies $X_{\omega, \text{uncertain}}$ and $X_{\overline{\omega, \text{uncertain}}}$ are set as 1% while the uncertainties for the mode shapes $X_{\Phi, \text{uncertain}}$ and $X_{\overline{\Phi, \text{uncertain}}}$ are set as 10%.

Figure 6-18 shows the lower bound value, the upper bound value, PoDE and DMI values of all the elements for Case 1. The DMI value of the 1st element is 44.71%, which is very close to the true value. The proposed Hybrid C-Jaya-TSA associated with the DMI by the non-probabilistic method can successfully identify the damage.

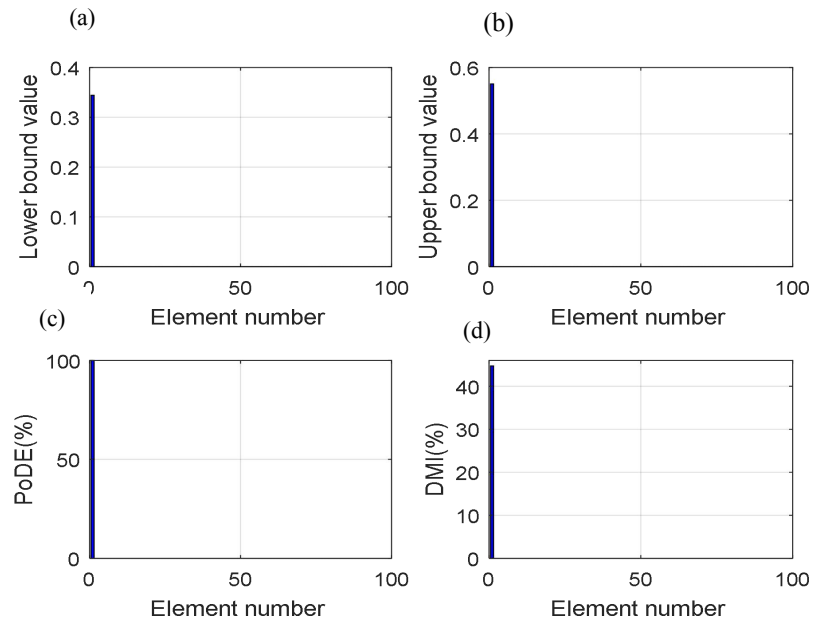


Figure 6-18 The lower bound, upper bound, DMI values of each element for Case 1 in the experimental verification: (a) Lower bound; (b) Upper bound; (c) PoDE; (d) DMI values.

For Cases 2 and 3, parameters setting for the algorithm are the same as those in Case 1. The regularization parameters are set as 0.02 and 0.0004, respectively. The same uncertainty levels as Case 1 are assumed for natural frequencies and mode shapes. Figures 6-19 and 6-20 show respectively the obtained PoDE and DMI values for these two cases. It is clearly observed that the damage locations are accurately identified. PoDE values of the damaged elements are significant without any minor false identification results. For Case 2, the DMI value of the 1st element is 68.10%. For Case 3, the DMI values for the 1st and 50th element are 76.15% and 73.79%, respectively. Overall, the identification accuracy is good, even when the uncertainties are included. The results in the experimental studies demonstrate that the proposed Hybrid C-Jaya-TSA can locate damages accurately and identify the damage severities with a good accuracy, even the uncertainties present in the finite element model and experimental data.

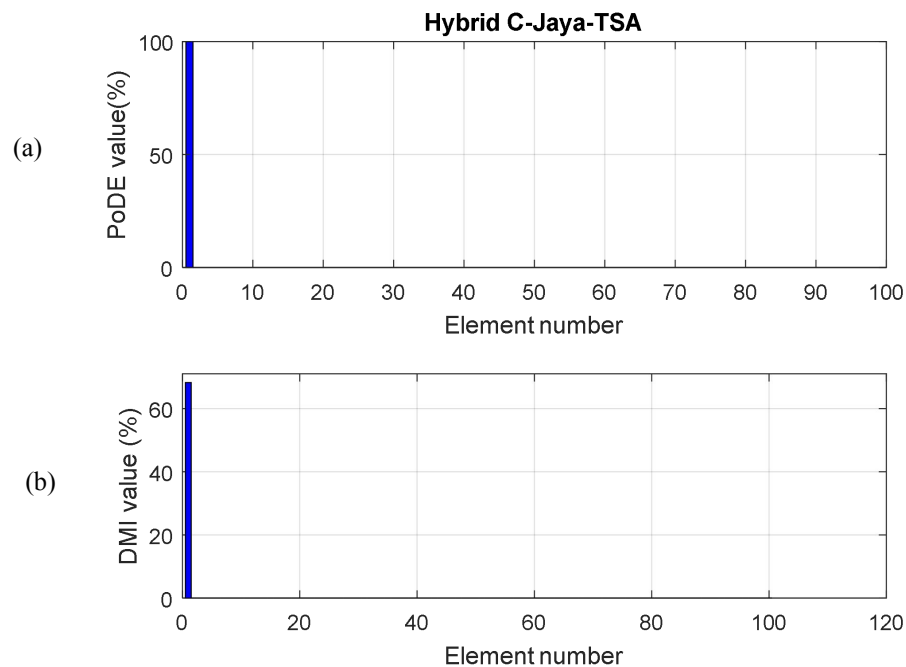


Figure 6-19 PoDE and DMI values of each element for Case 2 in the experimental verification:

a) PoDE; b) DMI.

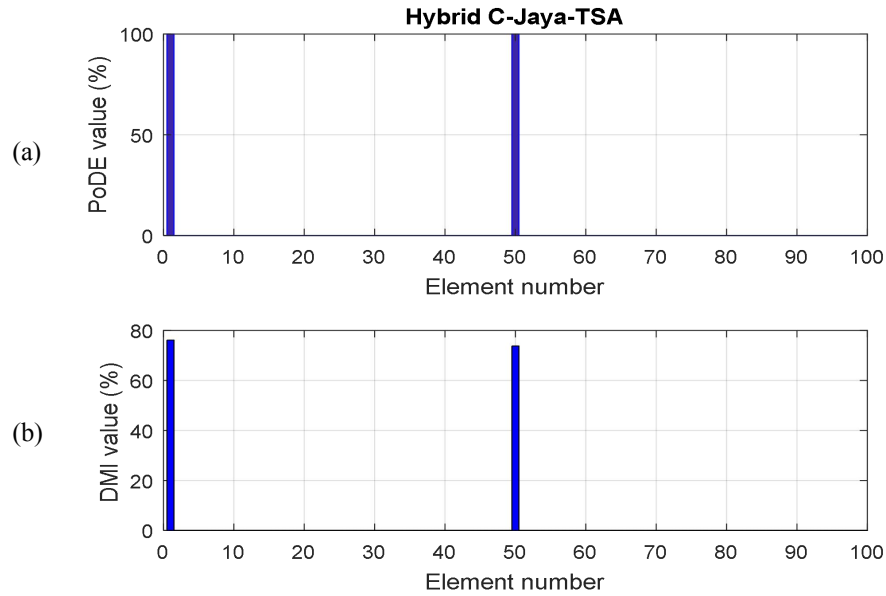


Figure 6-20 PoDE and DMI values of each element for Case 3 in the experimental verification:

a) PoDE; b) DMI.

6.6 Conclusions

In this study, a novel non-probabilistic method by using Hybrid C-Jaya-TSA is presented to conduct structural damage identification considering uncertainties in finite element modelling errors and measurement errors. The identification difficulties are increased since the damage identification analysis is underdetermined, with the quantity of the used modal data less than that of the total system parameters. The effectiveness and accuracy of the proposed method are verified by the numerical and experimental verifications. Several conclusions can be drawn:

- When optimizing high-dimension classical benchmarks, the developed Hybrid C-Jaya-TSA provides more competitive optimization results compared with the latest algorithms, indicating the effectiveness and necessity of the applied modifications for improving the existing swarm intelligence methods;

- When conducting the damage identification of complex civil engineering structures with uncertainties and modelling errors, the developed Hybrid C-Jaya-TSA combined with the non-probabilistic method based on interval analysis can localize the damages accurately and provide reliable damage quantification results by using DMI values;

- The results in the numerical and experimental studies demonstrate that the proposed method leads to better structural damage identifications with incomplete and uncertain modal data;

- Overall, the proposed approach can be potentially applied to the real structural health monitoring. The main reasons are listed as follows: a) The proposed method is efficient and accurate, even with a limited number of modal data, such as a few natural frequencies and partial mode shape values; b) Fewer controlling parameters are involved in the developed approach, compared with some existing swarm intelligence methods; c) The developed approach does not need to have good initial values and gradients information in the computation;

- In the future, this method will be extended to solve the long-term structural health monitoring problem, such as identifying modal information and calibrating the finite element models.

References

- Alkayem, N.F., Cao, M.S., & Ragulskis, M. (2019) Damage localization in irregular structures using intelligent FE model updating approach with a new hybrid objective function and social swarm algorithm. *Applied Soft computing*, 83, 105604.
- Beck, J.L., Au, S.K., Vanik, M.W. (1999) Bayesian probabilistic approach to structural health monitoring. *Journal of Engineering Mechanics*, 126(7), 738-745.
- Cai, Z.H., Gong, W.Y., Ling, C.X., & Zhang, H. (2011) A clustering-based differential evolution for global optimization. *Applied Soft Computing*, 11, 1363-1397.
- Chen, W.H., Lu, Z.R., Lin, W., Chen, S.H., Ni, Y.Q., Xia, Y., & Liao, W.Y., Theoretical and experimental modal analysis of the Guangzhou New TV Tower. *Engineering Structures*, 33(12), 3628-3646.
- Ding, Z.H., Li, J., Hao, H., & Lu, Z.R. (2019a) Structural damage identification with uncertain modelling errors and measurement noise by clustering based tree seeds algorithm. *Engineering Structures*, 165, 301-314.
- Ding, Z.H., Li, J., & Hao, H. (2019b) Structural damage identification using improved Jaya algorithm based on sparse regularization and Bayesian inference. *Mechanical Systems and Signal Processing*, 132, 211-231.
- Ding, Z.H., Liu, J.K., & Lu, Z.R. (2018) Parameters identification of chaotic systems based on artificial bee colony algorithm combined with cuckoo search strategy. *Science China Technological Science*, 61(3), 417-426.
- Ding, Z.H., Yao, R.Z., Li, J., & Lu, Z.R. (2018) Structural damage identification based on modified Artificial Bee Colony algorithm using modal data. *Inverse Problems in Science & Engineering*, 26(3), 422-442.
- Du, D.C., Vinh, H.H., Trung, V.D., Quyen, N.T.H., & Trung, N.T. (2017) An efficient multi-stage optimization approach for damage detection in plate structures. *Advances in Engineering Software*, 112, 76-87.
- Fan, W., & Qiao, P. (2011) Vibration-based damage identification methods: a review and comparative study. *Structural Health Monitoring*, 10(1), 83-111.
- Feng, D.M., & Feng, M.Q. (2018) Computer vision for SHM of civil infrastructure: From dynamic response measurement to damage detection - A review. *Engineering Structures*, 156, 105-117.
- Garcia-Macias, E., Ierimonti, L., Venanzi, I., & Ubertini, F. (2019) An innovative Methodology for Online Surrogate-Based Model Updating of Historic Buildings Using Monitoring Data. *International Journal of Architectural Heritage*, DOI: 10.1080/15583058.2019.1668495.
- Ghanem, W.A.H.M., & Janta, A. (2018) A cognitively inspired hybridization of artificial bee colony and dragonfly algorithms for training multi-layer perceptions. *Cognitive Computation*, 10(6), 1096-1134.
- Ghosh, S., Kaur, M., Bhullar, S., & Karar, V. (2019) Hybrid ABC-BAT for solving short-term hydrothermal scheduling problems. *Energies*, 12, 551.
- Hou, R.R., Xia, Y., Bao, Y.Q., & Zhou, X.Q. (2018) Selection of regularization parameter for L_1 -regularized damage detection. *Journal of Sound and Vibration*, 423, 141-160.
- Jadon, S.S. (2017) Hybrid Artificial Bee Colony algorithm with Differential Evolution. *Applied Soft Computing*, 58, 11-24.

- Jahangiri, M., Najafgholipour, M.A., Dehghan, S.M., & Hadianfard, M.A. (2019) The efficiency of a novel identification method for structural damage assessment using the first vibration mode data. *Journal of Sound and Vibration*, 458, 1-16.
- Kang, F., Li, J.J., & Xu, Q. (2012) Damage detection based on improved particle swarm optimization using vibration data. *Applied Soft Computing*, 12(8), 2329-2335.
- Kim, N.I., Kim, S., & Lee, J. (2019) Vibration-based damage detection of planar and space trusses using differential evolution algorithm. *Applied Acoustic*, 148, 308-321.
- Li, J., & Hao, J. (2016) A review of recent research advances on structural health monitoring in Western Australia. *Structural Monitoring and Maintenance*, 3(1), 33-49.
- Lin, X.X., Huang, M., & Lu, Z.R. (2017) Hybrid sensitivity matrix for damage identification in axially functionally graded beams. *Applied Mathematical Modelling*, 41, 604-617.
- Lu, X.B., Lu, Z.R. & Liu, J.K. (2013) A two-step approach for crack identification in beam. *Journal of Sound and Vibration*, 332, 282-293.
- Naik, M.K., Samantaray, L., & Panda, R. (2015) A hybrid CS-GSA algorithm for optimization. *Studies in Computational Intelligence*, 611, 3-35.
- Padil, K.H., Bakhary, N., & Hao, H. (2017) The use of a non-probabilistic artificial neural network to consider uncertainties in vibration-based-damage detection. *Mechanical Systems and Signal Processing*, 83, 194-209.
- Pathirage, C.S.N., Li, J., Li, L., Hao, H., Liu, W.Q., & Ni, P.H. (2018) Structural damage identification based on autoencoder neural networks and deep learning. *Engineering Structures*, 172, 13-28.
- Pramanik, P & Malti, M.K. (2019) An inventory model for deteriorating items with inflation induced variable demand under two level partial trade credit: A hybrid ABC-GA approach. *Engineering Applications of Artificial Intelligence*, 85, 194-207.
- Rao, R.V. (2016) Jaya: a simple and new optimization algorithm for solving constrained and unconstrained optimization problems. *International Journal of Industry Engineering Computation*, 7, 19-34.
- Senel, F.A., Gokce, F., Yuksel, A.S. & Yigit, T. (2019) A novel hybrid PSO-GWO algorithm for optimization problems. *Engineering with Computers*, 35(4), 1359-1373.
- Sun, H., Lus, H., & Betti, R. (2013) Identification of structural models using a modified Artificial Bee Colony algorithm. *Computers & Structures*, 116, 59-74.
- Tam, T.T., Dinh-Cong, D., Lee, J., & Nguyen-Thoi, T. (2020) An effective deep feed forward neural networks (DFNN) method for damage identification of truss structures using noisy incomplete modal data. *Journal of Building Engineering*, DOI: 10.1016/j.jobe.2020.101244.
- Titurus, B & Friswell, M.I. (2008) Regularization in model updating. *International Journal for Numerical Methods in Engineering*, 75, 440-478.
- Tsogka, C., Daskalakis, E., Comanducci, G., & Ubertini, F. (2017) The stretching method for Vibration-Based Structural Health Monitoring of Civil Structures. *Computer-Aided Civil and Infrastructure Engineering*, 32(4), 288-303.
- Tran-Ngoc, H., Khatir, S., De Roeck, G., Bui-Tien, T., Nguyen-Ngoc, L., & Abdel Wahab, M. (2018) Model updating for Nam O Bridge using particle swarm optimization algorithm and genetic algorithm. *Sensors*, 18(12), 4131-4146.

- Ubertini, F., Cavalagli, N., Kita, A., Comanducci, G. (2018) Assessment of a monumental masonry bell-tower after 2016 central Italy seismic sequence by long-term SHM. *Bulletin of Earthquake Engineering*, 16(2), 775-801.
- Wang, X., Qiu, Z., & Elishakoff, I. (2008) Non-probabilistic set-theoretic model for structural safety measure. *Acta Mechanica*, 198 (1-2), 51-64.
- Wang, X., Xia, Y., Zhou, X., & Yang, C. (2014) Structural damage measure index based on non-probabilistic reliability model. *Journal of Sound and Vibration*, 333(5), 1344-1355.
- Xu, Z., Zhang, H., & Wang, Y. (2010) $L_{1/2}$ regularization. *Science China Information Sciences*, 53(6), 1159-1169.
- Yi, T.H., Li, H.N., & Zhang, X.D. (2012) A modified monkey algorithm for optimal sensor placement in structural health monitoring. *Smart Material and Structures*, 21(10), 105033.
- Yu, L., & Li, C. (2014) A global artificial fish swarm algorithm for structural damage detection. *Advances in Structural Engineering*, 17(3), 331-346.
- Yuen, K.Y., & Katafygiotis, L.S. (2003) Bayesian fast Fourier transform approach for modal updating using ambient data. *Advances in Structural Engineering*, 6(2), 81-95.
- Zhou, X.Q., Xia, Y., & Weng, S. (2015) L_1 regularization approach to structural damage detection using frequency data. *Structural Health Monitoring*, 14(6), 571-582.

CHAPTER 7 SIMULTANEOUS IDENTIFICATION OF STRUCTURAL DAMAGE AND NONLINEAR HYSTERESIS PARAMETERS BY AN EVOLUTIONARY ARTIFICIAL NEURAL NETWORK BASED ON TIME DOMAIN DATA

ABSTRACT⁶

This paper presents a new approach for simultaneous identification of structural damage and nonlinear hysteresis parameters of nonlinear structures by using an evolutionary Artificial Neural Network (ANN) based on K-means Jaya algorithm and time domain vibration response data. ANN is an effective tool to tackle complex problems in numerous fields. However, the back propagation algorithm, which is conducted based on gradient descent, is an important component of training ANN. With vanishing gradients, ANN may suffer the local minimal during the training process. To over this disadvantage, a type of swarm intelligence method, named the K-means Jaya, is employed to improve the training of ANN parameters (weight and bias) by minimizing the discrepancies between real outputs and desired ones and then using these parameters to develop the networks. To evaluate the performance of the proposed approach, numerical studies on a nonlinear Single Degree Of Freedom (SDOF) system and a nonlinear five-story benchmark building model subjected to the seismic loading are conducted. A high level noise is introduced into acceleration response data to simulate the strong measurement noise for the nonlinear system identification. Identification results demonstrate that the evolutionary ANN combined with K-means Jaya, termed as an ANN-K-means Jaya, is more accurate than other swarm intelligence methods. The proposed approach can be used effectively for identifying nonlinear structural damage and nonlinear hysteresis model parameters simultaneously.

7.1 Introduction

Structural damage identification acts as a vital role in evaluating structural integrity since civil infrastructure is inevitably accumulating damage during the

⁶Ding, Z., Li, J., Hao, H. (2020). Simultaneous identification of structural damage and nonlinear hysteresis parameters by an evolutionary artificial neural network based on time domain data. *International Journal of Non-linear Mechanics* (Under review)

in-service period. To monitor structural conditions for reducing the maintenance cost and prevent catastrophic failures of structures, numerous methods have been developed for structural damage identification (Farrar & Worden, 2007). Among these studies, vibration based methods via utilizing the dynamic vibration characteristics, i.e. natural frequencies and mode shapes, etc., or vibration time domain responses for damage identification, have attracted an amount of interests and attentions.

For frequency domain based methods, Yan and Golinval (2005) used the state subspace method integrating with the flexibility to localize damages in beam structures. Lu et al. (2017) proposed a hybrid sensitivity method to conduct damage identification for axially functionally graded beams, in which only the first several natural frequencies and several vibration response measurements are required. Esfandiari et al. (2020) applied the changes in principle components of frequency response functions to formulate the objective function, and then the least square method was utilized to optimize the objective function to identify structural damages. This method was verified using a truss and a frame structure. Furthermore, the wavelet methods (Ren & Sun, 2008; Cao et al., 2012; Yazdanpanah et al., 2020), the stochastic subspace identification method (Altunisik et al., 2017) and the power spectral density method (Zheng et al., 2015), have been respectively employed for structural damage identification. On the other hand, structural damage identification methods using time domain measurement data have also been developed in the recent years. Hu et al. (2017) formulated the objective function based on acceleration responses and then used the homotopy continuation algorithm to identify the cracks in beam structures. Lu and Wang (2017) proposed an enhanced sensitivity method to conduct structural damage identification, in which a trust-region constraint was introduced to enhance the performance of the standard sensitivity method. The Extended Kalman Filter (EKF) (Yang et al., 2006; Xie & Feng, 2012) has been applied to perform online system identification in the time domain.

However, some of the above-mentioned methods (Lu et al., 2017; Esfandiari et al., 2020; Hu et al., 2017; Lu & Wang, 2017) require good initial system parameters and an accurate estimation of the gradients. The state-subspace method (Yan & Golinval,

2005), the wavelet-based methods (Ren & Sun, 2008; Cao et al., 2012; Yazdanpanah et al., 2020), and the filter based methods (Yang et al., 2006; Xie & Feng, 2012) are easily affected by high-level measurement noise. These unfavorable conditions might restrict the practical applications of these traditional methods, especially for some large-scale structures or nonlinear structures.

In contrast, machine learning methods can be used to overcome the abovementioned drawbacks, since machine learning based methods can learn and make predictions via datasets instead of the explicit formulations (Ding et al., 2019a). Many studies by using machine learning methods, mainly including the artificial neural networks (ANN), have been conducted for structural damage identification. Abdeljaber et al. (2018) proposed using convolutional neural networks for damage identification of joints in a steel frame. Maity and Saha (2004) used the strain and displacement data for damage identification of a simple cantilever beam using a back-propagation ANN. Padil et al. (2017) developed a non-probabilistic ANN to perform structural damage identification considering system uncertainties. Nadith et al. (2018) proposed the deep auto-encoder neural networks to identify structural damage, in which the first several natural frequencies and mode shapes were employed as the input and structural damage locations and extents were identified as the output. Liu et al. (2014) presented the Rough Sets (RS) theory combining with ANN to conduct damage identification. An information entropy based discretization in RS was used for dimension reduction and then ANN was applied for the following identification. Elshafey et al. (2013) developed a methodology based on the feed-forward back-propagation and the radial basis neural network to identify cracks for both thick and thin concrete elements.

Nevertheless, because of the usage of back-propagation algorithms based on gradient descent, a main shortcoming of ANN is the potential problem of local minimal when the network generates relative complex error surfaces with many local best points. When utilizing some traditional deterministic optimization techniques, if a selected initial point is far away from the global minimum, the optimization problem would converge to the local minimal instead of the global one. Previous studies (Curry & Morgan, 1997; Gupta & Sexton, 1999; Valian et al., 2011) have reported this local minimal problem relevant to the

back-propagation algorithm. Swarm intelligence techniques, i.e. Genetic Algorithm (GA) (Wang, 2009), Particle Swarm Optimization (PSO) algorithm (Chen & Yu, 2017) and Artificial Bee Colony (ABC) algorithm (Sun et al., 2013), have been used effectively for various types of optimization problems in recent years. These algorithms belong to global search techniques and have a higher likelihood to obtain global minimal and to avoid local minimal. Therefore, some remarkable successes by combining ANN and swarm intelligence methods to tackle complex problems in different fields have been obtained. For example, Geethanjali et al. (2008) concluded that using the PSO to train multi-layered neural networks is more effective than the back-propagation algorithm, for detecting an internal fault and distinguishing with other operating conditions of power transforms. Other combinations, i.e., a combination of GA and ANN, namely, GA-ANN (Yazdanmehr et al., 2009) and Imperialist Competitive Algorithm based ANN (ICA-ANN) (Toghyani et al., 2016), and Differential Evolutionary based ANN (DE-ANN) (Nguyen et al., 2016) have been developed to deal with complex production units problem and the stirling heat engine's power prediction.

Apart from the abovementioned algorithms, a new type of swarm intelligence method, named as Jaya algorithm (Rao & Saroj, 2017), has gained its attention. The most obvious advantage of the Jaya algorithm is that there is no special controlling parameters in this algorithm. To enhance the performance of the Jaya algorithm, K-means clustering is introduced into the Jaya algorithm by Ding et al. (Ding et al., 2019b) and the optimization performance of the Jaya algorithm has been greatly improved but the simple algorithmic structure of the Jaya algorithm is still kept. Therefore, the K-means Jaya algorithm is potentially promising to replace back-propagation algorithms for training ANN.

Regarding structural damage identification, existing studies (Yan & Golinval, 2005; Lu et al., 2017; Esfandiari et al., 2020; Ren & Sun, 2008; Cao et al., 2012; Yazdanpanah et al., 2020; Altunisik et al., 2017; Zheng et al., 2015; Hu et al., 2017; Lu & Wang, 2017; Ding et al., 2019a; Maity & Saha, 2004; Padil et al., 2017; Pathirage et al., 2018) focus more on the linear structures. In real applications, when structures have severe damages, nonlinear behaviors would be observed (Lu et al., 2017; Katsaras et al., 2008), especially under strong excitations. To describe the nonlinear behavior resulting from

structural damages, several nonlinear hysteretic models, such as Preisach, Ischinskii, Bouc-Wen and bilinear models (Charalampakis & Dimou, 2010), have been presented. Identifications of these nonlinear models are also important to understand the structural vibration behavior and condition (Lu et al., 2017). However, few researches on the simultaneous identification of structural damage and nonlinear hysteretic models have been conducted. The measurement noise inevitably exist in the identification process. However, the noise level in many studies (an & Golinval, 2005; Lu et al., 2017; Esfandiari et al., 2020; Ren & Sun, 2008; Cao et al., 2012; Yazdanpanah et al., 2020; Altunisik et al., 2017; Zheng et al., 2015; Hu et al., 2017; Lu & Wang, 2017; Ding et al., 2019a) follows a certain pattern with a moderate level. Under certain situations, very significant noise could be observed and the influence of a strong noise on the identification performance should be investigated to demonstrate the robustness of the developed methods.

This paper proposes a new approach by combining ANN and K-means based Jaya algorithm for simultaneous identification of structural damage and nonlinear hysteresis parameters. Specifically, in the training stage to obtain the weights and bias parameters for the designed ANN, the *K*-means Jaya algorithm is used to replace the back-propagation algorithm. As mentioned above, the *K*-means Jaya algorithm equips stronger global optimization capacity compared with the traditional gradient information based back-propagation algorithm. Therefore, using the *K*-means Jaya algorithm could more effectively train the ANN. The integrated algorithm is termed as ‘ANN-*K*- means Jaya’. Numerical studies are conducted on a benchmark structure with an improved Dahl hysteresis model (Wang & Liao, 2011) to demonstrate the accuracy and efficiency of the proposed approach. The simultaneous identification of structural damage and hysteretic model parameters is conducted for verifying the performance of the proposed approach. Furthermore, a relatively high level noise is introduced into acceleration data to simulate the case with strong measurement noise for the identification. State-of-the-Art swarm intelligence methods, including *K*-means Jaya (Ding et al., 2019b), Improved Tree Seeds Algorithm (Ding et al., 2019c), Best Neighbor-guided ABC (Hu et al., 2019), and the traditional ANN method are also used for comparison with the proposed ANN-*K*-means Jaya algorithm in terms of the calculation efficiency

and identification accuracy.

7.2 Nonlinear Hysteretic Model and Parameter Identification

7.2.1 Improved Dahl hysteresis model

This section briefly reviews the improved Dahl hysteresis model (Wang & Liao, 2011). The equation of motion of the Single Degree Of Freedom (SDOF) nonlinear system considering the hysteretic models can be expressed as

$$\begin{cases} m\ddot{u} + c\dot{u} + ku + \alpha \cdot r = \mathbf{F}(t) \\ \dot{r} = f(r, u, \dot{u}, \mathbf{p}) \\ u(0) = u_0, \dot{u}(0) = \dot{u}_0, r(0) = r_0 \end{cases} \quad (7.1)$$

where u is the displacement; u_0, \dot{u}_0 and r_0 are respectively the initial displacement, velocity and restoring force of the nonlinear system; and m, c, k and \mathbf{F} denote the mass, damping, stiffness and excitation respectively. The restoring force $\alpha \cdot r$ can be obtained based on the proposed improved Dahl hysteresis model, in which the parameter α is used to control the shape of the force-displacement responses.

The hysteretic behavior describes the memory-based relationship between the displacement u and the r , which can be generally defined as

$$\dot{r} = f(r, u, \dot{u}, \rho) \quad (7.2)$$

where $f(\cdot)$ is the nonlinear function denoting the hysteresis behavior, and ρ denotes the effective controlling parameter. Generally, Bouc-Wen model (Lu et al., 2017; Ding et al., 2019b) is commonly used to represent the hysteresis response. In this article, instead of using the Bouc-Wen model, an improved Dahl hysteresis model, as shown in Figure 7-1, is introduced to simulate the nonlinear hysteresis response.

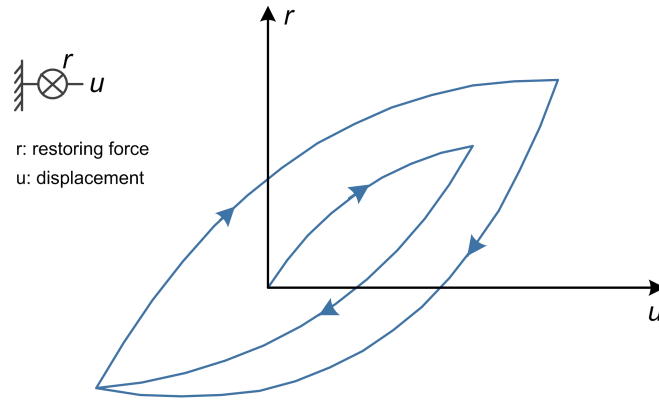


Figure 7-1 The improved Dahl nonlinear hysteretic model.

The improved Dahl model can well represent the hysteretic force-displacement response in the small displacement region and can be expressed as

$$\dot{r} = \rho(\dot{u} - |\dot{u}|r) \quad (7.3)$$

where ρ represents the controlling coefficient; r is the restoring force. The improved Dahl model could be used to describe the hysteresis phenomenon. Compared to the Bouc-Wen model, fewer controlling parameters are involved in the improved Dahl model. Furthermore, the model parameter vector \mathbf{p} can be defined as follow

$$\mathbf{p} = [k_0, c_0, \alpha, \rho]^T \quad (7.4)$$

It ought to be noted that different model vector \mathbf{p} could generate different nonlinear dynamic responses.

7.2.2 Nonlinear Model Parameter Identification

To well describe a nonlinear system with the improved Dahl model, Figure 7-2 presents a Single Degree Of Freedom (SDOF) nonlinear system, which is used as an example to demonstrate the dynamic response calculation of a nonlinear system.

Firstly, substitute the Eq.(7.3) into the Eq.(7.1) and use the Runge-Kutta method is used to solve Eq. (7.1) to obtain the dynamic responses. Similarly, the equation of motion of a nonlinear Multi Degree Of Freedom (MDOF) system or structure can be built.

In this article, $F(t)$ and $u(t)$ are respectively defined as two vectors comprising the input and the output data; $\mathbf{t} = t_1, t_2, \dots, t_k$ represents the time instant series and $u(t_k)$ denotes the dynamic response at the time instant t_k . As mentioned above, it is noted from Eq. (7.1) that when using different model vector \mathbf{p} , different dynamic responses would be obtained. Therefore, the analytical dynamic response $\hat{u}(t_k)$ under the model vector $\hat{\mathbf{p}}$ at the time instant t_k can be expressed as follows

$$\hat{u}(t_k) = f(\hat{\mathbf{p}}, t_k) \quad (7.5)$$

When using the swarm intelligence methods to conduct nonlinear model identification, the discrepancy between the calculated and measured responses can be used to formulate the objective function, which is defined as (Ding et al., 2019)

$$g(\hat{\mathbf{p}}) = \sum_{i=1}^{n_{res}} \sum_{k=1}^{n_{time}} (\hat{u}_i(t_k) - u_i(t_k)) \cdot (\hat{u}_i(t_k) - u_i(t_k))^T \quad (7.6)$$

where n_{res} is the quantity of the available measurements that are used for updating, which relies on the number of sensors used in the dynamic test; n_{time} is the number of sample points in each measured response; $u_i(t_k)$ denotes the measured dynamic response.

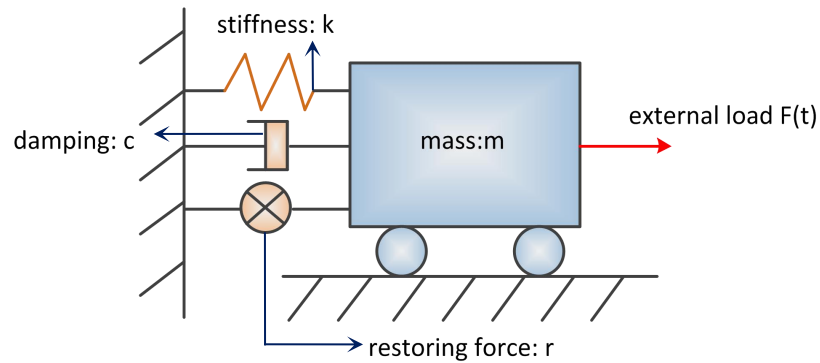


Figure 7-2 The improved Dahl model in SDOF system.

When using machine learning methods for the nonlinear system identification, a number of training samples are required. These samples can be obtained with different

model vector $\hat{\mathbf{p}}$. The input to the training can be the dynamic responses $\hat{u}(t_k)$, and the output is the corresponding model vector $\hat{\mathbf{p}}$.

7.3 Methodology

7.3.1 Artificial Neural Network

ANN is developed in the shape of a parallel distributed network inspired by human nervous system. The distinct feature of ANN is the capacity to learn from datasets to improve its prediction performance. Thus, the trained neural networks can be used for parameter identification, classification and pattern recognition, etc. ANN usually contains three main components, namely the input layer, hidden layer and output layer. Each layer comprises a set of neurons connected with each other by training parameters (weights and bias). Every neuron possesses a processing element with synaptic input connections based on the quantity of the processing neurons in the previous layer and a single output. Many neural network architectures have been developed, and multilayer perception neural networks are one of the most frequently used models. Multilayer perception neural networks contain one or more hidden layers of neurons linked between the input and output layers. Neurons of one hidden layer connect only to neurons of the immediately preceding and immediately following layers. The overview of a three-layer network is shown in Figure 7-3.

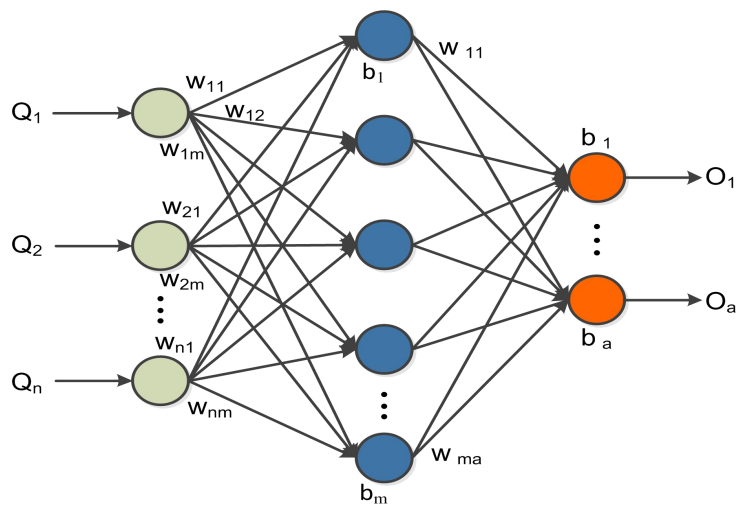


Figure 7-3 Three-layer neural network architecture.

Observed from Figure 7-3, the transfer process between neurons in layers could be found. The input layer receives input patterns $(Q_1 \dots Q_n)$, and then the input is transmitted to hidden layers. The hidden layer possesses several processing units and has an important role to bridge between the input layer and the output layer. Each element in the preceding layers is fully connected to the following ones, and these connections are based on training parameters, i.e. weight and bias. The whole transfer process is defined by two equations. The first one is a propagation function, which computes the input to a neuron from the output of its predecessor neurons and their connections as a weighted sum plus the bias.

$$input_a = \sum_j^n w_{ja} \cdot x_j + b_a; (j=1,2,\dots,n) \quad (7.7)$$

where x_j denotes the output of the j th processing neuron of the input layer, w_{ja} is the synaptic weight ratio that links the j th and a th processing neurons; b_a is the bias ratio between input and hidden layers; j and a are the processing neurons in the input and hidden layers, n is the number of processing neurons in the input layers. There are m total processing neurons in the output layers. $input_a$ represents the input to the a th processing neuron of the hidden layer.

When Equation (7.7) is calculated, the second equation is an activation function used to restrict the value range of the output neurons. The activation function could be a monotonically increasing linear or nonlinear function (Ertugrul, 2018). A sigmoid activation function is employed in this study. Output results $output_a$ are acquired from the output layer as follows

$$output_a = \frac{1}{1 + e^{-input_a}}; (a=1,2,\dots,m) \quad (7.8)$$

where $input_a$, calculated by Equation (7.7), denotes the input of the a th processing neuron; and $output_a$ is the output of the a th processing neuron in the output layer.

Training parameters, i.e. weight and bias, are the most important factors that could determine the success of the trained network. The process of training the network is to

adjust training parameters by minimizing the difference between the calculated output and labelled ones based on training datasets. Generally, the algorithms used for training are the back-propagation methods, which are based on gradient descent. Using these gradient-based algorithms for training would make the network converge to local minimal if the network generates complex error surface with too many local minimal points. To minimize the possibility to face this situation, K-means Jaya (Ding et al., 2019b), which is an EA based on global search techniques, is employed to minimize the difference between calculated outputs and desired ones for training the network parameters. Specifically, the K-means Jaya replaces back-propagation algorithms to determine training parameters including weight and bias. The trained network is used to identify structural damages and nonlinear hysteresis model parameters. A number of samples are generated as training datasets. Acceleration responses are treated as the input to the network, and the output is the vector of structural damage and nonlinear model parameters. Afterwards, acceleration responses in the testing datasets are used as the input and the obtained output provides the identification results.

7.3.2 K-means Jaya algorithm

Jaya algorithm is a powerful swarm intelligence method inspired by the conception that the feasible solution acquired for a given problem ought to move towards the best solution and avoid the worst solution (Rao & Saroj, 2017). Specifically, for each feasible solution, the way of creating its offspring is to move closer to the success (i.e. approaching the best solution) and avoid the failure (i.e. escaping from the worst solution). When generating the offspring, the objective function values are calculated and compared to determine whether this solution or its offspring comes into the next iteration (the selection process is also termed as ‘Greedy Selection Rule’) (Ding et al., 2019b). Three main steps are involved in the Jaya algorithm, which are briefly summarized.

7.3.2.1 Initialization

It is assumed that a colony is randomly generated in the search space and there

contains CS solutions. Every solution is marked as θ_h , which comprises u variables ($\theta_h = [\theta_1, \theta_2, \dots, \theta_u]$). These variables could be generated as

$$\theta_{h,u} = \theta_{h,u}^L + \text{rand}(0,1) \cdot (\theta_{h,u}^U - \theta_{h,u}^L) \quad (7.9)$$

where $\theta_{h,u}$ denotes the uth variable of θ_h ; $\text{rand}(0,1)$ denotes a random number in a range from 0 to 1; $\theta_{h,u}^U$ and $\theta_{h,u}^L$ represent the upper and lower bound values, respectively.

7.3.2.2 Local search strategy

When completing initialization, the local search strategy is operated. Assuming that $\theta_{h,u,C}$ represents the value of the uth dimension of the hth solution at the Cth iteration, the offspring $\theta'_{h,u,C}$ generated by this value is calculated as

$$\theta'_{h,u,C} = \theta_{h,u,C} + r_{1,u,C} \cdot (\theta_{best,u,C} - |\theta_{h,u,C}|) - r_{2,u,C} \cdot (\theta_{worst,u,C} - |\theta_{h,u,C}|) \quad (7.10)$$

where $r_{1,u,C}$ and $r_{2,u,C}$ are two random numbers within in the range $[0,1]$. $\theta_{best,u,C}$ and $\theta_{worst,u,C}$ are respectively the values of the uth variable for the best solution and the worst one in the current iteration.

7.3.2.3 Greedy selection mechanism

With calculations for all dimensions based on Eq. (7.10), the offspring $\theta'_{h,C}$ is obtained. The objective function values of $\theta_{h,C}$ and $\theta'_{h,C}$ are calculated and the solution corresponding to better objective function value will be kept in the next iteration. The algorithm will be continually run until the termination condition is satisfied, i.e., the maximum iteration number is reached.

The standard Jaya algorithm is illustrated above. To make the Jaya algorithm more powerful, the K-means clustering mechanism and a special search equation for the best solution (Ding et al., 2019b) is employed to enhance the standard Jaya algorithm's performance, termed as "K-means Jaya". The specific procedures are illustrated as

follows.

7.3.2.4 K-means clustering

The clustering technique is a useful tool to discover the inherent pattern in any given datasets. Therefore introducing the clustering technique into the swarm intelligence methods would be effective and efficient by making full use of the colony information (Cai et al., 2011). Among all clustering techniques, the K-means clustering is the simplest yet effective. During the early iterations of the Jaya algorithm, conducting the K-means clustering is straightforward and beneficial to improve the algorithm's convergence performance (Ding et al., 2019a). The specific steps of operating K-means clustering are described here

Step 1: $K = 0.1 \cdot CS$ initial clustering centers C_1, C_2, \dots, C_k are randomly selected from the CS individuals $[\theta_1, \theta_2, \dots, \theta_{CS}]$.

Step 2: The remaining solutions are delivered to these clustering centers according to their shortest distance to these centers. The distance between any two individuals (i.e., θ_z and θ_c) is determined by the Manhattan distance

$$d(\theta_z, \theta_c) = \|\theta_z - \theta_c\| = \sum_{v=1}^u \text{abs}(\theta_{z,v} - \theta_{c,v}) \quad (7.11)$$

Step 3: When completing the clustering once, each clustering center may attract several solutions, which can be used to calculate new clustering centers C'_1, C'_2, \dots, C'_k , as follows

$$C'_e = \frac{1}{E_n} \sum_{\theta_r \in c_e} \theta_r \quad (7.12)$$

Step 4: Finally, another K parent solutions from the colony will be randomly chosen and then combined with the newly-calculated clustering centers as a new set, marked as τ . The objective function values of the solutions will be calculated in the set τ , and these values are sorted from the smallest to the largest. The first K individuals are put into the colony.

7.3.2.5 A new updating equation for the best solution

In the standard Jaya algorithm, the best solution plays a critical role in the optimization process, since it guides other solutions to its region. To prevent the premature convergence of the algorithm, a new updating equation that concentrates on the global search is introduced here (Ding et al., 2019b; Gao et al., 2015)

$$\theta'_{best,u,C} = \theta_{best,u,C} + rand \cdot (\theta_{h,u,C} - \theta_{best,u,C}) \quad (7.13)$$

where $\theta_{best,u,C}$ represents the value of the uth dimension of the best solution at the Cth iteration and $\theta'_{best,u,C}$ denotes its offspring value, $\theta_{h,u,C}$ means the value of the uth dimension of an arbitrary solution in the colony. The randomly selected solution will be used to generate the offspring of the best solution and such randomness can be helpful in preventing premature convergence.

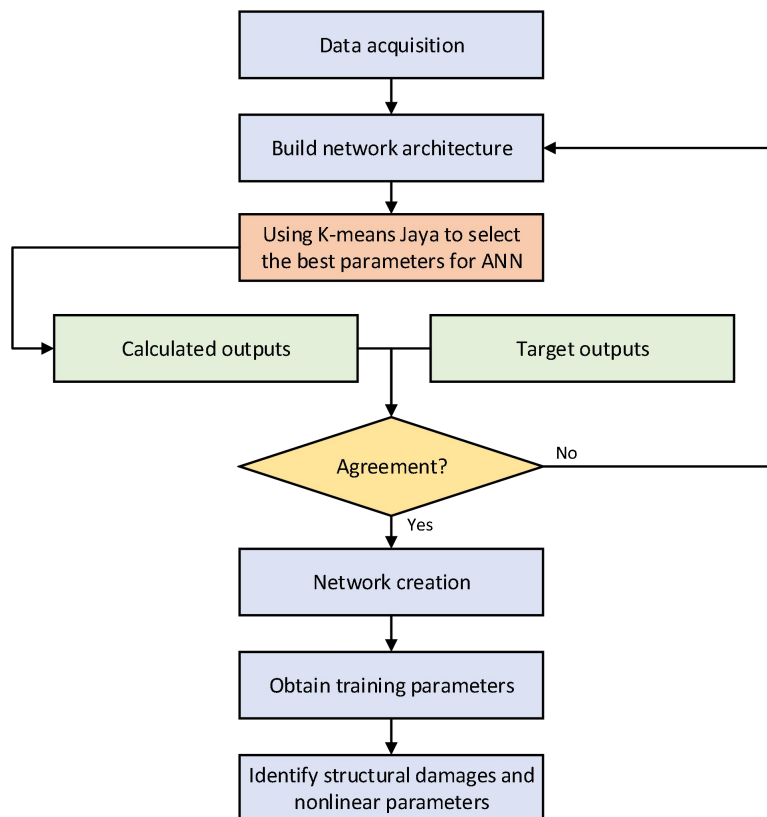


Figure 7-4 Flowchart of using the proposed ANN-K means Jaya for nonlinear model identification.

Herein, the K-means Jaya algorithm is demonstrated. The simple structure of the

standard Jaya algorithm is still kept in the K-means Jaya algorithm, which is used to replace the back-propagation algorithms in training weights and bias of the designed ANN. To demonstrate the procedure of the proposed approach, Figure 7-4 presents the flowchart of using the developed approach, namely ANN-K means Jaya, to conduct the nonlinear structural damage and model parameter identification.

7.4 Numerical studies

The first numerical example is a nonlinear SDOF system with the improved Dahl hysteresis model, as shown in Figure 7-1. The model vector of this system is $\mathbf{p}=[1,0.2,1,0.6]$, which is to be identified. The external loading is defined as $F(t)=\cos(t)$. The hysteresis phenomenon with model vector $\mathbf{p}=[1,0.2,1,0.6]$ for $t \in [0,30]$ is shown in Figure 7-5.

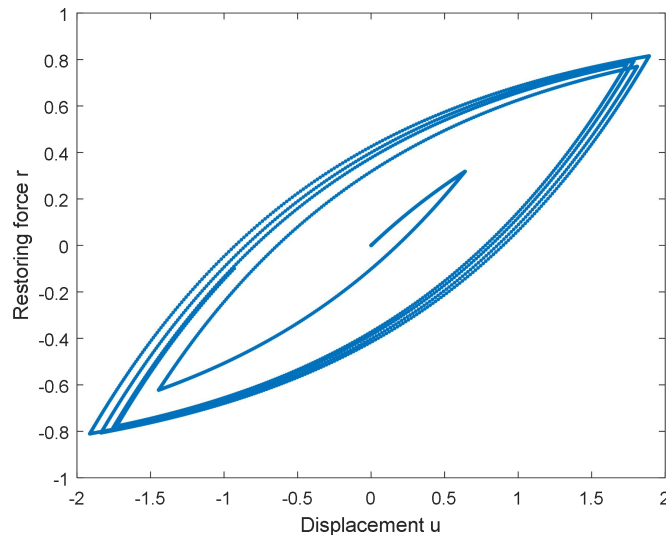


Figure 7-5 Nonlinear system behavior with an improved Dahl hysteresis model.

7.4.1 Training data generation

The acceleration data will be used for the identification. When using the ANN-K means Jaya for nonlinear model parameter identification, a number of samples are required for training. In this studies, 600 samples of acceleration data under sinusoidal excitations are obtained by using randomly generated model vectors. Similar as Ref.

(Ding et al., 2019c), the input for training ANN with K-means Jaya is the 3 seconds responses with a sampling frequency of 100 Hz. In the randomly generated 600 samples, the first 420 samples are employed as the training datasets while the remaining 180 samples are used as the testing datasets. Furthermore, to avoid the ‘dimension disaster’ and to save the computational demand, Principle Component Analysis (PCA) technique (Golival, 2017; Lever et al., 2017) is carried out to process the acceleration data before training. The working mechanism of the principle components are entirely equivalent to finding the eigenvectors of the covariance matrix. Each eigenvector corresponds to one principal component, and the principal component with the largest variance is the most important one. In this study, the first fifteen principle components, which covers over 95% of the variability in data, are used for the training and testing.

7.4.2 Parameters setting for the ANN-K means Jaya for a SDOF system

A relatively simple ANN-K means Jaya model is used for the nonlinear SDOF system identification. Namely, one hidden layer with 10 neurons is designed for the proposed method. The sigmoid function is employed as the activation function for all the layers. For the parameter setting of the K-means Jaya algorithm, the number of initial random solutions is $CS = 100$ and the maximum iteration number is 5000 or the deviation from two consecutive iterations of objective function value is lower than 10^{-8} . Similar as Ref. (Pathirage et al., 2018), additional measurement noise is added into the data. 10% random noise in the acceleration responses in order to train the network model to be more robust to noisy measurements. 30 runs are repeated by using the proposed algorithm, and the mean values and the standard deviations (std.) are recorded as the final identification result.

7.4.3 Training process and identification results

Figure 7-6 shows the iteration process of the objective function values. The objective function for the proposed ANN-K means Jaya represents the Mean Square Error (MSE) value between the calculated output and the target output. The objective function values are at the order of 10^{-5} after iterations, which means that the

discrepancy between calculated outputs and desired ones is sufficiently small and also indicates that the training of weights and bias parameters is successful. Figure 7-7 shows the fitted results from the 1st parameter to the 4th parameter in the model vector \mathbf{P} based on the training datasets (the first 420 samples) by using the proposed approach. It can be observed that the fitted results are close to the labels of training data. This good agreement further demonstrates the satisfactory training process by using the proposed approach. Figure 7-8 shows the regression of the testing dataset. It can be found that the normalized data are almost distributed along the 45-degree line and the R-value for all variables are higher than 0.99, indicating that a very good agreement between network output and target label results is achieved. The trained network will be used for nonlinear model parameter identification. 20% noise is introduced into the acceleration responses to simulate the uncertainties in vibration measurement. It should be noted that the noise level is much higher than that in Refs. (Cao et al., 2012; Yazdanpanah et al., 2020; Zheng et al., 2015; Hu et al., 2017; Lu & Wang, 2017; Lu et al., 2017; Ding et al., 2019c). As regarding the identification, the trained network will be used to identify the above-mentioned model parameter $\mathbf{p} = [1, 0.2, 1, 0.6]$. The final identification results are shown in Table 7-1. Good identification results are obtained and the maximum relative error of the proposed approach is only 0.45%, demonstrating the good robustness and accuracy of the proposed ANN-K means Jaya, even with severe noise effect.

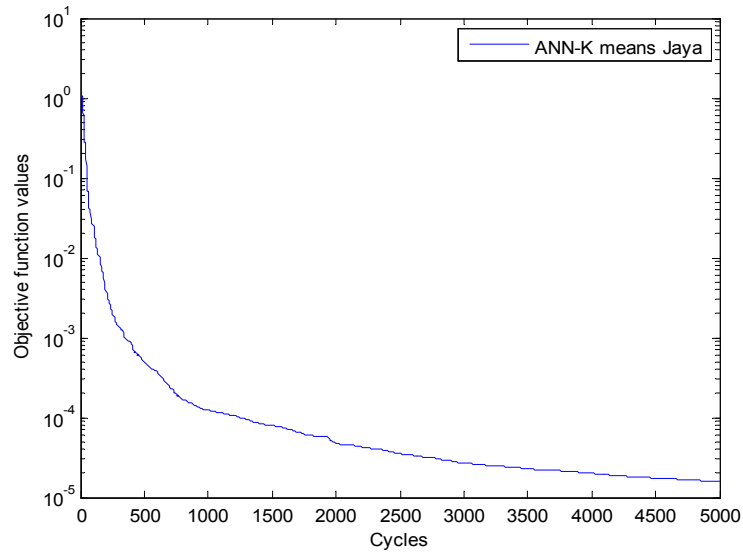


Figure 7-6 Iterations of objective function values for the network training process of the nonlinear SDOF system.

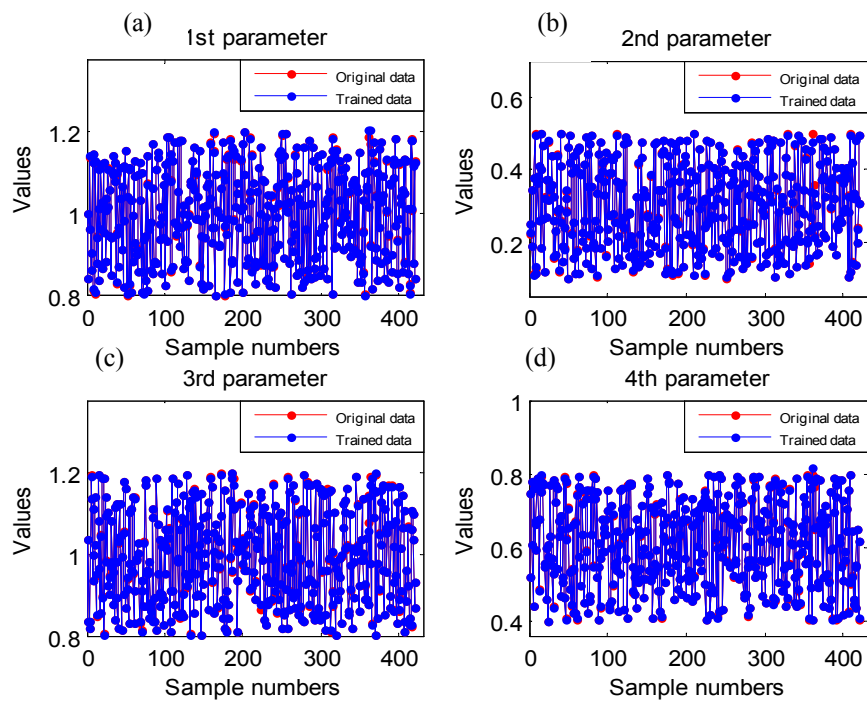


Figure 7-7 Fitted results on all parameters in the model vector based on the training dataset by using the proposed method, (a): k_0 ; (b): c_0 ; (c) α (d): ρ .

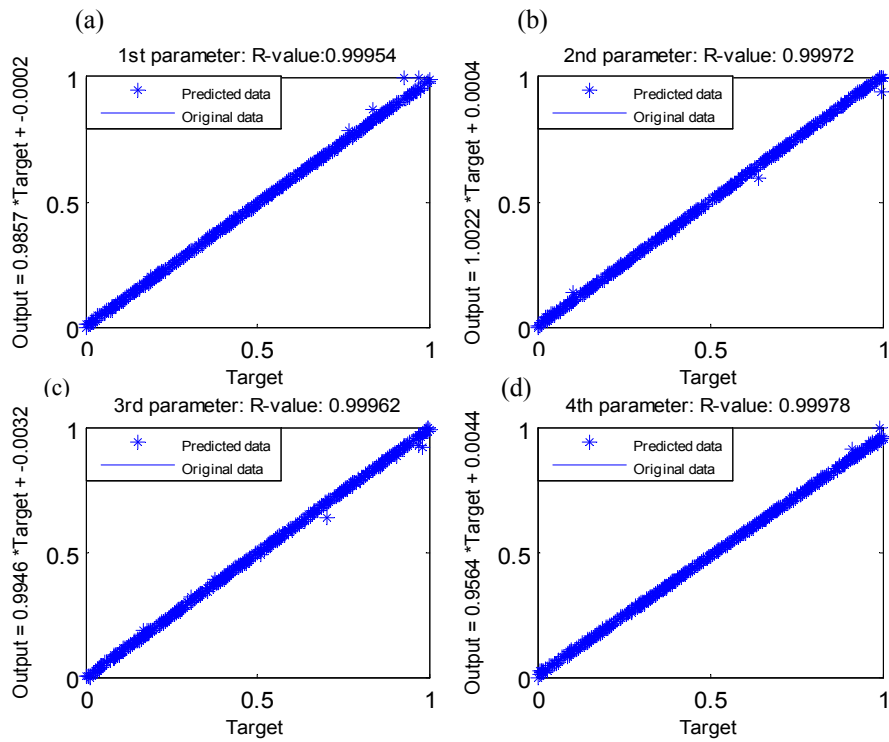


Figure 7-8 Regression results on all parameters in the model vector based on the testing datasets by using the proposed method, (a): k_0 ; (b): c_0 ; (c) α (d): ρ .

7.4.4 Comparisons with state-of-the-art swarm intelligence technique

In this section, several state-of-the-art swarm intelligence techniques, including the K-means Jaya (Ding et al., 2019b), Levy Tree Seeds Algorithm (Ding et al., 2019c) and Best Neighbor-guided ABC (Hu et al., 2019) are introduced for comparison. Swarm intelligence methods conduct the nonlinear model parameter identification by optimizing Eq. (7.7). The input data is the 3 seconds acceleration responses. 20% noise is also introduced to simulate the uncertainties. In terms of the setting of parameters for the algorithms, the number of initial random solutions is $CS = 100$ and the maximum iteration number is 100. Specifically, for the Levy Tree Seeds Algorithm, ST is set as 0.45, the number of conducting Levy flight for the best solution is set as 100. For the Best Neighbor-guided ABC, the parameter $limit$ is set as 200 and the neighbor range is 5. Each algorithm is independently run 30 times, and the mean values and the standard deviations (std.) are obtained.

Figure 7-9 presents the evolutionary processes of the objective function values from the abovementioned three swarm intelligence techniques. The objective function for the swarm intelligence methods represents the discrepancy between the measured and calculated acceleration responses, as shown in Eq. (7.7). It needs around 80 cycles for the Levy Tree Seeds Algorithm and K-means Jaya algorithm to converge. Furthermore, the final values acquired by the Levy Tree Seeds Algorithm and K-means Jaya algorithm are smaller than that acquired by the Best Neighbor-guided ABC. The identification results by these three EAs are also listed in Table 7-1. The maximum relative error from the Best Neighbor-guided ABC, the Levy Tree Seeds Algorithm and the K-means Jaya algorithm are respectively 23.35%, 6.80%, and 5.85%. The proposed ANN-K means Jaya significantly outperforms the other three swarm intelligence methods with a lower relative error. Furthermore, the standard deviation values from the proposed method are significantly less than those acquired by the swarm intelligence methods, which means the proposed method is more stable in system parameter identification of the nonlinear SDOF system. In addition, the numerical computations are conducted on a laptop with an Intel i5 processor and 16-GB RAM for computing and the computational times of each algorithm is also given, as observed in Table 7-1. The required computational time for the proposed method is the most, since the proposed ANN-K means Jaya requires more time for network training. However, the proposed approach can provide the most accurate identification results.

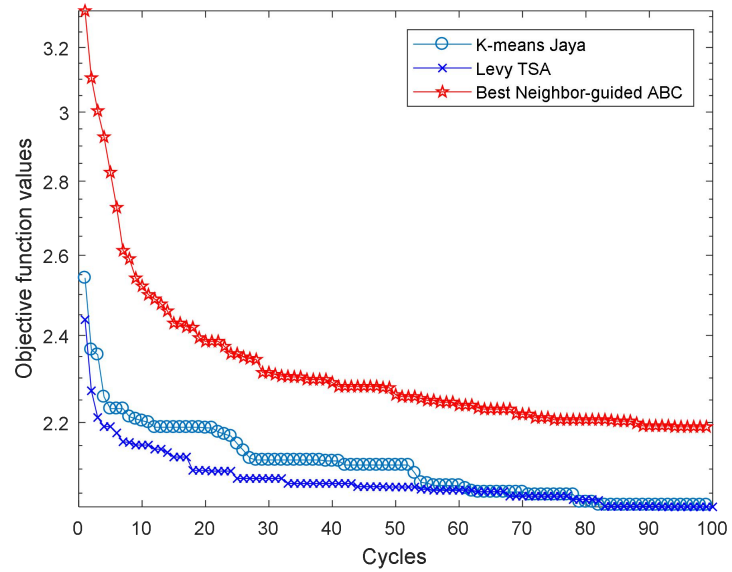


Figure 7-9 Evolutionary processes of objective function values based on state-of-the-art swarm intelligence methods.

Table 7-1 Identified results for a nonlinear SDOF system with improved Dahl model.

Parameters	True values	ANN-K means Jaya		Best Neighbor-guided ABC		Levy Tree Seeds Algorithm		K-means Jaya	
		Mean value	std.	Mean value	std.	Mean value	std.	Mean value	std.
		p1	1	1.0041	0.0002	1.0626	0.0282	1.0117	0.0122
p2	0.2	0.1976	0.0000	0.2467	0.0533	0.2136	0.0200	0.2117	0.0373
p3	1	1.0045	0.0001	0.9881	0.0406	0.9870	0.0087	0.9852	0.0077
p4	0.6	0.5971	0.0000	0.5792	0.0381	0.6110	0.0069	0.5849	0.0082
Maximum relative error (%)		0.45		23.35		6.80		5.85	
Computational time of a run (minutes)		45		20		25		10	

7.5 Identification for a MDOF system

In this section, a MDOF system with a smart controlling device, is used to further verify the performance of the proposed approach. A five-storey building structure (Wu & Samali, 2002; Yu et al., 2018) is used here as an example, as shown in Figure 7-10.

Structural properties of this five-storey building model, including mass, stiffness and damping coefficients, are listed in Table 7-2. The detailed finite element modeling (FEM) process of this benchmark model is referred to Refs. (Katsaras et al., 2008; Lu et al., 2017), in which the shear model is used to simulate this building. The N-S component of El Centro ground motion recorded at the Imperial Valley Irrigation District substation in El Centro, California during the earthquake on 19 May 1940, is used as the external excitation. To simulate the behavior of the seismic isolation device, in this article, the improved Dahl hysteresis model is introduced in the first floor. The parameters α and ρ in the improved Dahl hysteresis model are set as 0.7 and 0.8, respectively. Structural damage is assumed as the stiffness reduction of a specific element and the damage status of a structure is quantified through a series of damage index δ (Ding et al., 2019a). For example, if the damage index of an arbitrary element (h) is equal to 0.1, it means 10% stiffness reduction is introduced in this element, namely, $\delta_h = 0.1$. In this study, simultaneous identification of structural damages and nonlinear hysteresis parameters is conducted.

Table 7-2 Structural properties of the five-storey benchmark building model (Yu et al., 2018).

Floor no.	Mass (Kg)	stiffness (kN/m)	Damping (kN s/m)
1	214	1146	0.0584
2	207	3124	0.1117
3	207	3156	0.1128
4	207	3156	0.1100
5	207	2978	0.1233

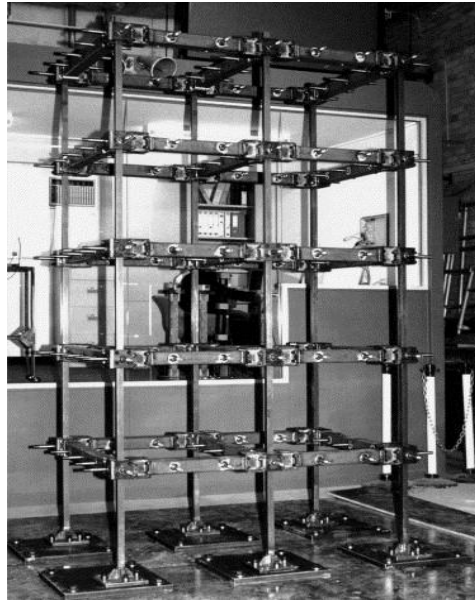


Figure 7-10 Five-storey benchmark building model (Yu et al., 2018).

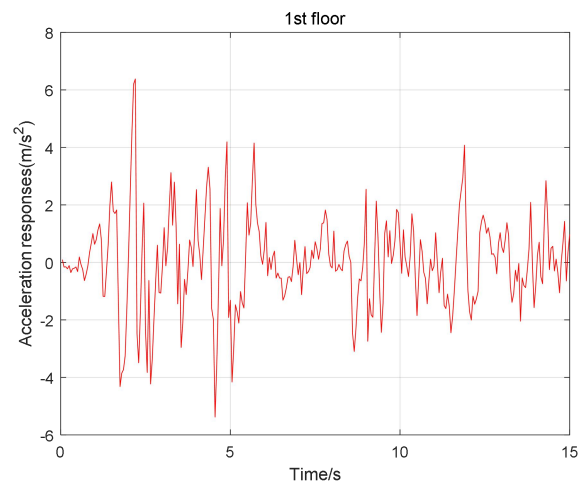


Figure 7-11 The acceleration response of the 1st floor.

7.5.1 Training data generation

It is assumed that the ground excitation is known in advance, namely, the input data is the acceleration responses of the 1st floor under the EI central seismic excitation. Figure 7-11 shows the acceleration responses of the first floor of the intact building under the abovementioned seismic excitation, which lasts 15 seconds with a sampling frequency of 100 Hz. Considering that the proposed ANN-K means Jaya has the best performance in the previous numerical studies on a SDOF system, therefore only the proposed approach is used for the following identification. 1000 sample datasets are

generated randomly, in which the first 700 samples are employed as the training dataset while the remaining 300 samples are used as the testing dataset. Then PCA is used to process the input acceleration data and the first thirty principal components, which also covers over 95% of the variability in data, are used for the training and testing.

7.5.2 Parameters setting for the ANN-K means Jaya

One hidden layer with 10 neurons (Padil et al., 2017) is designed for the ANN-K means Jaya. The output of the network includes structural parameters and nonlinear model parameters. The sigmoid function is served as the activation function for all the layers. Regarding the parameters setting for the K-means Jaya, the number of initial random solutions is $CS=100$. The termination condition is defined as the maximum iteration number is reaching 100 or the deviation from two consecutive iterations of the objective function value is lower than 10^{-8} . Additional 10% measurement noise is added into the acceleration response data in order to train the neural network model robust to noisy measurements. This example is also conducted on a laptop with an Intel i5 processor and 16 GB RAM for computing. The proposed ANN-K means Jaya is carried out 30 runs independently, and the mean values and the standard deviations (std.) are recorded as the final identification result.

7.5.3 Training process and identification results

Figure 7-12 shows the iteration situation of the objective function value for the training process. It can be found that the objective function value is at the magnitude order of 10^{-5} after around 4500 cycles, which means the discrepancy between calculated outputs and desired ones is sufficiently small enough and also means that the training of weights and bias parameters is successful. To further demonstrate the effectiveness of the trained network, Figure 7-13 presents the regression results of the samples from the testing dataset. The normalized data are basically distributed along the 45-degree line and the R-values for all these parameters are higher than 0.96, indicating that a close agreement between output and target results is achieved. Then this trained network is used for simultaneous structural damage and nonlinear

parameter identification. The required calculation time for the training process lasts around 70 minutes for each run.

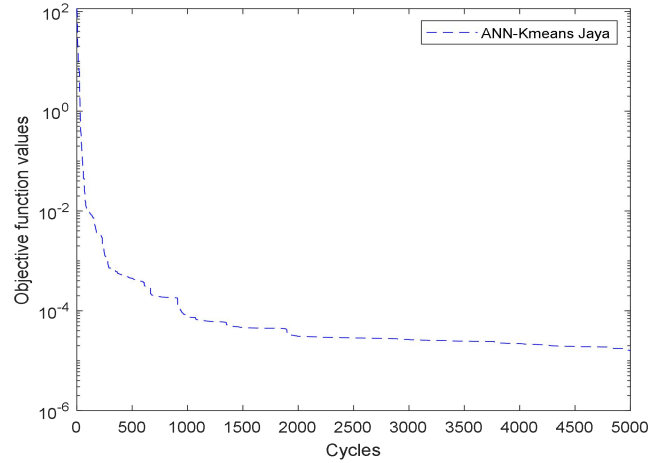


Figure 7-12 Iterations of objective function values for the network training process of the nonlinear MDOF system.

Two cases, which are not included in the training dataset, namely, Case 1 and Case 2, are introduced for testing the performance of the trained network. A small single damage is defined in Case 1 with 5% reduction in the stiffness of the 3rd floor. Therefore, the model parameter $\mathbf{P}_1 = [\delta_1, \delta_2, \delta_3, \delta_4, \delta_5, \alpha, \rho]$ for Case 1 is $\mathbf{P}_1 = [0, 0, 0.05, 0, 0, 0.7, 0.8]$. Multiple damages are defined in Case 2 with 20% reduction in the stiffness of the 1st, 3rd and 5th floors, respectively. Thus, the model parameter $\mathbf{P}_2 = [\delta_1, \delta_2, \delta_3, \delta_4, \delta_5, \alpha, \rho]$ for Case 2 is $\mathbf{P}_2 = [0.2, 0, 0.2, 0, 0.2, 0.7, 0.8]$. 20% measurement noise is introduced into the acceleration responses of the 1st floor, which are used as the input to the network. Furthermore, the traditional back propagation algorithm based ANN is also introduced for comparison. The identification results obtained from the mentioned two methods are shown in Table 7-3.

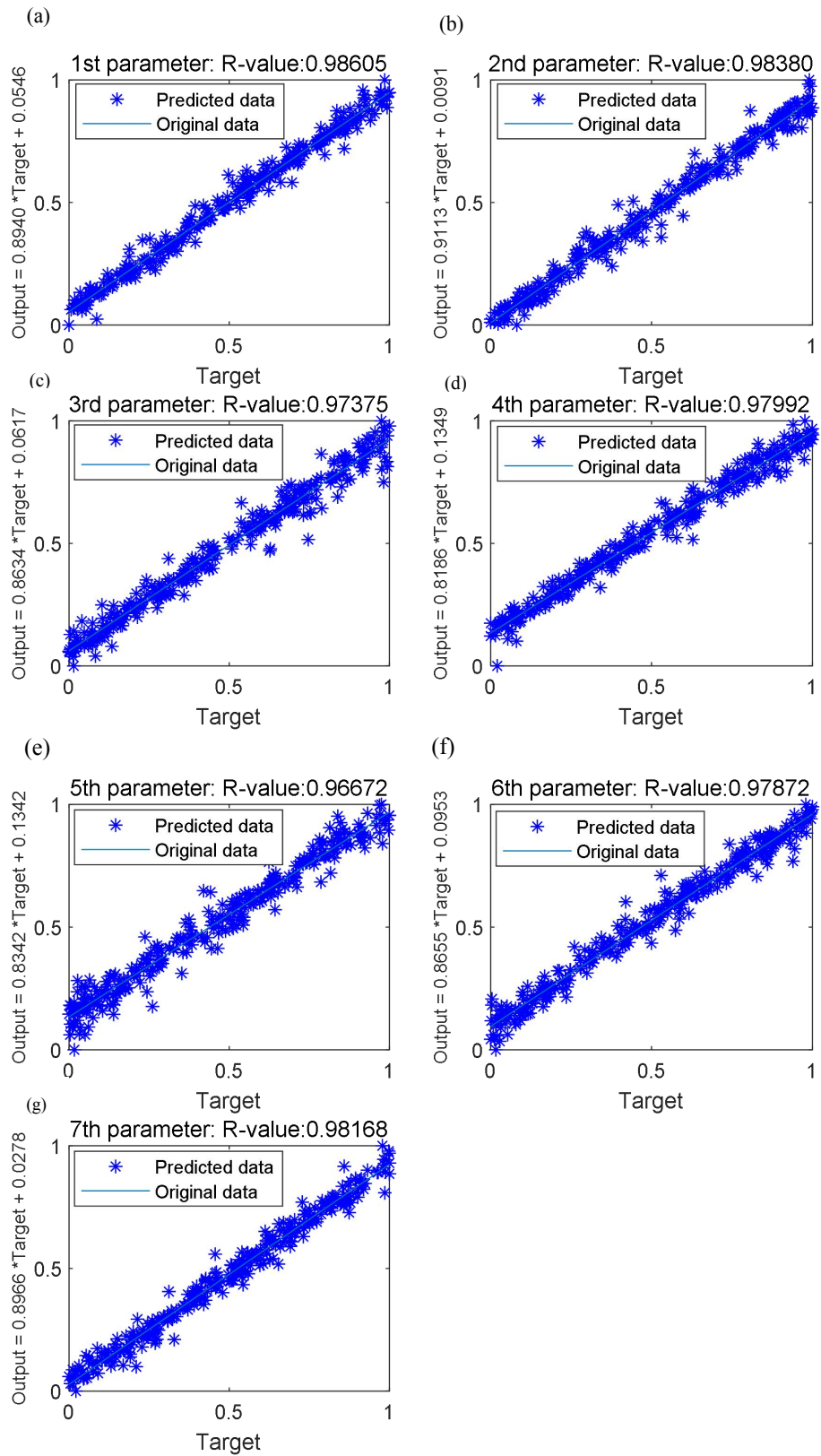


Figure 7-13 Regression results on all parameters in the model vector based on the testing dataset by using the proposed method; (a) δ_1 ; (b) δ_2 ; (c) δ_3 ; (d) δ_4 ; (e) δ_5 ; (f) α ; (g)

ρ .

For Case 1, the maximum identification relative error from the ANN and the proposed method are respectively 9.60% and 2.60%. For Case 2, the maximum relative error from the proposed ANN-K means Jaya is 2.61% while that by using ANN is 11.55%. The superiority of the proposed approach is demonstrated in terms of the identification accuracy. Compared with the results from the nonlinear SDOF system, the identification error for the MDOF system is increased. However, it should be noted that the five-storey benchmark building structure and its external excitation are more complex, and the maximum relative error in the identification results of this nonlinear MDOF system is less than 3%. Overall, good results by using the proposed approach are obtained for the simultaneous identification of structural damages and nonlinear hysteresis parameters, which demonstrates the effectiveness and accuracy of the proposed approach.

Table 7-3 Identified results for a nonlinear MDOF system with improved Dahl model.

Parameter	True values	Case 1			True values	Case 2		
		ANN-K means Jaya Mean values	ANN-K means Jaya std.	ANN Identification value		ANN-K-means Jaya Mean values	ANN-K-means Jaya std.	ANN Identification value
δ_1	0	0	0	0.001	0.2	0.1998	0.0000	0.1877
δ_2	0	0.001	0.0001	0	0	0.002	0.0001	0.001
δ_3	0.05	0.0487	0.0001	0.0452	0.2	0.1956	0.0001	0.1899
δ_4	0	0	0	0.002	0	0.003	0.0002	0.005
δ_5	0	0	0	0.001	0.2	0.1968	0.0003	0.1769
α	0.7	0.6885	0.0002	0.6765	0.7	0.6817	0.0002	0.6739
ρ	0.8	0.7982	0.0001	0.7786	0.8	0.7934	0.0003	0.7751

7.6 Conclusions

This paper proposes a new approach for structural damage and nonlinear model parameter identification of nonlinear structures. The recently developed K-means Jaya algorithm is used to train the parameters of an ANN, which is then used for structural damage and nonlinear model parameter identification. The improved Dahl model, with few controlling parameters, but can well describe the hysteresis phenomenon is used in this study. High-level noise is added into the acceleration responses to simulate the

uncertainties in the data used in the identification analysis. Numerical studies are conducted on a SDOF system for identifying the nonlinear model parameters, and on a MDOF system for the simultaneous identification of structural damages and nonlinear model parameters. The following conclusions are drawn from the obtained results:

- For the SDOF system, the proposed ANN-K means Jaya performs better than several state-of-the-art swarm intelligence methods, in terms of the identification accuracy;

- For the MDOF system identification, although only using one acceleration response, the proposed approach still provides good identification results for both structural damages and nonlinear model parameters. The accuracy of identification results from the proposed approach is better than that obtained by the traditional ANN method;

- Overall, the proposed ANN-K means Jaya equips good robustness and is an effective tool to conduct more complex system identification of nonlinear structures.

References

- Abdeljaber, O., Avci, O., Kiranyaz, M.S., Boashash, B., Sodano, H., & Inman, D.J. (2018) 1-D CNNs for structural damage detection: verification on a structural health monitoring benchmark data. *Neurocomputing*, 275, 1308-1317.
- Altunisik, A.C., Okur, F.Y. & Kahya, V. (2017) Structural identification of a cantilever beam with multiple cracks: Modeling and Validation. *International Journal of Mechanical Sciences*, 130, 74-89.
- Cai, Z.H., Gong, W.Y., Ling, C.X., & Zhang, H. (2011) A clustering-based differential evolution for global optimization. *Applied Soft Computing*, 11, 1363-1397.
- Cao, M.S., Li, C., Su, Z.Q., & Xu, H. (2012) A multi-scale pseudo-force model in wavelet domain for identification of damage in structural components. *Mechanical Systems and Signal Processing*, 28, 638-659.
- Charalampakis, A.E., & Dimou, C.K. (2010) Identification of Bouc-Wen hysteretic systems using particle swarm optimization. *Computers and Structures*, 88, 1197-1205.
- Chen, Z.P., & Yu, L. (2017) A novel PSO-based algorithm for structural damage detection using Bayesian multi-sample objective function. *Structural Engineering & Mechanics*, 63(6), 825-835.
- Curry, B., & Morgan, P. (1997) Neural networks: a need for caution. *Omega*, 25, 123-133.
- Ding, Z.H., Li, J., Hao, H., & Lu, Z.R. (2019a) Structural damage identification with uncertain modelling errors and measurement noise by clustering based tree seeds algorithm. *Engineering Structures*, 165, 301-314.
- Ding, Z.H., Li, J., & Hao, H. (2019b) Structural damage identification using improved Jaya algorithm based on sparse regularization and Bayesian inference. *Mechanical Systems and Signal Processing*, 132, 211-231.
- Ding, Z.H., Li, J., Hao, H., & Lu, Z.R. (2019c) Nonlinear hysteretic parameter identification using an improved Tree-seed algorithm. *Swarm and Evolutionary Computation*, 46, 69-83.
- Elshafey, A.A., Dawood, N & Marzouk, H. (2013) Crack width in concrete using artificial neural networks. *Engineering Structures*, 52, 676-686.
- Ertugrul, O.F. (2018) A novel type of activation function in artificial neural networks: Trained activation function. *Neural Networks*, 99, 148-157.
- Esfandiari, A., Nabiyani, M.S., & Rofooei, F.C. (2020) Structural damage detection using principle component analysis of frequency response function data. *Structural Control & Health Monitoring*, <https://doi.org/10.1002/stc.2550>.
- Farrar, R.C., & Worden, K. (2007) An introduction to structural health monitoring. *Philosophical Transactions of the Royal Society A*, 365, 303-315.
- Gao, W.F., Chan, F.T.S., Huang, L.L., & Liu, S.Y. (2015) Bare bones artificial bee colony algorithm with parameter adaption and fitness-based neighborhood. *Information Science*, 316, 180-200.
- Geethanjali, M., Slochanal, S.M.R., & Bhavani, R. (2008) PSO trained ANN-based differential protection scheme for power transformers. *Neurocomputing*, 71, 904-918.
- Golinval, J.C. (2017) Damage Detection in structures based on Principle Component Analysis of Forced Harmonic Responses. *Procedia Engineering*, 199, 1912-1918.

- Gupta, J.N., & Sexton, R.S. (1999) Comparing backpropagation with a genetic algorithm for neural network training. *Omega*, 27, 679-684.
- Hu, L., Huang, M. & Lu, Z.R. (2017) Crack identification of beam structures using homotopy continuation algorithm. *Inverse Problems in Science and Engineering*, 25(2), 169-187.
- Hu, P., Deng, C.S., & Wu, Z.J. (2019) Best neighbor-guided artificial bee colony algorithm for continuous optimization problems. *Soft Computing*, 23, 8723-8740.
- Katsaras, C.P., Panagiotakos, T.B., & Kolias, B. (2008) Restoring capacity of bilinear hysteretic seismic isolation systems. *Earthquake Engineering and Structural Dynamics*, 37, 557-575.
- Lever, J., Krzywinski, M., & Altman, N. (2017) Principal Component Analysis. *Nature Methods*, 14, 641-642.
- Liu, C.Y., Wu, X., Wu, N., & Liu, C.Y. (2014) Structural damage identification based on rough sets and artificial neural network, *The Scientific World Journal*, 201, 193284.
- Lin, X.X., Huang, M., & Lu, Z.R. (2017) Hybrid sensitivity matrix for damage identification in axially functionally graded beams. *Applied Mathematical Modelling*, 41, 604-617.
- Lu, Z.R., & Wang, L. (2017) An enhanced response sensitivity approach for structural damage identification: Convergence and Performance. *International Journal for Numerical Methods in Engineering*, 111, 1231-1251.
- Lu, Z.R., Yao, R.Z., Wang, L., & Liu, J.K. (2017) Identification of nonlinear hysteretic parameters by enhanced response sensitivity approach. *International Journal of Non-Linear Mechanics*, 96, 1-11.
- Maity, D., & Saha, A. (2004) Damage assessment in structure from changes in static parameter using neural networks, *Sadhana*, 29, 315-327.
- Nguyen, V.T., Bui, T., & Hasegawa, H. (2016) A gait generation for biped robot based on artificial neural network and improved self-adaptive differential evolution algorithm, *International Journal of Machine Learning and Computing*, 6(6), 260-266.
- Padil, K.H., Bakhary, N., & Hao, H. (2017) The use of a non-probabilistic artificial neural network to consider uncertainties in vibration-based-damage detection. *Mechanical Systems and Signal Processing*, 83, 194-209.
- Pathirage, C.S.N., Li, J., Li, L., Hao, H., Liu, W.Q., & Ni, P.H. (2018) Structural damage identification based on autoencoder neural networks and deep learning. *Engineering Structures*, 172, 13-28.
- Rao, R.V., & Saroj, A. (2017) A self-adaptive multi-population based Jaya algorithm for engineering optimization. *Swarm and Evolutionary Computation*, 37(4), 1-26.
- Ren, W.X., & Sun, Z.S. (2008) Structural damage identification by using wavelet entropy. *Engineering Structures*, 30(10), 2840-2849.
- Sun, H., Lus, H., & Betti, R. (2013) Identification of structural models using a modified Artificial Bee Colony algorithm. *Computers & Structures*, 116, 59-74.
- Toghyani, S., Ahmadi, M.H., & Kasaeian, A. (2016) Artificial neural network, ANN-PSO and ANN-ICA for modelling the Stirling engine. *International Journal of Ambient Energy*, 37, 456-468.
- Valian, E., Mohanna, S., & Tavakoli, S. (2011) Improved cuckoo search algorithm for feedforward neural network training. *International Journal of Artificial Intelligence & Applications*, 2, 36-43.

- Wang, D.H., & Liao, W.H. (2011) Magnetorheological fluid dampers: a review of parametric modelling. *Smart Materials and Structures*, 20(2), 023001.
- Wang, G.S. (2009) Applications of hybrid genetic algorithm to system identification. *Structural Control & Health Monitoring*, 16(2), 125-153.
- Wu, Y.M., & Samali, B. (2002) Shake table testing of a base isolated model. *Engineering Structures*, 24, 1203-1215.
- Xie, Z.B., & Feng, J.C. (2012) Real-time nonlinear structural system identification via iterated unscented Kalman filter, *Mechanical Systems and Signal Processing*, 28, 309-322.
- Yang, J.N., Lin, S.L., Huang, H.W. & Zhou, L. (2006) An adaptive extended Kalman filter for structural damage identification. *Structural Health Monitoring*, 13(4), 849-867.
- Yazdanmehr, M., Anijdan, S.M., & Bahrami, A. (2009) Using GA-ANN algorithm to optimize soft magnetic properties of nanocrystalline mechanically alloyed Fe-Si powders. *Computational Materials Science*, 44, 1218-1221.
- Yazdanpanah, O., Mohebi, B., & Yakhchalian, M. (2020) Seismic damage assessment using improved wavelet-based damage-sensitive features. *Journal of Building Engineering*, <https://doi.org/10.1016/j.jobbe.2020.101311>.
- Yan, A., & Golinval, J.C. (2005) Structural damage localization by combining flexibility and stiffness methods. *Engineering Structures*, 27(12), 1752-1761.
- Yu, Y., Wang, C.Y., Gu, X.Y., & Li, J.C. (2018) A novel deep learning-based method for damage identification of smart building structures. *Structural Health Monitoring*, 18(1), 147592171880413.
- Zheng, Z.D., Lu, Z.R., Chen, W.H., & Liu, J.K. (2015) Structural damage identification based on power spectral density, sensitivity analysis of dynamic responses. *Computers & Structures*, 146, 176-184.

CHAPTER 8 CONCLUSIONS AND RECOMMENDATIONS

8.1 Main findings

This thesis develops and improves swarm intelligence methods, neural network methods, and hybrid methods to conduct structural identification considering uncertainties. The major contributions and findings in this thesis are briefly summarized below:

Chapter 2 presents the clustering based Tree Seeds Algorithm to perform structural damage identification. The modal data is used to formulate the objective function. The developed algorithm and the objective function are described. Numerical simulations and experimental verifications reveal that: (1) The proposed method could identify damages more accurately than those acquired by some other swarm intelligence methods; (2) Even though relatively high-level uncertainties is introduced, the proposed method could still acquire satisfactory results; (3) The proposed method could also be seen as a useful tool for model updating, especially for simple structures (usually the total element number is less than 100).

Chapter 3 presents a novel method for nonlinear structural parameter identification. The Lévy flight mechanism and a new updating equation are employed to modify the original Tree Seeds Algorithm. The acceleration responses are used to formulate the objective function. The numerical examples show that: (1) The proposed algorithm could effectively identify three representative nonlinear models; (2) Using different types of response data as the input, the proposed method could still identify these parameters accurately. (3) The proposed algorithm shows obvious improvements in identification accuracy compared with the enhanced sensitivity method. Therefore, the proposed method is a better tool for nonlinear parameter identification.

Chapter 4 investigates the application of the Jaya algorithm in structural damage identification. A novel objective function, which is modified by using the sparse regularization technique and the Bayesian inference, is proposed. A relatively large-scale truss structure and a vehicle-bridge model are employed as the numerical example and the experimental verifications. It is observed that: (1) The proposed

objective function is more sensitive to structural damage compared with traditional one; (2) The proposed method could yield more competitive identification results compared with some traditional optimization methods; (3) The proposed method incorporating with the proposed objective function can be used to identify the parameters of relatively large-scale structures.

Chapter 5 presents the development and application of the sparse deep belief neural network in solving the undetermined structural damage identification problem. To enhance the capacity of the standard deep belief neural network, the sparse constraint is introduced. Numerical and experimental studies show that: (1) Due to the introduction of the sparse constraints, the performance of the deep belief neural network has been obviously enhanced; (2) Compared with the swarm intelligence methods, the proposed method has distinctive advantages in damage localization; (3) Even only the first several natural frequencies are available, the proposed method could provide satisfactory identification of a frame structure; (4) However, the proposed method requires more time for calculation.

Chapter 6 investigates the hybridization of the Tree Seeds Algorithm and the Jaya algorithm to perform structural damage identification of the Guangzhou New TV tower benchmark structural model and an experimental beam structure. To effectively curb the effects posed by the uncertainties, the interval analysis method is introduced and a damage index, termed as the 'DMI' value, is employed to quantify structural damages. It was observed that even though only limited modal data is used, the proposed method incorporating with the DMI values could yield reliable probabilistic identification.

Chapter 7 studies the hybridization of the K means Jaya algorithm and the Artificial Neural Network to conduct the simultaneous identification of structural damages and nonlinear hysteresis parameters. To enhance the performance of the Artificial Neural Network, the K means Jaya algorithm is applied to replace the back-propagation algorithm during the training process. The acceleration responses are employed as the input while the output is the identified parameters. The final identification results show that the proposed method is capable of identifying these parameters, and better than those acquired by some swarm intelligence methods and the

Artificial Neural Network. Overall, although the algorithmic structure of hybrid algorithms become more complex, the hybrid methods equip potentials to solve more complex identification problems. The complexity here mainly arises from the fact that the targets to be identified is more complex and contains different types of parameters.

8.2 Recommendations for future study

In the present work, swarm intelligence methods are developed and improved to conduct structural parameters identification. Good identification results can be acquired. Following investigations could be conducted in the future study:

1. Experimental verifications carried out in this study are relatively simple. More complex and practical experimental models can be used to verify the effectiveness and efficiency of the proposed methods.

2. The damage model is assumed as the linear stiffness reduction, which does not cover all the possible damage scenarios. Therefore, more refined damage models can be investigated.

3. These methods can be extended to tackle the identification problem of practical civil engineering structures, such as highway bridges and buildings. For example, DBN can be potentially used to conduct the SHM data recovery. Those swarm intelligence algorithms can be employed to conduct the identification of linear and nonlinear structures with limited measurements and the optimal sensor placement.

APPENDIX I ATTRIBUTION OF AUTHORSHIP

To whom it may concern

I, ZhengHao Ding, contributed (carried out numerical simulations, analysed numerical results and wrote the manuscript which was revised and edited by other co-authors) to the papers entitled below.

Structural damage identification with uncertain modelling error and measurement noise by clustering based tree seeds algorithm

Nonlinear hysteretic parameter identification using an improved tree-seed algorithm

(.....)

I, as a co-author, endorse that this level of contribution by the candidate indicated above is appropriate.

(Jun Li) (.....)

(Hong Hao) (.....)

(Zhongrong Lu) (.....)

To whom it may concern

I, ZhengHao Ding, contributed (carried out numerical simulations, analysed numerical results and wrote the manuscript which was revised and edited by other co-authors) to the papers entitled below.

Structural damage identification using improved Jaya algorithm based on sparse regularization and Bayesian inference

Structural damage identification by sparse deep neural network using uncertain and limited data

Non-probabilistic method to uncertainty in structural damage identification based on Hybrid Jaya and Tree Seeds algorithm

Simultaneous identification of structural damage and nonlinear hysteresis parameters by an evolutionary artificial neural network based on time domain data

(.....)

I, as a co-author, endorse that this level of contribution by the candidate indicated above is appropriate.

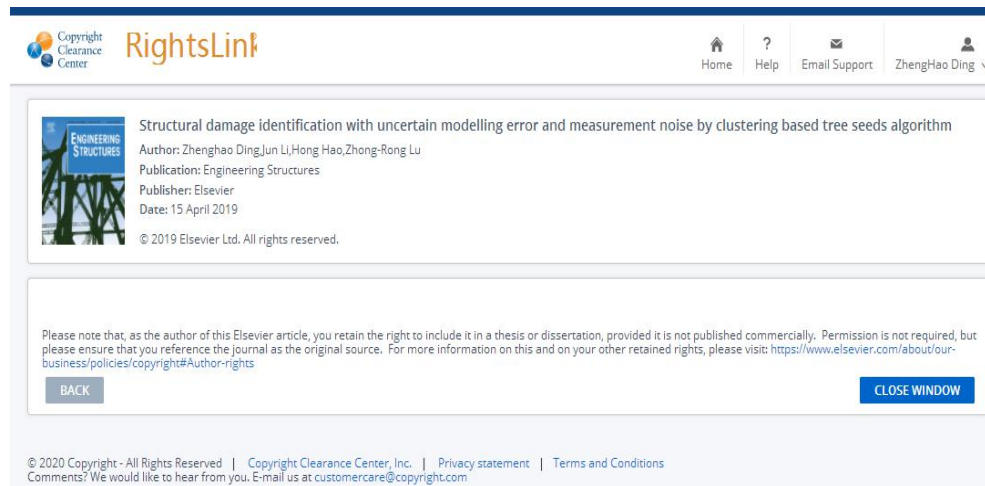
(Jun Li) (.....)

(Hong Hao) (.....)

APPENDIX II COPYRIGHT CLEARANC

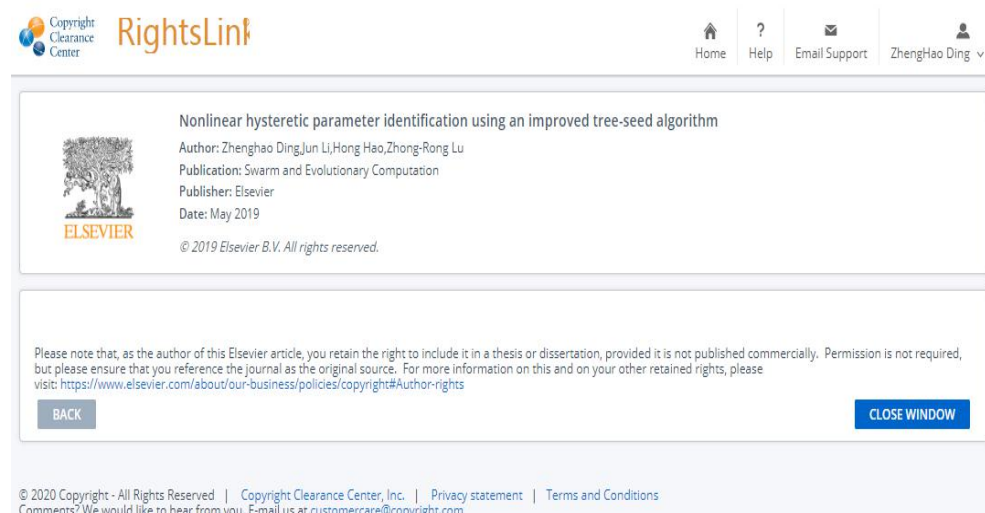
The proof of the rights, granted by publishers for the publication that forms the chapters of this thesis, to reproduce the contribution in the thesis are attached below

Ding, Z., Li, J., Hao, H., & Lu, Z. (2019). Structural damage identification with uncertain modelling error and measurement noise by clustering based tree seeds algorithm. *Engineering Structures*, 185, 301-314. <https://doi.org/10.1016/j.engstruct.2019.01.118>.



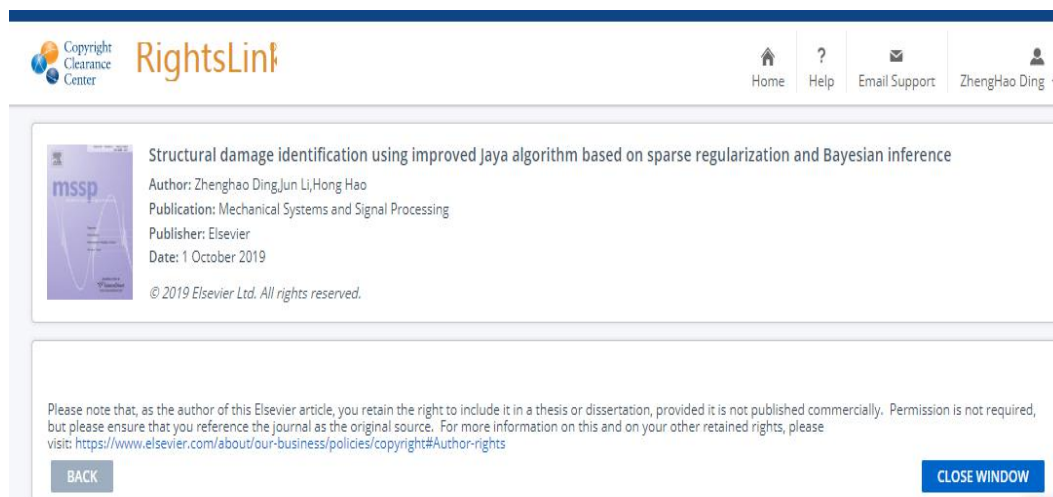
The screenshot shows a RightsLink notification from the Copyright Clearance Center. At the top, there is a navigation bar with the Copyright Clearance Center logo, the RightsLink logo, and links for Home, Help, Email Support, and a user profile for ZhengHao Ding. The main content area features a thumbnail of the journal cover for 'Engineering Structures' and the following text: 'Structural damage identification with uncertain modelling error and measurement noise by clustering based tree seeds algorithm', 'Author: Zhenghao Ding, Jun Li, Hong Hao, Zhong-Rong Lu', 'Publication: Engineering Structures', 'Publisher: Elsevier', and 'Date: 15 April 2019'. Below this is a copyright notice: '© 2019 Elsevier Ltd. All rights reserved.' A disclaimer follows, stating that the author retains the right to include the work in a thesis or dissertation, provided it is not published commercially. At the bottom of the notification are 'BACK' and 'CLOSE WINDOW' buttons. The footer contains copyright information for 2020 and contact details for the Copyright Clearance Center.

Ding, Z., Li, J., Hao, H., & Lu, Z. (2019). Nonlinear hysteretic parameter identification using an improved tree-seed algorithm. *Swarm and Evolutionary Computation*, 46, 69-83. <https://doi.org/10.1016/j.swevo.2019.02.006>.



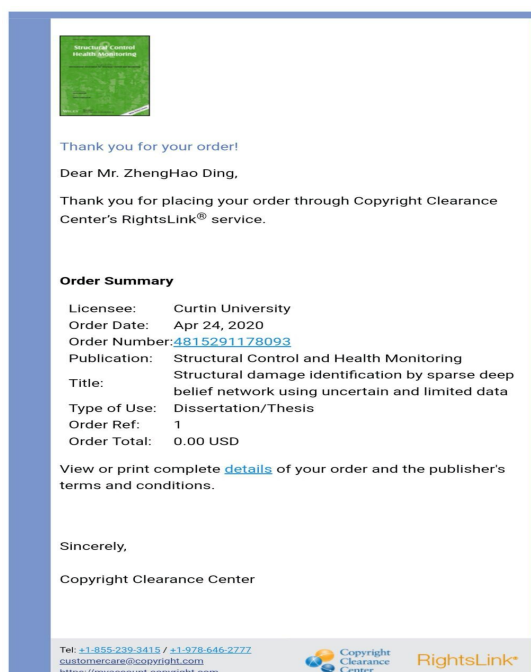
The screenshot shows a RightsLink notification from the Copyright Clearance Center. At the top, there is a navigation bar with the Copyright Clearance Center logo, the RightsLink logo, and links for Home, Help, Email Support, and a user profile for ZhengHao Ding. The main content area features a thumbnail of the journal cover for 'Swarm and Evolutionary Computation' and the following text: 'Nonlinear hysteretic parameter identification using an improved tree-seed algorithm', 'Author: Zhenghao Ding, Jun Li, Hong Hao, Zhong-Rong Lu', 'Publication: Swarm and Evolutionary Computation', 'Publisher: Elsevier', and 'Date: May 2019'. Below this is a copyright notice: '© 2019 Elsevier B.V. All rights reserved.' A disclaimer follows, stating that the author retains the right to include the work in a thesis or dissertation, provided it is not published commercially. At the bottom of the notification are 'BACK' and 'CLOSE WINDOW' buttons. The footer contains copyright information for 2020 and contact details for the Copyright Clearance Center.

Ding, Z., Li, J., & Hao, H. (2019). Structural damage identification using improved Jaya algorithm based on sparse regularization and Bayesian inference. *Mechanical Systems and Signal Processing*, 132, 211-231. <https://doi.org/10.1016/j.ymssp.2019.06.029>.



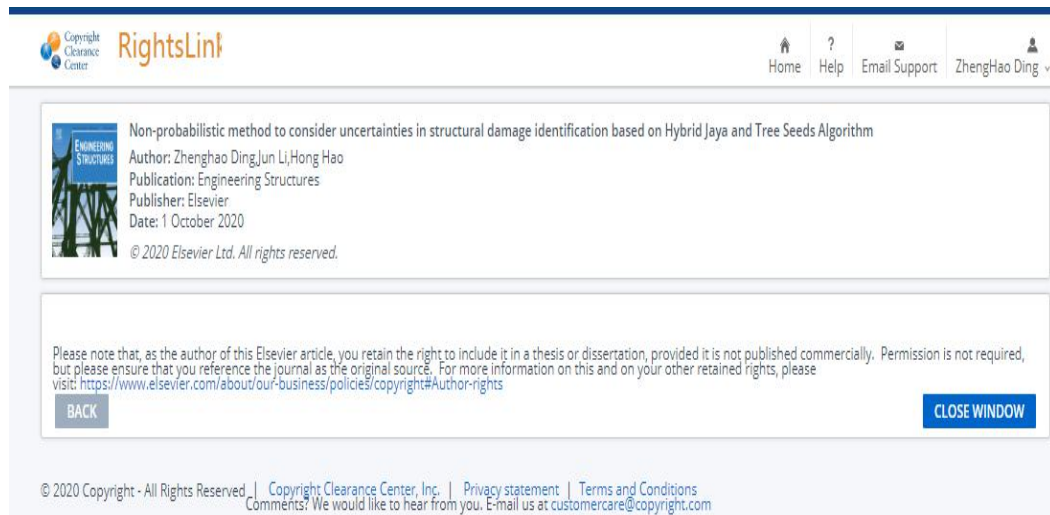
The screenshot shows the RightsLink interface for the article "Structural damage identification using improved Jaya algorithm based on sparse regularization and Bayesian inference". The interface includes the Copyright Clearance Center logo, the article title, author information (Zhenghao Ding, Jun Li, Hong Hao), publication details (Mechanical Systems and Signal Processing, Elsevier, October 2019), and a copyright notice. A disclaimer at the bottom states that the author retains the right to include the work in a thesis or dissertation. Navigation buttons for "BACK" and "CLOSE WINDOW" are visible.

Ding, Z., Li, J., & Hao, H. (2020). Structural damage identification by sparse deep belief neural network using uncertain and limited data. *Structural Control & Health Monitoring*, 27(5), e2522. <https://doi.org/10.1002/stc.2522>.



The screenshot shows an order confirmation email. It begins with a thank you message and identifies the recipient as Mr. ZhengHao Ding. The email thanks the customer for using the RightsLink service and provides an order summary. The summary includes the licensee (Curtin University), order date (Apr 24, 2020), order number (4815291178093), publication title (Structural Control and Health Monitoring), and the specific article title. It also lists the type of use (Dissertation/Thesis), order reference (1), and total cost (0.00 USD). A link is provided to view complete details. The email is signed off by Copyright Clearance Center. Contact information and logos for Copyright Clearance Center and RightsLink are at the bottom.

Ding, Z., Li, J., & Hao, H. (2020). Non-probabilistic method to uncertainty in structural damage identification based on Hybrid Jaya and Tree Seeds algorithm, *Engineering Structures*, 220, 110925. <https://doi.org/10.1016/j.engstruct.2020.110925>.



The screenshot shows a RightsLink interface. At the top left is the Copyright Clearance Center logo and the RightsLink text. On the top right, there are navigation links for Home, Help, Email Support, and a user profile for ZhengHao Ding. The main content area displays the following information:

- Title: Non-probabilistic method to consider uncertainties in structural damage identification based on Hybrid Jaya and Tree Seeds Algorithm
- Author: Zhenghao Ding, Jun Li, Hong Hao
- Publication: Engineering Structures
- Publisher: Elsevier
- Date: 1 October 2020
- Copyright notice: © 2020 Elsevier Ltd. All rights reserved.

Below this information is a disclaimer: "Please note that, as the author of this Elsevier article, you retain the right to include it in a thesis or dissertation, provided it is not published commercially. Permission is not required, but please ensure that you reference the journal as the original source. For more information on this and on your other retained rights, please visit: <https://www.elsevier.com/about/our-business/policies/copyright#Author-rights>".

At the bottom of the window, there are two buttons: "BACK" and "CLOSE WINDOW".

© 2020 Copyright - All Rights Reserved | Copyright Clearance Center, Inc. | Privacy statement | Terms and Conditions
Comments? We would like to hear from you. E-mail us at customer-care@copyright.com

BIBLIOGRAPHY DISCLAIMER

Every reasonable effort has been made to acknowledge the owners of copyright material. I would be pleased to hear from any copyright owner who has been omitted or incorrectly acknowledged.